Role of angiopoietin-like 4 in tumor growth.

Zhu, Pengcheng.

2011

Zhu, P. C. (2011). Role of angiopoietin-like 4 in tumor growth. Doctoral thesis, Nanyang Technological University, Singapore.

https://hdl.handle.net/10356/46431

https://doi.org/10.32657/10356/46431

THE ROLE OF ANGIOPOIETIN-LIKE 4 IN TUMOR GROWTH

ZHU PENGCHENG

School of Biological Sciences

A thesis submitted to the Nanyang Technological University
in partial fulfillment of the requirement for the degree of
Doctor of Philosophy

2011

To My Family .

ACKNOWLEDGEMENTS

It is a pleasure to thank those who made this thesis possible.

I owe my deepest gratitude to my supervisor Dr. Tan Nguan Soon, Andrew, for his sound guidance and constructive criticism during my PhD days. He has made available his support in a number of ways. His wide knowledge and his logical way of thinking have provided a good basis for the present thesis. And his perpetual energy and enthusiasm in research have always been a motivation for me. As a result, research life became smooth and rewarding for me.

It is an honor for me to thank my project collaborators for their valuable input: Prof. Ding Jeak Ling (National University of Singapore), Prof. Petra Boukamp (German Cancer Research Center, Germany), Dr. Sander Kersten (Wageningen University, The Netherlands), Dr. Hoi Yeung Li (Nanyang Technological University, Singapore), Dr. Juin Yit Pan and Dr. Tan Suat Hoon (National Skin Center, Singapore). This thesis would not have been possible without their great help.

My sincere thanks are due to the official referees, Prof. Walter Wahli, Assoc Prof. Vincent T.K. Chaw, and Assoc Prof. Lin Chun Ling Valerie, for their detailed review, constructive criticism and excellent advice during the preparation of this thesis.

All my lab buddies made it a convivial place to work. In particular, I would like to thank Tan Ming Jie for his friendship and all his technical help. All other folks, including Mintu Pal, William Tan, Kelvin, Siew Hui, Yan Yih, Ivan and Lakshmi, and many others had inspired me in research and life through our interactions during the long hours in the lab. Thanks. I also wish to thank my friends outside the lab especially those I met in the soccer fields for their great company and joy.

I owe my loving thanks to my wife Tiantian, my parents and sisters. Without their encouragement and understanding it would have been impossible for me to finish this work.

The financial support of the Nanyang Technological University is gratefully acknowledged.

TABLE OF CONTENTS

Page

LIST OF FIGURES

LIST OF TABLES

LIST OF ABBREVIATIONS

AJ	adherens junction
ANGPTL4	angiopoietin-like 4
AP-1	activated protein-1
A-5RT3$_{ANGPTL4}$	angiopoietin-like 4-knockdown A-5RT3
A-5RT3$_{CTRL}$	srambled siRNA control A-5RT3
A-5RT3$_{Nox1}$	Nox1-knockdown A-5RT3
A-5RT3$_{Nox2}$	Nox2-knockdown A-5RT3
A.U.	arbitrary unit
B	Bound fractions
Bad	B-cell lymphoma-associated death promoter
BAK	B-cell lymphoma-2 homologous antagonist killer
BAX	B-cell lymphoma-2-associated X protein
BCC	basal cell carcinoma biopsy
BCL2	B-cell lymphoma-2
BCL-XL	B-cell lymphoma-extra large
BID	BH3 interacting domain death agonist
BIM	B-cell lymphoma-2 interacting mediator of cell death
bFGF	basic fibroblast growth factor
BSA	bovine serum albumin
B16F10$_{ANGPTL4}$	angiopoietin-like 4-knockdown B16F10
B16F10$_{CTRL}$	scrambled siRNA control B16F10
cAMP	cyclic adenosine monophosphate
cANGPTL4	C-terminal ANGPTL4
CM	conditioned medium
CXCR4	C-X-C chemokine receptor type 4
Cox	cycloxygenase
DAPI	4',6-diamidino-2-phenylindole
DMEM	dulbecco's modified eagle's medium
EC	endothelial cell
ECM	extracellular matrix
EDTA	ethylenediaminetetraacetic acid
EGFR	epidermis growth factor receptor
EMT	epithelial to mesenchymal transition
EPR	electron paramagnetic resonance spectroscopy
ERK-1	extracellular signal-regulated kinase-1
ERK-2	extracellular signal-regulated kinase-2
FAK	focal adhesion kinase
FBS	fetal bovine serum
FIAF	fasting induced adipose factor
FN	fibronectin
FOXO	forkhead box O1
GF	growth factor
GFR	growth factor receptor
GPX	glutathione peroxidase
GSK-3β	glycogen synthase kinase-3beta
GTPase	guanosine triphosphatase
HaCaT	human immotalized keratinocytes

HEPES	(4-(2-hydroxyethyl)-1-piperazineethanesulfonic acid)
HFARP	hepatic fibrinogen/angiopoietin-related protein
HIF	hypoxia-inducible factors
HRP	horseradish peroxidase
HSC	human suquamous cell carcinoma cell
$HSC_{ANGPTL4}$	angiopoietin-like 4-knockdown HSC
HSC_{CTRL}	scrambled siRNA control HSC
H&E	haematoxylin and eosin staining
H_2O_2	hydrogen peroxide
H^+	positive hydrogen cation
IF	immunofluorescence
IGF	insulin-like growth factor
IgG	immunoglobulin G
IMD	integrin-mediated death
IL	interleukin
IL-3	interleukin-3
ILK	integrin-linked kinase
JNK	c-Jun N-terminal kinase
Ka	association rate constant
Kd	dissociation rate constant
K_D	equilibrium dissociation constant
kd	knockdown
KGF	keratinocyte growth factor
K_{off}	dssociation rate constant
KO	knockout
K_{on}	association rate constant
LCM	laser capture microdissection
LC-MS/MS	liquid chromatography-tandem mass spectrometry
LN-5	laminin-5
Lox	lipoxygenases
L27	60S ribosomal protein L27
mAb	monoclonal antibody
MAPK	mitogen-activated protein kinase
MAPK activator	mAPK kinase
MAPKK activator	mAPKK kinase
MAPKKK	mitogen-activated protein kinase kinase kinase
$MA\text{-}MB\text{-}231_{CTRL}$	srambled siRNA control MA-MB-231
$MA\text{-}MB\text{-}231_{Nox1}$	Nox1-knockdown MA-MB-231
$MA\text{-}MB\text{-}231_{Nox2}$	Nox2-knockdown MA-MB-231
MEK/ERK	mitogen-activated protein kinase kinase/extracellular regulated kinase
mit C	mitomycin C
mAb	monoclonal antibody
MMP	matrix metalloproteinase
Mn SOD	manganese superoxide dismutase
M-PEK	proteoextract native membrane protein extraction kit
mRNA	messenger ribonucleic acid
nANGPTL4	N-terminal ANGPTL4
NADH	nicotinamide adenine dinucleotide

NADPH	nicotinamide adenine dinucleotide phosphate
NF-kB	nuclear factor kappa-light-chain-enhancer of activated B cells
NHE	Na^+/H^+ transporter
Nox	nicotinamide adenine dinucleotide phosphate oxidase complex
NS	normal skin
OTC	organotypic coculture
O_2^-	superoxide
·OH	hydroxyl
PAK	p21-activated kinase
pAb	polyclonal antibody
PARP	poly (ADP-ribose) polymerase
PBS	Phosphate buffered saline
PCR	polymerase chain reaction
PDGF	platelet-derived growth factor
PDGF-B	platelet-derived growth factor-B
PDK-1	phosphoinositide-dependent kinase-1
pERK1/2	phosphorylated extracellular signal-regulated kinase 1/2
pFAK	phosphorylated focal adhesion kinase
pHc	cytosolic pH
PI	propidium iodide
PI3K	phosphotidylinositol 3-kinase
PKBα/Akt	protein kinase B alpha
PKC	protein kinases C
PKCα	protein kinases C alpha
PMSF	phenylmethylsulphonyl fluoride
PNS	peri-tumor normal samples
PPAR	peroxisome-proliferator-activated receptor
PPARα	peroxisome-proliferator-activated receptor alpha
PPARβ/δ	peroxisome-proliferator-activated receptor beta/delta
PPARγ	peroxisome-proliferator-activated receptor gamma
PTEN	phosphatase and tensin homologue
PTK	protein tyrosine kinase
PTP	protein tyrosine phosphatase
PUMA	p53 upregulated modulator of apoptosis
PVDF	polyvinylidene Fluoride
pVHL	von hippel-lindau tumor suppressor
qPCR	quantitative real-time polymerase chain reaction
redox	reduction and oxidation
RNAi	ribonucleic acid interference
ROS	reactive oxygen species
Rpl27	60S ribosomal protein L27
RTK	receptor tyrosine kinase
RU	response unit
SCC	squamous cell carcinoma biopsies
S2 cells	Schneider 2 cells
SD	standard deviation
SDF-1	stromal-derived factor 1
SDS	sodium dodecyl sulfate
SDS-PAGE	sodium dodecyl sulfate-polyacrylamid gel electrophoresis

SEM	standard error of the mean
siRNA	small interfering ribonucleic acid
SMAD	mothers against decapentaplegic homolog
SPARC	secreted protein acidic and rich in cysteine
SPR	surface plasmon resonance
Src	sarcoma viral oncogene homolog
TBS	Tris-buffered saline
TBST	Tris-buffered saline with Tween-20
TER	tranendothelial electrical resistance
TGF	transforming growth factor
TGFβ	transforming growth factor-beta
Tie-1	tyrosine kinase-1
Tie-2	tyrosine kinase-2
TJ	tight junction
HMVEC	human microvascular endothelial cell
TNF-α	tumor necrosis factor-alpha
TSP	thrombospondin
TUNEL	terminal deoxynucleotidyl transferase dUTP nick end labeling
MCLA	2-methyl-6-(p-methoxyphenyl)-3, 7-dihydroimidazo-[1, 2-a]-pyrazin-3-one
wk	week
WHO	world health organization
WT	widetype
Zn/Cu SOD	zinc/copper superoxide dismutase

SUMMARY

Cancer is a leading cause of death worldwide. Tumor cells exploit various signaling molecules to promote their growth and metastasis. The angiopoietin-like 4 protein (ANGPTL4) has well-studied roles in metabolism, yet its role in cancer biology remains undefined. Herein, by using human tumor tissue arrays, tumor cell lines and human skin tumor samples, we found that elevated ANGPTL4 expression is widespread in most known tumor types. Treating cancer cells with ANGPTl4-targeted RNAi or monoclonal antibodies imparts a significant decrease in in vivo tumor growth and induces apoptosis in cancer cell lines upon anoikis challenge. Mechanistic investigation suggests that tumor-derived ANGPTL4 interacts with integrins to stimulate the NADPH oxidase-dependent production of O_2^-. A high ratio of O_2^-:H_2O_2 oxidizes/activates Src, triggering the PI3K/PKBα and ERK pro-survival pathways to confer anoikis resistance, thus promoting tumor growth. ANGPTL4 deficiency results in diminished O_2^- production and a reduced O_2^-:H_2O_2 ratio, creating a cellular environment conducive to apoptosis. In all, we show that enhanced expression of ANGPTL4 is common in tumors, and tumor-derived ANGPTL4 activates integrin-related, oxidant-dependent survival pathways, despite the loss of matrix attachment, suggesting ANGPTL4 as an important novel player in redox-mediated cancer progression. Our findings suggest that anticancer strategies focusing on redox-based apoptosis induction in tumors are viable.

PUBLICATION LIST

1. **Zhu P**, Tan MJ, Roystan H, Tan CK, Chong HC, Pal M, Lam CRI, Boukamp P, Pan JY, Tan SH, Kersten S, Li HY, Ding JL, Tan NS. The angiopoietin-like 4 sustains an elevated pro-survival intracellular O_2^-:H_2O_2 ratio and confers anoikis resistance to tumor. (*Cancer Cell 19, 401-4*).
2. Goh YY*, Pal M*, Chong HC*, **Zhu P**, Tan MJ, Punugu L, Yau YH, Tan CK, Roystan H, Tan SM, Tang MBY, Ding JL, Kersten S, Tan NS. Angiopoietin-like 4 interacts with integrins β1 and β5 to modulate keratinocyte migration (*Am. J. Pathol. 177, 2791-280,* *Authors contributed equally).
3. Goh YY*, Pal M*, Chong HC, **Zhu P**, Tan MJ, Punugu L, Tan CK, Roystan H, Sze SK, Tang MBY, Ding JL, Kersten S, Tan NS. Angiopoietin-like 4 interacts with matrix proteins to modulate wound healing (*J.Biol.Chem. 285:32999-33009,* *Authors contributed equally).
4. Roystan H*, Teo Z*, Chong HC, **Zhu P**, Tan MJ, Tan CK, Lam CRI, SNG MK, David Leong, Tan SM, Ding JL, Li HY, Tan NS. Angiopoietin-like 4 disrupts endothelial integrity via integrin α5β1-mediated Rac/PAK signaling and declustering of VE-cadherin and claudin-5. (*Blood*, in press. *Authors contributed equally).
5. **Zhu P**, Goh YY, FANG CHA, KERSTEN S, Tan NS. Diverse roles of angiopoietin-like 4. (Invited review, in submission to *Biosciences Report*).
6. Tan MJ*****, Sng MK*, Teo ZQ*, **Zhu P***, and Tan NS*. Functions of angiopoietin-like 4 (ANGPTL4) in human cancer. (* equal contribution) (*British Journal of Cancer*, in revision).

1. INTRODUCTION

1.1) Cancer Overview

Cancer is now the leading cause of death worldwide. According to the 2008 GLOBOCAN study which was released in 2010 by the World Health Organization (WHO), there were an estimated 12.7 million new cancer cases and 7.6 million cancer-related deaths in 2008. There are over 100 different types of cancer, and each is classified by the type of cell that is initially affected. The most commonly diagnosed cancers worldwide are skin, lung, prostate, breast and colorectal cancers (see worldwide cancer incidence rates in Figure I); while the most common causes of cancer deaths are from lung (1.38 million, 18.2% of the total), stomach (0.74 million, 9.7%), liver (0.69 million, 9.2%), colorectal (0.61 million, 8.1%), and breast cancers (0.46 million, 6.1%). The cause of cancer development varies and could be perplexing, as an individual's risk of developing cancer depends on many factors, including exposure to carcinogens and genetic make-up, among others. Extensive exposure to carcinogens may raise the chance of cancer development, but genetic mutations are the ultimate culprit, which essentially comprise the activation of oncogenes or inactivation of tumor suppressor genes. The main cause of lung cancer is smoking, particularly of cigarettes, which contains over 60 known carcinogens, including radioisotopes from the radon decay sequence, nitrosamine, and benzopyrene (Hecht, 2003). Additionally, nicotine appears to depress the immune response to malignant growths in exposed tissue (Sopori, 2002). Genetically, mutations or/and amplifications in *K-ras*, epidermal growth factor receptor (*EGFR*) or/and *TP53* genes are most commonly found in lung cancers (Herbst et al., 2008). Several genetic polymorphisms are also associated with lung cancer (Devereux et al., 1996). People

with polymorphisms in genes coding for interleukin-1 (Engels et al., 2007), cytochhrome P450 (Wenzlaff et al., 2005), caspase-8 (Son et al., 2006) and XRCC1 (Yin et al., 2007) are more likely to develop lung cancer after exposure to carcinogens. Stomach cancer, is mainly caused through infection by *Helicobacter pylori*, especially for cancers in the lower (distal) part of the stomach (Bevan and Houlston, 1999). Genetic mutations of *CDH1* (Tamura et al., 1996), *APC* (Hsieh and Huang, 1995), *PTEN* (Nelen et al., 1997), *PJS1* (Jenne et al., 1998) and *TP53* (Moll and Schramm, 1998) genes are reported to contribute to the predisposition of stomach cancer. Risk factors that most commonly contribute to liver cancer are chronic infection with hepatitis C or hepatitis B viruses and chronic heavy alcohol use. Genetically, *MYC* and *TGF-α* amplifications, *CTNNB1* and *PIK3CA* mutation, *HGF*, *IGF-2* and *hTERT* overexpression, and defective in *RB1*, *TP53*, *CDKN2A*, *IGFR-2* and *PTEN* genes are related to liver carcinogenesis and metastases (Chen et al., 2010). Exposure to potential carcinogens from diet and cigarette smoking or virus (e.g. HPV) infection may be associated to colorectal cancer. Genetically, the Wnt-APC-β-catenin signaling pathway is commonly found mutated in colorectal cancers; while the *TP53* and *TGF-β* genes usually undergo deactivating mutations (Markowitz and Bertagnolli, 2009). Exposure to many environmental compounds, e.g. xenoestrogens, bisphenol A, aromatic amines, benzene and DDT, could increase breast cancer risk (Brody et al., 2007). Genetically, accumulated gene mutations in *BRCA1 (breast cancer 1)*, *BRCA2*, *ESRs* (estrogen receptors), *PGR* (progesterone receptor), *Her2/neu* or/and *TP53* are commonly found in breast cancer patients (Struewing et al., 1997).

Surprisingly to all, despite all the vast sums of money and time spent on the fundamental basic biology of cancer and all the clinical studies, we have made very little, if any, real progress in cancer death rates over the last 50-70 years. An

examination of the annual statistical data compiled by the American Cancer Society reveals that the rate of mortality from cancer has changed very little over the past 50 years (Labat-Robert and Robert, 2007), and deaths from cancer are projected to continue to rise. With an estimated 21.4 million new cases diagnosed annually, over 13.2 million deaths from cancer are predicted to occur worldwide in 2030. In other words, cancer remains and will remain a major challenge for basic research as well as in the clinic.

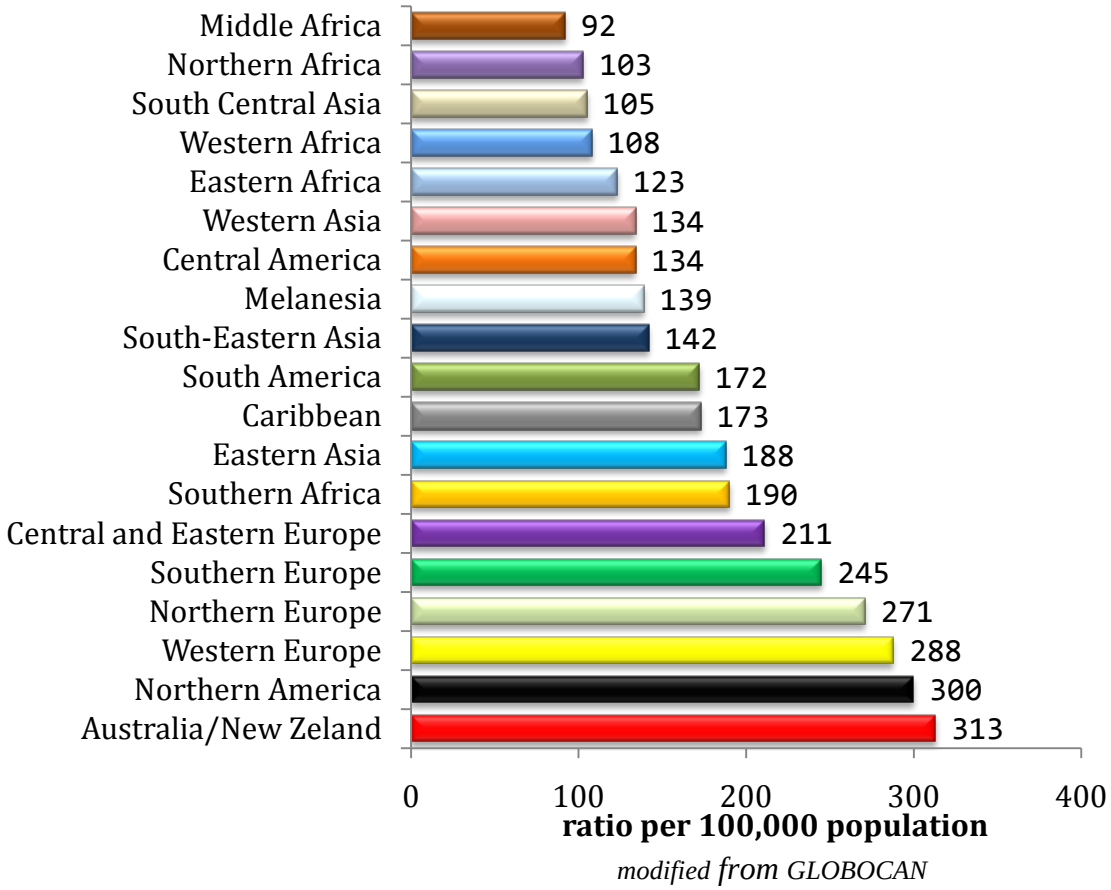

Figure I. Cancer incidence rates worldwide in 2008.

Cancer (malignant tumor/neoplasm) is a complex disease that arises from dysfunctional cells, which proliferate uncontrollably and disrupt tissue organization. Normal cells, under steady-state conditions, proliferate as needed to replace

themselves as they age or become injured. However, this process can go awry, resulting in uncontrolled proliferation and formation of a tumor, which can be benign or malignant. Benign tumors are generally slow growing, enclosed within a fibrous capsule and noninvasive, and they morphologically resemble their cellular precursor. If a benign tumor is not close to critical vascular or neural tissue, prompt diagnosis and treatment frequently result in a cure. In contrast, malignant tumors rarely encapsulate but grow rapidly, invade regional tissues, have morphologic abnormalities such that their tissue of origin may be unrecognizable, and metastasize. The term "metastasis" was coined in 1829 by Jean Claude Recamier and is now defined as "the transfer of disease from one organ or part to another not directly connected to it" (Talmadge and Fidler, 2010).

Metastasis is a primary clinical challenge because its onset is unpredictable and increases the clinical damage to the host exponentially. Thus, metastasis is the primary cause of death in patients with cancer (Fidler, 1999), causing 90% of deaths among solid tumor patients (Gupta and Massague, 2006). The process of cancer metastasis is highly selective and consists of a series of sequential, interrelated steps, each of which can be rate limiting. To produce clinically relevant lesions, metastatic cells must complete all steps of this process. After initial transformation and growth of cells, creation of new blood vessels (vascularization) must occur if a tumor mass (primary tumor) is to exceed 1 mm in diameter. The synthesis and secretion of several pro-angiogenic factors by tumor and host cells and the absence of antiangiogenic factors play key roles in establishing a capillary network from the surrounding host tissues (angiogenesis). Next, local invasion of the host stroma occurs (the collection of invasive neoplastic cells is now considered a malignant cancer) as a consequence of the enhanced expression of a series of enzymes (e.g. collagenase). Once the invading

cells penetrate the lymphatic or vascular channels (intravasation), they may grow there, or a single cell or clumps of cells may detach and be transported within the circulatory system. The tumor emboli must survive immune and non-immune defenses and the turbulence of circulation, arrest and lodge in the capillary beds of receptive organs, and then “extravasate” (i.e. escape the blood vessel lumen by penetrating the organ parenchyma - the tissue residing just outside the vessel walls and capillary basement membrane). After extravasation, the cancer cells must proliferate and establish a micrometastasis (or secondary tumor, growth of which requires both development of a vascular supply and evasion of host defense cells); this new tumor may subsequently grow and colonize other distant tissues (Fidler, 2003; Steeg, 2006; Langley and Fidler, 2007; Singh et al., 2007; Suresh, 2007; Talmadge and Fidler, 2010) (Figure II).

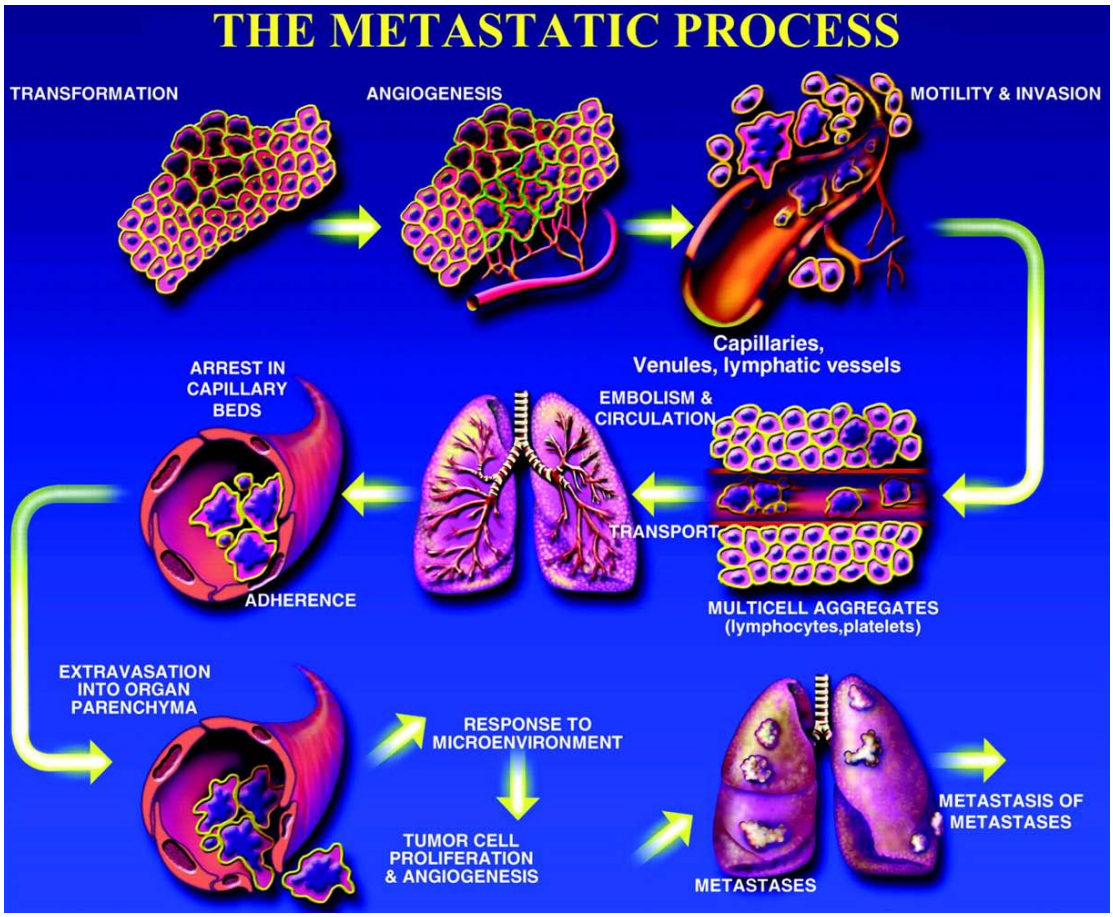

Figure II. Pathogenesis of cancer metastasis.

The process of cancer metastasis consists of sequential, interlinked, and selective steps. The outcome of each step is influenced by the interaction of metastatic cells with homeostatic factors. Each step of the metastatic process is considered rate-limiting in that failure of a tumor cell to complete any step effectively terminates the process. Therefore, the formation of clinically relevant metastases represents the survival and growth of unique subpopulations of cells that preexist in primary tumors. Numerous chemokines play multifaceted roles in tumor growth, invasion and metastasis (Langley and Fidler, 2007).

1.1.1) Signal Regulation in Cancer

Cancer cells create their own signals that allow sustained growth and duplication. Understanding the cellular and molecular mechanisms of the origins of cancer can provide clues about the role of molecules and genes in cancer progression in humans and thus provide therapeutic strategies for clinical applications (Suresh, 2007). However, experience has proved that merely targeting cancer cells themselves is not sufficient to cure a metastatic cancer. Succeeding metastatic cells have undergone changes in their proliferative, survival, migratory and invasive abilities and can be viewed as the winners of a "metastasis decathlon" (Crissman, 1986). It is now well established that genetic alterations in the tumor cells *per se* are not sufficient to allow tumor progression and metastasis to occur, but that a metastasis favorable stromal environment is needed as well. By analogy with the architecture of organs, tumors are not only composed of a "parenchyma" formed by the neoplastic cells, but also of a supportive "stroma", consisting of specific extra-cellular matrix (ECM) components, fibroblasts, adipocytes, vascular cells, smooth muscle cells and cells of the hematopoietic system (Mueller and Fusenig, 2004). During tumor progression and metastasis, an active crosstalk occurs between tumor cells and the stroma that is mainly mediated by direct cell-cell contact or paracrine cytokine and growth factor signaling and is reminiscent of the communication between epithelial and mesenchymal cells during embryonic development (Kopfstein and Christofori, 2006). As early as in 1889, Stephen Paget proposed the famous "seed and soil" theory, which is still well-accepted today. A current definition of the "seed and soil" hypothesis encompasses three principles (Fidler, 2003). First neoplasms are biologically heterogeneous and contain genotypically and phenotypically diverse subpopulations of tumor cells, each of which have the potential to complete some steps, but not all of

the steps in the metastatic process. The recent advent of laser-capture microdissection (LCM), which allows for the isolation of specific tumor cells (Simone et al., 1998), provides an appropriate method to analyze tumor-cell heterogeneity. Second, the process of metastasis is highly selective. Although some of the steps in this process contain stochastic elements, on the whole metastasis favors the survival and growth of a few subpopulations of cells that pre-exist within the parent neoplasm. Third, and perhaps most important for the design of new cancer therapies, is the idea that metastases can only develop in specific organs. The microenvironments of different organs ("soil") are biologically unique. The outcome of metastasis depends on multiple interactions ("cross-talk") between metastasizing cells via normal homeostatic mechanisms, which the tumor cells can usurp. The therapy of metastases, therefore, should be targeted not only against the cancer cells themselves, but also against the homeostatic factors that promote tumor cell growth, survival, angiogenesis, invasion and metastasis. In other words, a better understanding of the molecular mechanisms that regulate the process of metastasis and of the complex interactions between the metastatic cells and the host factors may provide a biological foundation for the design of more effective therapies (Fidler, 1999; Hanahan and Weinberg, 2000; Fidler, 2003).

1.1.2) HIF and Cancer

Tumor hypoxia was first proposed by radiation oncologists in the 1950s as a frequent cause of solid tumors' failure to respond to radiotherapy. Today, it is evident that tumor hypoxia and the critical molecular mediators of hypoxia - hypoxia-inducible factors (HIFs) - regulate multiple steps of tumorigenesis including tumor formation and progression, as well as response to therapy (Rankin and Giaccia, 2008).

HIFs (HIF1, 2, and 3) are transcription factors that mediate cellular adaptations to oxygen deprivation. Over 100 direct HIF target genes have been identified that regulate a number of cellular processes, including glucose metabolism, angiogenesis, erythropoiesis, proliferation, and tumor invasion (Semenza, 2001). In contrast to HIF1 and HIF2, the role of HIF-3 in the hypoxic regulation of target gene expression in vivo is not well understood (Rankin and Giaccia, 2008). HIF1α and HIF2α are commonly upregulated in a variety of human tumors, including bladder, breast, colon, glial, hepatocellular, ovarian, pancreatic, prostate, and renal tumors (Rankin and Giaccia, 2008); elevations in HIF1 and HIF2 expression levels often correlate with poor patient outcome in various types of cancer. Hypoxia is the best-characterized stimulus of HIF activation in tumors, and therefore HIF is used as a known hypoxic marker (Talks et al., 2000). HIF can also be activated in tumors under normoxic conditions through genetic alterations in the oxygen-signaling pathway (Iliopoulos et al., 1996; Maxwell et al., 1999). Tumorigenesis involves a number of alterations in cell physiology that contribute to malignant growth (Hanahan and Weinberg, 2000). Importantly, HIFs have been found to promote key steps in tumorigenesis, including angiogenesis, metabolism, proliferation, metastasis, and differentiation. For example, HIF activation correlates with metastasis in multiple tumors and can promote metastasis through the regulation of key factors governing tumor cell metastatic potential, including E-cadherin, lysyl oxidase, C-X-C chemokine receptor type 4 (CXCR4), and stromal-derived factor 1 (SDF-1); HIF can also indirectly regulate cellular processes such as proliferation and differentiation through interactions with other signaling proteins such as c-Myc and Notch. In summary, there are multiple mechanisms by which HIF can become activated and promote tumor progression (Rankin and Giaccia, 2008). In addition, an understanding

of tumor cell metabolism, apoptosis, migration, differentiation, angiogenesis, oxygenation and related issues involving the tumor-host relationship, wherein HIF1 and HIF2 directly or indirectly play critical overlapping/distinct roles, is becoming essential to studies of cancer biology as well as to the design of more effective forms of cancer therapy (Vogelstein and Kinzler, 2004; Calzada and del, 2007) (Figure III).

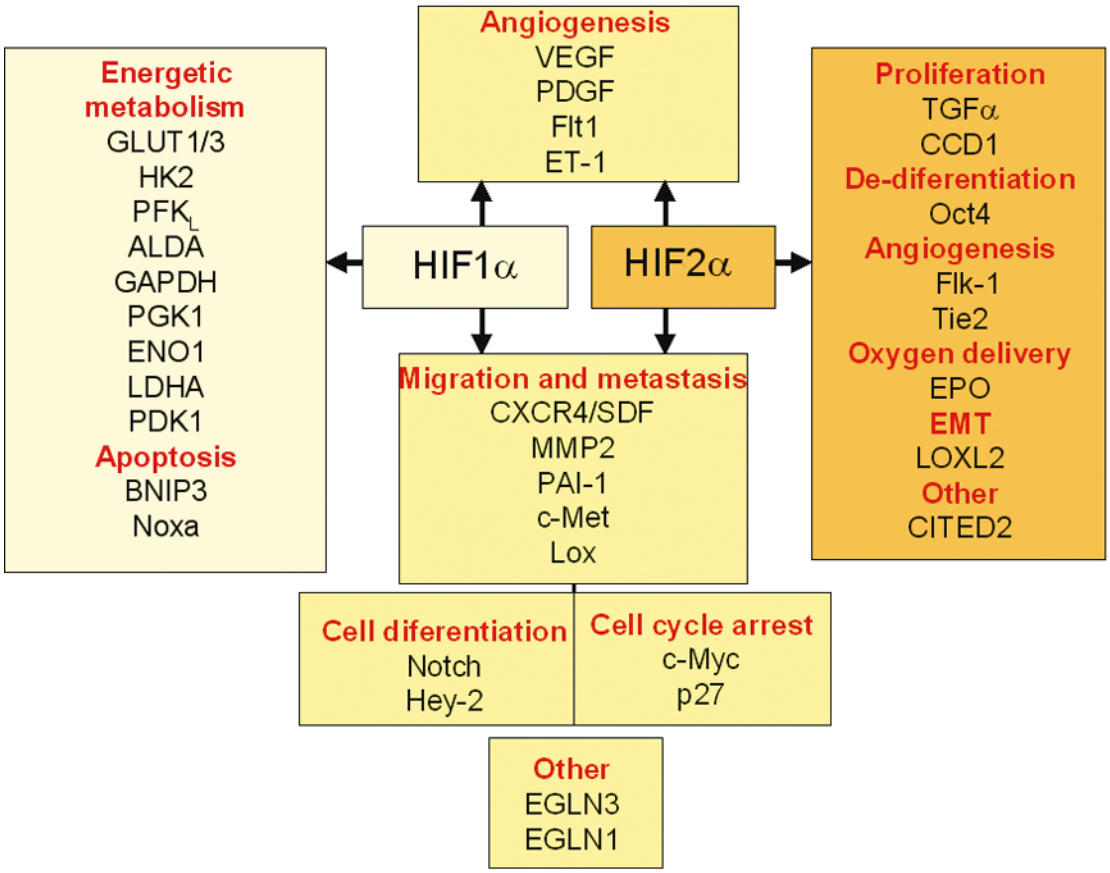

Figure III. Overview of HIF target genes.

HIF1α and HIF2α regulate overlapping and distinct genes. They share the regulation of genes involved in angiogenesis, migration and metastasis and cell differentiation. HIF1α specifically regulates genes involved in energetic metabolism, cell cycle arrest and apoptosis, while HIF2α specifically regulates expression of the stem cell factor gene Oct-4 and two genes involved in cell proliferation, cyclin D1 and the growth factor TGFα (picture adapted from Calzada and del, 2007).

1.1.3) PPARs and Cancer

Peroxisome proliferator-activated receptors (PPARs) are ligand-activated intracellular transcription factors and members of the nuclear hormone receptor superfamily. The PPAR subfamily consist of three subtypes encoded by distinct genes denoted PPARα (NR1C1), PPARβ/δ (NR1C2) and PPARγ (NR1C3), all of which are activated by specific ligands (Desvergne and Wahli, 1999). As transcription factors that require activation, the PPARs modulate the expression of target genes in response to ligand binding. Physiological ligands of PPARs include fatty acids and their derivatives, leukotrienes and prostaglandins. PPARs form heterodimers with retinoic X receptors, and upon ligand binding, modulate gene expression of downstream target genes dependent on the presence of co-repressors or co-activators. (Tan et al., 2003)

The three subtypes of PPAR exhibit distinct tissue distributions, reflecting their biological functions. PPARα is predominantly expressed in hepatocytes, cardiomyocytes and the proximal tubule cells of the kidney (Braissant et al., 1996), serving as a sensor of xenobiotics and lipids in the regulation of energy combustion, hepatic steatosis (fatty degradation), lipoprotein synthesis, inflammation and liver cancer (Devchand et al., 1996; Kersten et al., 1999; Delerive et al., 2001; Pyper et al., 2010). In rodents, sustained activation of PPARα by either exogenous or endogenous agonists leads to the development of hepatocellular carcinoma resulting from sustained oxidative and possibly endoplasmic reticulum stress and liver cell proliferation (Pyper et al., 2010). PPARβ/δ is ubiquitously expressed and plays various roles in metabolism. Recent investigations have demonstrated high PPARβ/δ expression in a variety of tissues, e.g. skin, skeletal muscle, adipose tissue, inflammatory cells, heart, and various types of cancer (Kliewer et al., 1994; Martin, 1995; Braissant et al., 1996; Lemberger et al., 1996). The function of PPARβ/δ in

different types of cancer is highly controversial at present. This controversy might result from the different experimental models used and also from the varying contributions of PPARβ/δ to inflammation, endothelial cell proliferation, and tumor cell proliferation, differentiation and apoptosis. Because all these processes are critical for cancer growth, different approaches could give rise to opposing results (Wagner and Wagner, 2010). PPARγ is highly expressed in adipocytes where it influences lipid storage and glucose metabolism (Desvergne and Wahli, 1999). PPARγ is also widely expressed in many tumors, including lung, prostate, colon, breast, duodenal, thyroid and bladder (Mansure et al., 2009). However, the role of PPARγ in cancer remains controversial. On one hand, it has been reported that PPARγ agonists exerted a growth suppressive effect in a chemically induced model of colon cancer in mice (Dai and Wang, 2010). On another, recent studies has implied that PPARγ enhances angiogenesis in obesity and cancer via the induction of ANGPTL4 (Gealekman et al., 2008; Tian et al., 2009), and plays an important role in carcinogenesis (Mansure et al., 2009). Thus, a more detailed analysis is warranted to clarify the role of PPARγ in tumor development as well as to dissect the molecular basis of its potential tumor effect (Nakagama, 2010). Taken together, the activation of PPARα leads to a pro-tumor effect, at least in rodents, while the roles of PPARβ/δ and PPARγ in cancer are still controversial.

1.1.4) Molecules of the 14-3-3 Family and Cancer

The 14-3-3 proteins are abundant and highly conserved acidic polypeptides of 28-33 kDa, of which seven family members (β, γ, ε, σ, ζ, τ and η) are found in mammals (Aitken, 2006). The 14-3-3 proteins self-assemble into homo- and hetero-

dimers in order to interact with a diverse array of up to 200 cellular proteins, mostly via a phosphorylated serine/theronine motif. By binding to a diverse array of interacting/binding partners/proteins, 14-3-3 controls mitogenic signal transduction, cell cycle progression, metabolism, oncogenesis, and apoptosis (Porter et al., 2006). Increases in 14-3-3 expression have been associated with a multitude of human epithelial cancers. These include increased expression of 14-3-3ζ in lung cancer (Shoji et al., 1994; Qi et al., 2005), oral squamous cell carcinomas (Arora et al., 2005), stomach cancers (Jang et al., 2004), breast cancer (Zang et al., 2004) and in papillomavirus-induced carcinomas (Huber et al., 2004); increased 14-3-3β, γ and τ expression in lung cancer biopsies (Qi et al., 2005); and increased expression 14-3-3γ in chemotherapy-resistant melanomas (Sinha et al., 2000). The ability of 14-3-3 proteins to bind and regulate various oncogenic gene products as well as various tumor suppressor gene products points to a potential role in cancer (Tzivion et al., 2006), and pharmacological interference with 14-3-3 proteins has been suggested as a strategy to counteract cancer (Wurtele et al., 2003).

Deregulation of the balance between survival and apoptosis is a hallmark of cancer (Hanahan and Weinberg, 2000), and 14-3-3 proteins contribute to this process in multiple ways (Morrison, 2009). The binding of 14-3-3 has often been found to enhance the activity of proteins with proliferative or survival functions, such as Ras GTPase, which initiates the activation of the extracellular signal-regulated kinase (ERK) cascade (Tzivion et al., 2006). Another way that 14-3-3 influences the balance between survival and apoptotic signaling is by antagonizing the activity of proteins that promote cell death and senescence (Porter et al., 2006). 14-3-3 proteins can suppress apoptosis through interactions with core components of the mitochondrial apoptotic machinery, such as BCL-2 antagonist of cell death (Bad), BCL-2 interacting

mediator of cell death (BIM) and BCL-2 associated x protein (BAX), and through interactions with proteins that transmit apoptotic signals, including the stress-responsive kinase ASK1 (MEKK5) and the forkhead box O1 (FOXO) transcription factors. Kinases with pro-survival functions, such as PKB/Akt (protein kinase B), Rsk and PIM, are often responsible for generating the 14-3-3 docking sites on these molecules, and the binding of 14-3-3 frequently promotes the relocalization of these pro-apoptotic proteins away from their site of action. For example, the Bad-14-3-3 interaction causes Bad to be retained in the cytoplasm, thus preventing Bad from dimerizing with BCL-XL at the mitochondria and mediating the release of BAX from BCL-XL-mediated inhibition. (Shoji et al., 1994; She et al., 2005; Porter et al., 2006; Morrison, 2009) (Figure IV) In short, 14-3-3 plays pivotal roles in the control of apoptosis and survival signaling, indicating its substantial cancer therapeutic potentials.

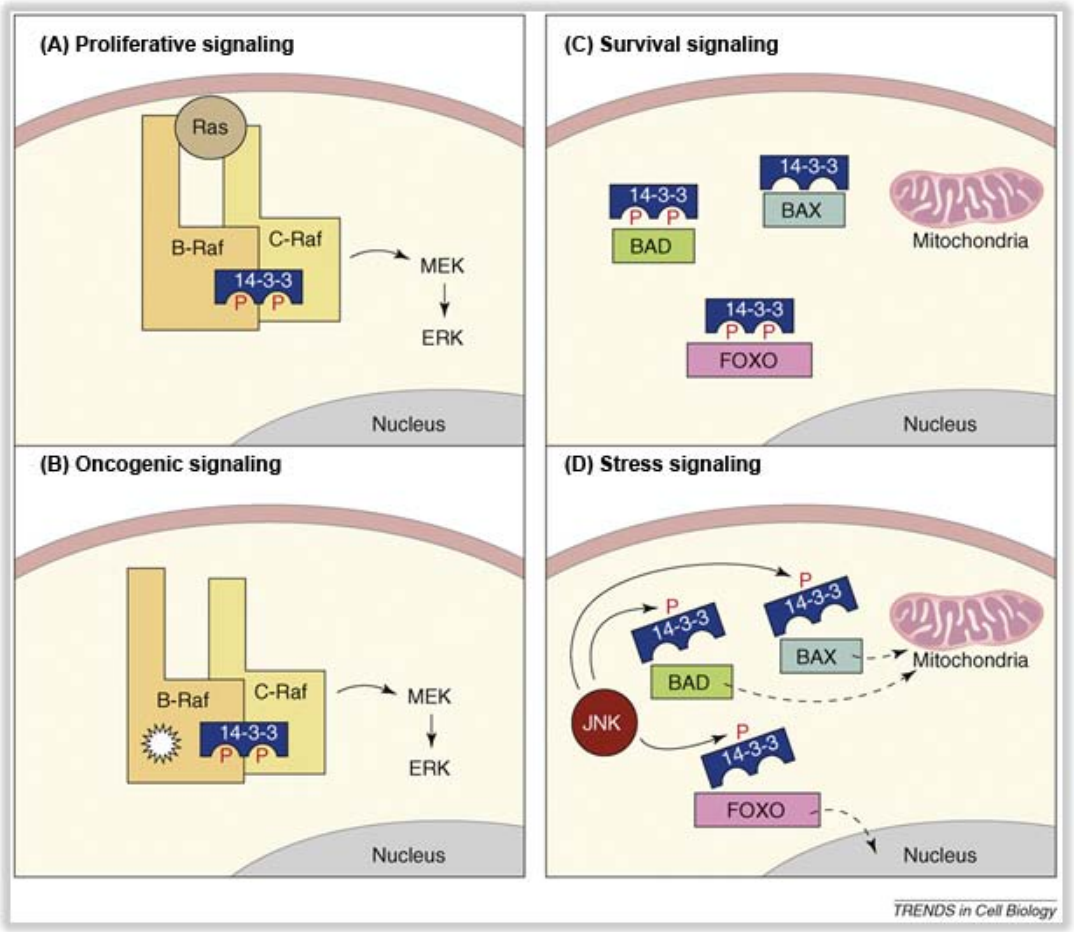

Figure IV. Functions of 14-3-3 in proliferative, oncogenic, survival and stress signaling.

(A) Under proliferative signaling conditions, 14-3-3 binding is required for the Ras-dependent heterodimerization of B-Raf and C-Raf and contributes to the full kinase activation of C-Raf.

(B) Under oncogenic B-Raf signaling conditions, 14-3-3 mediates the constitutive heterodimerization of B-Raf and C-Raf and is required for the transforming potential of kinase-impaired B-Raf mutants (indicated by starburst shape).

(C) Under survival signaling conditions, 14-3-3 binding inactivates numerous pro-apoptotic proteins, such as Bad, BAX and the FOXO transcription factors, by sequestering them from their sites of action such as the mitochondria and the nucleus.

(D) Under stress signaling conditions, activated JNK disrupts 14-3-3 binding to several pro-apoptotic proteins by directly phosphorylating the 14-3-3 proteins themselves, thus, enabling the apoptosis regulators to localize to their site of action (Morrison, 2008).

1.2) Integrins, ROS and Anoikis Resistance in Cancer

1.2.1) Integrins and Anoikis Resistance in Cancer

Cell to matrix adhesion is a key factor for the maintenance of cellular homeostasis, and the disruption of this interaction has adverse effects on cell survival. In most non-transformed cells, it leads to a specific type of apoptosis known as "anoikis"which is important for development and tissue homeostasis. By contrast, anoikis-resistance or anchorage-independent growth is a hallmark of transformed cells. It is suggested to have crucial roles during tumorigenesis, particularly during the metastatic spreading of cancer cells, because tumor cells must survive in different foreign microenvironments before they can colonize distant organs (Hanahan and Weinberg, 2000; Tsatsanis and Spandidos, 2004; Simpson et al., 2008). Although the signaling mechanisms involved in anoikis and anoikis resistance are still not completely understood, many of the signal transduction pathways activated upon detachment of the cell from the matrix are quite similar to those that occur during apoptosis. Protein kinase signaling pathways, such as those involving mitogen-activated protein kinase (MAPK) and focal adhesion kinase (FAK), are vital for the regulation of anoikis. Furthermore, the existence of anoikis implies that integrin signaling regulates critical components of the apoptotic machinery, because integrins are the major matrix receptors *in vivo* (Zhan et al., 2004).

Integrins are a family of transmembrane glycoproteins composed of 18 α and 8 β subunits, non-covalent combinations of which allow formation of an array of 24 integrin heterodimers (Guo and Giancotti, 2004). Integrins regulate cell viability through their interaction with the extracellular matrix and can sense mechanical forces arising from the matrix and convert these stimuli to chemical signals capable of

modulating intracellular signal transduction. Integrins expressed by tumor cells and host cells can contribute directly to the control and progress of metastatic dissemination (Felding-Habermann, 2003). During tumor development, changes in integrin expression, intracellular control of integrin functions and signals derived from integrin-ligand binding affect upon the ability of tumor cells to interact with their environment and enable metastatic cells to convert from a sessile, stationary phenotype to a migratory, invasive phenotype. Integrins are involved in each step of the metastatic cascade and affect tumor cell survival and interaction with changing environments while in transit from the primary tumor to distant target organs. For example, when activated by integrin ligation, FAK can suppress anoikis in favor of tumor cell survival by signaling through phosphotidylinositol 3-kinase (She et al., 2005) to PKB/Akt (Frisch et al., 1996; Khwaja et al., 1997). Furthermore, integrin signaling promotes the expression of the anti-apoptotic protein BCL-2 (Zhang et al., 1995) and suppresses the expression of the pro-apoptotic factor BIM (Reginato et al., 2003). However, unligated integrins can negatively influence the malignant properties of tumor cells (Giancotti and Ruoslahti, 1990; Varner et al., 1995; Stupack et al., 2001) by activation of apoptotic pathways inducing a form of death known as IMD (integrin-mediated death). The tumor cells can develop various mechanisms to escape IMD that contribute to their metastatic behavior (Stupack et al., 2006). Extracellular factors such as insulin-like growth factor (IGF)-1/2 or interleukin (IL)-3 (Lotem and Sachs, 1996; Butt et al., 1999), intracellular signals from mutant Ras or activated Src (Khwaja et al., 1997), and deletion of the tumor suppressor phosphatase and tensin homologue (PTEN) (Tamura et al., 1999) all contribute to anoikis resistance in cancer cells, presumably through activation of PI3K-PKB/Akt signaling.

1.2.2) ROS and Cancer

The cellular oxidation and reduction (redox) environment is influenced by the production and removal of reactive oxygen species (ROS; "redox signaling"). The major reactive oxygen species include oxygen radicals such as superoxide (O_2^-) and hydroxyl (·OH) as well as non-radical derivatives of molecular oxygen (O_2) such as hydrogen peroxide (H_2O_2). Whereas O_2^- and H_2O_2 do not exhibit strong reactivity with other bio-molecules, their reaction generates the highly reactive ·OH radical, which probably accounts for most of the oxidative damage attributed to ROS (Pervaiz and Clement, 2007). Although in mammalian cells intracellular ROS such as O_2^- and H_2O_2 are generally considered to be toxic byproducts of respiration through the mitochondrial electron-transport chain, recent evidence suggest that the production of these ROS might be an integral component of membrane receptor signaling. ROS can be "purposely" generated by stimulus-induced activation of membrane-bound enzyme systems, such as NADPH oxidase complexes (Noxes), xanthine oxidases, Lipoxygenases (Loxes) and Cycloxygenase (Coxes) (Pervaiz and Clement, 2007; Sarsour et al., 2009; Pani et al., 2010). Activation of these ROS generating intracellular systems results in one electron reduction of molecular oxygen to generate O_2^-, which is readily dismutated by the superoxide dismutases (SODs; cytosolic Zn/Cu SOD and mitochondrial Mn SOD) to produce H_2O_2. These two products of molecular oxygen can in turn react with each other to generate the highly damaging ·OH radical. Cellular ROS levels may function as "second messengers" that regulate numerous cellular processes including proliferation and apoptosis (Sarsour et al., 2009).

A delicately and tightly regulated cellular redox level is a necessity for normal physiological functioning such as wound healing and aging, and loss of cellular redox

control can lead to various disorders and diseases including diabetes, cardiovascular diseases, fibrosis, neurodegenerative diseases and cancer. Under physiological conditions, the deleterious potential of these reactive oxygen intermediates is counterbalanced by the cells' anti-oxidant defense arsenal, which comprised of the O_2^- scavenger enzyme SOD and the H_2O_2 scavengers catalase and glutathione peroxidase (GPX) (Pervaiz and Clement, 2002). The levels of these anti-oxidant enzymes vary from tissue to tissue (Oberley et al., 2000), and therefore the overall redox state of a cell is a product of its ROS-generating potential and its inherent ability to prevent toxic ROS build-up activation of the quenching mechanisms. A significant digression from this tightly controlled balance could lead to an abnormal accumulation of ROS and render the cell oxidatively stressed, which is usually associated with either disordered cell death (necrosis) or programmed cell death (apoptosis) (Chandra et al., 2000). There is also mounting evidence demonstrating that ROS act as second messengers in intracellular signaling cascades that induce and maintain the oncogenic phenotype of cancer cells (Liou and Storz, 2010).

ROS are tumorigenic by virtue of their ability to increase cell proliferation, survival, cellular migration, and to induce DNA damage leading to genetic lesions that initiate tumorigenicity and sustain subsequent tumor progression. Carcinoma cells produce ROS at elevated rates *in vitro* and *in vivo*, as well as many tumors appear persistent to oxidative stress (Storz, 2005). According to a "canonical" view, ROS contribute to carcinogenesis and the malignant progression of tumor cells: they drive genomic damage and genetic instability; they act as signaling intermediates transducing mitogenic and survival inputs by growth factor receptors and adhesion molecules; and they promote cell motility and shape the tumor microenvironment by inducing inflammation/repair and angiogenesis (Pani et al., 2010). However, it is also

known that ROS can induce cellular senescence and cell death and can therefore function as anti-tumorigenic agents (Storz, 2005). Therefore, the mechanisms by which cells respond to reactive oxygen species depends on the tissue and cell background, the location of ROS production and particularly the concentration of individual ROS species. In fact, in 2007, Pervaiz and Clement proposed that the tight control of the ratio between O_2^- and H_2O_2 is of crucial importance for the fate of a cancer cell. They believe that O_2^- predominance supports cell survival and promotes oncogenesis, whereas a shift in favor of H_2O_2 prevents carcinogenesis by facilitating cell death signaling (Figure V) (Pervaiz and Clement, 2007; Pervaiz et al., 2009).

Intracellular environmental factors (e.g. pH) are also tightly regulated by ROS in cancer cells. A decrease in intracellular O_2^- or an increase in H_2O_2 results in an acidic shift of the cytosolic pH (pHc), a phenomenon commonly observed during receptor or drug-induced apoptosis (Thangaraju et al., 1999; Clement et al., 2003). This acidification of the intracellular milieu could be a function of H_2O_2-mediated activation of PARP (poly (ADP-ribose) polymerase), leading to depletion of cellular NADH (nicotinamide adenine dinucleotide) and ATP (adenosine-5'-triphosphate) stores and culminating in the inhibition of critical ATP-driven pH regulators, such as the Na^+/H^+ transporter (NHE) (Hirpara et al., 2001). In contrast to acidification, which promotes caspase activation and death (Segal and Beem, 2001), an alkaline cytosolic milieu is invariably found in tumor cells (7.12–7.65 versus 6.99–7.20 in normal tissues); this effect has been attributed to the increase in the ability of tumor cells to secrete H^+ ions into the interstitial environment, an activity that increases with tumor aggressiveness (Gillies et al., 2002). The mechanism behind this reverse pH gradient (acidic extracellular milieu and alkaline pHc) involves oncogene-dependent activation/stimulation of NHE1 (Hagag et al., 1987). Whether this increase in pHc is a

cause or effect of the transformation process remains debatable. Interestingly, recent evidence appears to directly implicate NHE1 as a downstream target of intracellular ROS (Akram et al., 2006). Intriguingly, the redox regulation of NHE1 and its effect on cell survival and death appeared independent of its pump activity, thereby pointing to a novel survival mechanism in tumor cells that could be linked to increased expression but not necessarily increased pump activity of NHE1 (Akram et al., 2006). All of these ROS- and cancer-related observations present novel intracellular targets for the development and design of effective anti-cancer drugs.

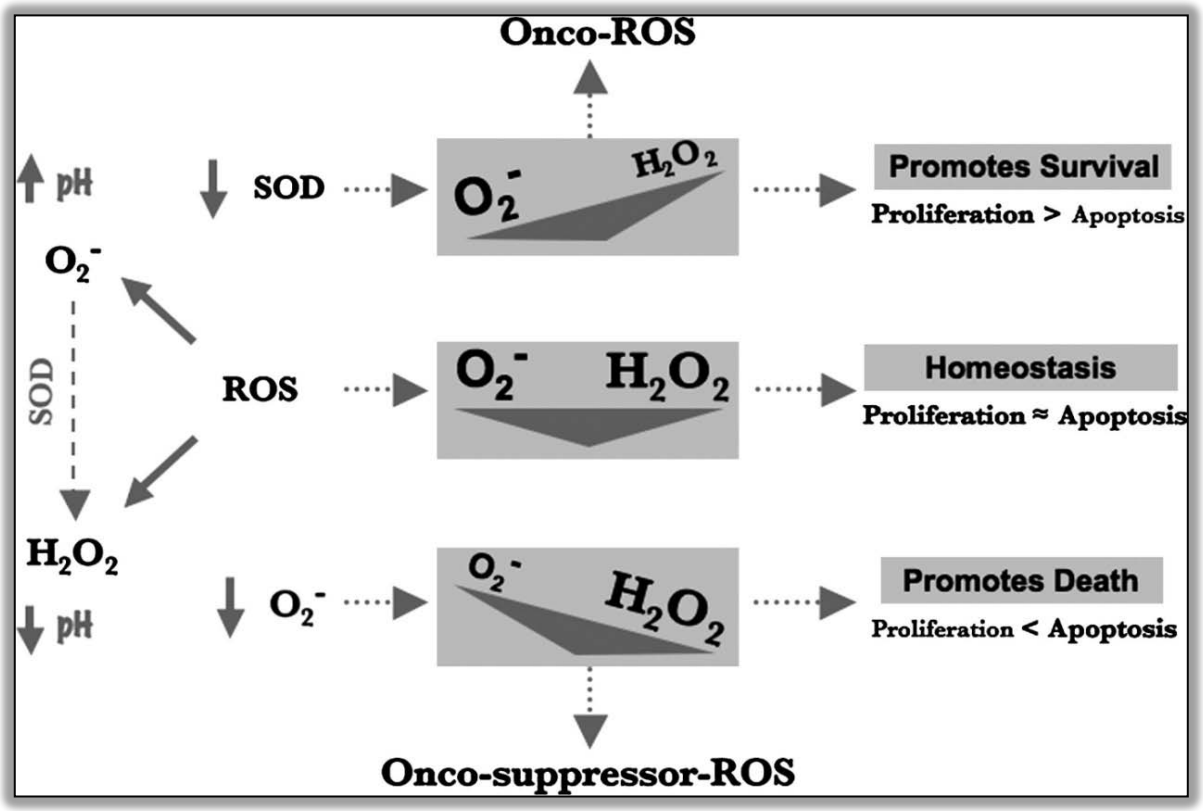

Figure V. The divergent signaling by O_2^- and H_2O_2.

Homeostatic growth is a function of a tight balance between intracellular O_2^- and H_2O_2. A tilt in favor of O_2^- promotes cell survival by an increase in intracellular pH and inhibition of cell death signaling. In contrast, an increase in H_2O_2, which could be due to higher SOD activity in the cells, results in a significant decrease in pH and creates an intracellular milieu conducive for apoptotic execution. In view of this, O_2^- serves as an oncogenic ROS, whereas H_2O_2 functions as a tumor-suppressor ROS (Pervaiz et al., 2009).

1.2.3) Integrin and ROS Signals in Cancer

Cell adhesion and migration is largely dependent on integrin binding to the extracellular matrix. Cell migration is intimately linked to degradation of the extracellular matrix, and activation matrix metalloproteinases (MMPs) and attachment-independent survival/anoikis resistance are two prerequisites for cancer cell invasion and metastasis (Chiarugi and Fiaschi, 2007; Svineng et al., 2008; Chiarugi, 2008). Also it has become increasingly clear that integrins convey several of the signals that result in increased ROS production upon ligand binding (Chiarugi and Fiaschi, 2007; Chiarugi and Buricchi, 2007). In addition, a large body of evidence supports the idea that the mitogenic signaling triggered by integrin and growth factor receptors (GFRs) acts through the production of a transient burst of ROS. Both growth factor (GF) and integrin stimulation leads to an increase in intracellular oxidants through the activation of the PI3K cascade, which in turn promotes Rac1 activation (Chiarugi et al., 2003; Chiarugi and Cirri, 2003; Rhee, 2006; Finkel, 2006). In response to GFR or integrin ligation, the small GTPase Rac1 translocates to the plasma membrane and induces production of ROS. ROS are mainly produced by NADPH-oxidases (Noxes), though 5-lipoxygenase (Lox) and mitochondria release of ROS are also reported to be involved (Werner and Werb, 2002; Chiarugi and Giannoni, 2005; Taddei et al., 2007). The GTPase Rac1 is activated by integrin engagement and is needed for activation of all three systems, although the exact mechanism for the involvement of Rac in the latter two systems is not known. Numerous studies have implicated the involvement of Nox complexes in integrin-mediated ROS production (Honore et al., 2003; Sangrar et al., 2007), but the exact mechanism of integrin induction of Nox-mediated ROS production is not fully understood. The Nox family of ROS-generating NADPH oxidases consists of the

following 7 members: Nox1-5, Duox1 and Duox2. Nox1-3 activities are Rac1-dependent, with Nox1 predominantly found in the colon, Nox2 in phagocytes and Nox3 in the inner ear (Krause, 2004). One plausible mechanism for integrin-Nox mediated ROS production is via the activation of Rac1, which is involved in regulation of Nox1, Nox2, and Nox3 complexes (Bedard and Krause, 2007).

The signaling properties of ROS are largely due to the reversible oxidation of redox-sensitive target proteins that contains low pKa cysteines (Rhee, 2006; Chiarugi and Fiaschi, 2007). Protein oxidation can be reversed by thiol donors such as glutathione, glutaredoxin, peroxiredoxins, and thioredoxin. Proteins vulnerable to oxidation include transcription factors, protein tyrosine kinases (PTKs), such as Src family kinases and some receptor tyrosine kinases (RTKs), protein tyrosine phosphatases (PTPs) and small GTPases (Chiarugi, 2005; Rhee, 2006).

1.2.4) ROS and Anoikis Resistance

During tumor progression, several cellular features undergo change, including proliferation capacity and the ability of cells to grow outside their confined milieu, leading them to metastasize, a major problem in cancer treatment. In untransformed cells, mitogenic pathways as such Ras/Rac/Rho GTPases, Src kinase and PI3K/PKB are regulated by integrin-mediated ECM contact. As a result, the growth of these cells is anchorage dependent. In contrast, constitutive activation of each of these routes has been described in cancer cells, with consequent reductions in their GF and ECM dependence (Figure VI) (Giancotti, 2000; Comoglio et al., 2003). Therefore, as introduced previously, the ability to grow independently of anchorage (i.e., anoikis

resistance) is an essential feature of cancer cells, yet how it is acquired is a central question in cancer biology.

Expression of certain oncogenes can grant protection from anoikis, mimicking integrin-dependent signals and allowing oncogene-expressing cells to survive under conditions in which normal cells undergo apoptosis (Giancotti, 2000). It is now accepted that ROS production is constitutively increased in several cancers, likely leading to constant activation of transcription factors as NF-κB and AP-1 and genotoxic oxidative stress (Woo et al., 2000; Chiarugi and Cirri, 2003; Finkel, 2006). Evidence indicates that ROS are further involved in tumor initiation, progression and maintenance. Ras mitogenic activity is superoxide-dependent, while a sustained ROS increase following overexpression of Nox1 leads to cell transformation and an aggressive tumor phenotype (Chiarugi and Giannoni, 2005). In addition, abnormal generation of ROS following activation of the c-Met proto-oncogene leads to cell transformation and malignant growth (Ferraro et al., 2006), while Rac-dependent redox signals increase secretion of metalloproteases and induce epithelial-mesenchimal transition (EMT) (Radisky et al., 2005), two key features of invasive cancers. Therefore, in cancer cells, sustained ROS generation may inhibit phosphatases or activate kinases, thereby shifting the balance towards tyrosine phosphorylation of intracellular proteins, and finally the assembly of the mitotic machinery (Chiarugi, 2005). In line with this idea, it has been reported that the ability of two Src oncogenes (v-Src and Y527FSrc) to sustain anchorage- and GF-independent growth depends on their redox regulation (Giannoni et al., 2005).

Ligand-independent RTK activation can lead to the constitutive generation of pro-survival cues in cancer cells by mimicking autocrine signals. Some authors have speculated that excess ROS production associated with cell transformation leads to the

release or deregulated costimulatory signals that are normally (and transiently) triggered by the cell/ECM interface, thus leading to persistent anchorage-related signals allowing for loss of growth dependence on ECM (Chiarugi, 2008). In this view, the kinase Src is widely recognized as the main factor in maintaining pro-survival signals in cancer cells that are resistant to anoikis. Indeed, Src activation is a required step for anoikis resistance in both osteosarcoma and lung adenocarcinoma cells (Wei et al., 2004; Diaz-Montero et al., 2006). In prostate carcinoma cells, resistance to apoptotic stimuli is achieved through a specific redox upregulation of Src activity. In particular, these anchorage-independent cells undergo a switch to constitutive Rac1-dependent oxidative stress, leading to association of the oxidized/activated Src with epidermal growth factor receptor (EGFR), phosphorylation of the receptor and sustained ECM-independent survival (Giannoni et al., 2009). Although specific studies on the role of PTP redox cues in allowing cell survival are lacking, it is likely that redox signaling can contribute to anoikis resistance in cancer cells through both Src activation and PTP inhibition.

Anchorage-independent growth results in several cellular changes including loss of contact inhibition, alterations in motility and adhesiveness, as well as in changes in cytoskeletal organization. Transformation of cells by various oncogenes leads to actin filament and focal adhesion disruption, and inhibition of actin polymerization, thus suggesting an essential role for actin dynamics in the oncogenic transformation and motility of cancer cells (Giancotti, 2000; Comoglio et al., 2003). Also, it is believed that amplified and sustained ROS production associated with cell transformation might result in actin oxidation/glutathionylation, thus disturbing cytoskeletal dynamics (Chiarugi, 2008). However, a full elucidation of the specific

targets of redox signaling in cancer cells is necessary for the understanding of the transformation/metastatic redox signature.

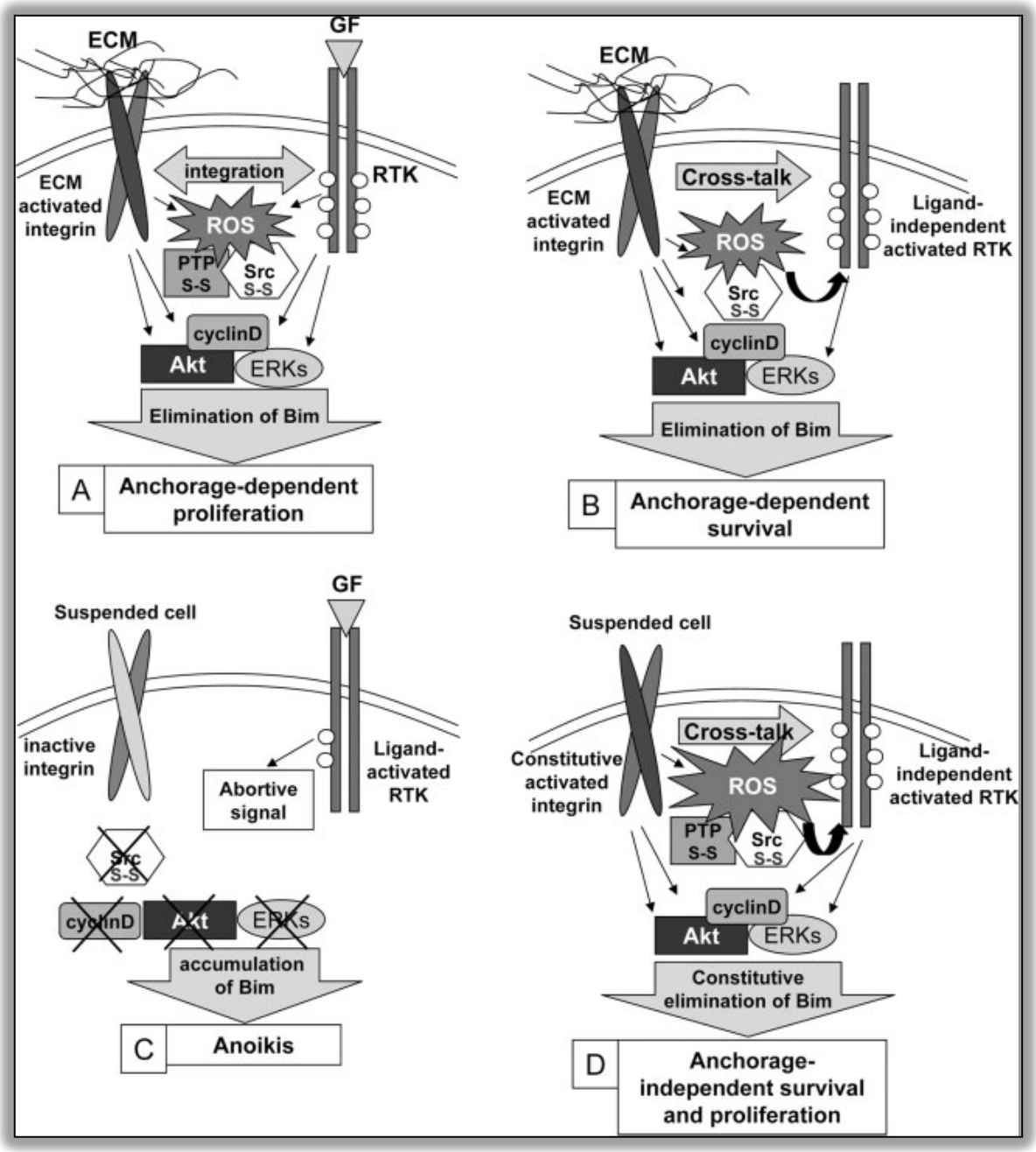

Figure VI. Redox signaling in anchorage-dependent cell growth and anchorage–indpendent cell survival and growth.

(A) Integrin and RTKs cooperate to sustain anchorage-dependent cell growth coordinating an integrated signal through redox-dependent and independent pathways leads to degradation of the pro-apoptotic protein Bim and allows proper execution of mitosis.

(B) ECM-adherent cells in absence of mitogenic stimuli undergo an integrin-dependent redox signalling, leading to Src-mediated ligand-independent RTK activation, sustaining a signal granting for survival but not for proliferation.

(C) Nontransformed cells lacking anchorage to ECM undergo anoikis due to the lack of integrin-mediated redox signalling acting on Src kinase. GFs produce abortive signal, not allowing either survival or proliferation and committing cell to anoikis.

(D) Cancer cells lack the dependence on ECM contact for redox signalling, thereby undergoing to a constitutive oxidative stress. This leads to sustain a constitutive ligand-independent RTK signal allowing for both survival and proliferation of anchorage-independent cells (Chiarugi, 2008).

1.2.5) Summary of the Molecular Programs in Anoikis Resistance of Cancer

Resistance to anoikis is a hallmark of metastatic cancer cells, especially because anchorage-independent growth is a distinct property of different types of human malignancies (Hanahan and Weinberg, 2000; Chiarugi and Giannoni, 2008; Simpson et al., 2008). The underlying mechanisms rendering tumor cells resistant to anoikis are not fully understood, but it has been postulated that they may be comprised of upregulated survival signals and inhibited of apoptotic pathways (Figure VII) (Chiarugi, 2008).

One strategy that allows early-stage tumor cells to circumvent anoikis is to acquire constitutive activity in the pathways responsible for cell survival, such as those transduced by PI3K, MEK/ERK and NF-kB, through either the constitutive activation of the pathways themselves or the loss of pathway inhibitors. In some cases, tumor cells acquire autocrine growth factor loops that activate these survival pathways. For example, in melanoma, one of the earliest alterations is the acquisition of an autocrine basic fibroblast growth factor (bFGF) signaling loop (Nesbit et al., 1999).

Another strategy used by cancer cells to avoid anoikis is to change the pattern of integrin expression, so that the cells perceived attachment to their favored ECM when in fact no such ECM is present. Only transformed melanocytes can survive in the altered environment of the dermis, this survival being due in part to the de novo expression of the correct integrins. For example, αVβ3 is important for adhesion of melanoma cells to dermal collagen and the suppression of anoikis (Montgomery et al., 1994), most likely by altering the Bcl2/Bax ratio (Petitclerc et al., 1999).

Emerging evidence suggests that ROS also play a fundamental role in conferring anoikis resistance to cancer cells. It is now largely accepted that cancer cells exhibit a higher amount of intracellular ROS with respect to their untransformed counterparts. The oxidative intracellular milieu is constantly observed to strongly correlate with resistance to anoikis. For example, high amounts of intracellular ROS accounts for the constitutive oxidation and activation of the Src kinase in metastatic prostate carcinoma cells, allowing constitutive Src-dependent and ligand-independent phosphorylation of EGFR and leading to the activation of pro-survival pathways (Giannoni et al., 2008).

The epithelial to mesenchymal transition (EMT) is an essential process that occurs during both physiologic and pathologic conditions (Savagner, 2001). Such a transition, which is necessary for proper embryonic development, also provides a convenient system for epithelium-derived tumors to become highly invasive and rapidly metastasize (Savagner, 2001; Thiery, 2002), following a mechanism resembling a reactivation of the embryonic program of EMT. In both embryonic and tumorigenic EMT, migrating cells change their relationship with the ECM and gain the ability to overcome anoikis, to grow and survive in inappropriate locations, ultimately colonizing distant organs. The activation of several mesenchymal genes in epithelial cells is critical for EMT and for the suppression of the apoptotic program. Molecules such as Snail, Twist, HGF/Met and NF-kB play a role in the acquisition of anoikis resistance during the process of EMT (Chiarugi, 2008).

Another key player that promotes anoikis resistance, thus ensuring tumor cell spreading during the metastatic process, is hypoxia (Sullivan and Graham, 2007). Intratumoral hypoxia is an indicator of poor patient prognosis and is associated with a malignant phenotype characterized by uncontrolled tumor growth, increased tumor

cell invasiveness and metastatic potential, angiogenesis, and the development of resistance to radiotherapy and chemotherapy (Brizel et al., 1996; Chiarugi and Giannoni, 2008). The mechanism by which hypoxia is able to induce escape from anoikis has not been yet fully clarified.

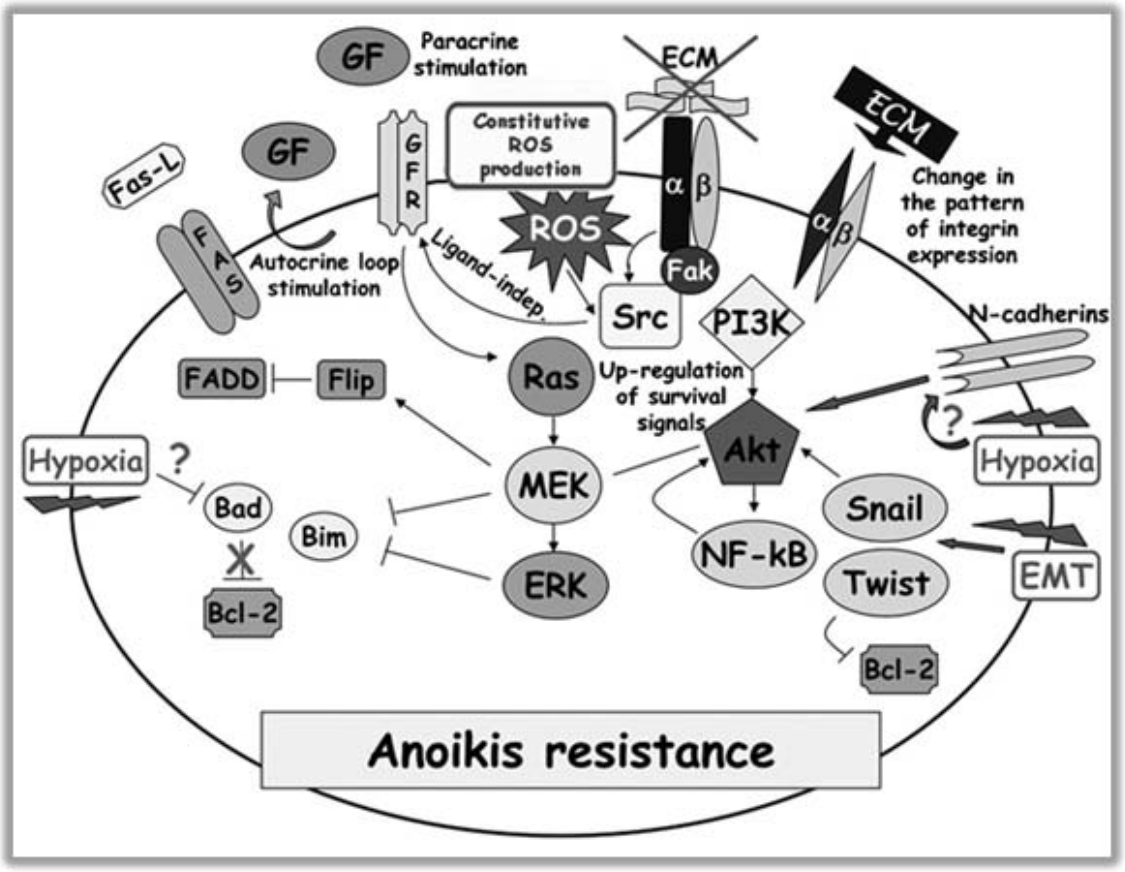

Figure VII. Signaling pathways conferring anoikis resistance to cancer cells.

Acquisition of anoikis resistance is achieved through the involvement of different strategies which converge on the stimulation of survival signals and/or on the inhibition of apoptotic pathways. Cells can circumvent anoikis by acquiring constitutive activity of survival pathways (i.e. PI3K/PKB, MEK/ERK and NF-kB) by means of an autocrine growth factor loops or by a paracrine stimulation of the neighbouring cells. Another strategy to avoid anoikis is to change the pattern of integrin expression, so that the correct environmental survival signals are received. ROS constitutively upregulated in cancer cells, are additional key player in conferring anoikis resistance by transducing pro-survival signals through a ligand-independent activation of GF. Hypoxia-mediated increase in ROS production may also concur to overcome anoikis, through a redox-mediated down-regulation of pro-apoptotic factors. EMT is another fundamental strategy to evade the anoikis barrier. The up-regulation of several transcription factors (Snail, Twist, NF-kB), by activating survival genes, such as the PI3K/PKB cascade, is critical for EMT success and for the overcoming of the apoptotic program (Chiarugi and Giannoni, 2008).

1.3) Angiopoietin-like 4 (ANGPTL4)

ANGPTL4, also known as hepatic fibrinogen/angiopoietin-related protein (HFARP), peroxisome proliferator-activated receptor-γ (PPARγ) angiopoietin-related gene (PGAR) and fasting-induced adipose factor (FIAF), was first described in mouse hepatocytes during a search for novel genes in hepatocytes during fasting, and in adipocytes during adipogenesis (Kersten et al., 2000; Yoon et al., 2000). As a glycosylated secretory protein with a predicted molecular weight of approximately 46 kDa, ANGPTL4 is characterized by the presence of a 25 amino acid-long signal peptide at its N-terminus. It also contains an N-terminal coiled-coil domain (nANGPTL4) and a C-terminal angiopoietin/fibrinogen-like domain (cANGPTL4). Based on its amino acid sequence similarity, the protein belongs to the family of angiopoietin-like proteins (ANGPTLs) but does not bind to the Tie1 or Tie2 receptor (Kim et al., 2000). The ANGTLl4 protein exists as an oligomer containing intermolecular disulfide bonds. Oligomerized ANGPTL4 undergoes proteolytic processing to release its carboxyl fibrinogen-like domain, which then circulates as a monomer. The N-terminal coiled-coil domain of ANGPTL4 mediates its oligomerization and is sufficient to form higher order oligomeric structures (Mandard et al., 2004; Ge et al., 2004). It has been reported that ANGPTL4, via its N-terminal coiled-coil domain, binds to lipoprotein lipase and converts the enzyme from a catalytically active dimers to an inactive monomers, (Sukonina et al., 2006) affecting lipid metabolism. These findings demonstrate a novel property of angiopoietin-like proteins and suggest that oligomerization and proteolytic processing of ANPTL4 may regulate its biological activities *in vivo* (Ge et al., 2004).

ANGPTL4, which is produced widely in the body, has been well documented as a vital endocrine signal involved in the regulation of lipid and glucose metabolism

(Kersten et al., 2000; Kersten, 2005; Xu et al., 2005). It was previously identified as a novel adipocytokine that is upregulated by nuclear hormone receptors PPARs (Kersten et al., 2000; Mandard et al., 2004) and by hypoxia (Belanger et al., 2002). ANGPTL4 protein expression can be detected in various tissues and in the blood plasma (Mandard et al., 2004; Mandard et al., 2006), suggesting that it has an endocrine function. Its plasma abundance is increased by fasting and decreased by chronic high fat feeding (Kersten et al., 2000; Lichtenstein et al., 2010). The expression of ANGPTL4 is stimulated by hypolipidemic fibrate drugs and insulin-sensitizing thiazolidinediones (Mandard et al., 2004). The expression of this gene is upregulated during fasting conditions in both hepatocytes and white adipose tissue, which are primary sites for triglyceride and lipid metabolism (Mandard et al., 2006; Koliwad et al., 2009; Legry et al., 2009). Recent findings based on genome-wide transcriptional profiling also show that ANGPTL4 transcription can be cooperatively activated by functional interaction between PPARβ/δ and transforming growth factor-β (TGFβ) pathways in human myofibroblasts (Kaddatz et al., 2010). To date, its expression has been noted in liver, adipose tissue, blood plasma, pancreas, kidney, intestine, brain, placenta and skin (Mandard et al., 2004; Kersten et al., 2000; Yoon et al., 2000), suggesting multiple functions for this protein.

1.3.1) ANGPTL4 – Roles in Energy Metabolism

The role of ANGPTL4 in lipid regulation has been thoroughly studied and is well defined. Overexpression of ANGPTL4 severely impairs the clearance of plasma triglycerides and stimulates adipose tissue lipolysis, resulting in the redirection of lipids from storage into circulation and the uptake of fatty acids and cholesterol into

tissues (Mandard et al., 2006; Lichtenstein, 2007). ANGPTL4 also regulates triglyceride metabolism and adiposity (Koster et al., 2005; Mandard et al., 2006). The hypertriglyceridemic effect of ANGPTL4 is attributable to inhibition of LPL-dependent VLDL lipolysis by conversion of LPL dimers to monomers. ANGPTL4 upregulation of cholesterol synthesis in the liver is secondary to inhibition of LPL- and HL-dependent hepatic cholesterol uptake (Lichtenstein et al., 2007). In studies using anti-ANGPTL4 antibody and ANGPTL4 knockout mice, ANGPTL4 has been shown to have lipid-lowering effects (Desai et al, 2007). Moreover, downregulation of ANGPTL4 in the intestine is essential for the increase in adipose mass induced by intestinal microbiota (Backhed et al., 2004). Stimulation of cardiac ANGPTL4 gene expression by dietary fatty acids via PPARβ/δ is part of a feedback mechanism aimed at protecting the heart against lipid overload and consequently fatty acid-induced oxidative stress (Georgiadi et al., 2010). ANGPTL4 also plays important roles in glucose metabolism. A group of scientists found that the serum levels of ANGPTL4 are lower in type 2 diabetes patients than in healthy individuals. Their studies demonstrated that ANGPTL4 decreases blood glucose and improves glucose tolerance in mice but induces hyperlipidemia and hepatic steatosis (Xu et al., 2005). These findings are in accordance with the notion that PPARγ, as the direct transcriptional regulator of ANGPTL4, also plays vital roles in glucose metabolism; PPARγ agonists are already in clinical use for the treatment of type 2 diabetes. Subsequently, the same group found that overexpression of ANGPTL4 in mice alters mitochondrial activities and modulates the amino acid metabolic cycle in liver tissue (Wang et al., 2007).

Recently, a Korean group demonstrated that hypothalamic ANGPTL4 is regulated by physiological appetite regulators and mediates their anorexigenic effects via inhibition of hypothalamic AMPK activity, suggesting that ANGPTL4 plays an

important role in the central regulation of energy metabolism (Kim et al., 2010). All these studies suggest that ANGPTL4 is a crucial physiological regulator of lipid and glucose metabolism that may provide potential therapeutic strategies for complex metabolic disorders (Oike et al., 2005).

1.3.2) ANGPTL4 - Roles in Angiogenesis and Cancer

In contrast to its well-studied roles in metabolism, the potential role of ANGPTL4 in the growth and development of cancer and metastasis (including angiogenesis) has just emerged and remains unclear and contradictory.

Growth and metastasis of solid tumors depend on angiogenesis i.e. the formation of new blood vessels that originate from the existing vascular system. Tumor-induced angiogenesis is mainly sustained by the production and secretion of angiogenic factors, e.g. the vascular endothelial growth factor (Gealekman et al., 2008) and angiopoietins, which originate from the tumor and stroma cells (Marme, 2001). Due to the significant similarity between ANGPTLs and angiopoietins, the potential involvement of ANGPTL4 in angiogenesis has been a subject of study. Early in 2000, Kim et al. found that recombinant ANGPTL4 protects endothelial cells from apoptosis and characterized it as a pro-angiogenic factor (Kim et al., 2000). Subsequently, recombinant ANGPTL4 was also found to significantly promote *in vitro* tube formation of porcine aortic endothelial cell and murine angiogenesis *in vivo* (Zhu et al., 2002). A year later, ANGPTL4 was again proposed as a pro-angiogenic factor produced during ischemia and in conventional renal cell carcinoma (Le et al., 2003). Interestingly but not surprisingly, a study conducted on arthritis also suggests a role for ANGPTL4 in angiogenesis (Hermann et al., 2005). A recent study,

although lacking in mechanistic explanation, has provided more details on the role of ANGPTL4 in angiogenesis by showing that TGFβ primes breast tumors for the seeding lung metastasis through ANGPTL4, which is induced by TGFβ via the SMAD signaling pathway in cancer cells that are about to enter the circulation. ANGPTL4 enhances the cancer cells' subsequent retention in the lungs, disrupts vascular endothelial cell-cell junctions, increases the permeability of the lung capillaries, and facilitates the trans-endothelial passage of tumor cells, thus promoting the vital steps of metastasis (Padua et al., 2008). ANGPTL4 was reported to be involved in the functional partitioning of postnatal intestinal lymphatic and blood vessels (Backhed et al., 2007). Despite the elusive role of PPARγ in tumors as aforementioned, a wealth of most recent studies has implied that PPARγ enhances angiogenesis in obesity and cancer via the induction of ANGPTL4 (Gealekman et al., 2008; Tian et al., 2009). However, ANGPTL4 was also been suggested as an anti-angiogenic factor by many researchers. Inhibition of angiogenesis and vascular permeability by ANGPTL4 was observed using corneal neovascularization and Miles permeability assays (Ito et al., 2003). It was also discovered that ECM-bound but not soluble ANGPTL4 inhibits endothelial cell adhesion, migration and sprouting (Cazes et al., 2006). This study also indicated that interaction with the ECM is heparin/heparan-sulfate-proteoglycan dependent and that the matrix-associated and soluble forms of ANGPTL4 (through its N-terminal coiled-coil domain) regulated the bioavailability (Cazes et al., 2006) of this glycan (Chomel et al., 2009). cANGPTL4 exists as a monomer whose function is still relatively unclear, but it has been implicated in the maintenance of vascular endothelial integrity (Yang et al., 2008). Because both pro- and anti-angiogenic effects of ANGPTL4 have been observed, a clear conclusion cannot be drawn.

In addition to angiogenesis, ANGPTL4 has also been implicated in other steps of cancer growth and metastasis. ANGPTL4 has been identified as one of the genes that most highly predict breast cancer to lung metastasis (Minn et al., 2005; Steeg, 2006). Further studies indicated that TGFβ increases cancer metastasis through ANGPTL4 which modulate endothelial integrity to mediate lung metastasis seeding (Padua et al., 2008). ANGPTL4 mRNA is expressed in the perinecrotic areas of various human tumors and is highly upregulated in epithelial tumor cells from clear-cell renal carcinoma (Le et al., 2003). A recent study has also demonstrated the high expression of ANGPTL4 in human gastric cancers. Moreover, this elevated expression of ANGPTL4, although not linked with overall patient survival, was proposed to promote venous invasion (Nakayama, 2010). Almost simultaneously, they proposed that ANGPTL4 may play an important role in metastasis through lymphovascular invasion, and may potentially affect prognosis (Shibata et al., 2010). In addition, a total of 13 genes, including ANGPTL4, were identified as a compact *in vivo* hypoxia signature that predicts a poor outcome in multiple tumor types (Hu et al., 2009; Murata et al., 2009). Similarly, Wang et al. found that combined expression of ANGPTL4 and tenascin C mRNA predicts prognosis of oral tongue squamous cell carcinoma (Wang et al., 2010). All these studies demonstrate that ANGPTL4 is an important participant in tumor promotion. However, other groups have proposed that ANGPTL4 is involved in the opposite side of cancer development; that it acts as an anti-tumor factor. In one study, ANGPTL4 was shown to inhibit growth of human liver carcinomas inoculated in nude mice (Li et al., 2004). ANGPTL4 was also reported to prevent metastasis through inhibition of angiogenesis, tumor cell motility and invasion (Cazes et al., 2006; Galaup et al., 2006). Interestingly, Klopper et al. showed that treatment with LGD1069, a retinoid X receptor-selective agonist and a

novel treatment for anaplastic thyroid cancer resulted in a significant, dose-dependent decrease in xenograft tumor growth accompanied by a significant increase (6.5-fold) in ANGPTL4 mRNA expression (Klopper et al., 2008). These events were positively correlated with decreased tumor vascularization and increased necrosis, suggesting that ANGPTL4 may be a potential mediator of the effects of retinoid treatment on anaplastic thyroid cancer. Thus, all these findings suggest that ANGPTL4 is potentially involved in cancer biology, but its exact role and the possible underlying mechanism are elusive and under debate; thus extensive further investigation is needed. Furthermore, a thorough and general study of the gene expression profile of ANGPTL4 in various tumors is required; these results may provide insight into the link between ANGPTL4 and cancer development.

1.3.3) ANGPTL4 - Roles in Wound Healing and Other Functions

The involvement of ANGPTL4 in keratinocyte migration during wound healing is a completely new, interesting area of study. As a secreted protein, ANGPTL4 in its various forms is likely to interact with specific membrane-bound receptors that initiate intracellular cascades leading to appropriate cellular responses, e.g. cell migration. Recent data demonstrate that ANGPTL4 is elevated after injury. ANGPTL4 produced by wound keratinocytes coordinates cell-matrix communication in several ways. First, ANGPTL4 specifically interacts with vitronectin and fibronectin in the wound bed and regulates the availability of local extracellular matrix. Second, ANGPTL4 specifically interacts with integrins β1 and β5 residing on the surface of the wound keratinocytes, which activate integrin-mediated intracellular

signaling, allow for selective integrin recycling, enhances cell migration, and accelerates the wound healing process (Goh et al., 2010a; Goh et al., 2010b).

In addition, recent studies demonstrated that the deletion of ANGPTL4 gene leads to enhanced oxidative stress in the heart, both after an acute oral fat load and after prolonged high fat feeding (Georgiadi et al., 2010). Furthermore, ANGPTL4 protects against the severe proinflammatory effects of saturated fat by inhibiting fatty acid uptake into mesenteric lymph node macrophages (Lichtenstein et al., 2010).

1.4) Rationale of the Present Study

In response to stresses such as hypoxia and inflammation in the tumor microenvironments, tumor cells exploit various signaling molecules to sustain and promote their growth, invasiveness and metastasis (Fidler, 1999; Singh et al., 2007). The constitutive activation of intracellular signaling by these molecules in tumor cells causes changes in cellular functions, including increased proliferation and the ability of cells to grow outside of their original confined milieu, which lead to metastasis (Pani et al., 2009; Westhoff and Fulda, 2009). Among these changes, the loss of dependence on integrin-mediated extracellular matrix contact for growth (i.e., anoikis resistance) is an essential feature of tumor cells. However, the mechanism by which anoikis resistance is acquired remains an unsolved problem in cancer biology. Extensive research during the past two decades has revealed the mechanism by which continued oxidative stress can lead to chronic inflammation, which could in turn mediate most chronic diseases including cancer (Reuter et al., 2010). Although low levels of ROS regulate cellular signaling and play an important role in normal cell proliferation, recent studies show that tumors exhibit an excessive or persistent

elevation of ROS (specifically the superoxide anion O_2^-) and utilize a redox-based mechanism to evade death by anoikis (Pervaiz and Clement, 2002; Pervaiz and Clement, 2007; Chiarugi, 2008; Giannoni et al., 2009). Previous studies have indicated that ROS are involved in tumor initiation, progression and maintenance. Furthermore, deregulated ROS production is also associated with an invasive tumor phenotype. Oncogenic and mitogenic Ras activity is superoxide-dependent, and a sustained increase in ROS following the overexpression of Nox1 leads to cell transformation and aggressive tumor metastasis (Suh et al., 1999; Komatsu et al., 2008). Elevated production of ROS following activation of the c-Met proto-oncogene leads to cell transformation and malignant growth (Ferraro et al., 2006), and Rac-dependent redox signals increase the secretion of metalloproteases and induce the epithelial-mesenchymal transition (Wu, 2006), both of which are key features of invasive cancers. Thus, a clear understanding of the underlying redox-based anoikis escape mechanism and its connection to malignancy will provide new insights into therapeutic interventions.

In this regard, the secreted adipocytokine protein angiopoietin-like 4 (ANGPTL4) was recently linked to tumor progression. ANGPTL4 was previously identified as a novel paracrine and possibly endocrine regulator of lipid metabolism (Oike et al., 2005); it is also a target of PPARs (Kersten et al., 2000) and hypoxic signaling (Kersten et al., 2000; Belanger et al., 2002). Emerging studies implicate tumor-derived ANGPTL4 in cancer metastasis via its effect on endothelial integrity. However, whether ANGPTL4 promotes or inhibits vascular permeability and thus metastasis remains controversial. Intense research has revealed tumor-promoting roles for hypoxia, inflammation and the wound microenvironment in the development and progression of cancer (Dvorak et al., 1986; Balkwill and Mantovani, 2001; Coussens

and Werb, 2002; Gonda et al., 2009; Kalluri, 2009; Finger and Giaccia, 2010; Chiodoni et al., 2010). Observations to date suggest that oxidative stress-associated ROS, chronic inflammation, and cancer are closely linked. Oxidative stress can activate a variety of transcription factors including NF-κB, AP-1, p53, HIF-1α, PPAR-γ, β-catenin/Wnt, and Nrf2. Activation of these transcription factors can lead to the expression of over 500 different genes, including genes for growth factors, inflammatory cytokines, chemokines, cell cycle regulatory molecules, and anti-inflammatory molecules (Reuter et al., 2010). Current results from our lab implicate the adipocytokine ANGPTL4 as a novel modulator of wound healing and cell migration (Goh et al., 2010a; Goh et al., 2010b), and thus potentially involved in cancer metastasis. Recent reports demonstrate that ANGPTL4 gene expression is one of the best predictor of breast cancer metastasis to the lung (Minn et al., 2005; Padua et al., 2008). The expression of ANGPTL4 is highly upregulated in clear cell renal-cell carcinoma (Le et al., 2003; Verine et al., 2010) and oral tongue squamous cell carcinoma (Wang et al., 2010). In addition, tumor-derived ANGPTL4 has been shown to promote metastasis by disrupting vascular integrity (Padua et al., 2008). The reason for these apparently conflicting results and the underlying mechanism of ANGPTL4 activity in tumor cells have not been clarified, hampering our understanding of its precise role in cancer metastasis. More importantly, the global expression pattern of ANGPTL4 in different types of tumors has yet to be fully investigated, and the pathological relevance of ANGPTL4 in cancer biology remains largely undefined.

In the present report, we examined the expression pattern of ANGPTL4 in various types of human tumor cells and found that an elevated level of ANGPTL4 is a common feature of many tumor types. Next, we found that suppression of ANGPTL4, by the use of either RNAi or a monoclonal antibody significantly impaired the growth

of tumor cells *in vivo* and their resistance to anoikis *in vitro*. Further study regarding the underlying mechanism of ANGPTL4 activity led us to propose that tumor cells express ANGPTL4 to modulate intracellular O_2^- levels, conferring anoikis resistance to tumor cells and promoting tumorigenesis. Therefore, ANGPTL4 is a potential therapeutic target in cancer treatment.

2. MATERIALS AND METHODS

2.1 Antibodies and Reagents

Antibodies and reagents used in this study: cyclinD1, integrins β1 and β5 (Chemicon); caspase-3, cleaved caspase-3 (R&D systems); PCNA, β-tubulin, 14-3-3β, 14-3-3σ, Zn/Cu SOD, ERK1, p(T202/Y204)ERK1/2, Nox1, Nox2, secondary HRP-conjugated antibodies (Santa Cruz Biotechnology); c-Src, p(Y416)Src, FAK, p(Y397)FAK, PKBα, p(S473)PKBα, p(T308) PKBα (Cell Signaling Technology); pan-14-3-3 and Bad (Abcam); Na^+/H^+ exchanger 1 (NHE), Bax and cleaved PARP (Millipore); GTP-Rac1 and total Rac1 (Upstate Biotechnology); Ki67 (NovaCastra); secondary Alexa488-conjugated antibodies, 2-methyl-6-(4-methoxyphenyl)-3, 7-dihydroimidazo[1, 2-a]pyrazin-3-one, hydrochloride (MCLA) and Amplex® Red Hydrogen Peroxide/Peroxidase Assay Kit (Invitrogen). pFIV lentivirus-based siRNA vector and packaging kit and Interferon Response Detection kit were from System Biosciences. Acetyl ester was from Molecular Probes. Transfection reagent ExGen 500 and restriction enzymes were from Fermentas. Unless specified, all other reagents were obtained from Sigma.

2.2 Human Tumor Samples

Human basal cell carcinoma biopsies (BCCs) and squamous cell carcinoma biopsies (SCCs) along with their paired peri-tumor normal samples (PNSs) were provided by Dr. Pan, Dr. Tan (National Skin Centre, Singapore) and purchased from Asterand plc, USA. BCC, SCC and PNS samples, inclusive of epithelia and stroma, were subjected to protein and RNA extraction for immunoblotting and qPCR analyses, respectively.

Commercial tumor tissue arrays #MTU951 and #MET961 (Pantomics, Inc., USA) were utilized to study the expression profile of ANGPTL4 in a large human tumor set by immunofluorescence imaging. The #MTU951 human tumor tissue array contains 40 tumor types, covering most of the common benign, malignant and metastatic tumors originating from 27 anatomic sites, and the #MET961 human cancer metastasis tissue array consists of 48 cases of metastatic cancers from >8 anatomic sites. The two tissue arrays were probed with the anti-cANGPTL4 polyclonal antibody followed by Alexa488 goat-anti-rabbit IgG. Images were taken using MIRAX MIDI with Plan-Apochromatic 20x/0.8 objective (with equal exposure and gain), and each image was automatically stitched using MIRAX Scan software (Carl Zeiss). The 3D heatmaps were generated using IMARIS software (Bitplane Scientific Software). In the heatmaps, the X- and Y- axes represent the length and width, whereas the Z axis represents the IF intensity. The gray value (IF intensity) was obtained from three biopsies using TissueQuest software (TissueGnostic GmbH).

2.3 Laser Capture Microdissection (LCM)

For LCM samples, epithelial and stromal fractions were microdissected from 8-µm-thick sectioned tissues using a PALM Microbeam Axio Observer Z1 (Carl Zeiss). LCM tissues were collected into microfuge tubes with opaque AdhesiveCaps (Carl Zeiss). RNA was extracted using Optimum™ FFPE RNA Isolation kit (Ambion) pooled from eight LCM tissues. Five ng of RNA was amplified using a Full Spectrum Complete Transcriptome RNA Amplification kit (System Biosciences) prior to qPCR as previously described (Chong et al., 2009; Goh et al., 2010a).

2.4 Cell Culture

HaCaT is an immortalized but non-tumorigenic human keratinocyte line. II-4 and A-5RT3 are tumorigenic HaCaT derivatives kindly provided by the German Cancer Research Center (DKFZ, Germany). HSC is a human squamous cell carcinoma line provided by Prof. Aso (Yamagata University School of Medicine, Japan), and MDA-MB-231 (breast adenocarcinoma) by Assoc Prof. Ling (Nanyang Technological University). Other lines used were murine melanoma B16F10 and human tumor lines used were Alexander (malignant hepatoma), A549 (lung carcinoma), Hela (cervix adenocarcinoma), huH-1 (hepatoma), Kato III (stomach signet ring cell carcinoma), MCF7 (breast adenocarcinoma) and T24 (bladder carcinoma). All cells were maintained in Dulbecco's modified Eagle's medium (DMEM; Hyclone, USA) supplemented with 10% heat-inactivated fetal bovine serum (FBS, Hyclone), except for A549, huH-1, Kato III which were maintained in RPMI-1640 (Hyclone) with 10% FBS. Cells were cultured at 37 ºC, 5% CO_2 and 75% humidified incubator.

2.5 Immunoblot Analysis

Total protein was extracted from cells or tumor tissues/cells with ice-cold lysis buffer (20 mM $Na_2H_2PO_4$, 250 mM NaCl, 1% Triton-100, 0.1% SDS). Equal amount of protein extracts were resolved by SDS-PAGE and electrotransferred onto PVDF membranes. Membranes were processed according to standard procedure and proteins were detected by chemiluminesence (Millipore, USA). β-tubulin was used as loading and transfer control.

2.6 Total RNA Isolation and Quantitative Real-time PCR (qPCR)

Total RNA was extracted and qPCR was performed. Expression was related to the housekeeping gene 60S ribosomal protein *L27* (*L27*) which did not change under any of the experimental conditions studied. The sequence of primers is available in the Table 1. For focused mRNA array, genes whose expression was changed significantly (> 2-fold) were listed and heatmaps were generated using Orange Canvas 1.0 software.

Table 1. Sequences of Quantitative Real-time PCR (qPCR) Primers.

GenBank Accession	Official Symbol	Sense Primers (5' → 3')	Antisense Primers (5' → 3')
NM_004324	*BAX*	GGGTGGTTGGGTGAGACTC	AGACACGTAAGGAAAACGCATTA
NM_014417	*BBC3*	GACCTCAACGCACAGTACGAG	AGGAGTCCCATGATGAGATTGT
NM_138578	*BCL2L1*	TGCGTGGAAAGCGTAGACAAG	GCTGCTGCATTGTTCCCATA
NM_004050	*BCL2L2*	GCGGAGTTCACAGCTCTATAC	AAAAGGCCCCTACAGTTACCA
NM_001196	*BID*	GACAGCATGGACCGTAGCATC	AGGTGCGTAGGTTCTGGTTAATA
NM_001166	*BIRC2*	GTTTCAGGTCTGTCACTGGAAG	TGGCATACTACCAGATGACCA
NM_182962	*BIRC3*	TCCTGGATAGTCTACTAACTGCC	GCTTCTTGCAGAGAGTTTCTGAA
NM_033292	*CASP1*	TCCAATAATGGACAAGTCAAGCC	GCTGTACCCCAGATTTTGTAGCA
NM_001230	*CASP10*	ATTGGTCCCAAGACATGAAGAC	TGTTCCCTGTTTGTCCACTCT
NM_032982	*CASP2*	AAACGAGGTTCCTGGTACATCG	TCCTTGATAAGTGCGTTCACC
NM_033340	*CASP7*	AGTGACAGGTATGGGCGTTC	GAGGTTGCAGTCTTCCGAGAT
NM_001237	*CCNA2*	GATGGTAGTTTTGAGTCACCACA	CACGAGGATAGCTCTCATACTGT
NM_053056	*CCND1*	GCTGGAGCCCGTGAAAAAGA	CTCCGCCTCTGGCATTTTG
NM_000075	*CDK4*	CAGATGGCACTTACACCCGTG	GCAGCCCAATCAGGTCAAAGA
NM_004935	*CDK5*	GCCGCAATGTGCTACACAG	GAGTAACAGCGGACGGGAATC
NM_000389	*CDKN1A*	GTCACTGTCTTGTACCCTTGTG	CGGCGTTTGGAGTGGTAGAAA
NM_000076	*CDKN1C*	ACATCCACGATGGAGCGTC	GGAAGTCGTAATCCCAGCGG
NM_001278	*CHUK*	CAGCCATTTACCTGGCATGAG	GAGGGTCCCAATTCAACATCAA
NM_001303	*COX10*	CCAGCAAGTAAGACCCAAGCC	TCATCTCTTTCCACCGCTTTTC
NM_019887	*DIABLO*	GGTACAGACAGTGTTTGTGTGT	CTACTAAGGGAATGAGGCTCTGA
NM_000043	*FAS*	TATCACCACTATTGCTGGAGTCA	ACGAAGCAGTTGAACTTTCTGTT
NM_002417	*KI67*	TGTTCCCACTACACAATGTCTTG	ACTTACGCGAGACCAACAGTT
NM_021960	*MCL1*	GTGCCTTTGTGGCTAAACACT	AGTCCCGTTTTGTCCTTACGA
NM_001618	*PARP1*	GATGCCTATTACTGCACTGGG	CGGTCCTGCTTTTTAACCTTCAA
NM_022121	*PERP*	CAACCCTGCTGTCACTTACAT	AGGTCATCTTCGTAGTTGGGG
NM_182649	*PCNA*	ACACTAAGGGCCGAAGATAACG	CGGCATATACGTGCAAATTCAC
NM_002859	*PXN*	GCGGACTTGGAGTCTACCAC	TCCAGTTGGGTATGAGTAGGG
NM_001167	*XIA[*	GACAGGCCATCTGAGACACAT	GGGGTTAGGTGAGCATAGTCTG
NM_000687	*AHCY*	GCATCCGAGGCATCTCTGAG	GCCATAGAGGTTGTCAAACTTGC
NM_001713	*BHMT*	GACACCTTCATACCTTAGCTGC	ACAGGTTTACCGGATGCTATCAA
NM_012260	*HACL1*	CCTTCTTATCATCGGGAAAGGTG	CCCATAGGGGTGGGCAAAAAT
NM_000221	*KHK*	GCTATTCTGTGGACCTACGCT	AGTATAGGATGGTGCGGCTAC
NM_000429	*MATLA*	CATCAAGCACATCGGCTACGA	CCGAACATCAAACCCTGATCTC
NM_000274	*OAT*	TGCTGTCAACCAAGGGCATT	GCCTCCACTCCTGTATTCATAGG
NM_000988	*L27*	TGATGGCACCTCAGATCGC	AGAGTACCTTGTGGGCATTAGG

Note: Melt curve analysis was included to assure that only one PCR product was formed.

2.7 Suppression by RNA Interference (RNAi)

Small interfering RNAs (siRNAs) against human ANGPTL4, mouse ANGPTL4, Nox1, Nox2 and a scrambled sequence as control (control siRNA) were subcloned into the pFIV-H1/U6-puro pFIV/siRNA lentivirus system. The correct pFIV siRNA constructs were verified by sequencing using H1 primer. The sequences are shown in Table 2. Pseudovirus purification and transduction were performed as described (Chong et al., 2009). Briefly, transduction-ready pseudoviral particles (System Biosciences) were produced and harvested as described by the manufacturer. Transduced cells were enriched by puromycin (600-800 ng/ml) selection for 1 wk. The knockdown sub-cell lines were designated A-5RT3$_{ANGPTL4}$, B16F10$_{ANGPTL4}$, A-5RT3$_{Nox1}$, A-5RT3$_{Nox2}$, A-5RT3$_{ANGPTL4}$ Nox1 kd (double gene knockdown of ANGPTL4 and Nox1 in A-5RT3 cells) and A-5RT3$_{ANGPTL4}$ Nox2 kd (double gene knockdown of ANGPTL4 and Nox2 in A-5RT3 cells), and the non-targeted scrambled siRNA transduced lines were denoted as A-5RT3$_{CTRL}$ and B16F10$_{CTRL}$. The expression of endogenous ANGPTL4 in MDA-MB-231 cells was also suppressed using tetracycline-inducible pSingle-tTS-shRNA vector (Clontech). ANGPTL4 set 2 shRNA sequences were used (Table 2). Immunoblot and qPCR experimentations were used to assess the efficiencies of knockdown.

Table 2. Sequences of *ANGPTL4, NOX1, NOX2* and control siRNAs.

siRNA	Sense Primer (5' → 3')	Antisense Primer (5' → 3')
ANGPTL4* set 1	AAAGCTGCAAGATGACCTCAGATGGAGGCTG	AAAACAGCCTCCATCTGAGGTCATCTTGCAG
***ANGPTL4* set 2#**	TCGAGGCAGCACCTGCGAATTCAGCATCTGC ATTCAAGAGATGCAGATGCTGAATTCGCAGG TGCTGCTTTTTTACGCGTA	AGCTTACGCGTAAAAAGCAGCACCTGCGAAT TCAGCATCTGCATCTCTTGAATGCAGATGCT GAATTCGCAGGTGCTGCC
***ANGPTL4* set 3**	AAAGCAGCAGGATCCAGCAACTCTTCCACAA	AAAATTGTGGAAGAGTTGCTGGATCCTGCTG
***ANGPTL4* set 4**	AAAGGCTTAAGAAGGGAATCTTCTGGAAGAC	AAAAGTCTTCCAGAAGATTCCCTTCTTAAGC
NOX1	AAAGGGCCACAGATGGCTCCCTTGCCTCCAT	AAAAATGGAGGCAAGGGAGCCATCTGTGGC
NOX2	AAAGGGCCAGATGTTCTTTCTACAGAAGAAT	AAAAATTCTTCTGTAGAAAGAACATCTGGCC
Mouse *ANGPTL4*	AAAGCTGTGAGATGACTTCAGATGGAGGCTG	AAAACAGCCTCCATCTGAAGTCATCTCACAG
Control siRNA	AAAGCTGTCTTCAAGCTTGATATCGAAGACT	AAAATAGTCTTCGATATCAAGCTTGAAGACA

**ANGPTL4* Set 1 siRNA were used for lentivirus-mediated RNA interference due to its highest knockdown efficiency on A-5RT3 and B16F10 in this study.

 # ANGPTL4 set 2 shRNA was cloned into pSingle-tTS-shRNA vector (Clontech) and used for doxycycline-inducible knockdown in MDA-MB-231 cells.

2.8 In Vivo Tumorigenicity Assay

BALB/c athymic nude female mice (20-22 g), aged 5-6 weeks, and WT C57BL/6J female mice (20-25 g), aged 6-8 weeks, were purchased from A*STAR Biological Resources Centre, Singapore.WT C57BL/6J female ANGPTL4 and ANGPTL4-knockout (KO) mice were used (Koster et al., 2005). All animals were maintained in pathogen-free conditions. The animal studies were approved by the Institutional Animal Care and Use Committee (IACUC0092), Nanyang Technological University, and all experiments were carried out in strict compliance with their regulations.

For nude mice experiments, 5×10^5 cells (A-5RT3$_{CTRL}$ or A-5RT3$_{ANGPTL4}$) were injected subcutaneously (*s.c.*) into the interscapular region of each nude mouse (n = 5 for each group). The injection site was rotated to avoid site bias. The injected tumor cells were allowed to grow for 8 weeks. The subcutaneous xenograft tumors were externally measured with a Vernier caliper every other day, and tumor volume was estimated using the equation, $V = (L \times W^2)/2$, where L is the length of the major axis of the tumor, and W is the length of the minor axis. Mice were sacrificed at the end of the experiment (week 8), and their tumors were harvested for further analyses. To test the effect of the number of injected cells on tumorigenicity, nude mice were inoculated with 0.5 ×, 2 × and 8 $\times10^6$ A-5RT3$_{CTRL}$ or A-5RT3$_{ANGPTL4}$ cells as above. Experiments were terminated at week 4 accordingly to IACUC protocol, because tumor volume in the 8 × 10^6 inoculation group approached 3000 mm^3. For the antibody treatment, nude mice (n = 6 for each group) were implanted with A-5RT3 as described above. One week post implantation, 30 mg/kg/week of either mAb11F6C4 or isotype control IgG were intravenously (*i.v.*) administered once weekly for 4 weeks. The dose of antibody and delivery mode was consistent with studies using

mAb14D12, another anti-ANGPTL4 monoclonal antibody (Desai et al., 2007). Mice were sacrificed after treatments, and tumors were harvested for further analyses.

KO mice and cANGPTL-treated C57BL/6J mice studies were performed as previously described (Sun and Lodish, 2010). Briefly, 1×10^6 $B16F10_{CTRL}$ (scrambled control cells) or $B16F10_{ANGPTL4}$ (ANGPTL4 knockdown cells) were *s.c.* injected into the interscapular region of the indicated mice (n = 4-6 in each group). Mice were *i.v.* treated with either 3mg/kg of cANGPTL4 or control PBS three times a week. All of the animals were monitored, and tumor volume was measured as above. Mice were sacrificed at the end of the experiment (day 15), and tumors were harvested for imaging.

2.9 Generation of cANGPTL4 and Antibodies

Recombinant ANGPTL4 proteins were purified from the conditioned medium of stable cANGPTL4-expressing S2 cells by preparative isoelectric membrane electrophoresis as previously described (Goh et al., 2010a). Rabbit polyclonal antibodies against the C-terminal region and N-terminal region of human ANGPTL4 were produced in-house as previously described (Goh et al., 2010a). Monoclonal antibodies (mAbs) against human cANGPTL4 (a.a. 186-406) were made according to standard protocols (Ward et al., 1999). Briefly, mice were immunized with adjuvant conjugated-cAngptl4. The spleen of the mouse was then removed, and a single cell suspension was prepared. These cells were fused with myeloma cells and cultured in hybridoma selection medium (HAT; Gibco). The fused cells were cultured in microtiter plates with peritoneal macrophages for 48 h post-fusion ($2\text{-}4 \times 10^6$ cells/ml). The cultures were maintained in a 5% CO_2 humidified incubator for 7-21 days, and routinely fed with HAT medium. mAbs in medium were first screened using ELISA to identify positive

clones. Positive clones were expanded and recloned by a limiting dilution technique to ensure monoclonality. Next, SPR was performed to determine the binding kinetics of mAbs. Global fitting of the data to a Langmuir 1:1 model was used to determine the association (k_{on}), dissociation (k_{off}) and affinity constant (K_D) using Scrubber2 (BioLogic Software Pte Ltd). mAb 11F6C4 was chosen for immunotherapy and other experiments based on its superior k_{on}, k_{off} and K_D values as well as its ability to block interaction between cANGPTL4 and integrins.

2.10 Surface Plasmon Resonance (SPR) Analysis

The purified fibrinogen-like fragment of ANGPTL4 (cANGPTL4) was immobilized onto ProteOn GLC chip by amine coupling, as recommended by the manufacturer (Bio-Rad). Different concentrations of integrins were introduced into the GLC chip at a flow rate of 25 µl/min for 5 min with running buffer (50 mM Tris, pH 8.0 and 100 mM NaCl). Polyclonal anti-cANGPTL4 antibodies against the immobilized cANGPTL4 determined the R_{max} value to be 423.1 resonance unit (RU). Global fitting of the data to a Langmuir 1:1 model was used to determine the association (k_{on}), dissociation (k_{off}) and affinity constants (K_D) using Scrubber2 (BioLogic Software Pte Ltd). The experimental R_{max} values of integrins β1 and β5 for cANGPTL4 were determined to be 365.6 and 341.9 RU, respectively. The affinity constants of the 6 mAbs for ANGPTL4 were determined using the One-Shot Kinetics protocol as described by manufacturer (Bio-Rad).

2.11 In Situ Proximity Ligation Assay (PLA)

DUOLink™ *in situ* PLA (OLink Biosciences) was performed on tumor biopsies or cells as described (Tan et al., 2009). The paired-primary antibodies used in the present study were rabbit anti-p(Y397)FAK and mouse anti-FAK antibodies, rabbit anti-pan-14-3-3 and mouse anti-Bad antibodies, and mouse anti-cANGPTL4 with either rabbit anti-β1, β3 or β5 integrin antibodies. As a negative control, PLA was performed using only anti-FAK, anti-pan-14-3-3 or anti-nANGPTL4 antibodies, respectively. Briefly, sections/cells were fixed with 4% paraformaldehyde for 15 min. The slides were washed twice with PBS, blocked for 1 h at room temperature with 2% BSA in PBS containing 0.1% Triton-X, followed by incubation with the indicated antibody pairs overnight at 4 ^{o}C. PLA was performed as recommended by the manufacturer (OLink Biosciences). Images were taken using an LSM710 META confocal laser scanning microscope with a Plan-Apochromat 63x/1.40 Oil objective and ZEN 2008 software (Carl Zeiss).

2.12 Rho GTPases Assay

Active GTP-bound Rac1 was quantified as previously described (Tan et al., 2009) with minor modifications. Briefly, 500 μg of the indicated tumor biopsies lysates were incubated with 2 μg of configuration-specific monoclonal anti-Rac1-GTP antibody (GTP-Rac1; NewEast Biosciences). GTP-Rac1-bounded antibodies were immunoprecipitated with Sepharose Protein G/A beads. Bound proteins were solubilised in Laemmli's buffer, resolved by SDS-PAGE, and immunoblotted using polyclonal antibody against Rac1. Total Rac1 was detected using total lysate. Anti-Rac1 antibodies for immunblot were from Cytoskeleton Inc.

2.13 Membrane Protein Extraction

HEK293T cells were transfected with either empty mammalian expression vector pEF1-mycA (Invitrogen) or vector carrying cDNAs encoding human integrins β1, β3 and β5 by means of ExGen 500. Forty-eight hours post-transfection, cell membranes were first isolated using ProteoExtractNative Protein Extraction Kit (Calbiochem) and subjected to enrichment by sucrose step gradient (Tang et al., 2006). The proteins were dialyzed against PBS prior to SPR analysis.

2.14 Soft Agar and Anoikis Assay

A-5RT3$_{CTRL}$ and A-5RT3$_{ANGPTL4}$ cells were used in soft agar assay. 0.6% Noble agar (Sigma Aldrich) in DMEM with 10% FBS was allowed to solidify in 6-well plates, and 1×10^4 cells were plated in 0.3% Noble agar in DMEM with 10% FBS on top. Tumor-cell colonies were stained with 1 mg/ml thiazolyl blue tetrazolium in PBS after 4 weeks.

Cells were subjected to an anoikis assay. Briefly, anoikis was induced by forced suspension, wherein 5.0×10^5 cells were seeded onto DMEM equilibrated agarose (1.0%, i.e. 1g of agarose in 100 ml of DMEM) in the presence of either 10 μg/ml of pre-immune IgG or mAb11F6C4. For MBA-MD-231, cells were exposed to 1 μg/ml doxycyline for 24 h to knockdown ANGPTL4 prior anoikis. For rescue experiments, cells were subjected to anoikis in the presence of either the indicated concentrations of exogenous recombinant cANGPTL4 or vehicle (PBS). Cells were harvested at the indicated time points, and analyzed for apoptosis by FACS analysis. The apoptotic indices of attached cells were determined immediately after harvesting with trypsin.

2.15 Caspase Activity Assay

Cells were subjected to anoikis as described above. The activities of caspases 2, 3, 6, 8 and 9 were measured with Apotarget caspase colorimetric protease assay kit (Biosource International, Camarillo,CA) according to the manufacturer's instructions. The $O.D._{405nm}$ was measured, and the fold increase in caspase activity was determined by direct comparison with the level of the $A\text{-}5RT3_{CTRL}$ or cognate pre-immune IgG treated cells.

2.16 Electron Paramagnetic Resonance (EPR) Measurement of O_2^-

Entire excised tumor biopsies were enzymatically dispersed into single cell suspensions. The tissue was minced and incubated in digestion buffer containing 1 mg/ml hyaluronidase, 1 mg/ml collagenase D and 100 unit/ml DNase (Sigma-Aldrich) in a 37^oC shaking incubator for 2h. The dispase and hyaluronidase digests were pooled and filtered through a 70 μm Nylon cell strainer. Cells were washed, pelleted and resuspended in PBS containing 3% FBS. Equal amount of cells were used for EPR measurement of O_2^-. Direct trapping of superoxide in aqueous media was performed using the spin trap DEPMPO, which forms a relatively stable superoxide adduct. EPR spectra were recorded at room temperature with a Bruker D-200 ER spectrometer, operating at X-band with a TM 110 cavity with a quartz flat cell. The EPR parameters were set at 100 KHz, X-band microwave frequency, 9.5 GHz; microwave power, 20 mW; modulation amplitude, 1 G; time constant, 160 s; scan time, 50 s; and receiver gain, 5×10^5. The EPR spectra represent the averaged signals of 10 scans. EPR signal amplitude at 3480 G represents the pure line, corresponding only to the superoxide adduct. All experiments were performed in triplicates.

2.17 Measurement of O_2^- by MCLA

Production of O_2^- from tumor cells was measured using an O_2^--sensitive luciferin derivative, 2-methyl-6-(p-methoxyphenyl)-3, 7-dihydroimidazo[1, 2-a]pyrazin-3-one (MCLA; Invitrogen). Cells (5×10^4) were trypsinized, washed, lysed in Krebs buffer and treated either individually or combinatorially for 0.5 h with the following chemicals: 10 mM Tiron, 20 µM diphenyleneiodonium chloride (DPI,) or 500 µM apocynin, 50 µM rotenone and 3 or 6 µg/ml monoclonal human anti-cANGPTL4 antibody mAb11F6C4. MCLA (2 µM) was added, and the luminescent signal was recorded immediately thereafter for 1 min with a GloMax® 20/20 Luminometer (Promega).

2.18 Measurement of H_2O_2 by Amplex Red Assay

Intracellular H_2O_2 was measured as previously described (Wagner et al., 2005). We performed two control experiments to verify that we were measuring H_2O_2. The specificity of the assay for H_2O_2 was verified with catalase, and the degradation of H_2O_2 or inhibition of the assay system by the sample was analyzed by determining the recovery of exogenously added H_2O_2. The fold change in the O_2-:H_2O_2 ratio of A-5RT3$_{ANGPTL4}$ and mAb11F6C4-treated tumor cells was determined by direct comparison with the value of either A-5RT3$_{CTRL}$ or control IgG-treated tumor cells, which were arbitrarily assigned the value of one.

2.19 Detection of Src Oxidation by Carboxymethylation

The detection of reduced Src was performed as described (Giannoni et al., 2009) with minor modifications. Cells were subjected to anoikis as described above. At the

indicated time, cells were then lysed with 500 μl lysis buffer (50 mM Tris-HCI, pH 7.5, 150 mM NaCl, 0.5% Triton X-100, 10 μg/ml aprotinin and 10 μg/ml leupeptin) containing 100 μM *N*-(biotinoyl)-*N*'-(iodoacetyl) ethylenediamine. Lysates were clarified by centrifugation and c-Src was immunoprecipitated using specific anti-c-Src antibodies. Immunocomplexes were resolved by SDS-PAGE and the biotinylated/reduced fraction of Src kinase was detected with horseradish peroxidase (HRP)-conjugated streptavidin and chemiluminesence.

2.20 Statistical Analyses

Statistical significance between two groups was analyzed using unpaired nonparametric test (Mann-Whitney test) or with a Student's *t*-test (SPSS, Inc.). All statistical tests were two-sided. A p-value of ≤ 0.05 was considered significant.

3. RESULTS

3.1 Elevated Expression of ANGPTL4 in Various Tumor Types.

To examine the expression profile of ANGPTL4 in known human tumors, we first screened its expression pattern on two commercially available human tumor tissue arrays, which cover most of the common benign, malignant and metastatic tumors originating from various anatomic sites. Via immunofluorescence with an anti-cANGPTL4 antibody, we observed widespread, elevated expressions of ANGPTL4 in all epithelial tumor samples compared to the corresponding normal tissues, regardless of anatomical site of origin (Figures 1 and 2). The level of immunofluorescence signal, however, varied among different types of tumor. Notably, the expression of ANGPTL4 increased as tumors progressed from a benign state to an invasive/metastatic state (Figure 2C).

Next, we determined the expression of ANGPTL4 on three human skin tumorigenic lines (HSC, II-4 and A-5RT3), 10 human squamous cell carcinoma (SCC) biopsies and 13 basal cell carcinoma (BCC) biopsies by quantitative real-time PCR (qPCR) and immunoblot analyses. Consistent with our prior results, we observed significant upregulation of ANGPTL4 mRNA and protein levels in these epithelial tumor cells when compared with the non-tumorigenic human skin line HaCaT or cognate peri-tumor normal samples (PNSs), respectively (Figures 3A-C). No difference was observed between normal skin biopsies (NS) and PNSs (Figures 3B and 3C). Interestingly, the three SCCs expressing the highest mRNA level of ANGPTL4 corresponded to an invasive prognosis (Figure 3B), underscoring our finding in tumor tissue arrays. In addition, polyclonal antibodies against either the N-

or C-terminus of ANGPTL4 detected only cANGPTL4 in these tumor lines, SCCs and BCCs (Figures 3).

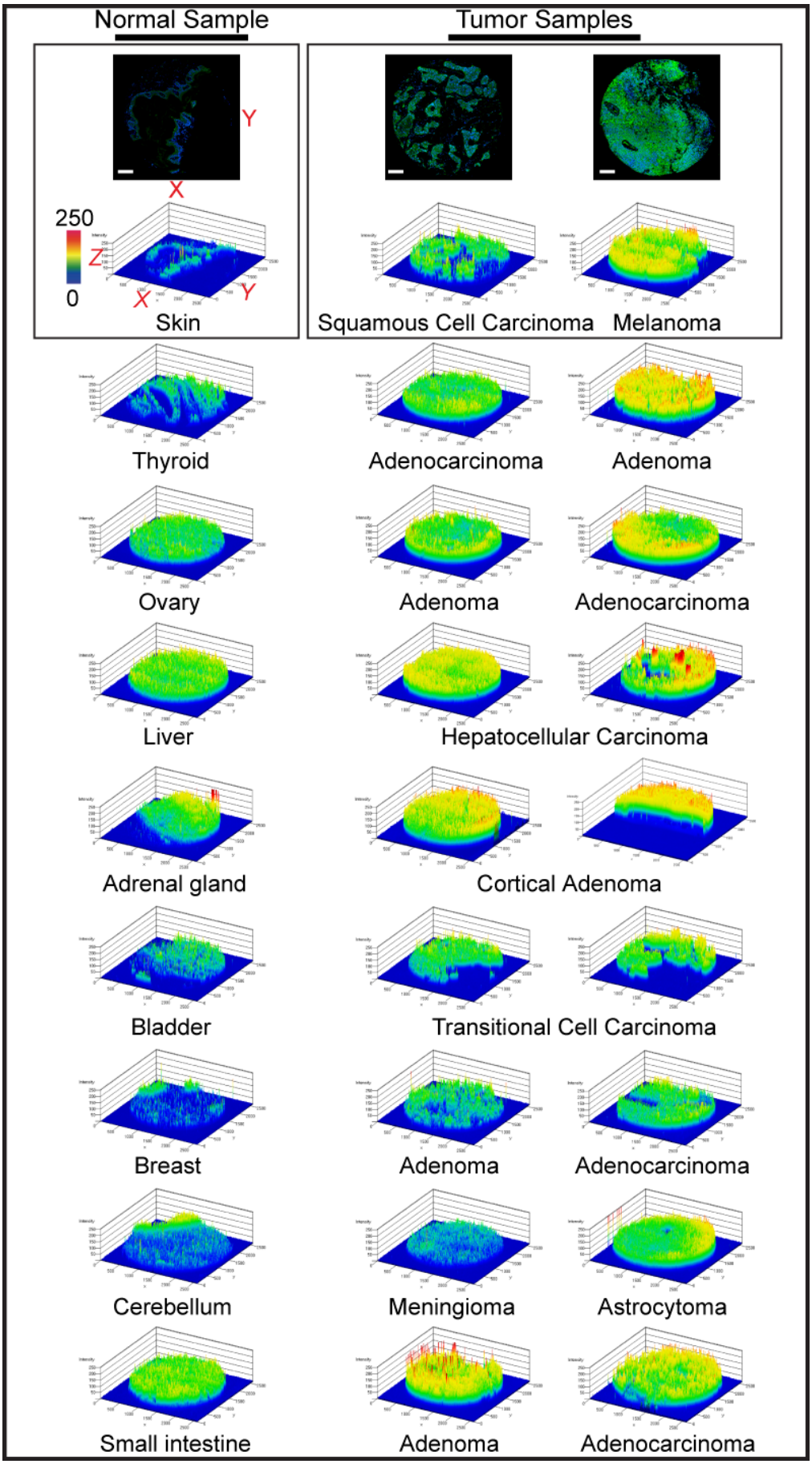

Figure 1. Elevated expression of ANGPTL4 in various tumors (tumor tissue array I).

ANGPTL4 expression varied among tumors procured from different anatomic sites. Heatmap profiles were generated from immunofluorescence (IF) images using IMARIS (Bitplane Scientific Software). X and Y axes represent the length and width; the Z axis represents IF intensity. Representative images of normal skin and skin tumor samples with corresponding heatmaps are shown. The heatmaps from the same anatomic sites are grouped horizontally. Scale bars represent 200 μm.

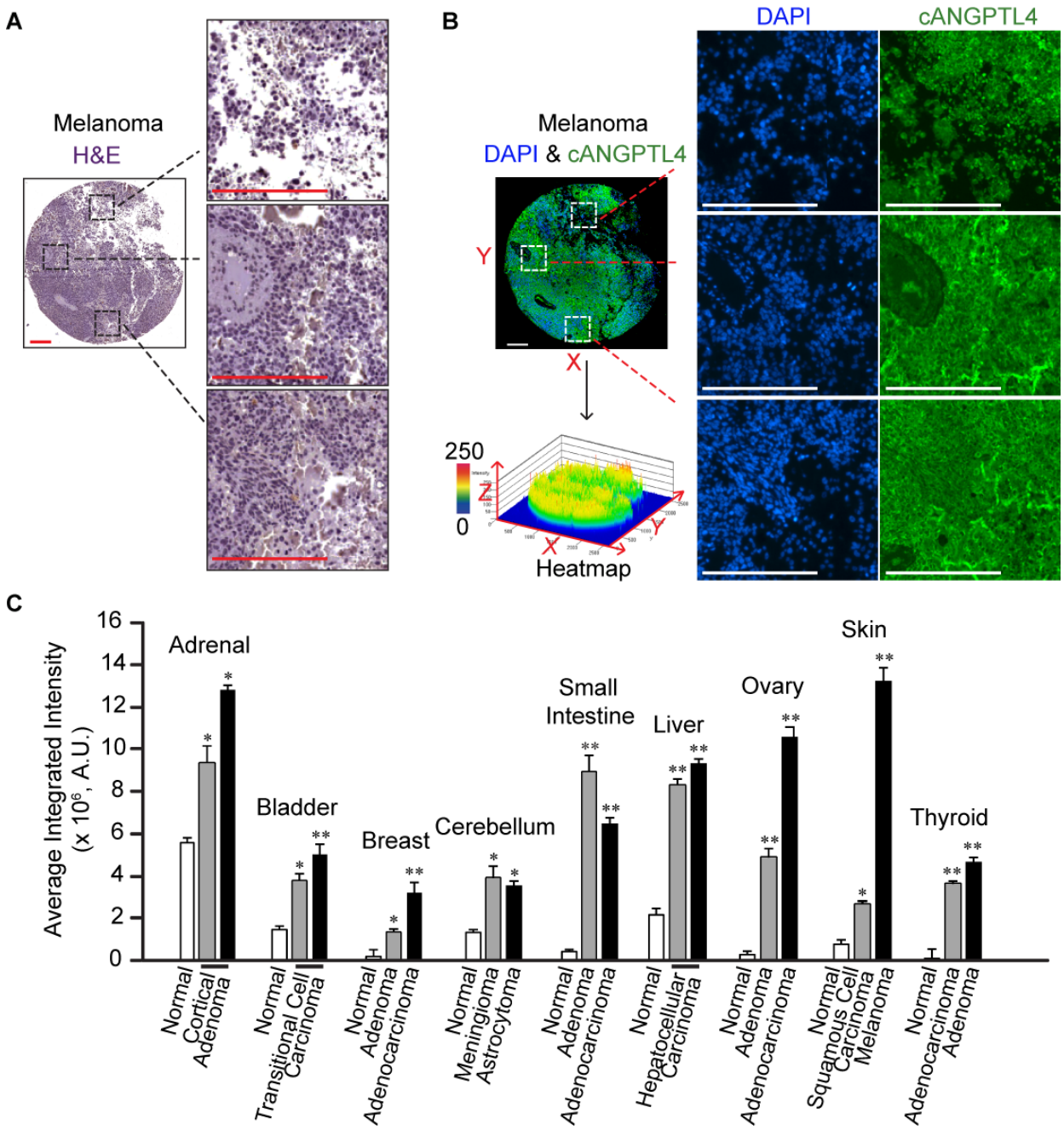

Figure 2. Elevated expression of ANGPTL4 in various tumors (tumor tissue array II).

(A and B) Haematoxylin and eosin (H&E) and immunofluorescence (IF) images of melanoma shown as a representative of the tumor tissue array in Figure 1. Higher magnification pictures randomly selected from the melanoma tissue are shown (H&E, right panel of A; DAPI and cANGPTL4, middle and right panels of B). The heatmap (left bottom panel of B) was transformed from the IF image (left upper panel of B) based on the gray value (IF intensity) of cANGPTL4. All scale bars represent 200 μm. **(C)** Average integrated gray value (IF) of cANGPTL4 from various normal and tumor tissues shown in Figure 1. Tissues from same anatomic site were grouped and compared. Results are representative of two independent experiments performed in duplicate. Values (mean ± SEM) were calculated from at least three biopsies and microscopic fields of each tissue. *$p < 0.05$; **$p < 0.01$.

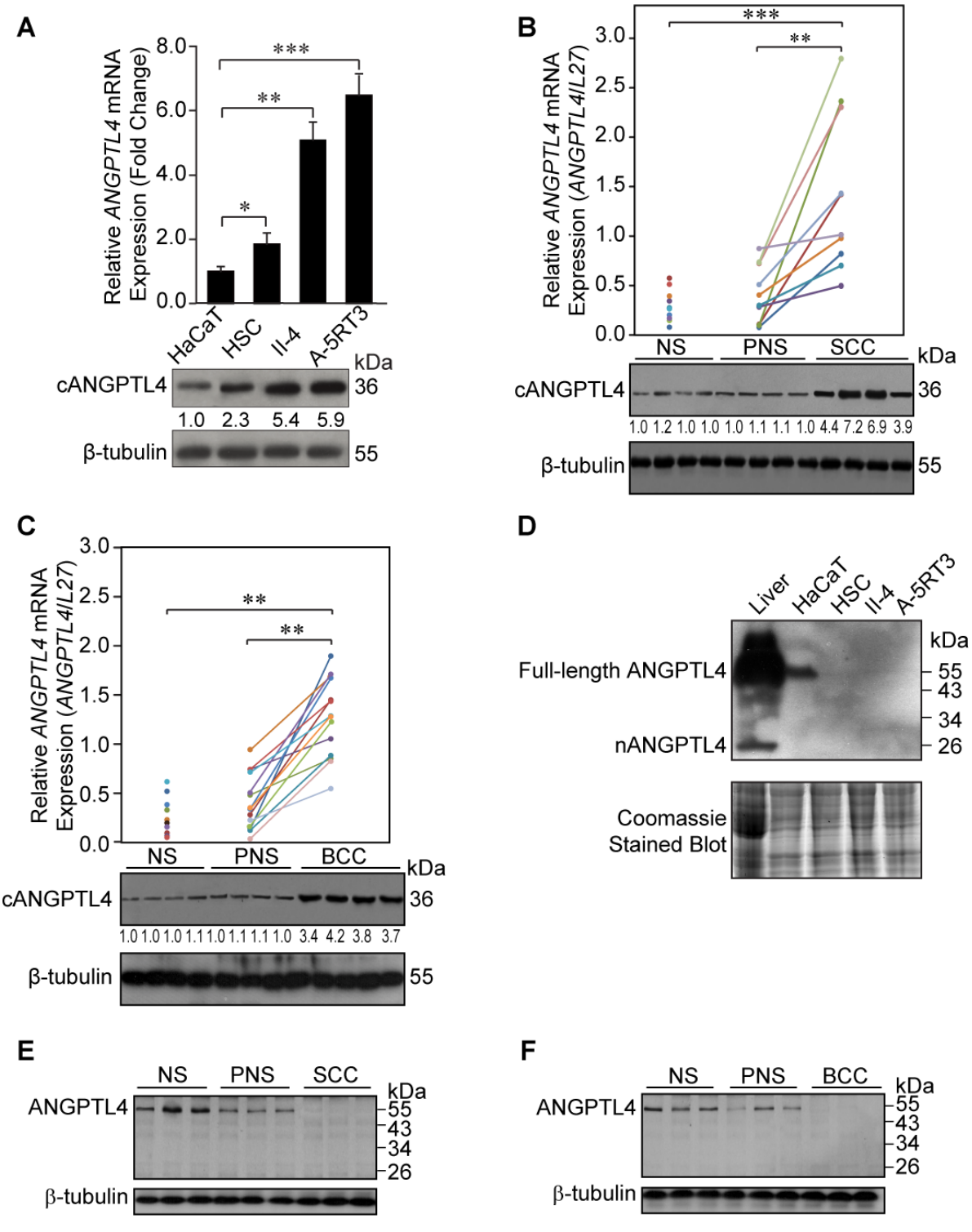

Figure 3. Elevated expression of ANGPTL4 in various tumor types (tumor cell lines and skin tumor biopsies).

(A) Relative ANGPTL4 mRNA and protein levels in non-tumorigenic HaCaT skin cell line and the tumorigenic skin cell lines HSC, II-4, and A-5RT3.

(B and C) Relative ANGPTL4 mRNA and protein levels in paired human squamous cell carcinoma (SCC) (B) or basal cell carcinoma (BCC) (C) and cognate peri-tumor normal sample (PNS). Skin biopsies from normal human skin (NS) served as additional controls. Three SCCs with the highest mRNA ANGPTL4 levels corresponded to an invasive prognosis.

(D-F) Immunoblot analysis using anti-nANGPTL4 antibody of tumorigenic skin lines HSC, II-4, and A-5RT3 (D), and human skin squamous cell carcinomas (SCCs) (E), basal cell carcinomas (BCCs) (F) along with cognate peri-tumor normal sample (PNS). Liver, non-tumorigenic skin line HaCaT and normal skin biopsies (NS) served as cognate positive controls. No full-length or nANGPTL4 was detected in indicated tumor cell line, BCCs or SCCs. Anti-nANGPTL4 antibody was previously described (Kersten et al., 2000).

All mRNA data shown are the means ± SD from two independent qPCR experiments performed in triplicate. Ribosomal protein *L27* (*L27*) was used as a reference housekeeping gene. *$p < 0.05$; **$p<0.01$; ***$p<0.001$. Immunoblot data are from three independent experiments performed in duplicate. Coomassie stained blot or β-tubulin served as loading and transfer controls.

The expression of ANGPTL4 is upregulated by hypoxia (Belanger et al., 2002) and by PPARs (Kersten et al., 2000) To understand the reason for the increased expression of ANGPTL4 in tumor cells, we examined the expression of hypoxia-inducible factor 1 alpha (HIF1α) and PPARs in the SCC samples. We found a concomitant upregulation of HIF1α with ANGPTL4 in SCCs when compared with PNSs (correlation coefficient = 0.88) (Figures 4A-B). Although no clear correlation was observed between the expression of ANGPTL4 and the three PPAR isotypes (Figures 4C-E), we cannot exclude an involvement of PPARs and/or other oncogenic pathways that enhanced the expression of cANGPTL4 in tumors. These results suggested that at least for SCCs, the elevated expression of ANGPTL4 reflects the tumor's hypoxic microenvironment. As a protein that is highly secreted by tumor cells, ANGPTL4 may perform an important paracrine or autocrine function in tumors. Therefore, we sought to determine the source of ANGPTL4 in tumors. We isolated epithelial tumor and stromal tissues, which consist mainly of fibroblasts, from SCCs and PNSs, using laser capture microdissection (LCM). qPCR and immunoblot analyses were then performed on these samples. Our results revealed that epithelial tumor cells, rather than tumor stroma, were the major contributor of ANGPTL4 in SCCs (Figure 4F). Further, only a low, baseline level of ANGPTL4 expression was found in normal PNS stroma and epithelia, suggesting that ANGPTL4 may have an autocrine role in tumors.

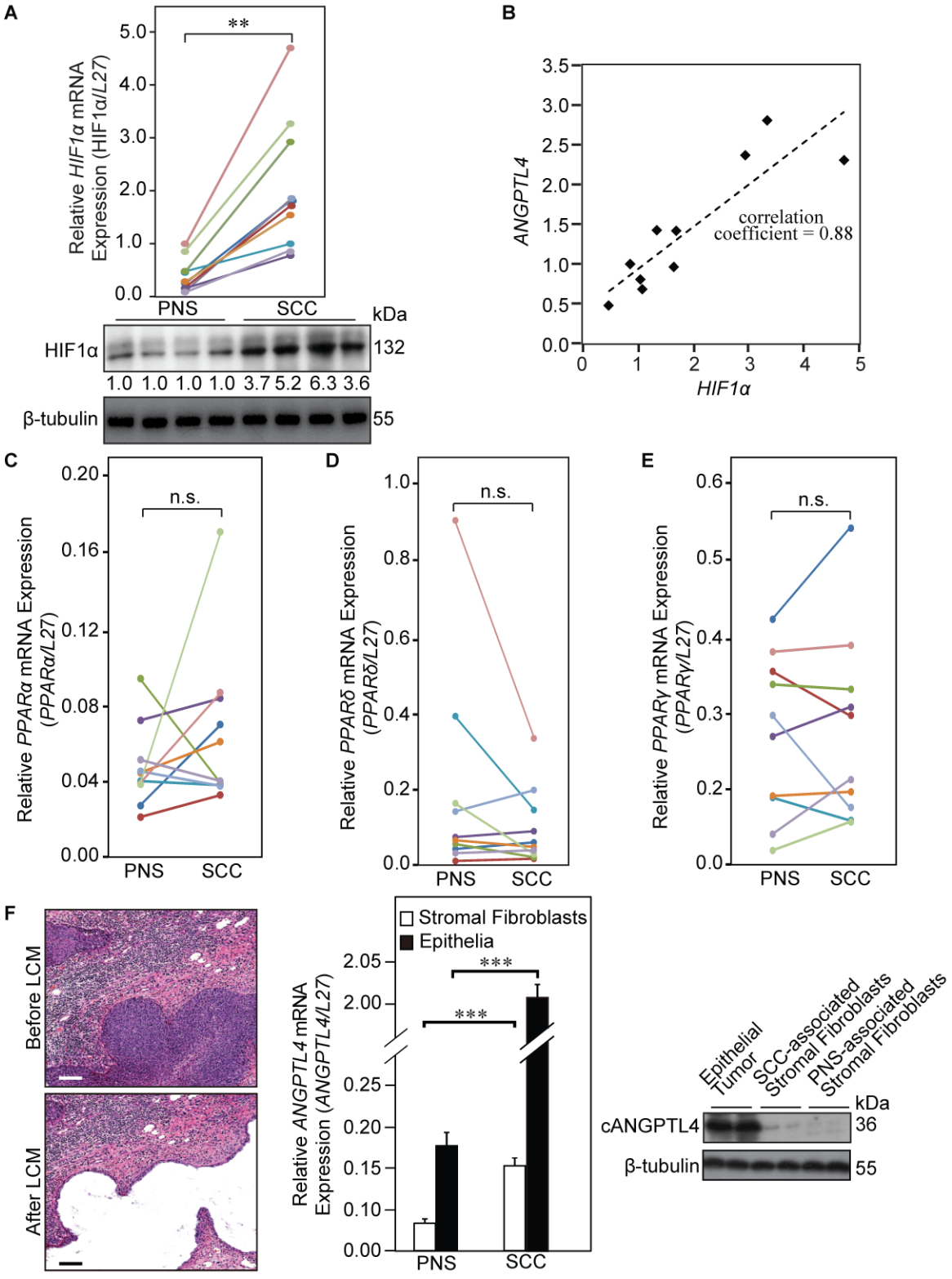

Figure 4. Involvement of HIF1α and PPARs in the upregulation of ANGPTL4 in various tumor types.

(A) Relative HIF1α mRNA and protein levels in paired human SCCs and PNSs. For qPCR results, data points from the same individual are linked by colored lines.

(B) HIF1α with ANGPTL4 mRNA levels were concomitantly upregulated in SCCs as compared with PNSs (correlation coefficient = 0.88). The individual mRNA expression levels of ANGPTL4 and HIF1α refer to Figure 3B and Figure 4A, respectively.

(C-E) Relative mRNA expressions PPARα (C), PPARδ (D) and PPARγ (E) in paired human SCCs and PNSs as determined by qPCR. Data spots from same individual were linked by coloured lines.

(F) Relative ANGPTL4 mRNA and protein levels in laser capture microdissected (LCM) epithelial cells and stromal fibroblasts from paired SCC and PNS. Hematoxylin and eosin images of an SCC section before and after LCM of epithelial tissue were shown in the left panel. Scale bars represent100 μm. Microdissected tissues were processed for qPCR (middle panel) and immunoblotting (right panel).

All qPCR Data shown are means ± SD from at least two independent experiments performed in triplicate. Ribosomal protein *L27* (*L27*) was used as a reference housekeeping gene. **p<0.01; ***p<0.001. n.s. represents not significant in the comparison between paired SCCs and PNSs. Immunoblot data are from at least two independent experiments performed in duplicate. β-tubulin served as loading and transfer control.

3.2 Suppression of ANGPTL4 Impairs In Vivo Tumor Growth.

Our findings revealed an elevated expression level of ANGPTL4 in tumors. Next, we investigated its biological relevance to tumor growth via RNAi. Four sets of siRNAs targeting different segments of the ANGPTL4 sequence were permanently introduced into the metastatic skin tumor line A-5RT3 (Mueller et al., 2001), and the sub-line with the highest knockdown efficiency (designated A-5RT3$_{ANGPTL4}$) was selected for subsequent studies. A non-targeting scrambled siRNA was also integrated into A-5RT3 (designated A-5RT3$_{CTRL}$), serving as a negative control. ANGPTL4 mRNA and protein levels were successfully suppressed > 85% in A-5RT3$_{ANGPTL4}$ when compared with the parental control A-5RT3 or the scrambled control A-5RT3$_{CTRL}$ (Figure 5A). The induction of interferon responses has been reported as a challenge to the specificity of some RNAi approaches (Bridge et al., 2003). To test whether the RNAi-mediated silencing of ANGPTL4 was associated with interferon responses, we measured the expression of several key interferon response genes by qPCR. No induction of *OAS1*, *OAS2*, *MX1* or *ISGF3γ* was detected in the A-5RT3$_{ANGPTL4}$ cells when compared with either wild-type, untreated A-5RT3 or A-5RT3$_{CTRL}$ cells (Figure 5B), verifying that our RNAi experiment did not produce an off-target effect.

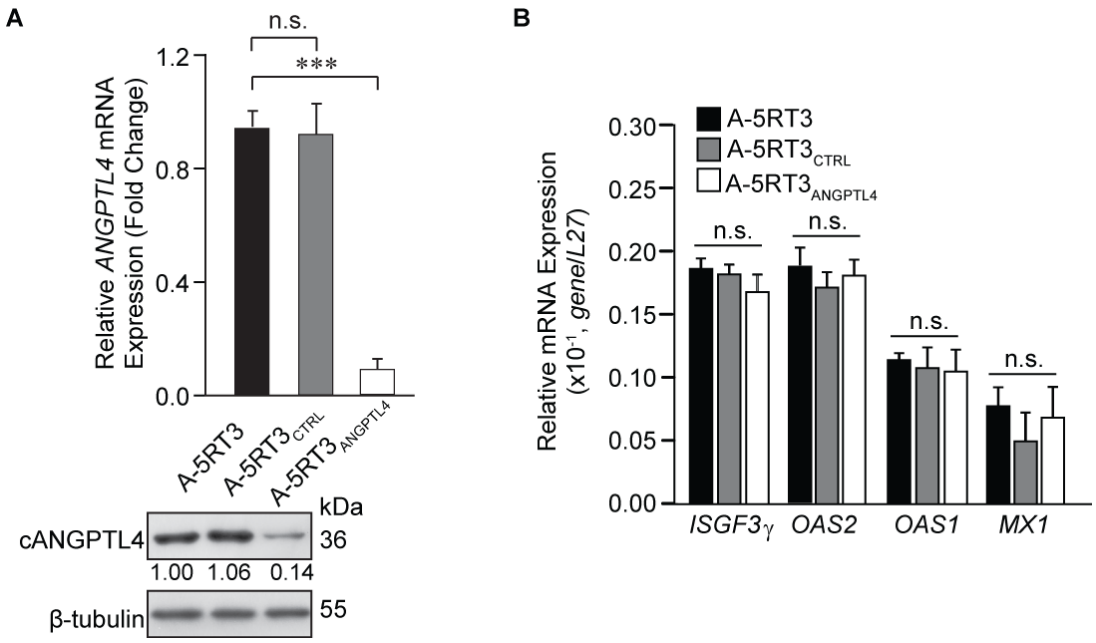

Figure 5. Knockdown of ANGPTL4 has no off-target effect in tumor cell A-5RT3.

(A) Relative ANGPTL4 mRNA and protein levels in A-5RT3 (parental), A-5RT3$_{CTRL}$ (scrambled control) and A-5RT3$_{ANGPTL4}$ (knockdown) cells. Immunoblot data are from three independent experiments performed in duplicate. β-tubulin served as a loading and transfer control.

(B) Relative mRNA levels of key interferon response genes: 2', 5'-oligoadenylate synthetase isoforms 1 and 2 (*OAS1, OAS2*), interferon-induced myxovirus resistance 1 (*MX1*) and interferon-stimulated transcription factor 3γ (*ISGF3γ*) in A-5RT3, A-5RT3$_{CTRL}$, and A-5RT3$_{ANGPTL4}$.

All qPCR results shown are mean ± SD from three independent qPCR experiments performed in triplicate. Ribosomal protein *L27* (*L27*) was used as a reference housekeeping gene. ***$p < 0.001$ and n.s. represents not significant.

As expected, the injection of A-5RT3$_{CTRL}$ cells into immunodeficient mice induced large primary tumors (~1000 mm^3) in all five mice at week 8, but A-5RT3$_{ANGPTL4}$-induced tumors displayed a 90% reduction in tumor growth (Figures 6A-B). To further exploit the effect of ANGPTL4 deficiency on tumor size depending on the amount of injected tumor cells, we injected various numbers (0.5×, 2.0× and 8×10^6) of A-5RT3$_{CTRL}$ and A-5RT3$_{ANGPTL4}$ cells into nude mice. Consistently, the A-5RT3$_{ANGPTL4}$-induced tumor growth was reduced when compared with corresponding amount of A-5RT3$_{CTRL}$-induced tumor, although the tumor growth reduction decreased when mice were implanted with increasing number of tumor cells (Figure 6C).

To strengthen the above observations, we subcutaneously implanted B16F10 cells into ANGPTL4-knockout (KO) and control (WT) mice. WT and KO mice were maintained in a C57BL/6J background, and the B16F10 melanoma was derived from the same background. Notably, B16F10 tumor cells implanted in KO mice grew significantly slower than those implanted in WT mice; at 15 days post implantation, the average tumor volume in KO mice was ~6-fold less than in WT mice (Figure 7A). The injection of ANGPTL4-knockdown (B16F10$_{ANGPTL4}$) cells into KO mice induced little tumor growth, and showed similar growth profile in WT mice compared to control B16F10 (B16F10$_{CTRL}$)-induced tumors in KO mice (Figure 7A). Conversely, WT mice implanted with B16F10$_{CTRL}$ cells and intravenously injected three times a week with recombinant N-terminal histidine-tagged cANGPTL4 showed greater tumor growth. The average tumor volume in cANGPTL4-treated mice was ~3-fold larger than PBS-treated mice (Figures 7B-D). B16F10$_{ANGPTL4}$-induced tumor growth was diminished in PBS-treated mice when compared to cANGPTL4-treated mice (Figure 7B). Thus, cANGPTL4 is essential for tumor growth in mouse model.

Next, we reasoned that treating mice injected with A-5RT3$_{CTRL}$ cells with an antibody which interferes with the action of ANGPTL4 would recapitulate the observation made with A-5RT3$_{ANGPTL4}$ cells. To this end, the monoclonal human cANGPTL4-directed antibody mAb11F6C4 was identified and produced for our immunotherapy experiment based on its superior k_{on}, k_{off} and K_D values, as determined by surface plasmon resonance (Cazes et al., 2006) (Figure 8A). Notably, immunosuppression of ANGPTL4 with mAb11F6C4 significantly attenuated *in vivo* tumor growth in immunodeficient mice, compared with control IgG-treated mice (n = 6 in each group) (Figures 8B and 8C).

Immunoblot and immunofluorescence analyses of A-5RT3$_{ANGPTL4}$-induced tumor biopsies indicated significantly reduced cell proliferation and enhanced cell apoptosis when compared with A-5RT3$_{CTRL}$-induced tumors (Figures 9A and 9B). A qPCR-focused array of A-5RT3$_{ANGPTL4}$-induced tumor biopsies further suggested increased expression of many pro-apoptotic genes, whereas expression of cell proliferation genes was diminished (Figure 9C; Table 3). Taken together, all the above observations clearly support a tumor-promoting role for cANGPTL4.

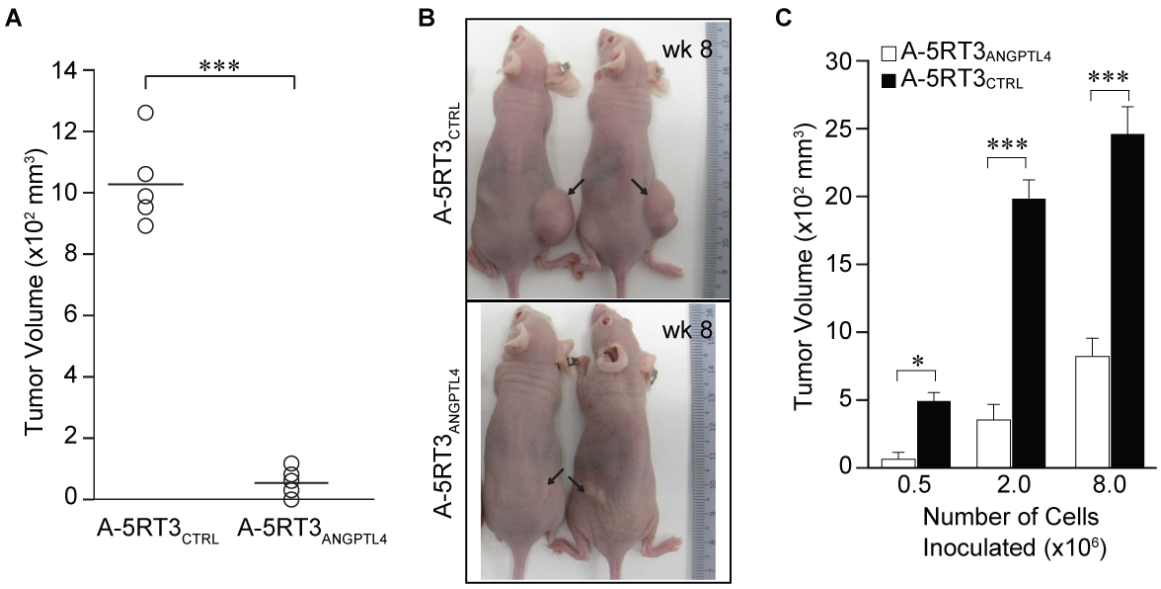

Figure 6. Suppression of ANGPTL4 impairs tumorigenicity.

(A) Size of xenograft tumors induced in nude mice by 5×10^5 of A-5RT3$_{ANGPTL4}$ or A-5RT3$_{CTRL}$ cells 8 weeks post-inoculation (n = 5 in each group). Each circle represents the mean size from three measurements on each mouse at wk 8.

(B) Representative pictures of A-5RT3$_{CTRL}$- and A-5RT3$_{ANGPTL4}$-induced tumors (week 8) in (A). Black arrows indicate inoculation sites.

(C) Mean size of xenograft tumors induced in nude mice by 0.5 ×, 2 × and 8×10^6 A-5RT3$_{ANGPTL4}$ or A-5RT3$_{CTRL}$ cells 4 weeks post-inoculation (each group). Values (mean ± SEM) were calculated from n = 5 (each group) mice. *$p < 0.05$; ***$p<0.001$.

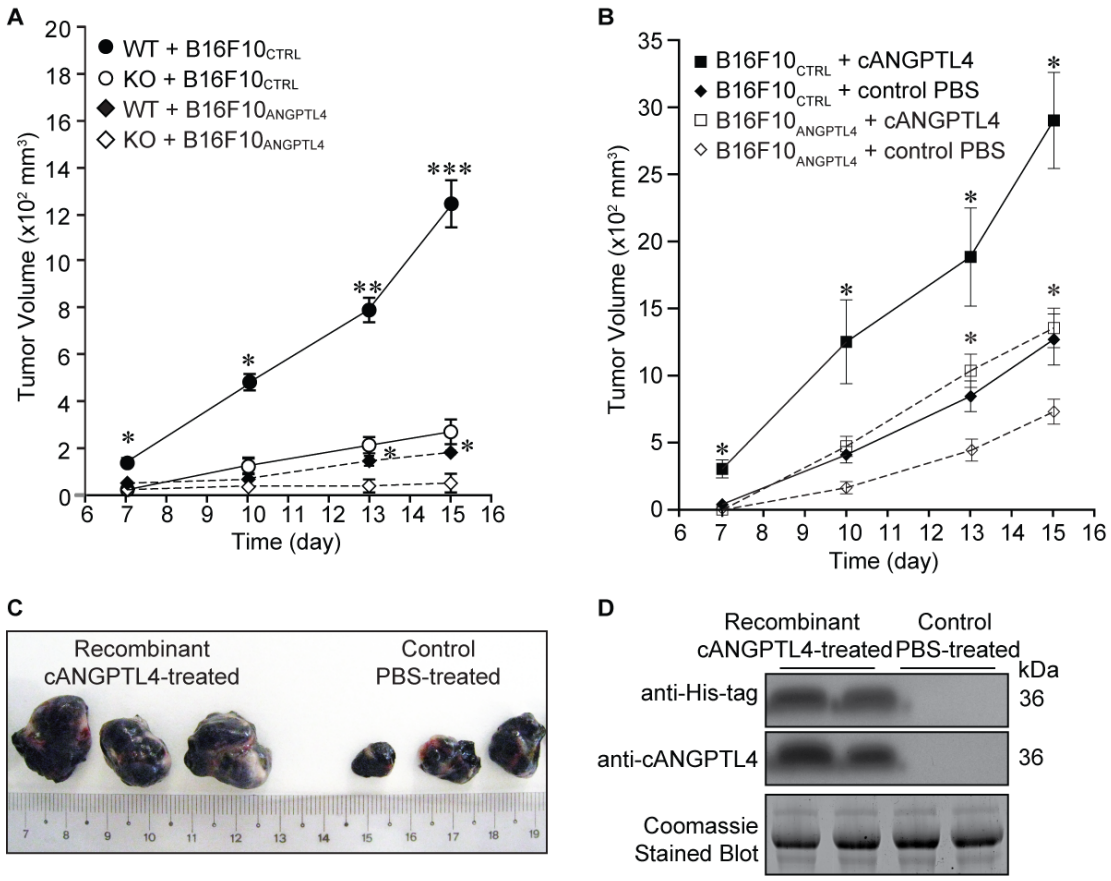

Figure 7. Suppression of ANGPTL4 reduces tumorigenicity and exogenously infused cANGPTL4 accelerates tumor growth.

(A and B) Size of tumor volume induced in ANGPTL-knockout (KO) and wild-type (WT) mice (A), and PBS- or recombinant cANGPTL4-treated C57BL/6J WT mice (B) by B16F10 melanoma ($B16F10_{CTRL}$, control) and ANGPTL4-knockdown ($B16F10_{ANGPTL4}$). Cells (1×10^6) were *s.c.* inoculated into each mouse. Mice were treated *i.v.* with either 3 mg/kg of cANGPTL4 or vehicle PBS three times a week (n = 6 in each group). Values are the means ± SEM from three measurements of each mouse. *$p < 0.05$; **$p<0.01$; ***$p<0.001$.

(C) Representative pictures of B16F10-induced tumors in C57BL/6J mice with *i.v.* treatments of either 3mg/kg of cANGPTL4 or control PBS three times a week and dissected 15 days after injection (scale bar 10 mm).

(D) Immunoblot detection of recombinant cANGPTL4 using anti-His-tag and anti-cANGTPL4 antibodies. Plasma samples from C57BL/6J mice 1 day post-treatment with cANGPTL4 or control PBS (as described in (B)) were used. Coomassie stained blot served as loading and transfer control. Experiments were repeated three times with consistent results.

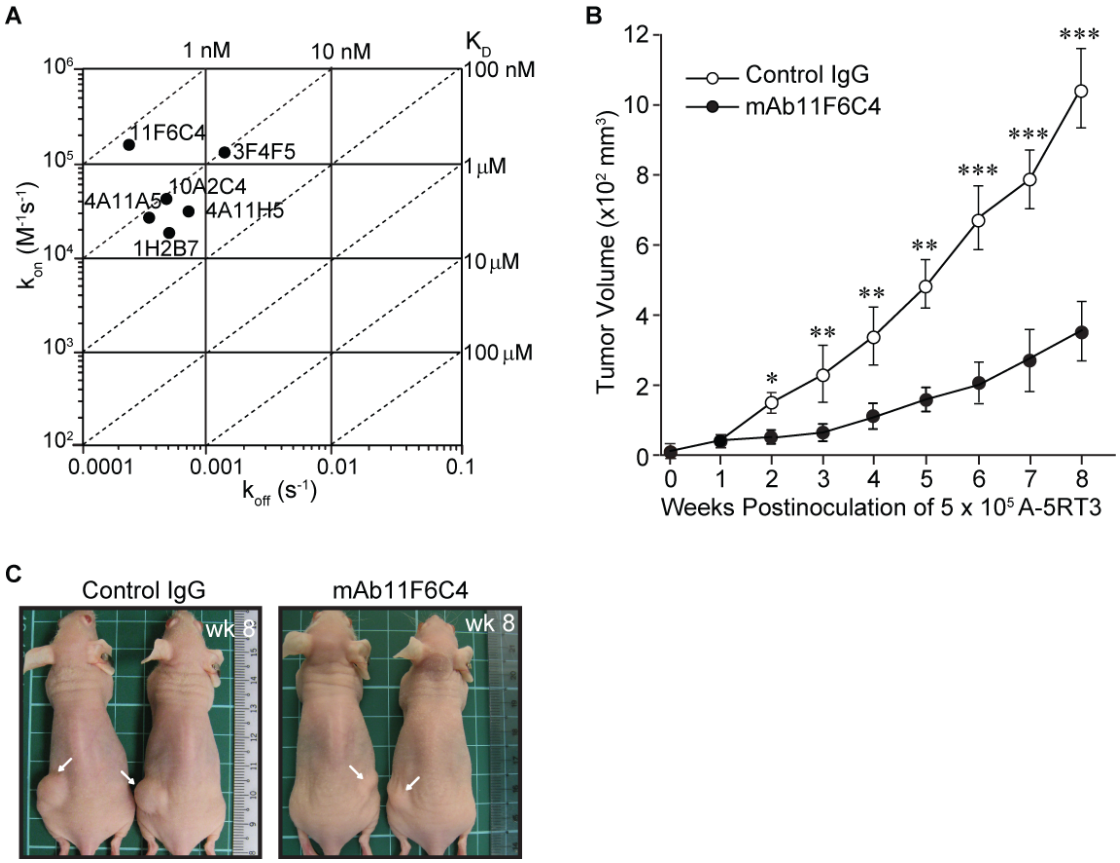

Figure 8. Immuno-suppression of ANGPTL4 impairs tumorigenicity.

(A) ANGPTL4 interaction kinetic maps for human mAbs, shown as association and dissociation rate constants (k_{on} and k_{off}), and a combination of k_{on} and k_{off} that results in the same affinity constant (K_D) values (diagonal lines) as determined by SPR. Labels in maps identify the six mAb clones. mAb11F6C4 was chosen for subsequent immunotherapy experiment based on its superior k_{on}, k_{off} and K_D values.

(B) Tumor volume in nude mice injected *s.c.* with 5×10^5 of A-5RT3 cells and treated *i.v.* with 30 mg/kg/week of either mAb11F6C4 or control IgG as a function of time (n = 6 in each group). Each circle represents the mean ± SEM from three measurements of each mouse. *$p < 0.05$; **$p<0.01$; ***$p<0.001$.

(C) Representative pictures of control IgG- or mAb11F6C4-treated nude mice (wk 8) as described in (B). White arrows indicate A-5RT3 cell inoculation sites.

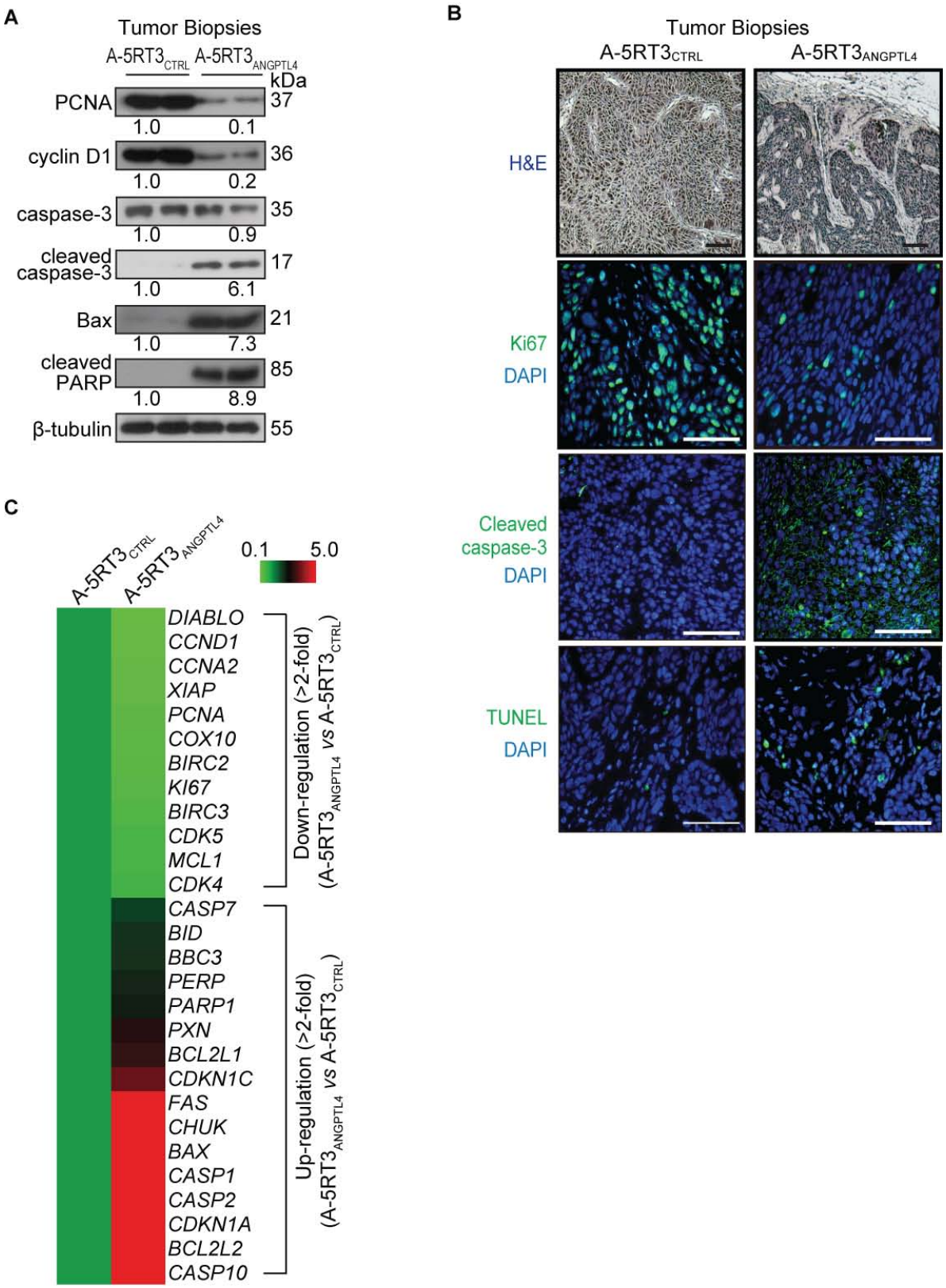

Figure 9. Suppression of ANGPTL4 reduces cell proliferation and enhances cell apoptosis *in vivo*.

(A) Immunoblot of proliferation (PCNA and cyclin D1), and apoptosis (cleaved caspase-3, Bax and cleaved PARP) markers in A-5RT3$_{ANGPTL4}$- and A-5RT3$_{CTRL}$-induced tumor biopsies. Immunoblot data are from three independent experiments performed in duplicate. β-tubulin served as a loading and transfer control.

(B) Hematoxylin and eosin (H&E) and immunofluorescence staining of A-5RT3$_{CTRL}$- and A-5RT3$_{ANGPTL4}$-induced tumor sections. Proliferating (Ki67) and apoptotic (cleaved caspase-3 or TUNEL) cells were identified using the indicated antibodies or assay. Sections were counterstained with DAPI (blue). Scale bars represent 40 μm.

(C) Heatmap showing genes up- and down-regulated in A-5RT3$_{ANGPTL4}$-induced tumors relative to A-5RT3$_{CTRL}$-induced tumors as determined by qPCR. Results were generated from three pairs of indicated tumors. Three independent qPCR experiments performed in triplicate. Ribosomal protein *L27* (*L27*) was used as a reference housekeeping gene. A detailed description of the genes and their expression is presented in Table 1.

All experiments were performed using tumor biopsies harvested from mice described in Figure 7 at wk 8.

Table 3. Relative fold change of gene expressions in A-5RT3$_{ANGPTL4}$-induced tumors as compared with that of A-5RT3$_{CTRL}$-induced tumors, related to Figure 9C.

Down-regulated (> 2-fold)		
Gene	**A-5RT3$_{CTRL}$**	**A-5RT3$_{ANGPTL4}$**
DIABLO	1.000	0.070
CCND1	1.000	0.102
CCNA2	1.000	0.119
XIAP	1.000	0.120
PCNA	1.000	0.177
COX10	1.000	0.223
BIRC2	1.000	0.247
KI67	1.000	0.269
BIRC3	1.000	0.345
CDK5	1.000	0.498
MCL1	1.000	0.500
CDK4	1.000	0.549
Unchanged (< 2-fold)		
SRC	1.000	0.968
TP53	1.000	0.871

Up-regulated (> 2-fold)		
Gene	**A-5RT3$_{CTRL}$**	**A-5RT3$_{ANGPTL4}$**
CASP7	1.000	1.927
BID	1.000	2.051
BBC3	1.000	2.075
PERP	1.000	2.246
PARP1	1.000	2.308
PXN	1.000	2.947
BCL2L1	1.000	3.112
CDKN1C	1.000	3.609
FAS	1.000	6.171
CHUK	1.000	6.353
BAX	1.000	8.363
CASP1	1.000	10.499
CASP2	1.000	10.560
CDKN1A	1.000	13.037
BCL2L2	1.000	14.671
CASP10	1.000	24.740

Note: The Gene expression levels in A-5RT3$_{CTRL}$-induced tumors were assigned value one.

3.3 ANGPTL4-Deficient Tumor Cells Showed Increased Susceptibility to Anoikis.

Anchorage-independent growth or anoikis resistance of tumor cells, a hallmark of tumor malignancy (Hanahan and Weinberg, 2000), can be investigated by tumor colony formation in soft agar and anoikis assays, which are well-established *in vitro* approaches to study and predict self-renewal and metastatic potentials of *in vivo* tumor cells (Salmon, 1984). Underscoring our *in vivo* findings, the colony-forming potential of A-5RT3$_{ANGPTL4}$ cells was dramatically undermined and formed significantly fewer (~85%) tumor colonies on soft agar than A-5RT3$_{CTRL}$ cells (Figure 10A and B). Furthermore, the A-5RT3$_{ANGPTL4}$ line was also more susceptible to anoikis, having 30% more apoptotic A-5RT3$_{ANGPTL4}$ cells, as well as significantly enhanced activities from caspases 2, 3, 8 and 9 when compared with A-5RT3$_{CTRL}$ cells after 2 h of anoikis (Figure 10C and 10D). The addition of exogenous recombinant cANGPTL4 reduced the apoptotic index of A-5RT3$_{ANGPTL4}$ cells in a dose-dependent manner (Figure 10E). Similarly, ANGPTL4 deficiency in human keratinocytes rendered these cells ~50% more susceptible to anoikis when compared to control keratinocytes, suggesting that a low amount of ANGPTL4 was also necessary to confer anoikis resistance in normal epithelial cells (Figure 11A). No difference in the apoptotic index was observed in adhered A-5RT3 cells or keratinocytes (Figure 11B and 11C).

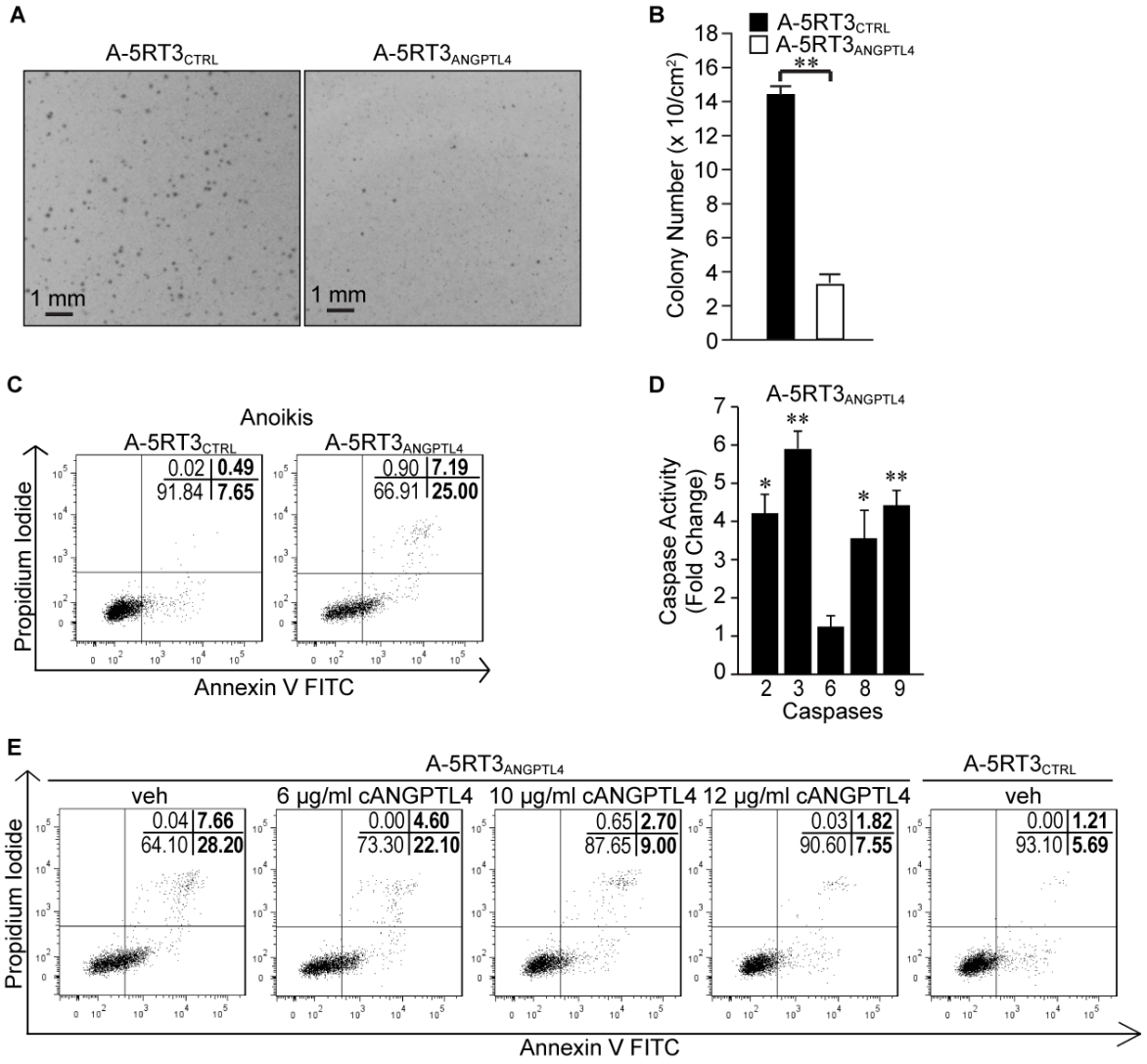

Figure 10. ANGPTL4 confers anoikis resistance to tumor cells.

(A) Representative pictures of colony assay results.

(B) Quantification of A-5RT3$_{CTRL}$ and A-5RT3$_{ANGPTL4}$ tumor colonies on soft agar (A).

(C) Percentage of apoptotic A-5RT3$_{CTRL}$ and A-5RT3$_{ANGPT4}$ after 2 h of anoikis, as analyzed by FACS (5000 events). The sum of Annexin V^+/PI^- (early apoptosis) and Annexin V^+/PI^+ (late apoptosis) cells were considered apoptotic. Values (bold) denote apoptotic cells (%).

(D) Relative activities of caspases 2, 3, 6, 8, 9 in A-5RT3$_{ANGPTL4}$ cells compared to A-5RT3$_{CTRL}$ cells (assigned value of one) after 2 h of anoikis.

(E) Percentage of anoikis-induced apoptotic A-5RT3$_{ANGPT4}$ cells in the presence of increasing exogenous recombinant cANGPTL4, as analyzed by FACS (5000 events). Vehicle (PBS)-treated A-5RT3$_{CTRL}$ and A-5RT3$_{ANGPT4}$ cells served as controls for comparison. The apoptotic index is described in (C).

All data (means ± SD) were obtained from at least three independent experiments performed in duplicate or triplicate. *$p < 0.05$, **$p < 0.01$.

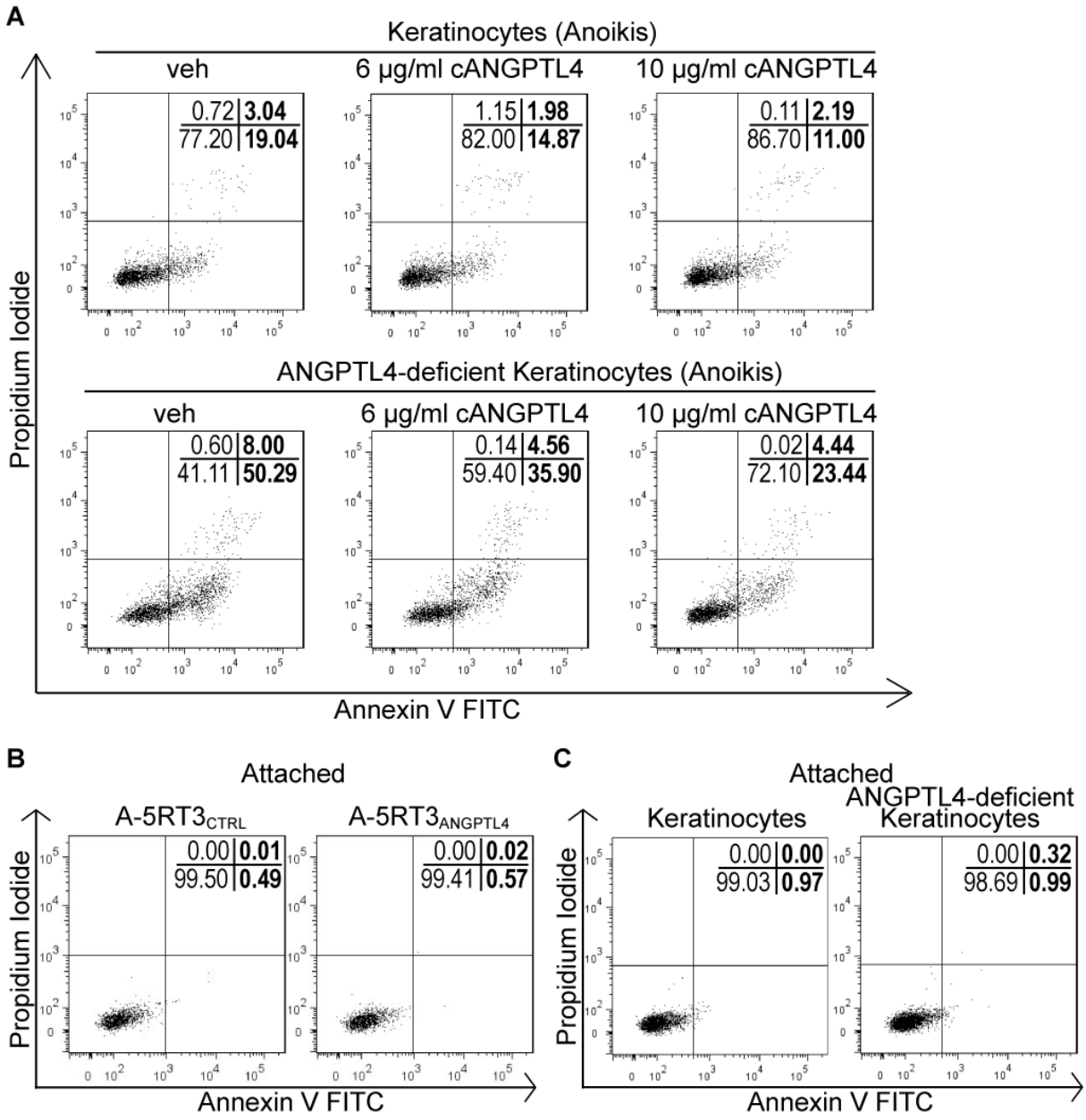

Figure 11. ANGPTL4 confers anoikis resistance to normal epithelial cells.

(A) Percentage of anoikis-induced apoptotic skin keratinocytes and ANGPTL4-deficient keratinocytes in the presence of increasing exogenous recombinant cANGPTL4 as analysed by FACS (5000 events). Vehicle (PBS)-treated keratinocytes and ANGPTL4-deficient keratinocytes served as cognate controls for comparison. Apoptotic index as described in (Figure 3B).

(B and C) Apoptotic index of adhered epithelial cells. A-5RT3$_{CTRL}$ and A-5RT3$_{ANGPT4}$ cells (B), and normal skin keratinocytes and ANGPTL4-deficient keratinocytes (C) were detached by trypsin, subjected for Annexin V and PI staining, and immediately analysed by FACS (5000 events). The sum of Annexin V^+/PI^- and Annexin V^+/PI^+ cells were considered dead. Values (bold) denote death rate (%).

All data (means ± SD) are obtained from at least four independent assays performed in triplicate. Representative pictures are shown.

3.4 ANGPTL4 Interacts with Integrins β1 and β5.

Our above findings indicate that ANGPTL4 endows tumor cells with resistance to anoikis and therefore sustains their growth, but the mechanism by which ANGPTL4 mediates this process is an unanswered question in our understanding of ANGPTL4 in cancer biology. Previous studies have revealed that anoikis is an integrin-dependent process (Zhan et al., 2004; Eble and Haier, 2006; Chiarugi, 2008). Thus, we hypothesize that ANGPTL4 also exerts its role in tumor cells through integrins-mediated signaling. To test this hypothesis, we first examined if cANGPTL4 can interact with integrins. Indeed, results obtained from SPR and ELISA assays showed that ANGPTL4 specifically interacts with integrins β1 and β5, but not with β3 (Figure 12A and 12B), and these interactions were blocked by either mAb11F6C4 (Figure 12C and 12D) or integrin-specific antibodies (Figures 12E-H). ANGPTL4 deficiency did not affect the expression of integrins β1, β3 and β5 (Figure 12I). An *in situ* proximity ligation assay (PLA) detected ANGPTL4-integrin complexes in both A-5RT3$_{CTRL}$-induced tumor biopsies and A-5RT3$_{CTRL}$ cells (Figure 13A and B), confirming that this interaction also exists *in vivo*. Further investigation revealed that integrin activation by ANGPTL4 binding triggered focal adhesion kinase (FAK) in A-5RT3$_{CTRL}$ tumors and cells, which were reduced by > 70% in A-5RT3$_{ANGPTL4}$ (Figures 13C-F). All of these findings were further corroborated by results from immunodetection FAK of tumor biopsies (Figure 14). Our findings suggest that ANGPTL4 secreted by epithelial tumor cells acts in an autocrine manner to hijack the integrin/FAK-regulated pathway, conferring anoikis resistance to tumors, and thus sustaining tumor growth.

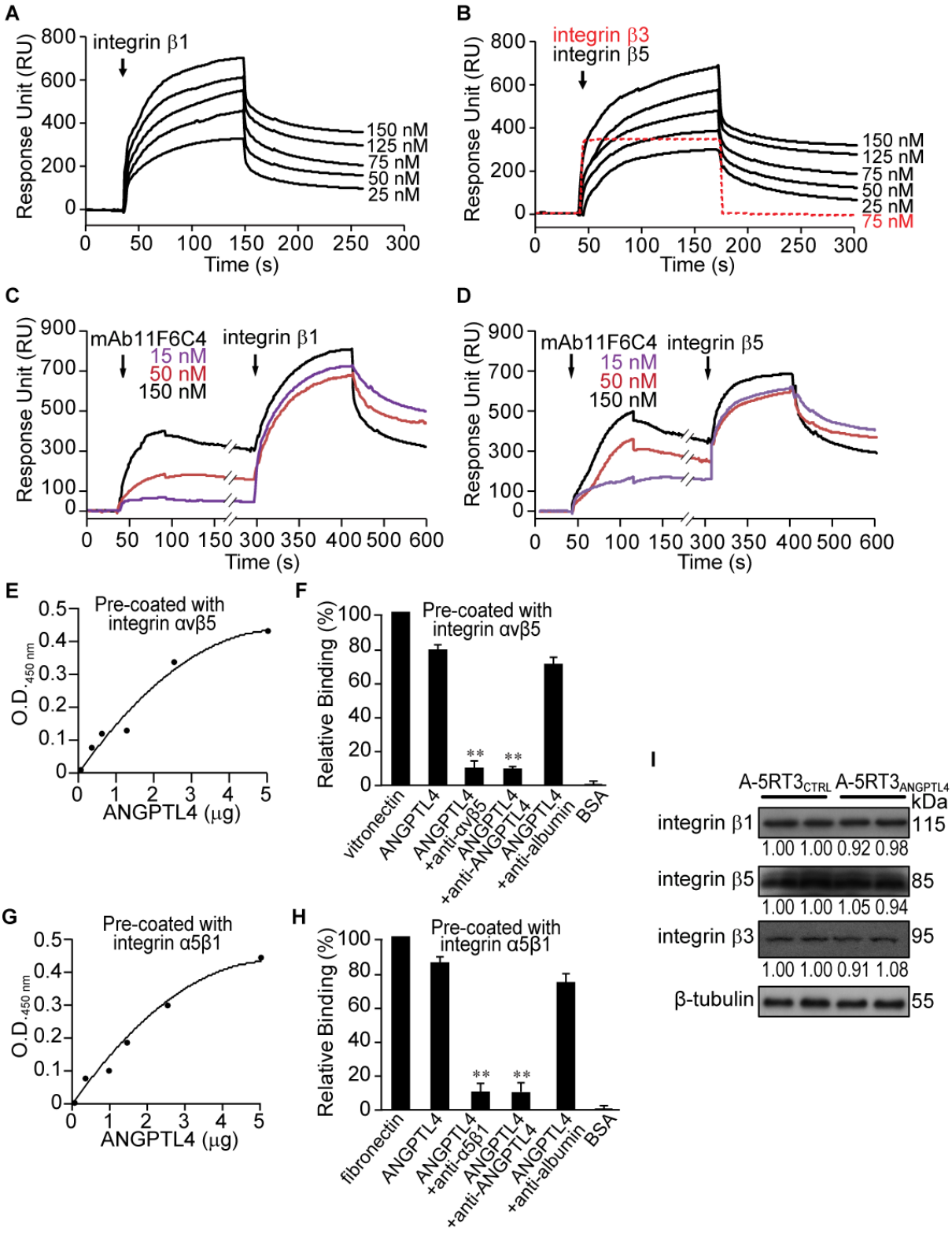

Figure 12. ANGPTL4 specifically interacts with integrins β1 and β5 but not with β3.

(A and B) Representative sensorgrams of three independent experiments showing binding profiles between immobilized-ANGPTL4 and integrin β1 (A) or integrin β5 (B). Integrin β3 (75 nM) did not show any detectable interaction (B, dotted red line). Sensorgrams were corrected against a reference flow cell with no immobilized protein. K_D ~10^{-7} M was determined after global fitting **(***Langmuir 1:1 model) using Scrubber2***.**

(C and D) Representative sensorgrams showing dose-dependent blocking of integrin β1 (C) and integrin β5 (D) to immobilized-ANGPTL4 by pre-injection with the indicated concentrations of mAb11F6C4.

(E-H) Dose-dependent ANGPTL4 bindings to immobilized integrin αvβ5 (E and F) and integrin α5β1 (G and H), which were specifically blocked by anti-cANGPTL4 as determined by ELISA.

(I) Immunoblot detects no significant difference in the protein expressions of integrins β1, β5 and β3 between A-5RT3$_{CTRL}$ and A-5RT3$_{ANGPTL4}$ cells

All experiments were repeated at least three times with consistent results. ** $p < 0.01$.

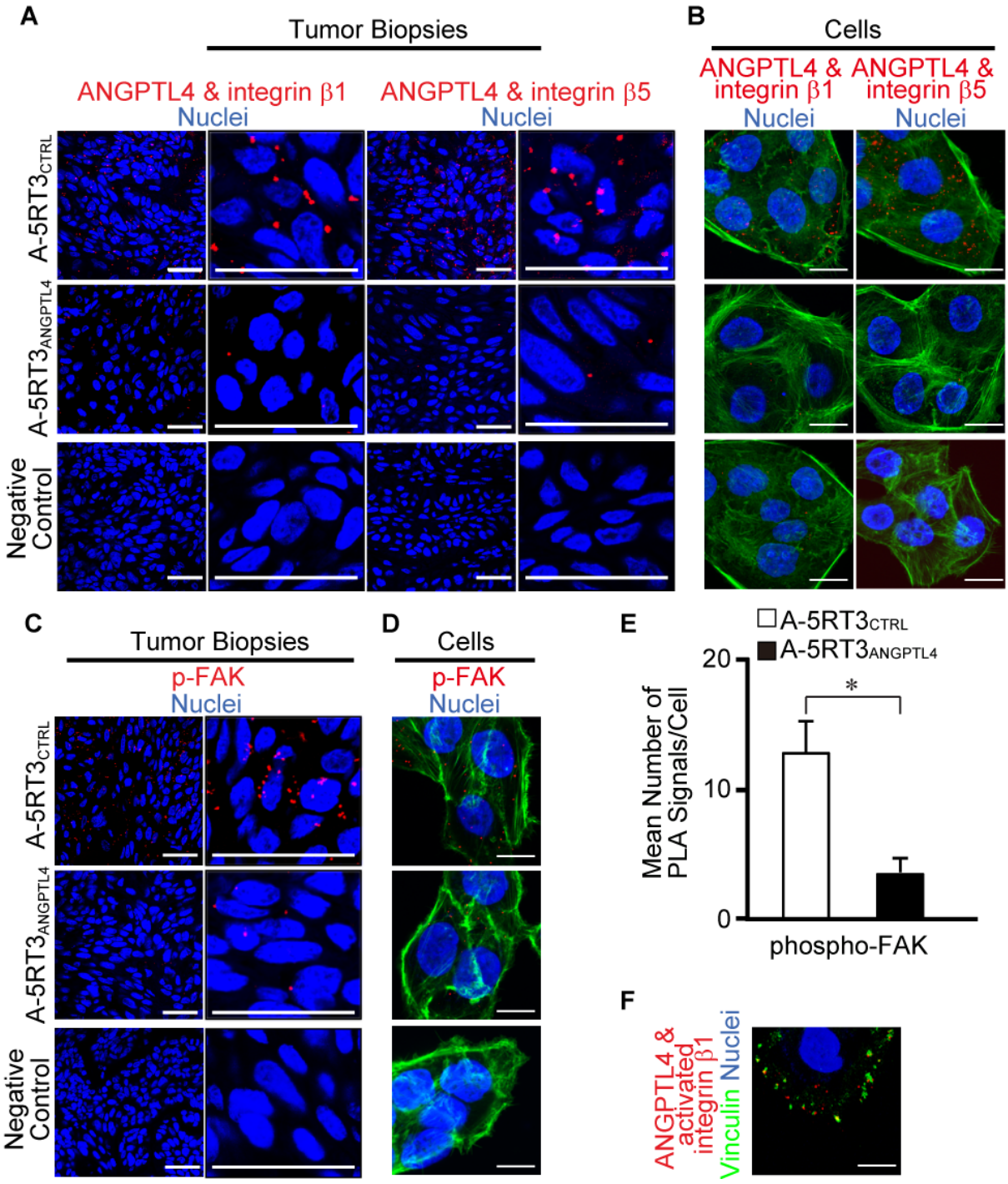

Figure 13. ANGPTL4 specifically interacts with integrins β1 and β5 but not with β3 to activate FAK.

(A and C) *In situ* PLA detection of ANGPTL4:integrin β1 (A, left two panels), ANGPTL4:integrin β5 (B, right two panels), and phosphorylated FAK (C) in A-5RT3$_{ANGPTL4}$- and A-5RT3$_{CTRL}$-induced tumor biopsies. Higher magnification images are shown in (A, 2nd and 4th panels; C, right panel). PLA signals are shown in red and nuclei are stained blue by Hoechst dye. Images were acquired in one z-plane using a Zeiss LSM710 META confocal laser scanning microscope.

(B and D) *In situ* PLA detection of ANGPTL4:integrin β1 and ANGPTL4:integrin β5 complexes (B), and of phosphorylated FAK (D) in A-5RT3$_{CTRL}$ and A-5RT3$_{ANGPTL4}$ cells. PLA signals are shown in red and nuclei are stained blue by Hoechst dye. The cells were also counterstained with Alexa488-phallodin for actin stress fibers (green).

(E) Graph shows mean number of phosphorylated FAK (as shown in Figure 13D) calculated from 200 A-5RT3$_{ANGPTL4}$ and A-5RT3$_{CTRL}$ cells (n = 3; total 600 cells) using BlobFinder software (Uppsula University). Error bars represent SD. *$p < 0.05$.

(F) *In situ* PLA detection of ANGPTL4:integrin β1(activated form) A-5RT3$_{CTRL}$ cells. PLA signals are shown in red and nuclei are stained blue by Hoechst dye. The cells were also counterstained with vinculin for focal adhesion complex (green).

Negative controls were performed with only anti-nANGPTL4 (A and B) or anti-FAK (C and D) antibodies. Images were acquired in one z-plane using a Zeiss LSM710 META confocal laser scanning microscope. Scale bars represent 40 μm. Experiments were performed using tumor biopsies harvested from A-5RT3$_{CTRL}$- or A-5RT3$_{ANGPTL4}$ -inoculated (5×10^5 cells each) nude mice at wk 8. All experiments were performed three or four times with consistent results.

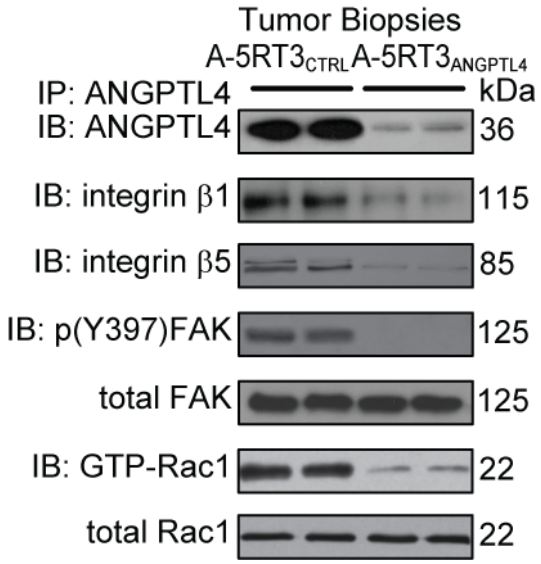

Figure 14. ANGPTL4 specifically interacts with integrins β1 and β5 to activate downstream pathways.

Immunoprecipitation and immunodetection of ANGPTL4, integrin β1, integrin β5, total FAK, phosphorylated FAK (pY397FAK), total Rac1 and GTP-bound Rac1 (GTP-Rac1), from the indicated tumor sections. A configuration-specific monoclonal anti-Rac-GTP antibody (NewEast Biosciences) was used for immunoprecipitation of GTP-Rac1. Total FAK served as a loading and transfer control. Experiments were performed using tumor biopsies harvested from A-5RT3$_{CTRL}$- or A-5RT3$_{ANGPTL4}$ -inoculated (5×10^5 cells each) nude mice at wk 8. All experiments in were repeated at least three times with consistent results.

3.5 ANGPTL4 Elevates the O_2^- Level and Maintains a High O_2^-:H_2O_2 Ratio in Tumor Cells.

ROS (e.g. O_2^- and H_2O_2) have long been recognized as important second messengers, functioning in the relay of intracellular signals in normal and cancer cells (Thannickal and Fanburg, 2000; Liou and Storz, 2010). ROS can be regulated through integrin engagement and an elevated O_2^- level or a relatively high O_2^-:H_2O_2 ratio, allowing tumor cells to survive and avoid anoikis (Pervaiz et al., 1999; Pervaiz and Clement, 2007; Pani et al., 2009; Pervaiz et al., 2009; Pani et al., 2010). In this regard, we assessed whether ANGPTL4-integrin interaction regulates ROS production in tumor cells. Using electron paramagnetic resonance spectroscopy (EPR) in combination with 5-(diethoxyphosphoryl)-5-methyl-1-pyrroline-N-oxide (DEPMPO) spin trapping, we measured a significant decrease in the O_2^- level in A-5RT3$_{ANGPTL4}$ cells compared to A-5RT3$_{CTRL}$ cells (Figure 15), suggesting that ANGPTL4 is vital in sustaining O_2^- production in tumor cells. To determine the source of O_2^-, similar experiments were performed using specific inhibitors that block the mitochondrial respiratory chain complex I and membrane-bound NADPH oxidase, which are two major producers of O_2^- in mammalian cells (Giannoni et al., 2008). Treatment of tumor cells with rotenone, a mitochondrial respiratory chain complex I inhibitor (Irani et al., 1997), did not alter their cellular O_2^- level (Figure 15), suggesting that this complex has little role in generating O_2^- in tumors. Further excluding mitochondria as the source of ANGPTL4-mediated O_2^- generation, our qPCR analysis showed no change in the expression of selected genes in the methionine/homocysteine metabolic cycle (Figure 16), as previously studied in db/db diabetic rodent hepatocytes (Wang et al., 2007). In contrast, the O_2^- level was significantly abrogated by using two different

NADPH oxidase inhibitors (Ushio-Fukai and Nakamura, 2008), diphenylene iodonium (DPI) and apocynin (Figure 15). ROS generated through the involvement of the small GTPase Rac1 and NADPH oxidase upon integrin engagement exert a mandatory role in transmitting a pro-survival signal that ensures tumor cells escape from anoikis (Joneson and Bar-Sagi, 1998; Giannoni et al., 2008). In accordance with these results, comparative immunoblot analyses of anti-cANGPTL4 immunoprecipitates from A-5RT3$_{CTRL}$- and A-5RT3$_{ANGPTL4}$-induced tumor lysates detected integrins β1 and β5, along with phosphorylated FAK and active GTP-bound Rac1, in A-5RT3$_{CTRL}$-induced tumors, but were significantly reduced in A-5RT3$_{ANGPTL4}$-induced tumors (Figure 14). To further validate the relevance of Rac1 in ANGPTL4-mediated O_2^- production, we next transiently transfected A-5RT3$_{CTRL}$ and A-5RT3$_{ANGPTL4}$ cells with dominant-negative Rac1 (T17N) and constitutively active Rac1 (G12V), respectively. We measured a significantly diminished O_2^- level in the former system and, conversely, an obviously rescued level of O_2^- production in the latter. The percentage of inhibition and recovery was consistent with the ~65% transfection efficiencies, as estimated using a GFP-expressing vector. The requirement of Rac1 suggested a Nox-dependent mechanism for O_2^- production. Thus, we examined the expression of Nox1 and Nox 2 in A-5RT3 (Figure 17A). Nox 3 is expressed predominantly in the inner ear and is involved in the biogenesis of otoconia/otoliths (Paffenholz et al., 2004). Next, we performed Nox1 and Nox2 knockdown (Nox1 kd and Nox2 kd, respectively) in A-5RT3$_{CTRL}$ and A-5RT3$_{ANGPTL4}$ cells (Figure 17B and 17C), and measured the O_2^- level using EPR (Figure 14). Our results indicated that Nox 1 NADPH oxidase is the predominant source of ANGPTL4-mediated O_2^- generation in tumor cells. As expected, the O_2^- level was completely abolished when treated with the superoxide scavenger Tiron, which serves

as a negative control for O_2^- measurements (Figure 15). These data were reproduced by a reliable chemiluminescence method using 2-methyl-6-(4-methoxyphenyl)-3,7-dihydroimidazo [1, 2-a] pyrazin-3-one hydrochloride (MCLA; Figure 18) (Munzel et al., 2002).

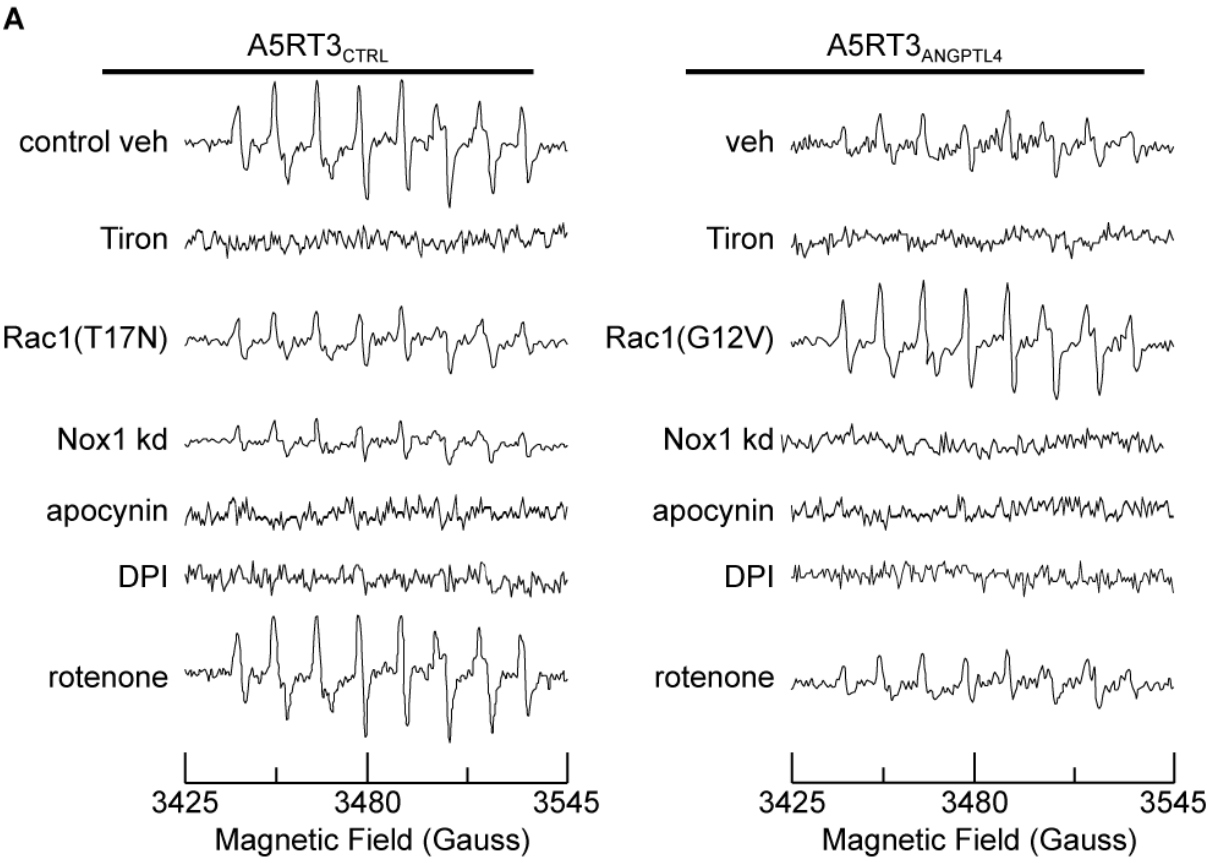

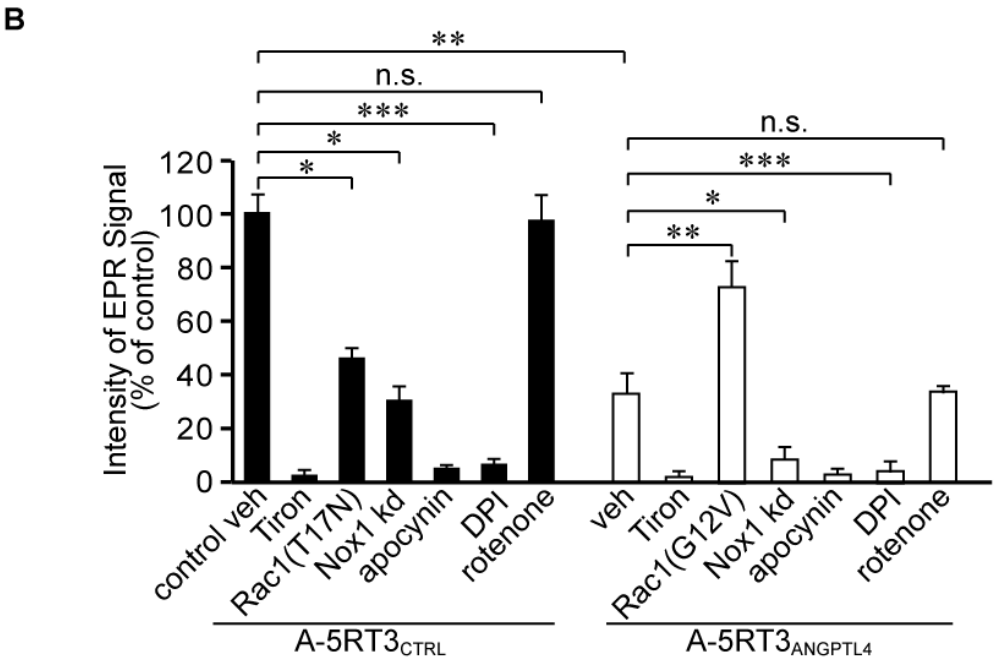

Figure 15. ANGPTL4 elevates O_2^- production in tumor cells.

(A) Representative EPR spectra of DEPMPO-superoxide spin adduct measuring O_2^- production from A-5RT3$_{CTRL}$ and A-5RT3$_{ANGPTL4}$ cells under various conditions (i.e. in the absence or presence of indicated chemicals or inhibitors; transiently transfected with vector expressing Rac1(T17N) or Rac1(G12V), respectively; transiently transfected with ON-TARGETplus siRNA (Dharmacon) against either Nox1 (Nox1 kd) or Nox2 (Nox2 kd)). The superoxide adduct of DEPMPO has hyperfine splitting constants of a_N=13.13 G; a_P=55.61 G; a^{β}_H =13.11 G; a^{γ}_H =0.71, 0.42, 0.7, 0.25, and 0.6 G.

(B) Relative EPR signal intensity at 3480 G as measured in (A). Tiron-treated measurement served as negative signal control.

All experiments were repeated at least three times with consistent results.

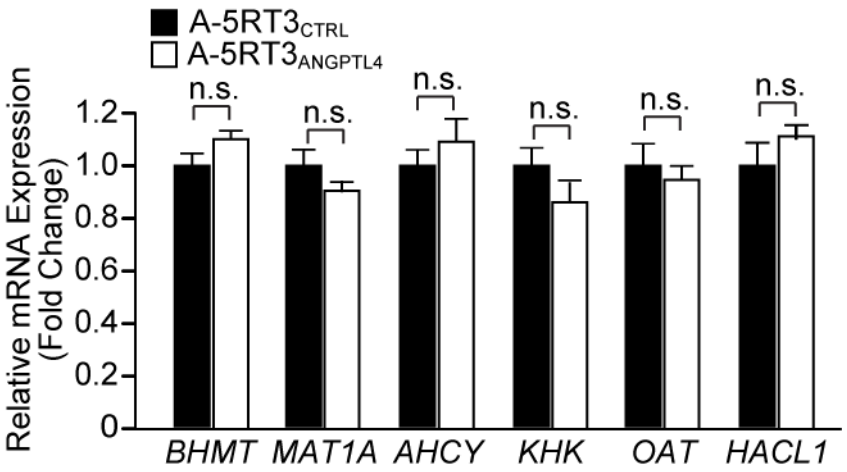

Figure 16. Suppression of ANGPTL4 has no effect in the methionine/homocysteine metabolic cycle of tumor cells.

Relative mRNA level of *BHMT*, *MAT1A*, *AHCY*, *KHK*, *OAT* and *HACL1* (representative genes in the methionine/homocysteine metabolic cycle) in A-5RT3$_{ANGPTL4}$ and A-5RT3$_{CTRL}$ cells as determined by qPCR. Experiments were repeated at least three times with consistent results.

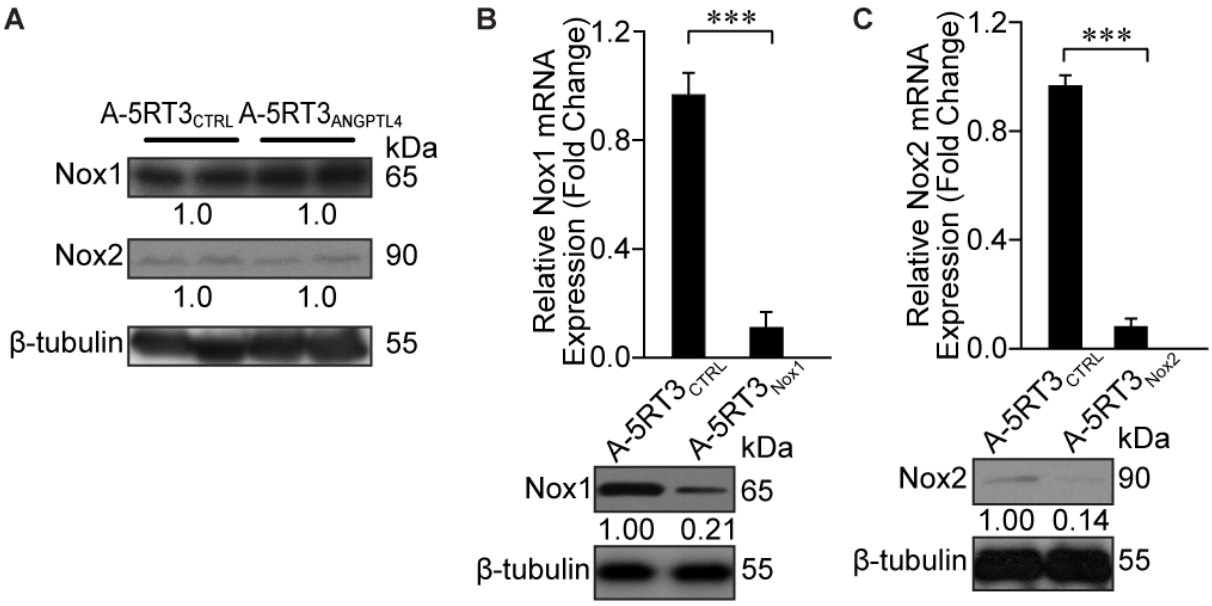

Figure 17. Suppression of Nox1 and Nox2 on tumor cells.

(A) Immunoblot of Nox1 and Nox2 in A-5RT3$_{CTRL}$ and A-5RT3$_{ANGPTL4}$ cells. β-tubulin served as a loading and transfer control.

(B and C) Relative fold change in Nox1 and Nox2 mRNA and protein levels in A-5RT3$_{CTRL}$ (scrambled control), A-5RT3$_{Nox1}$ (Nox1 knockdown) and A-5RT3$_{Nox2}$ (Nox2 knockdown) cells. All experiments were repeated at least three times with consistent results.

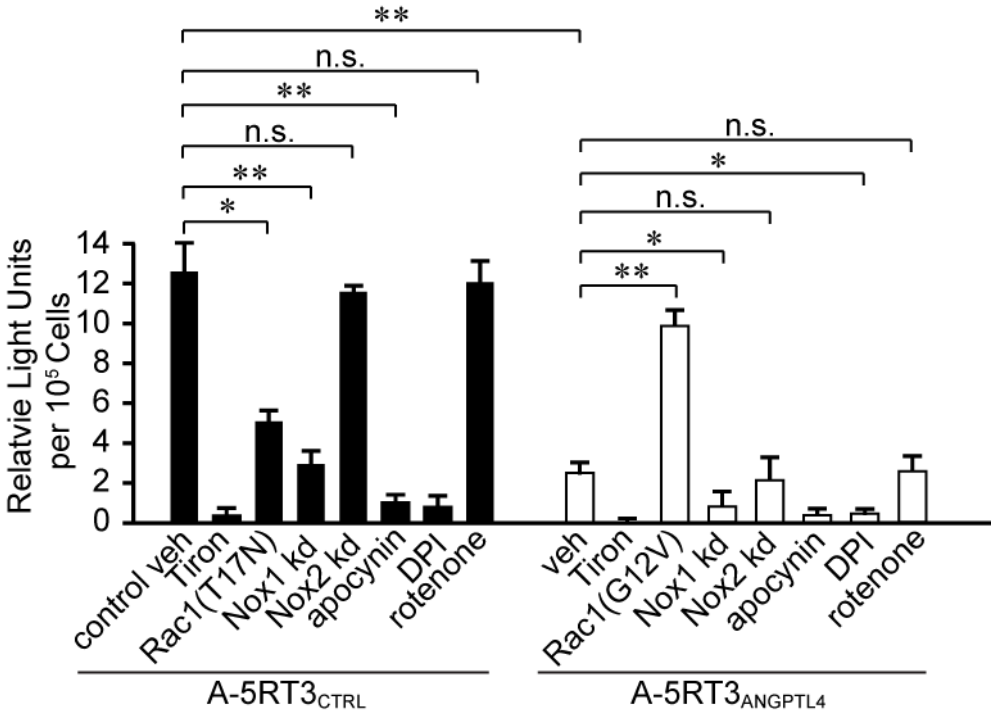

Figure 18. ANGPTL4 elevates O_2^- production in tumor cells (measured by MCLA).

Measurement of O_2^- levels using the MCLA assay in A-5RT3$_{CTRL}$ and A-5RT3$_{ANGPTL4}$ cells in various conditions (i.e. in the absence or presence of indicated chemicals or inhibitors; transiently transfected with vector expressing Rac1(T17N) or Rac1(G12V), respectively; transiently transfected with ON-TARGETplus siRNA (Dharmacon) against either Nox1 (Nox1 kd) or Nox2 (Nox2 kd)). A-5RT3$_{CTRL}$ treated with control veh and Tiron were used as positive and negative controls, respectively. Values were normalized to total proteins and presented as means ± SEM. Experiments were repeated at least three times with consistent results.

Next, we measured the level of H_2O_2 in tumor cells in the presence of a specific catalase inhibitor, 3-amino-l, 2, 4-triazole (Chance et al., 1979; Wagner et al., 2005). H_2O_2 levels in the A-5RT3$_{ANGPTL4}$ line were significantly higher than in A-5RT3$_{CTRL}$ cells (Figure 19A). Nox1 knockdown did not affect the H_2O_2 level, suggesting that ANGPTL4 modulated H_2O_2 production via a linked as-yet-unknown mechanism (Figure 19B). Notably, the lower O_2^- level and O_2^-:H_2O_2 ratio was concurrent with threefold more apoptosis and significantly enhanced caspase activities within 2 h of anoikis in A-5RT3$_{ANGPTL4}$ cells compared to A-5RT3$_{CTRL}$ cells (Figures 10B, 10C, 15 and 19A). Accordingly, we observed a reduced O_2^- level in A-5RT3$_{ANGPTL4}$-induced tumors compared to A-5RT3$_{CTRL}$-induced tumors, as determined by EPR (Figure 20), which was associated with increased apoptosis (Figure 9).

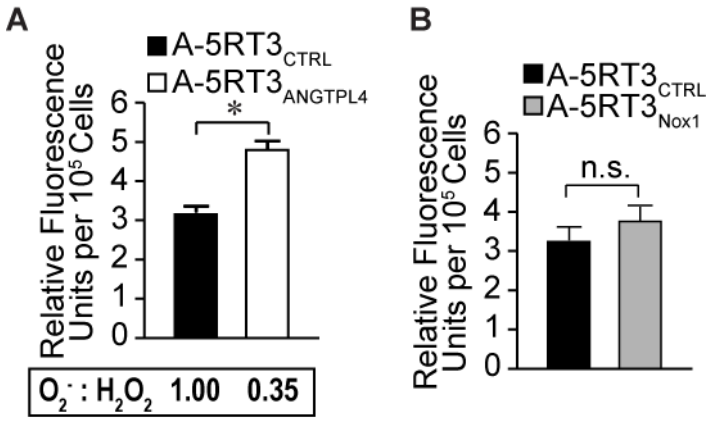

Figure 19. Suppression of ANGPTL4 but not Nox1 affects H_2O_2 Level in tumor cells.

Measurement of H_2O_2 levels using the Amplex red assay in comparison between A-5RT3$_{CTRL}$ and A-5RT3$_{ANGPTL4}$ cells (A), or between A-5RT3$_{CTRL}$ and A-5RT3$_{Nox1}$ cells (B). Arbitrary relative O_2^-:H_2O_2 ratios are shown in boxes (A). Values were normalized to total proteins and presented as means ± SEM. All experiments were repeated at least three times with consistent results. *$p < 0.05$; n.s. represents not significant.

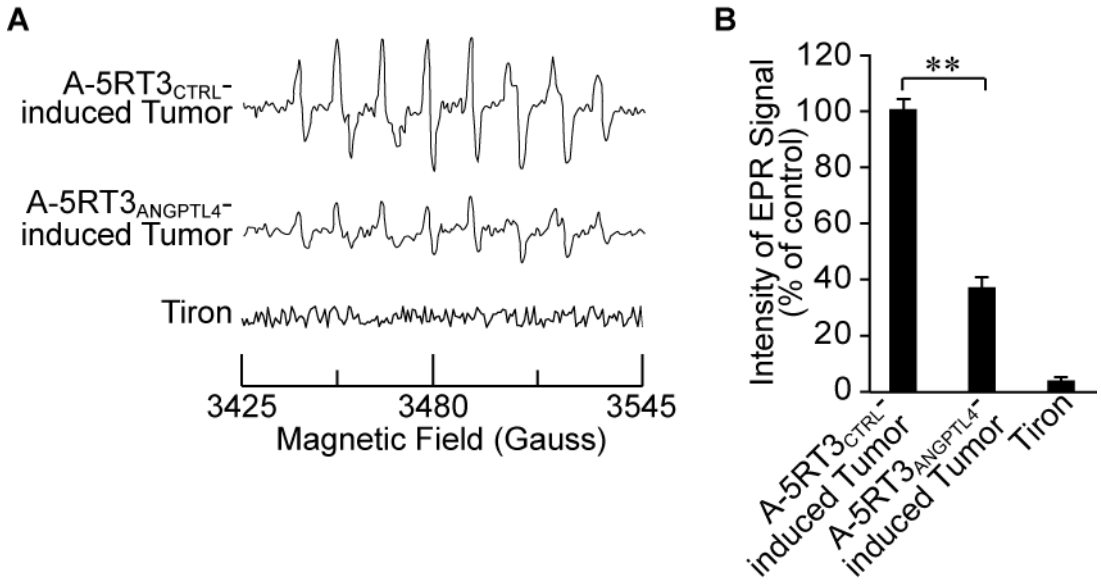

Figure 20. Suppression of ANGPTL4 reduces O_2^- level in tumor.

(A) Representative EPR spectra of DEPMPO-superoxide spin adduct from A-5RT3$_{CTRL}$- and A-5RT3$_{ANGPTL4}$-induced tumor biopsies. The superoxide adduct of DEPMPO has hyperfine splitting constants of a_N=13.13 G; a_P=55.61 G; a^{β}_H =13.11 G; a^{γ}_H =0.71, 0.42, 0.7, 0.25, and 0.6 G.

(B) EPR signal intensity at 3480 G measured in (A). Tiron-treated measurements served as negative signal controls. All experiments were repeated at least three times with consistent results. **$p < 0.01$.

To underscore the relevance of these findings to other cancers, similar experiments were performed using the breast cancer line MDA-MB-231, after using the monoclonal antibody mAb11F6C4 to dose-dependently neutralize endogenous cANGPTL4. We showed earlier that mAb11F6C4 was able to block cANGPTL4-integrin interaction (Figures 12C-H). Consistent with the above results, the immunosuppression of cANGPTL4 in MDA-MB-231 reduced the O_2^- level (Figure 21), lowered the O_2^-:H_2O_2 ratio (Figure 22A), and enhanced apoptosis (Figure 22B) and caspase activities (Figure 22C). The knockdown of Nox1 (Figure 23B) but not Nox2 reduced ANGPTL4-mediated O_2^- production (Figure 21) with little effect on H_2O_2 production (Figure 23D).

Taken together, these findings indicate that ANGPTL4 may protect tumor cells from anoikis via an NADPH oxidase-dependent O_2^- generation mechanism.

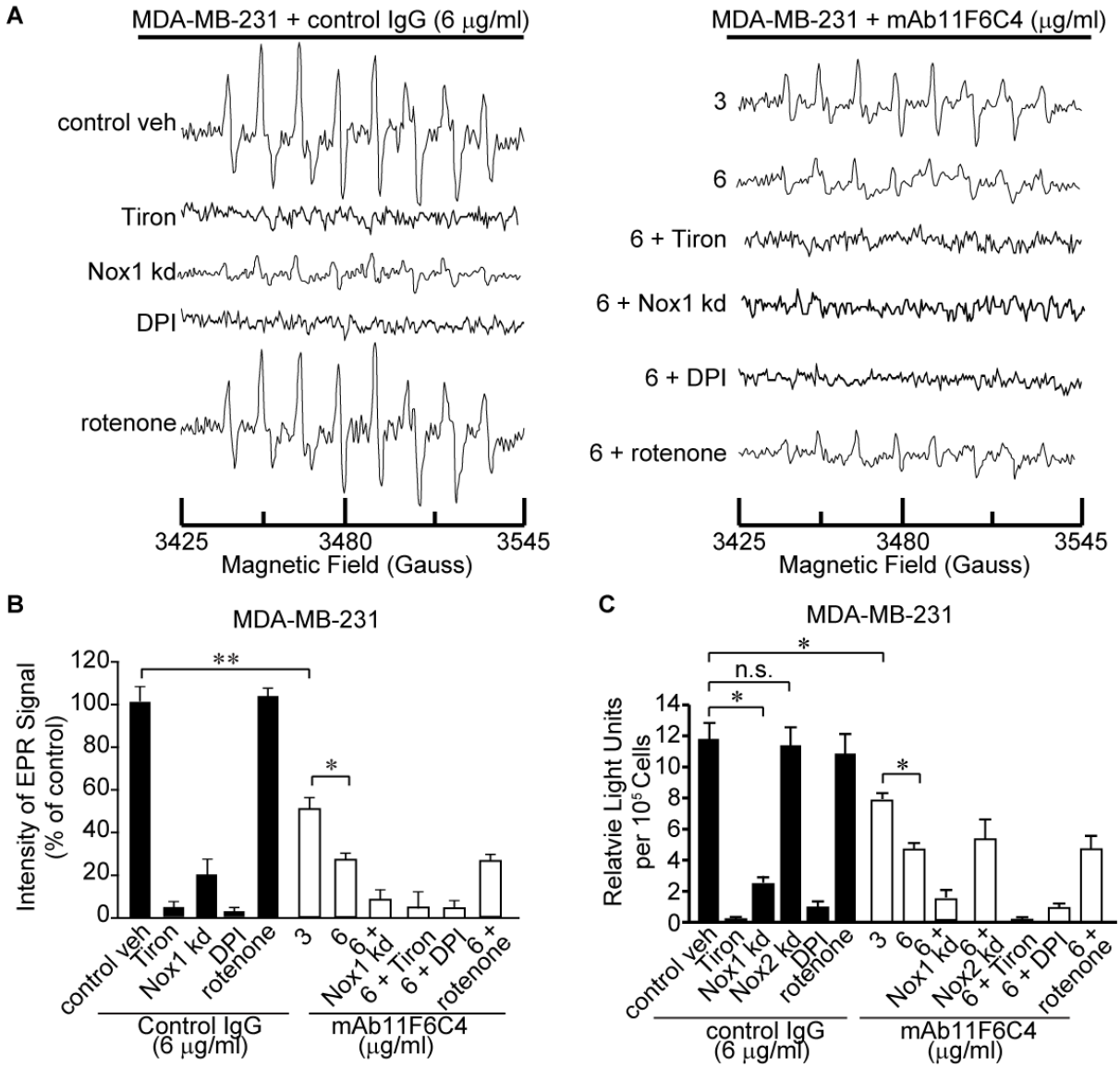

Figure 21. Immunosuppression of cANGPTL4 reduces the O_2^- in MDA-MB-231 tumor cells.

(A) Representative EPR spectra of DEPMPO-superoxide spin adduct measuring O_2^- production in MDA-MB-231 cells treated with mAb11F6C4 (3 or 6 µg/ml) or control IgG (6 µg/ml) under various conditions (i.e. in the absence or presence of indicated chemicals or inhibitors; transiently transfected with ON-TARGETplus siRNA (Dharmacon) against either Nox1 (Nox1 kd)). The superoxide adduct of DEPMPO has hyperfine splitting constants of a_N=13.13 G; a_P=55.61 G; a^{β}_H=13.11 G; a^{γ}_H=0.71, 0.42, 0.7, 0.25, and 0.6 G.

(B) EPR signal intensity at 3480 G measured in (A).

(C) Measurement of O_2^- levels using the MCLA assay in MDA-MB-231 cells treated with mAb11F6C4 (3 or 6 µg/ml) or control IgG (6 µg/ml) under various conditions (i.e. in the absence or presence of indicated chemicals or inhibitors; transiently transfected with ON-TARGETplus siRNA (Dharmacon) against either Nox1 (Nox1 kd) or Nox2 (Nox2 kd)).

Tiron was used as negative control. Values were normalized to total proteins and presented as means ± SEM. Experiments were repeated at least three times with consistent results.

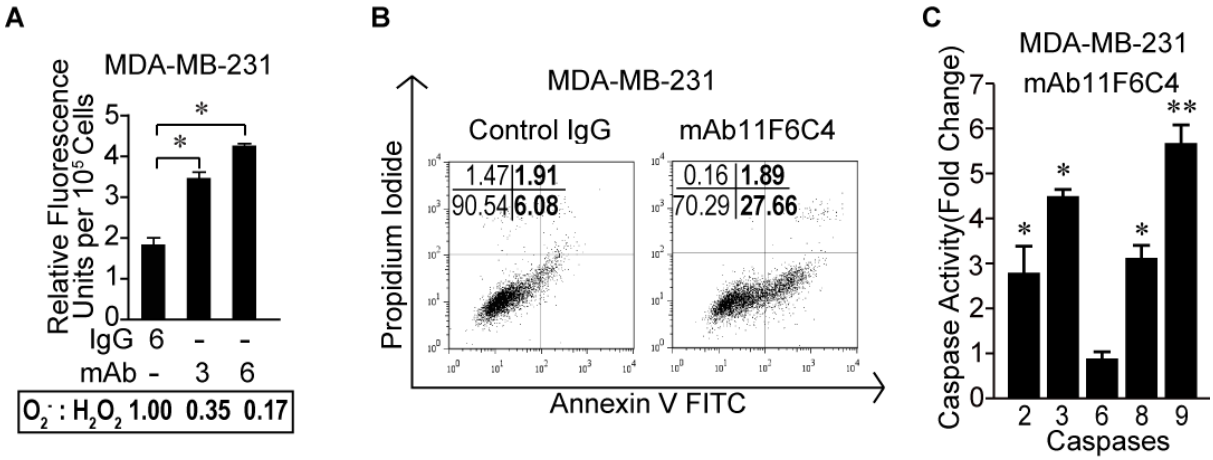

Figure 22. Immunosuppression of cANGPTL4 lowers the O_2^-:H_2O_2 ratio, and enhances apoptosis and caspase activities in MDA-MB-231 tumor cells.

(A) Measurement of H_2O_2 levels using the Amplex red assay in MDA-MB-231 cells treated with mAb11F6C4 (3 or 6 µg/ml) or control IgG (6 µg/ml). Arbitrary relative O_2^-:H_2O_2 ratios are shown in boxes.

(B) Percentage of apoptotic MDA-MB-231 after 2 h of anoikis as analyzed by FACS (5000 events). Apoptotic index is described in (Figure 10B). Values (bold) denote apoptotic cells (%) from three independent experiments.

(C) Relative activities of caspases 2, 3, 6, 8 and 9 in mAb11F6C4-treated MDA-MB-231 cells after 2 h of anoikis. Values (means ± SD) are from three independent experiments performed in triplicate. *$p < 0.05$; **$p < 0.01$. Fold-increase in caspase activity was calculated by comparison to pre-immune IgG-treated MDA-MB-231 cells.

Values were normalized to total proteins and presented as means ± SEM. Experiments were repeated at least three times with consistent results.

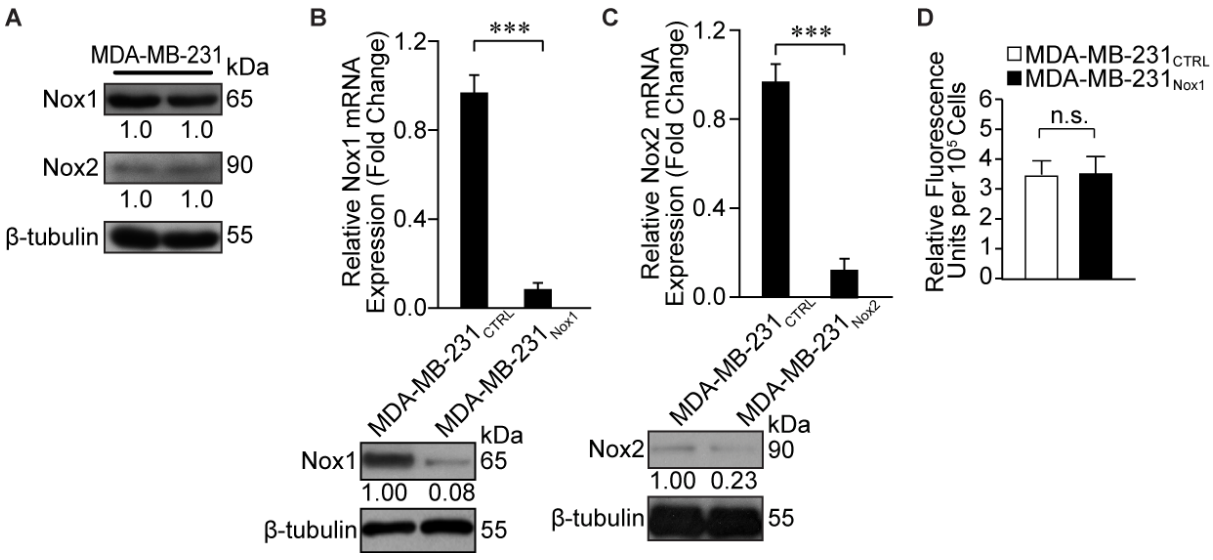

Figure 23. Suppression of Nox1 and Nox2 in MDA-MB-231 tumor cells.

(A) Immunoblot of Nox1 and Nox2 in MA-MB-231 cells. β-tubulin served as a loading and transfer control.

(B and C) Relative fold change in Nox1 and Nox2 mRNA and protein levels in MA-MB-231$_{CTRL}$ (scrambled control), MA-MB-231$_{Nox1}$ (Nox1 knockdown) and MA-MB-231$_{Nox2}$ (Nox2 knockdown) cells.

(D) Measurement of H_2O_2 levels using the Amplex red assay in the comparison between MA-MB-231$_{CTRL}$ and MA-MB-231$_{Nox1}$ cells. Values were normalized to total proteins and presented as means ± SEM.

All experiments were repeated at least three times with consistent results. ***$p < 0.001$.

3.6 ANGPTL4-mediated O_2^- Activates the Src, PI3K/PKBα and ERK Survival Pathways.

Reports have shown that ROS produced via integrin engagement oxidizes and activates Src, which stimulates the ERK and PKBα pro-survival pathways (Werner and Werb, 2002; Giannoni et al., 2008; Pani et al., 2009; Giannoni et al., 2009; Pani et al., 2010). Both pathways regulate the subcellular localization or stability of BH3-only apoptotic proteins (e.g. Bad and Bim), which are essential for executing anoikis (Bouillet and Strasser, 2002). Thus, we asked whether ANGPTL4-integrin engaged O_2^- generation employs these downstream signaling pathways to modulate tumor cell behavior. Indeed, immunoblot analyses revealed significantly diminished expression of oxidized/activated Src, phosphorylated PKBα and ERK1 in A-5RT3$_{ANGPTL4}$-induced tumors and A-5RT3$_{ANGPTL4}$ cells (Figures 24A and left panel of 24B). Similar immunoblot analyses performed in the presence of DPI and with Nox1 kd cells, which attenuate ANGPTL4-mediated O_2^- production, revealed severely diminished Src, PKBα and ERK1 activation, emphasizing the role of O_2^- in their activities (Figure 24B). The inhibition of PI3K by LY29402 and Wortmannin, a pivotal upstream mediator of PKBα, caused significantly (four-fold) more apoptosis of tumor cells within 2 h of anoikis challenge, reaching levels comparable to those of A-5RT3$_{ANGPTL4}$ cells (Figure 24C). In addition, inhibition of MEK1/2, the upstream signal of ERK1, by PD98059 also resulted in a significant enhancement of apoptotic cell numbers upon anoikis challenge, albeit to a lesser extent (~50%) compared to PI3K inhibitors (Figure 24C). These results suggest that the PI3K/PKBα and ERK1/2 downstream survival pathways are modulated and exploited by ANGPTL4 engagement in tumor cells, the former being the predominant pathway.

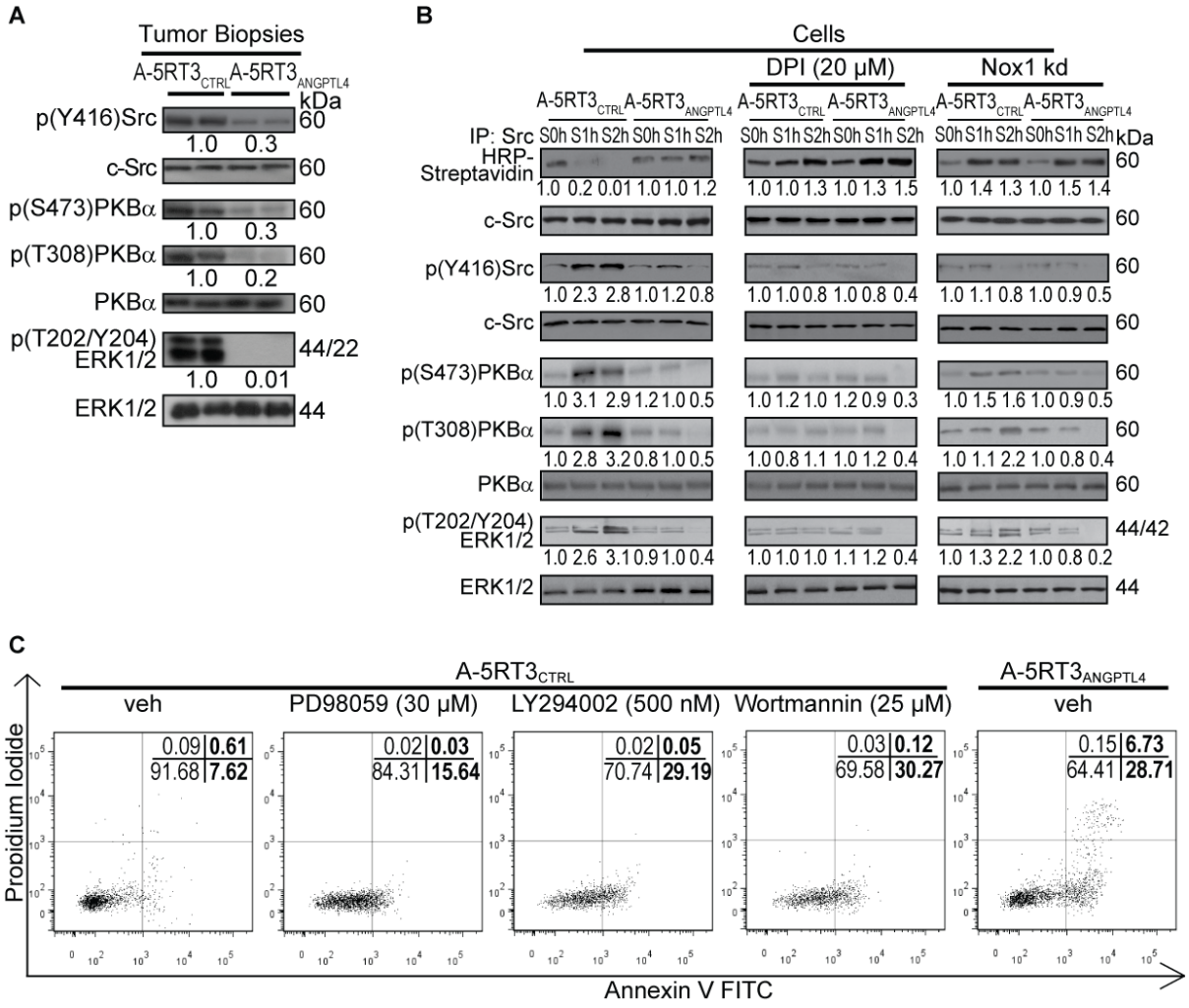

Figure 24. ANGPTL4-mediated O_2^- regulates Src and promotes the PI3K/PKBα and ERK survival pathways.

(A) Immunoblot of the indicated proteins in A-5RT3$_{ANGPTL4}$- and A-5RT3$_{CTRL}$-induced tumor biopsies. c-Src served as loading and transfer controls.

(B) Immunoblot of the indicated proteins in A-5RT3$_{ANGPTL4}$ and A-5RT3$_{CTRL}$ cells in the absence or presence of 20 μM DPI, and in Nox1 kd A-5RT3$_{ANGPTL4}$ and A-5RT3$_{CTRL}$ cells. The cells were suspended for 0, 1 and 2 h (S0h, S1h and S2h). Cell lysates were labeled with 100 μM *N*-(biotinoyl)-*N'*-(iodoacetyl) ethylenediamine to evaluate the Src redox state. An HRP-Streptavidin immunoblot performed on the anti-Src immunoprecipitate showing reduced Src. The immunoprecipitate was probed with anti-c-Src for normalization. Values (mean ± SD) represent the mean fold change against the values at respective S0h.

(C) Percentage of apoptotic A-5RT3$_{ANGPTL4}$ and A-5RT3$_{CTRL}$ cells, treated with either MEK inhibitor PD98059 or PI3K inhibitors LY294002 and Wortmannin, after 2 h of anoikis challenge and analyzed by FACS (5000 events).

All experiments were repeated at least three times with consistent results.

The 14-3-3 adaptor protein is known to act downstream of the above survival pathways by sequestering pro-apoptotic Bad from the mitochondria to prevent apoptosis (She et al., 2005). In agreement with these previous findings, the number of 14-3-3/Bad complexes and 14-3-3β/σ proteins was significantly reduced by ~70% in A-5RT3$_{ANGPTL4}$-induced tumors (Figure 25). The Na^+/H^+ exchanger 1 (NHE), which positively influences cell proliferation by maintaining an alkaline intracellular environment (Shibanuma et al., 1988; Akram et al., 2006) was also diminished in A-5RT3$_{ANGPTL4}$-induced tumors (Figure 25D), indicating that NHE plays a subsidiary role in ANGPTL4-mediated tumor cell growth. Upon oxidant challenge in tumor cells, the induction of superoxide dismutase (SOD) expression is muted, allowing tumor cell proliferation (Oberley, 2001; Pervaiz and Clement, 2007). In agreement with these studies, we found that expression of the cytosolic Zn/CuSOD was significantly enhanced in A-5RT3$_{ANGPTL4}$-induced tumors (Figure 25D), which indirectly contribute to the reduced O_2^-:H_2O_2 ratio in ANGPTL4-deficient tumor cells (see Figures 15, 18 and 19).

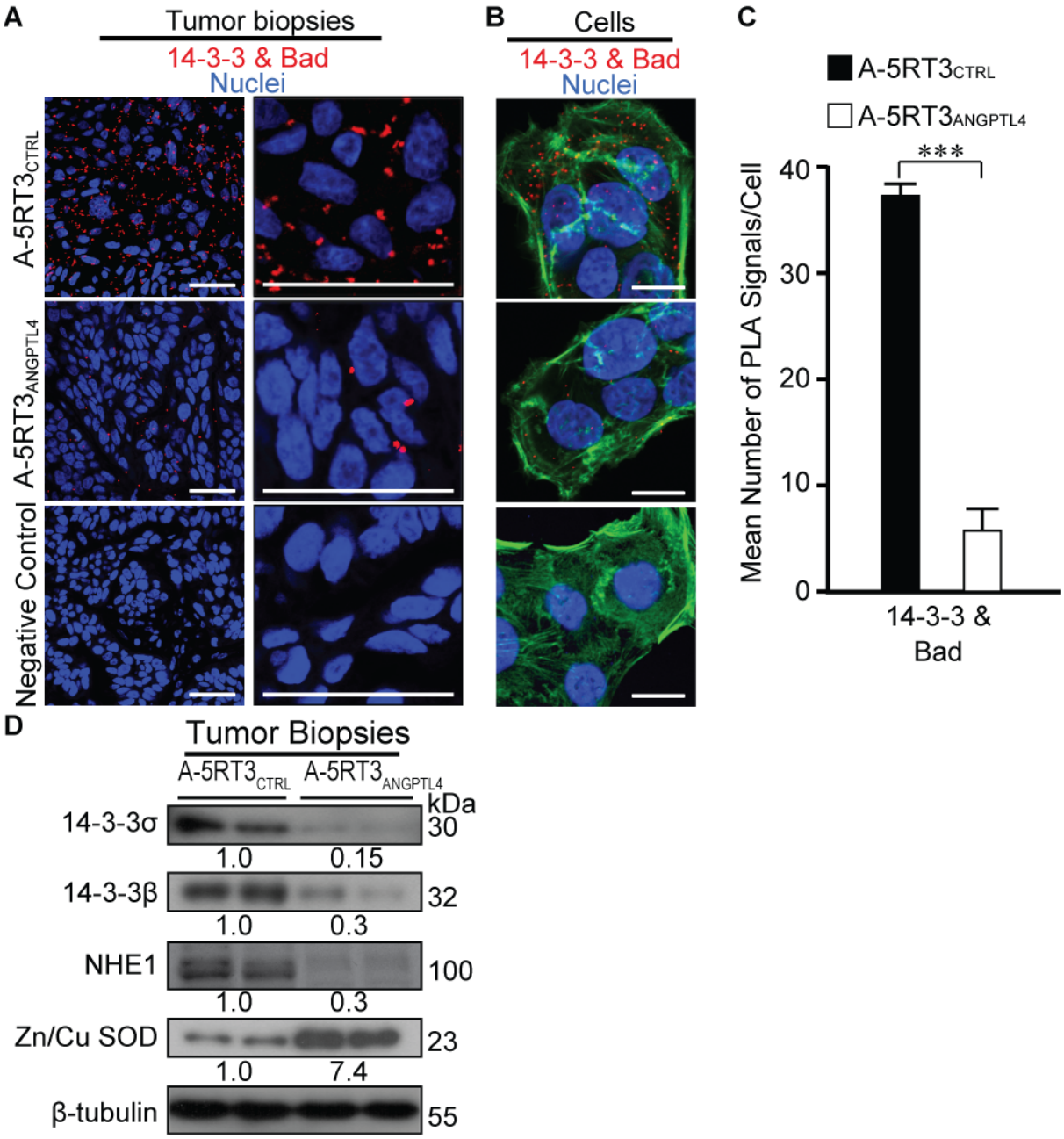

Figure 25. ANGPTL4-mediated O_2^- regulates players downstream of PI3K/PKBα and ERK survival pathways.

(A and B) *In situ* PLA detection of 14-3-3:Bad complexes in the indicated tumor sections (A) and cells (B). PLA signals are red dots and Hoechst stained nuclei are blue. The cells were counterstained with Alexa488-phallodin for actin stress fibers (green). Negative controls were performed with only anti-14-3-3 antibodies. Data shown are representative of three independent experiments. Scale bars represent 40 μm.

(C) Mean number of 14-3-3:Bad complexes (as shown in (B)) was calculated from 200 cells (n = 3; 600 cells total) using BlobFinder software. Error bars represent the SD. ***$p < 0.001$.

(D) Immunoblot of the indicated proteins in A-5RT3$_{ANGPTL4}$- and A-5RT3$_{CTRL}$-induced tumor biopsies. Values represent the mean fold change from four independent experiments. β-tubulin served as loading and transfer control.

3.7 ANGPTL4 Deficiency Abrogates O_2^- Production and Sensitizes Cancer Cells to Anoikis.

Our results revealed that the suppression of ANGPTL4, either by constitutive RNAi (Figure 15 and 18) or immunosuppression with mAb11F6C4 (Figure 21), results in a dose-dependent reduction of O_2^- levels. To underscore the importance of ANGPTL4 in the regulation of O_2^- production, maintenance of a high O_2^-:H_2O_2 ratio, and hence tumor survival, we examined the impact of reduced ANGPTL4 on anoikis in nine different cancer cell lines, in addition to A-5RT3 and MDA-MB-231 cells. Treatment with mAb11F6C4, which blocked cANGPTL4-integrin interaction, resulted in a dose-dependent reduction of O_2^- levels (40-80% for 6 µg/mL mAb11F6C4; Figure 26), a reduction in the O_2^-:H_2O_2 ratio (70-90% for 6 µg/mL mAb11F6C4; Figure 27), a three- to eight-fold increase in the activities of caspases 2, 3, 8 and 9 (Figure 28) and 30-60% more apoptotic tumor cells (Figure 29A), all indicating weakened anoikis resistance and further corroborating our previous observations with A-5RT3 and MDA-MB-231 cells. A higher percentage of apoptotic tumor cells were also observed using inducible RNAi against ANGPTL4 in the MDA-MB-231 line (Figure 29B). These findings indicate that ANGPTL4-mediated O_2^- production for anoikis resistance may be a common feature in tumor cells.

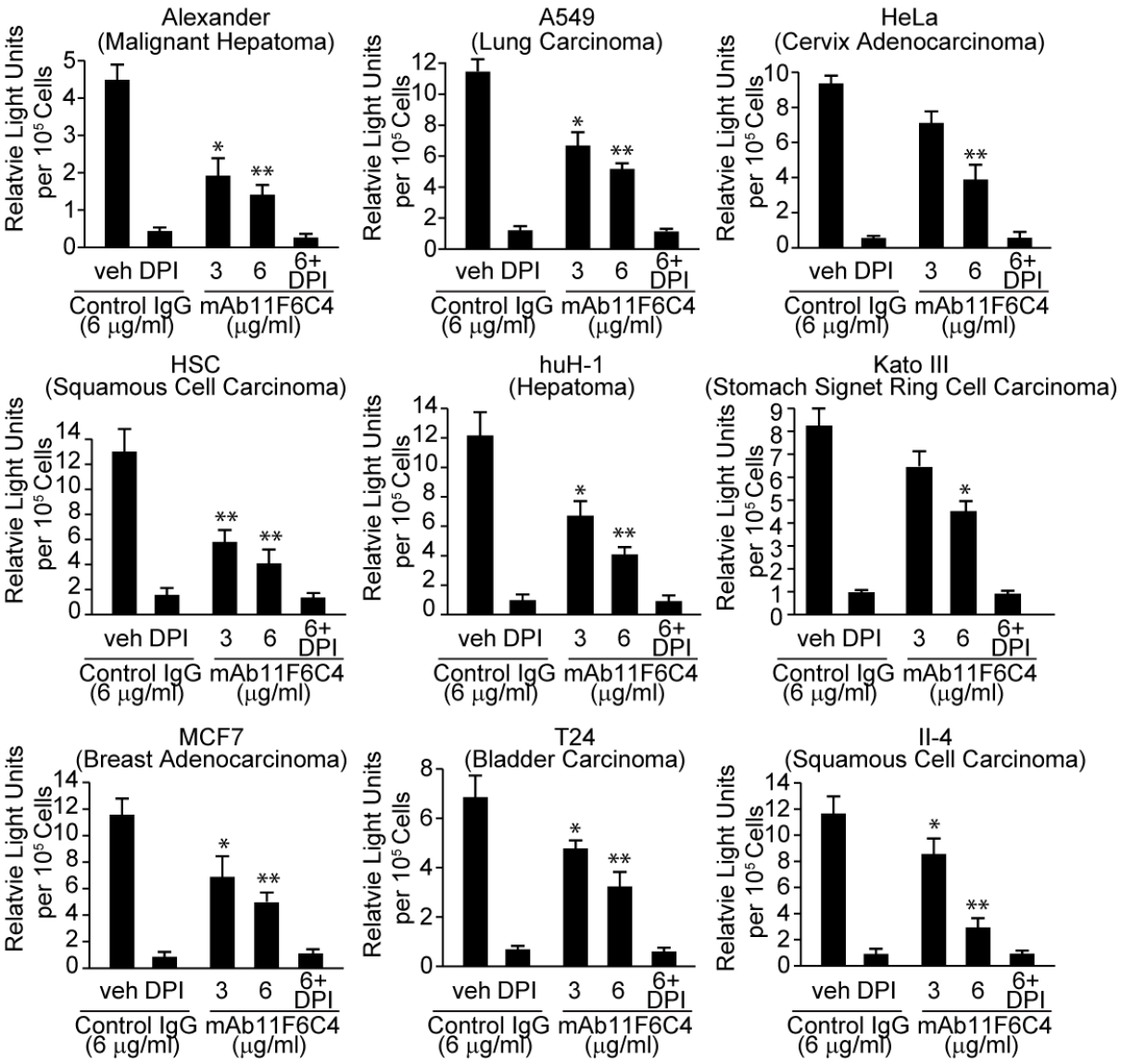

Figure 26. ANGPTL4 upregulates O_2^- production in nine tumor cell lines.

Measurement of O_2^- levels in nine different tumor lines using a chemiluminescence MCLA assay. Values (mean ± SD) are normalized to the total protein content. Three independent experiments were performed with consistent results. *p < 0.05; **p < 0.01.

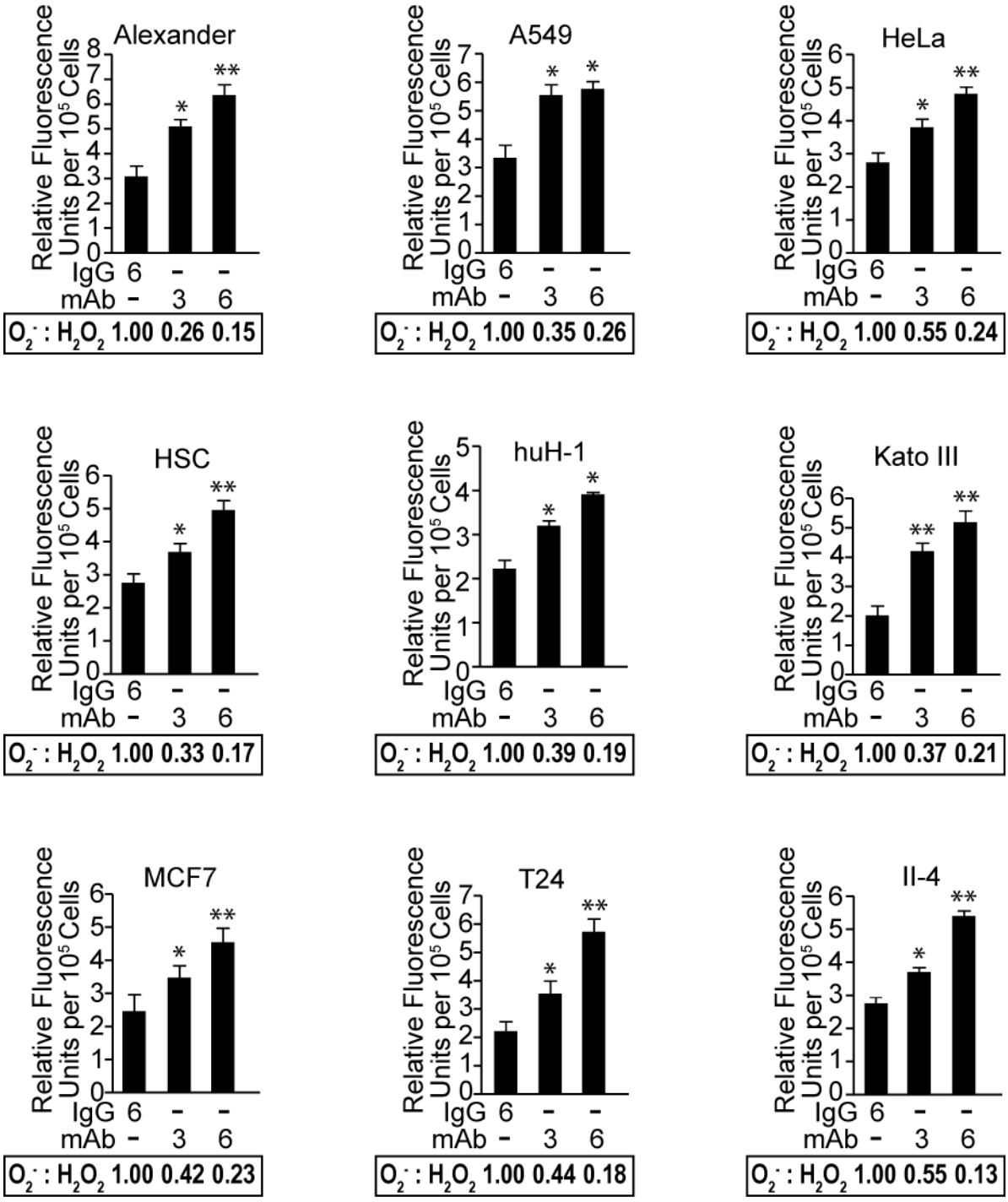

Figure 27. ANGPTL4 maintains a relatively high O_2^-:H_2O_2 ratio in nine tumor cell lines.

Measurement of H_2O_2 levels in nine different tumor lines using the Amplex red assay, in the presence of the specific catalase inhibitor, 3-amino-l, 2, 4-triazole. Arbitrary relative O_2^-:H_2O_2 ratios are shown in boxes. Values (mean ± SD) are normalized to the total protein content. Three independent experiments were performed with consistent results. *$p < 0.05$; **$p < 0.01$.

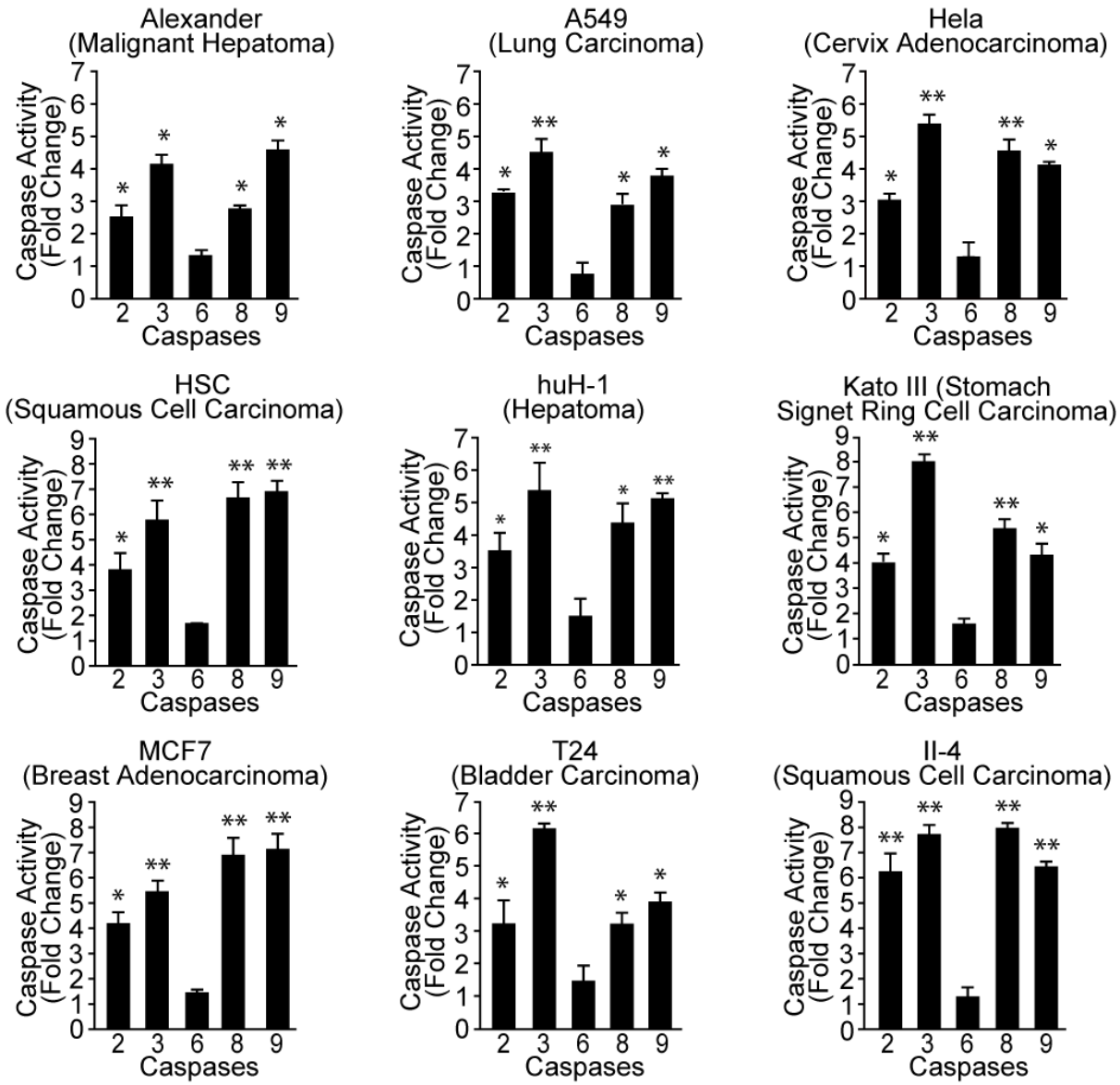

Figure 28. Deficiency of ANGPTL4 activates caspase activities in nine tumor cell lines.

Relative activities of caspases 2, 3, 6, 8 and 9 were measured after 2 h of anoikis. Fold-increase of caspase activities in mAb11F6C4 (6 μg/ml)-treated cells was calculated by comparing with the caspase activities of cells treated with pre-immune IgG (6 μg/ml). Values (mean ± SD) were obtained from at least three independent experiments with consistent results.*$p < 0.05$; **$p < 0.01$.

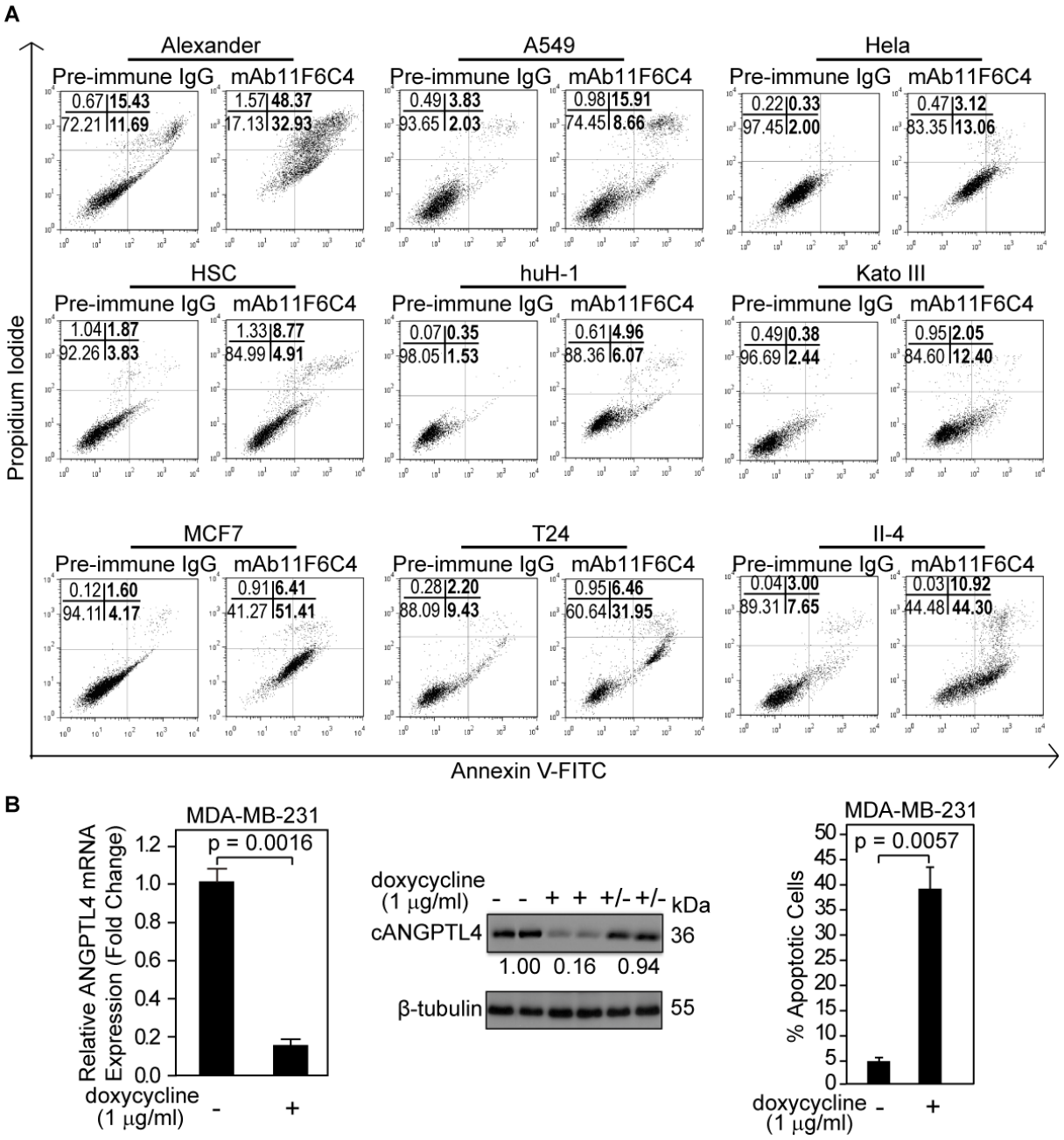

Figure 29. Suppression of ANGPTL4 induces apoptosis upon anoiks in various tumor cell lines.

(A) Apoptotic cells (%) in nine different tumor cell lines after 2 h of anoikis as analysed by FACS analysis (5000 events). Cells were treated with 10 μg/ml of control IgG or mAb11F6C4. Apoptotic index is as described in Figure 10B.

(B) Relative ANGPTL4 mRNA (left panel) and protein (middle panel) levels in MDA-MB-231, whose ANGPTL4 suppression was doxycycline-inducible. A stable MDA-MB-231 line that expresses an anti-ANGPTL4 shRNA was produced using the Knockout Singe Vector System (Clontech). Cells were grown in the absence (-) or presence (+) of doxycycline (1 μg/ml) for 24 h. +/- denotes the removal of doxycycline after 24 h of treatment. The right panel shows the percentage of apoptotic MDA-MB-231 cells as evaluated by anoikis assay. Data were obtained from three independent experiments with consistent results. $p < 0.05$.

4. DISCUSSION

It is known that in response to microenvironmental stresses such as hypoxia and chronic inflammation, tumor cells exploit various signaling molecules to promote their growth, invasiveness and metastasis (Balkwill and Mantovani, 2001; Coussens and Werb, 2002; Finger and Giaccia, 2010; Reuter et al., 2010). The loss of dependence on integrin-mediated ECM contact for growth (i.e., anoikis resistance) is an essential feature of tumor cells, but the mechanism by which anoikis resistance is acquired is a central problem in cancer biology (Hanahan and Weinberg, 2000; Chiarugi, 2003; Guo and Giancotti, 2004 Chiarugi and Giannoni, 2005; Chiarugi, 2008; Chiarugi and Giannoni, 2008). Our study demonstrated a novel role for tumor-secreted ANGPTL4, which conferred anoikis resistance to tumors via autocrine adhesion mimicry that stimulates a redox-based pro-survival pathway (Figure 30). Tumor-secreted ANGPTL4 interacted with integrins in an autocrine fashion to stimulate NADPH oxidase-dependent generation of $O_2^{\cdot-}$, promoting a high $O_2^{\cdot-}$:H_2O_2 ratio, and consequently activating downstream PI3K/PKBα and ERK. Our findings identify ANGPTL4 as an important novel redox player in cancer biology and suggest that anticancer therapeutics focused on redox-based apoptosis induction in tumors represent an exciting and viable strategy.

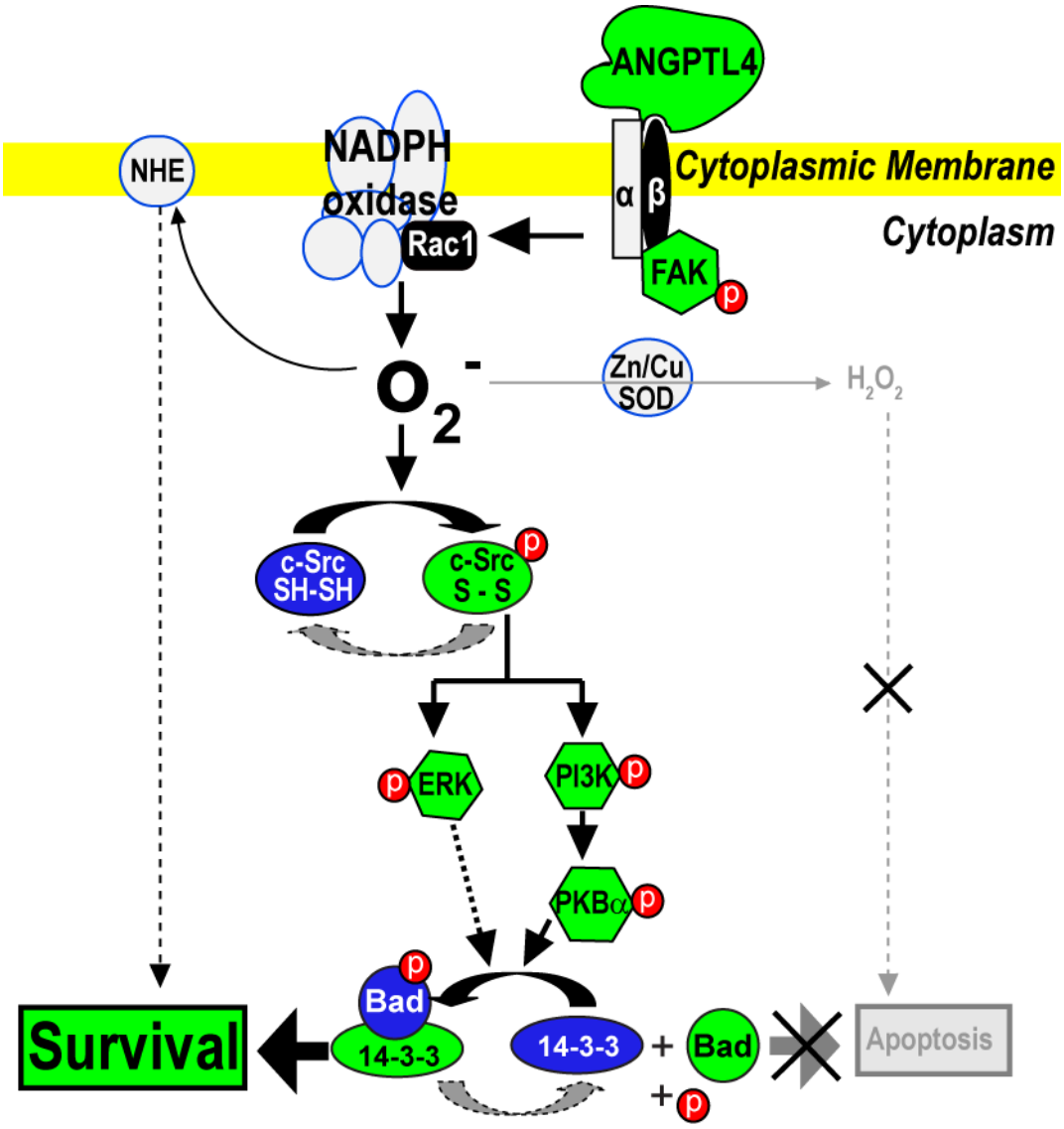

Figure 30. Schematic outline of ANGPTL4-mediated regulation of O_2^- production in tumors.

In an autocrine manner, tumor-derived ANGPTL4 specifically binds to integrins β1 or β5 and subsequently activates FAK and Rac1 activities, which further activates the NADPH oxidase-dependent generation of "*onco-ROS*" O_2^-, promoting a relatively high O_2^-:H_2O_2 ratio in tumor cells. This pro-oxidant intracellular milieu, which may subsidiary maintained through NHE, favors cell survival and proliferation by oxidizing/activating the Src machinery and therefore stimulates its downstream PI3K/PKBα- and ERK-mediated survival pathways. This further triggers the 14-3-3 adaptor protein to sequester pro-apoptotic Bad from mitochondria to prevent apoptosis and favor cell survival.

ANGPTL4 belongs to a group of secreted factors that has emerged to play important roles in lipid and glucose metabolism (Oike et al., 2005). Recently, our group found that ANGPTL4 interacts with specific integrins to modulate the signals that regulate cell migration and wound healing, two physiological aspects closely related to cancer metastasis (Goh et al., 2010a; Goh, 2010b). However, the biological importance of ANGPTL4 in tumor growth and spread has been poorly explored and underreported, leading to conflicting ideas regarding its precise role. To date, ANGPTL4 has been reported to be expressed in some human tumors, however, an extensive study of its expression profile in various human tumors is necessary. Consistent with few early findings, our data shows that elevated ANGPTL4 expression is a common feature of most known human tumor types. In addition, the tissue-specific and tumor-stage-dependent expression pattern indicated that ANGPTL4 may exert different effects in different stages of cancer progression. Full-length ANGPTL4 protein is proteolytically cleaved, giving rise to the N-terminal coiled-coil domain (nANGPTL4) and the C-terminal fibrinogen-like domain (cANGPTL4) fragments. Depending on the tissue examined, differential expression of the various domains of ANGPTL4 was observed (Kersten et al., 2000). These observations raise the intriguing possibility that the different domains of ANGPTL4 have distinct biological functions. It is now well-established that nANGPTL4 mediates its own oligomerization and binds to lipoprotein lipase to modulate lipoprotein metabolism (Li, 2006; Sukonina et al., 2006). In contrast, cANGPTL4 exists as a monomer, and its function is currently unknown. Furthermore, how cANGPTL4 triggers intracellular signaling to propagate its biological effect remains an unsolved question, hampering our understanding of the role of ANGPTL4. Our study showed that only cANGPTL4 was detected and elevated in many human tumor

cells, implying that the truncated cANGPTL4 is particularly essential for tumor cell growth. The predominant source of ANGPTL4 in tumors is the highly proliferative epithelial cells (apart from the stromal cells), indicating an autocrine manner of action for ANGPTL4 in tumors. Tumor epithelial cell-secreted cANGPTL4 specifically binds to integrins β1 and β5 on tumor cells and activates FAK and Rac1, which further stimulate NADPH oxidase-mediated O_2^- production via an autocrine pathway. However, it is conceivable that in tissues expressing high levels of cANGPTL4 at close proximity to the tumor site may transmit a paracrine signal. Although integrins alone are not oncogenic, integrin-mediated signalling is often required to enable tumor survival and influence tumor growth (Desgrosellier and Cheresh, 2010). Our findings demonstrated that ANGPTL4-mediated integrin engagement activates ROS production, which leads to a pro-survival signal and sustained anchorage-related signaling even in the absence of ECM and cell contact. The pro-oxidant intracellular environment led to redox-mediated activation of the Src machinery, and therefore stimulation of the downstream PI3K/PKBα and ERK pro-survival pathways. This further triggered the 14-3-3 adaptor protein to sequester the pro-apoptotic Bad protein from mitochondria, conferring resistance to anoikis and favoring tumor survival and growth. More importantly, our data indicate that cANGPTL4 can modulate integrin-mediated ROS signaling. This novel finding is a pivotal step toward a better mechanistic understanding of the role of ANGPTL4.

A cell's fate is determined by the cellular redox state, through a complicated regulation mechanism that is delicately maintained by intracellular ROS generators and antioxidant enzyme systems. Low or transient levels of intracellular ROS stimulate cellular signals essential for normal cellular functions. The dysregulation of intracellular ROS levels, resulting in an excessive level or persistent elevation of

ROS, has been linked to tumor growth, invasiveness and metastasis. Indeed, elevated levels of ROS are detected in almost all cancers (Liou and Storz, 2010). In line with previous reports and proposals (Pervaiz and Clement, 2007; Clement and Pervaiz, 2001), we found that not only an elevated level of O_2^- but also a high O_2^- :H_2O_2 ratio is important for cancer cells to sustain their tumorigenicity as well as their metastatic potential. Although exactly how this delicate balance is maintained remains to be investigated, our finding that the cytosolic enzyme Zn/Cu SOD expression was largely muted in A-5RT3$_{ANGPTL4}$-induced tumor may shed light on this issue (Oberley, 2001; Pervaiz and Clement, 2007). We found that the disruption of ANGPTL4-mediated redox signaling via genetic and antibody-mediated suppression of ANGPTL4 essentially reduced the activities of FAK, Rac1 and O_2^- production. These changes resulted in an increase in tumor cells' sensitivity to anoikis and impaired tumorigenesis. The $O_2^{-}\cdot$ production was measured by the reliable physical method EPR+DEPMPO spin trapping, in combination with a superoxide-sensitive chemical MCLA rather than the conventional dyes 2',7'-dichlorodihydrofluorescein diacetate (H_2DCFDA) and Dihydrorhodamine 123 (DHE), which have questionable specificities. ANGPTL4-stimulated NADPH oxidase activity, which leads to O_2^- production, can be inhibited by DPI and apocynin, two structurally and functionally distinct NADPH oxidase inhibitors (Ushio-Fukai and Nakamura, 2008; MacFarlane et al., 2009), but not by the mitochondrial complex I inhibitor rotenone. This suggests that O_2^- was “purposely” and enzymatically produced by NADPH oxidase, rather than as a by-product of mitochondrial activity. Further knockdown approaches indicated that Nox1 is the major source of O_2^- production. A dysregulated inflammatory response promotes tumorigenesis and malignancy by stimulating ROS production (Aggarwal and Gehlot, 2009; Pervaiz et al., 2009; Reuter et al., 2010). Although not

examined in this study, we cannot rule out the possibility that O_2^- requires Rac1 activation to function, such as cytosolic 5-lipooxygenase, may act in conjunction with ANGPTL4-stimulated NADPH oxidase activity to maintain an elevated intracellular O_2^- level for tumor growth (Chiarugi et al., 2003; Chiarugi, 2003; Chiarugi and Giannoni, 2005; Chiarugi and Fiaschi, 2007; Chiarugi, 2008). Two survival pathways, the PKBα and ERK, which have been shown to exert anoikis-suppressing effects (Zhan et al., 2004; Westhoff and Fulda, 2009), were both employed by ANGPTL4 to confer resistance to anoikis in tumor cells. However, numerous reports indicate that stimuli that invoke the activation of JNK, GSK3, SMAD, and EMT signaling pathways also confer anoikis resistance (Chiarugi, 2008). Therefore, it would be interesting to further investigate the involvement of ANGPTL4 in the regulation of these pathways, thus increase our comprehensive understanding of ANGPTL4 signals in the context of cancer.

The tumor microenvironment plays a pivotal role in modulating gene expression and epithelial tumor cell behavior. The tumor-promoting role of inflammation in the tumor microenvironment is well-recognized (Balkwill and Mantovani, 2001; Coussens and Werb, 2002; Aggarwal and Gehlot, 2009; Reuter et al., 2010; Chiodoni et al., 2010). The nuclear hormone PPAR, in particular the PPARγ and δ/β isotypes, play major roles in the regulation of inflammation and are implicated in tumorigenesis (Murphy and Holder, 2000; Panigrahy et al., 2005; Peters and Gonzalez, 2009; Wagner and Wagner, 2010). Although we did not observe any correlation between the expression levels of either PPARγ or β/δ, and that of their target gene ANGPTL4 in our analysis of PNS and SCCs, we cannot exclude their involvement and/or other oncogenic pathways or cell types in the tumor microenvironment that enhanced the expression of cANGPTL4 in tumors. It is also conceivable that PPARs in cancer-

associated fibroblasts play a more dominant role in the regulation of epithelial tumor growth. Indeed, we showed that PPARβ/δ-deficient fibroblasts can increase the proliferation of normal epithelial cells and SCCs via regulation of the interleukin-1 signaling pathway (Chong et al., 2009). The activation of interleukin-1 signaling enhances the growth of tumors, whereas its repression by an interleukin-1 receptor antagonist has an anti-tumor effect (Lewis et al., 2006).

Although no direct evidence has been shown, our findings and also that of others show elevated ANGPTL4 in various tumors (Ma et al., 2010; Nakayama et al., 2010; Verine et al., 2010; Wang et al., 2010; Hu et al., 2011; Nakayama et al., 2011; Zhu et al., 2011). Thus it is conceivable that the elevated ANGPTL4 could be a pre-malignant event in addition to its role in tumor survival. Indeed, our finding that hypoxic condition, which is similarly observed in tumor microenviorment, is closely correlated to the expression level of ANGPTL4. Our previous findings and others also demonstrate that ANGPTL4 is significantly elevated and involved during the wound healing process (Goh et al., 2010b) and inflammation (Gonzalez-Muniesa et al., 2010; Lichtenstein et al., 2010; Lu et al., 2010). And cancer is closely related to inflammation (Hanahan and Weinberg, 2011) and often considered as a chronic wound that never heals (Dvorak, 1986). It seems rather than pure coincidence but potentially related between the facts that both the wounding and tumorous epithelial cells secrete significant high amount of ANGPTL4. Nonetheless, in order to uncurtain this mystery, intensive in-depth studies and elegant experimental strategies are warranted.

In summary, our present study shows that ANGPTL4 is crucial for the survival and growth of tumor cells. We show that elevated expression of ANGPTL4 is

widespread in tumors. Tumor-derived ANGPTL4 confers anoikis resistance to tumor cells via autocrine adhesion mimicry. Furthermore, we provide evidence that tumor cells employ ANGPTL4 to hijack integrin-mediated signaling, modulating intracellular O_2^- levels to confer anoikis resistance to tumor cells and to enhance their tumorigenesis. Our findings identify ANGPTL4 as a novel tumor biomarker and redox factor in cancer biology, making ANGPTL4 a potential therapeutic target in cancer treatment and suggesting anticancer strategies focused on redox-based apoptosis induction in tumors.

5. FUTURE DIRECTIONS

Metastasis of primary malignancies is frequently characterized by a leaky vasculature and dynamic tumor-stroma interactions, aiding migration and invasion of the tumor mass across the endothelium (Sakaguchi et al., 2008; Joyce and Pollard, 2009). The endothelium provides a semi-permeable boundary between the bloodstream and the tumor. It consists of a monolayer of gate-keeping endothelial cells (ECs) held together via a network of transmembrane proteins linked to the actin cytoskeleton (Dejana, 2004). The paracellular permeability of endothelium is mediated mainly by endothelial adherens (AJ) and tight junction (TJ) proteins that connect adjacent ECs (Komarova and Malik, 2010). In addition, integrins also provide a scaffold for cell organization, proliferation and migration (Guo and Giancotti, 2004). Defects in endothelial leakiness, junction integrity and cellular organization have been implicated in cancer (van Nieuw Amerongen and van Hinsbergh, 2002; Sakaguchi et al., 2008). Inherently, tumor metastasis requires intimate communication between the tumor and ECs (Joyce and Pollard, 2009). However, little is known about the molecular mechanisms by which the tumor-endothelium communication disrupts endothelial integrity to facilitate the metastasis of tumor cells. Recent work revealed ANGPTL4 is one of the most highly expressed genes in distant metastases (Hu et al., 2009) and during breast cancer metastasis to the lung (Minn et al., 2005; Minn et al., 2007). In addition, tumor-derived ANGPTL4 was shown to promote cancer metastasis by disrupting vascular integrity (Padua et al., 2008). Despite evidences suggesting a role for ANGPTL4 in cancer metastasis, the underlying molecular mechanism by which ANGPTL4 modulates vascular leakiness and integrity is still unclear.

In view of these results, we hypothesized that tumor-derived ANGPTL4 may facilitate metastasis through the disruption of the endothelium barrier. Studies have shown that AJs and TJs are ubiquitous in EC cell-cell contacts and are responsible for the maintenance of ECs integrity (Bazzoni and Dejana, 2004; Dejana, 2004). Both structures are connected to the actin cytoskeleton via intracellular cytoplasmic ZO-1 (Itoh et al., 1997; Bazzoni and Dejana, 2004), and any perturbations to the endothelial integrity result in ZO-1 and actin cytoskeleton rearrangement (Eiselein et al., 2007). Our preliminary data showed that the endothelial junction integrity of confluent human microvascular endothelial cells (HMVEC) was disrupted upon treatment with recombinant ANGPTL4 as revealed by ZO-1 and actin immunostaining. This effect occurred in the presence of cycloheximide and actinomycin D, indicating that neither new protein synthesis nor transcription was necessary for this ANGPTL4-mediated action (Figure 31A). HMVEC junction integrity was disrupted when cell were cultured in conditioned medium (CM) containing ANGPTL4 secreted from A-5RT3$_{CTRL}$ but not in A-5RT3$_{ANGPTL4}$ CM, as indicated by ZO-1 and actin immunostaining. The effect was abolished in the presence of a monoclonal antibody (mAb11F6C4) against ANGPTL4, suggesting a major role for tumor-secreted ANGPTL4 in endothelial junction disruption (Figure 31B). These results were further validated by transendothelial electrical resistance (TER) monitoring for 24 hours post-ANGPTL4 treatment, which showed a rapid and dose-dependent increase in paracellular vascular permeability (Figure 31C) that was not due to apoptosis of the HMVECs (Figure 31D). Overall, these results indicate that tumor-secreted ANGPTL4 is a major pro-metastatic factor that acts via disruption of endothelial integrity. Therefore, we believe that further dissection of the underlying mechanism of this ANGPTL4-mediated effect whether integrin-dependent or –independent, will provide

novel molecular insights into the pro-metastatic role of ANGPTL4, thereby providing a potential therapeutic target for the treatment of metastatic and vascular diseases.

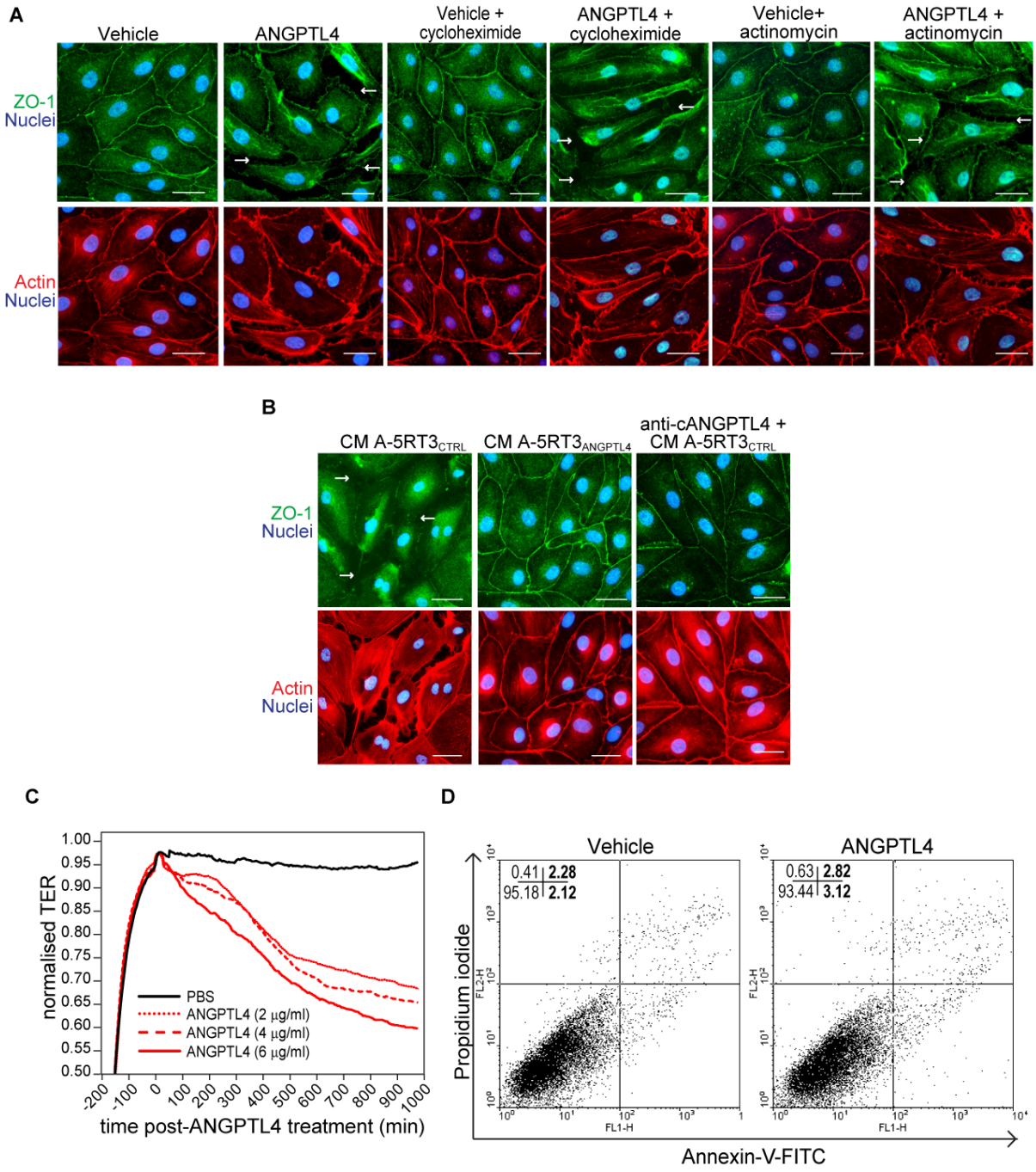

Figure 31. ANGPTL4 disrupts endothelial junction integrity.

(A and B) Immunofluorescence staining for ZO-1 of confluent human microvascular endothelial cells (HMVECs) monolayer treated **(A)** with 6 μg/ml of recombinant human ANGPTL4 in the presence or absence of cycloheximide and actinomycin, **(B)** with 3-day old serum-free conditioned medium (CM) from either A-5RT3$_{CTRL}$ in the presence or absence of anti-ANGPTL4 or A-5RT3$_{ANGPTL4}$. All treatments were for 3 hours. Nuclei were counterstained with DAPI and phallodin for actin stress fibers. Scale bar: 40 μm. White arrows indicate endothelial junction lesions.

(C) Transendothelial electrical resistance (TER) analysis of confluent monolayer HMVECs treated with indicated amount of recombinant ANGPTL4.

(D) FACS analysis of vehicle (PBS)- or ANGPTL4-treated HMVECs stained with annexin V-FITC/PI. The percentage of apoptotic cells (upper and lower right quadrants) is indicated in bold. Data obtained from 3 independent experiments.

Intensive studies are indispensible to further dissect the underlying mechanism of these observations. Early studies have shown that VE-cadherin and claudin-5 contribute to the control of paracellular permeability while integrin α5β1, which is localized to endothelial cell-cell junctions, also mediates endothelial leakiness (Lampugnani et al., 1991). Hence, we hypothesized that tumor-derived ANGPTL4 induces vascular leakiness and ultimately disrupts the endothelium barrier via direct interactions with specific junctional proteins. Surface plasmon resonance (SPR) and *in situ* proximity ligation assay (PLA) analyses will be utilized to evaluate the interaction properties of ANGPTL4 with VE-cadherin, claudin-5 and integrin α5β1. These potential interaction results will be further corroborated by blocking with neutralizing antibodies against VE-cadherin, claudin-5, integrin α5β1 and ANGPTL4. ANGPTL4-mediated endothelial disruption requires neither new protein synthesis nor transcription, thus suggests the activation of pre-existing intracellular signaling that culminates to vascular disruption. To this end, the expression and cellular distribution of Rac-GTP, Tiam and PAK, whose roles in endothelial contractility and barrier function are well-recognized (Stam et al., 1997; Stockton et al., 2004; Galan et al., 2009), will also be examined.

6. REFERENCES

Aggarwal, B.B. and Gehlot, P. (2009). Inflammation and cancer: how friendly is the relationship for cancer patients? Curr. Opin. Pharmacol. *9*, 351-369.

Airola, K. and Fusenig, N.E. (2001). Differential stromal regulation of MMP-1 expression in benign and malignant keratinocytes. J. Invest Dermatol. *116*, 85-92.

Aitken, A. (2006). 14-3-3 proteins: a historic overview. Semin. Cancer Biol. *16*, 162-172.

Akram, S., Teong, H.F., Fliegel, L., Pervaiz, S., and Clement, M.V. (2006). Reactive oxygen species-mediated regulation of the Na+-H+ exchanger 1 gene expression connects intracellular redox status with cells' sensitivity to death triggers. Cell Death. Differ. *13*, 628-641.

Arora, S., Matta, A., Shukla, N.K., Deo, S.V., and Ralhan, R. (2005). Identification of differentially expressed genes in oral squamous cell carcinoma. Mol. Carcinog. *42*, 97-108.

Backhed, F., Crawford, P.A., O'Donnell, D., and Gordon, J.I. (2007). Postnatal lymphatic partitioning from the blood vasculature in the small intestine requires fasting-induced adipose factor. Proc. Natl. Acad. Sci. U. S. A *104*, 606-611.

Backhed, F., Ding, H., Wang, T., Hooper, L.V., Koh, G.Y., Nagy, A., Semenkovich, C.F., and Gordon, J.I. (2004). The gut microbiota as an environmental factor that regulates fat storage. Proc. Natl. Acad. Sci. U. S. A *101*, 15718-15723.

Balkwill, F. and Mantovani, A. (2001). Inflammation and cancer: back to Virchow? Lancet *357*, 539-545.

Bazzoni, G. and Dejana, E. (2004). Endothelial cell-to-cell junctions: molecular organization and role in vascular homeostasis. Physiol Rev. *84*, 869-901.

Bedard, K. and Krause, K.H. (2007). The NOX family of ROS-generating NADPH oxidases: physiology and pathophysiology. Physiol Rev. *87*, 245-313.

Belanger, A.J., Lu, H., Date, T., Liu, L.X., Vincent, K.A., Akita, G.Y., Cheng, S.H., Gregory, R.J., and Jiang, C. (2002). Hypoxia up-regulates expression of peroxisome proliferator-activated receptor gamma angiopoietin-related gene (PGAR) in cardiomyocytes: role of hypoxia inducible factor 1alpha. J. Mol. Cell Cardiol. *34*, 765-774.

Bevan, S. and Houlston, R.S. (1999). Genetic predisposition to gastric cancer. QJM. *92*, 5-10.

Bouillet, P. and Strasser, A. (2002). BH3-only proteins - evolutionarily conserved proapoptotic Bcl-2 family members essential for initiating programmed cell death. J. Cell Sci. *115*, 1567-1574.

Braissant, O., Foufelle, F., Scotto, C., Dauca, M., and Wahli, W. (1996). Differential expression of peroxisome proliferator-activated receptors (PPARs): tissue distribution of PPAR-alpha, -beta, and -gamma in the adult rat. Endocrinology *137*, 354-366.

Bridge, A.J., Pebernard, S., Ducraux, A., Nicoulaz, A.L., and Iggo, R. (2003). Induction of an interferon response by RNAi vectors in mammalian cells. Nat. Genet. *34*, 263-264.

Brizel, D.M., Scully, S.P., Harrelson, J.M., Layfield, L.J., Bean, J.M., Prosnitz, L.R., and Dewhirst, M.W. (1996). Tumor oxygenation predicts for the likelihood of distant metastases in human soft tissue sarcoma. Cancer Res. *56*, 941-943.

Brody, J.G., Moysich, K.B., Humblet, O., Attfield, K.R., Beehler, G.P., and Rudel, R.A. (2007). Environmental pollutants and breast cancer: epidemiologic studies. Cancer *109*, 2667-2711.

Butt, A.J., Firth, S.M., and Baxter, R.C. (1999). The IGF axis and programmed cell death. Immunol. Cell Biol. *77*, 256-262.

Calzada, M.J. and del, P.L. (2007). Hypoxia-inducible factors and cancer. Clin. Transl. Oncol. *9*, 278-289.

Cazes, A., Galaup, A., Chomel, C., Bignon, M., Brechot, N., Le, J.S., Weber, H., Corvol, P., Muller, L., Germain, S., and Monnot, C. (2006). Extracellular matrix-bound angiopoietin-like 4 inhibits endothelial cell adhesion, migration, and sprouting and alters actin cytoskeleton. Circ. Res. *99*, 1207-1215.

Chance, B., Sies, H., and Boveris, A. (1979). Hydroperoxide metabolism in mammalian organs. Physiol Rev. *59*, 527-605.

Chandra, J., Samali, A., and Orrenius, S. (2000). Triggering and modulation of apoptosis by oxidative stress. Free Radic. Biol. Med. *29*, 323-333.

Chen, Z., Li, M., Yuan, Y., Wang, Q., Yan, L., and Gu, J. (2010). Cancer/testis antigens and clinical risk factors for liver metastasis of colorectal cancer: a predictive panel. Dis. Colon Rectum *53*, 31-38.

Chiarugi, P. (2003). Reactive oxygen species as mediators of cell adhesion. Ital. J. Biochem. *52*, 28-32.

Chiarugi, P. (2005). PTPs versus PTKs: the redox side of the coin. Free Radic. Res. *39*, 353-364.

Chiarugi, P. (2008). From anchorage dependent proliferation to survival: lessons from redox signalling. IUBMB. Life *60*, 301-307.

Chiarugi, P. and Buricchi, F. (2007). Protein tyrosine phosphorylation and reversible oxidation: two cross-talking posttranslation modifications. Antioxid. Redox. Signal. *9*, 1-24.

Chiarugi, P. and Cirri, P. (2003). Redox regulation of protein tyrosine phosphatases during receptor tyrosine kinase signal transduction. Trends Biochem. Sci. *28*, 509-514.

Chiarugi, P. and Fiaschi, T. (2007). Redox signalling in anchorage-dependent cell growth. Cell Signal. *19*, 672-682.

Chiarugi, P. and Giannoni, E. (2005). Anchorage-dependent cell growth: tyrosine kinases and phosphatases meet redox regulation. Antioxid. Redox. Signal. *7*, 578-592.

Chiarugi, P. and Giannoni, E. (2008). Anoikis: a necessary death program for anchorage-dependent cells. Biochem. Pharmacol. *76*, 1352-1364.

Chiarugi, P., Pani, G., Giannoni, E., Taddei, L., Colavitti, R., Raugei, G., Symons, M., Borrello, S., Galeotti, T., and Ramponi, G. (2003). Reactive oxygen species as essential mediators of cell adhesion: the oxidative inhibition of a FAK tyrosine phosphatase is required for cell adhesion. J. Cell Biol. *161*, 933-944.

Chiodoni, C., Colombo, M.P., and Sangaletti, S. (2010). Matricellular proteins: from homeostasis to inflammation, cancer, and metastasis. Cancer Metastasis Rev. *29*, 295-307.

Chomel C., Cazes, A., Faye, C., Bignon, M., Gomez, E., Ardidie-Robouant,C., Barret,A., Ricard-Blum,S., Muller,L., Germain,S., and Monnot,C. (2009). Interaction of the coiled-coil domain with glycosaminoglycans protects angiopoietin-like 4 from proteolysis and regulates its antiangiogenic activity. FASEB J. *23*, 940-949.

Chong, H.C., Tan, M.J., Philippe, V., Tan, S.H., Tan, C.K., Ku, C.W., Goh, Y.Y., Wahli, W., Michalik, L., and Tan, N.S. (2009). Regulation of epithelial-mesenchymal IL-1 signaling by PPARbeta/delta is essential for skin homeostasis and wound healing. J. Cell Biol. *184*, 817-831.

Clement, M.V., Hirpara, J.L., and Pervaiz, S. (2003). Decrease in intracellular superoxide sensitizes Bcl-2-overexpressing tumor cells to receptor and drug-induced apoptosis independent of the mitochondria. Cell Death. Differ. *10*, 1273-1285.

Clement, M.V. and Pervaiz, S. (2001). Intracellular superoxide and hydrogen peroxide concentrations: a critical balance that determines survival or death. Redox. Rep. *6*, 211-214.

Comoglio, P.M., Boccaccio, C., and Trusolino, L. (2003). Interactions between growth factor receptors and adhesion molecules: breaking the rules. Curr. Opin. Cell Biol. *15*, 565-571.

Coussens, L.M. and Werb, Z. (2002). Inflammation and cancer. Nature *420*, 860-867.

Crissman, J.D. (1986). Tumor-host interactions as prognostic factors in the histologic assessment of carcinomas. Pathol. Annu. *21 Pt 1*, 29-52.

Dai,Y. and Wang,W.H. (2010). Peroxisome proliferator-activated receptor gamma and colorectal cancer. World J. Gastrointest. Oncol. *2*, 159-164.

Dejana, E. (2004). Endothelial cell-cell junctions: happy together. Nat. Rev. Mol. Cell Biol. *5*, 261-270.

Delerive, P., Fruchart, J.C., and Staels, B. (2001). Peroxisome proliferator-activated receptors in inflammation control. J. Endocrinol. *169*, 453-459.

Desai, U., Lee, E.C., Chung, K., Gao, C., Gay, J., Key, B., Hansen, G., Machajewski, D., Platt, K.A., Sands, A.T., Schneider, M., Van, S., I, Suwanichkul, A., Vogel, P., Wilganowski, N., Wingert,J., Zambrowicz,B.P., Landes,G., and Powell,D.R. (2007). Lipid-lowering effects of anti-angiopoietin-like 4 antibody recapitulate the lipid phenotype found in angiopoietin-like 4 knockout mice. Proc. Natl. Acad. Sci. U. S. A *104*, 11766-11771.

Desgrosellier, J.S. and Cheresh, D.A. (2010). Integrins in cancer: biological implications and therapeutic opportunities. Nat. Rev. Cancer *10*, 9-22.

Desvergne, B. and Wahli, W. (1999). Peroxisome proliferator-activated receptors: nuclear control of metabolism. Endocr. Rev. *20*, 649-688.

Devchand, P.R., Keller, H., Peters, J.M., Vazquez, M., Gonzalez, F.J., and Wahli, W. (1996). The PPARalpha-leukotriene B4 pathway to inflammation control. Nature *384*, 39-43.

Devereux, T.R., Taylor, J.A., and Barrett, J.C. (1996). Molecular mechanisms of lung cancer. Interaction of environmental and genetic factors. Giles F. Filley Lecture. Chest *109*, 14S-19S.

Diaz-Montero, C.M., Wygant, J.N., and McIntyre, B.W. (2006). PI3-K/Akt-mediated anoikis resistance of human osteosarcoma cells requires Src activation. Eur. J. Cancer *42*, 1491-1500.

Dvorak, H.F., Galli, S.J., and Dvorak, A.M. (1986). Cellular and vascular manifestations of cell-mediated immunity. Hum. Pathol. *17*, 122-137.

Dvorak, H.F. (1986). Tumors: wounds that do not heal. Similarities between tumor stroma generation and wound healing. N. Engl. J. Med. *315*, 1650-1659.

Eble, J.A. and Haier, J. (2006). Integrins in cancer treatment. Curr. Cancer Drug Targets. *6*, 89-105.

Eiselein, L., Wilson, D.W., Lame, M.W., and Rutledge, J.C. (2007). Lipolysis products from triglyceride-rich lipoproteins increase endothelial permeability, perturb zonula occludens-1 and F-actin, and induce apoptosis. Am. J. Physiol Heart Circ. Physiol *292*, H2745-H2753.

Engels, E.A., Wu, X., Gu, J., Dong, Q., Liu, J., and Spitz, M.R. (2007). Systematic evaluation of genetic variants in the inflammation pathway and risk of lung cancer. Cancer Res. *67*, 6520-6527.

Felding-Habermann, B. (2003). Integrin adhesion receptors in tumor metastasis. Clin. Exp. Metastasis *20*, 203-213.

Ferraro, D., Corso, S., Fasano, E., Panieri, E., Santangelo, R., Borrello, S., Giordano, S., Pani, G., and Galeotti, T. (2006). Pro-metastatic signaling by c-Met through RAC-1 and reactive oxygen species (ROS). Oncogene *25*, 3689-3698.

Fidler, I.J. (1999). Critical determinants of cancer metastasis: rationale for therapy. Cancer Chemother. Pharmacol. *43 Suppl*, S3-10.

Fidler, I.J. (2003). The pathogenesis of cancer metastasis: the 'seed and soil' hypothesis revisited. Nat. Rev. Cancer *3*, 453-458.

Finger, E.C. and Giaccia,A.J. (2010). Hypoxia, inflammation, and the tumor microenvironment in metastatic disease. Cancer Metastasis Rev. *29*, 285-293.

Finkel, T. (2006). Intracellular redox regulation by the family of small GTPases. Antioxid. Redox. Signal. *8*, 1857-1863.

Frisch, S.M., Vuori, K., Ruoslahti, E., and Chan-Hui, P.Y. (1996). Control of adhesion-dependent cell survival by focal adhesion kinase. J. Cell Biol. *134*, 793-799.

Galan Moya, E.M., Le, G.A., and Gavard, J. (2009). PAKing up to the endothelium. Cell Signal. 21, 1727-1737.

Galaup, A., Cazes, A., Le, J.S., Philippe, J., Connault, E., Le, C.E., Mekid, H., Mir, L.M., Opolon, P., Corvol, P., Monnot, C., and Germain, S. (2006). Angiopoietin-like 4 prevents metastasis through inhibition of vascular permeability and tumor cell motility and invasiveness. Proc. Natl. Acad. Sci. U. S. A *103*, 18721-18726.

Ge, H., Yang, G., Huang, L., Motola, D.L., Pourbahrami, T., and Li, C. (2004). Oligomerization and regulated proteolytic processing of angiopoietin-like protein 4. J. Biol. Chem. *279*, 2038-2045.

Gealekman, O., Burkart, A., Chouinard, M., Nicoloro, S.M., Straubhaar, J., and Corvera, S. (2008). Enhanced angiogenesis in obesity and in response to PPARgamma activators through adipocyte VEGF and ANGPTL4 production. Am. J. Physiol Endocrinol. Metab *295*, E1056-E1064.

Georgiadi, A., Lichtenstein, L., Degenhardt, T., Boekschoten, M.V., van, B.M., Desvergne, B., Muller, M., and Kersten, S. (2010). Induction of cardiac Angptl4 by dietary fatty acids is mediated by peroxisome proliferator-activated receptor beta/delta and protects against fatty acid-induced oxidative stress. Circ. Res. *106*, 1712-1721.

Giancotti, F.G. (2000). Complexity and specificity of integrin signalling. Nat. Cell Biol. *2*, E13-E14.

Giancotti, F.G. and Ruoslahti, E. (1990). Elevated levels of the alpha 5 beta 1 fibronectin receptor suppress the transformed phenotype of Chinese hamster ovary cells. Cell *60*, 849-859.

Giannoni, E., Buricchi, F., Grimaldi, G., Parri, M., Cialdai, F., Taddei, M.L., Raugei, G., Ramponi, G., and Chiarugi, P. (2008). Redox regulation of anoikis: reactive oxygen species as essential mediators of cell survival. Cell Death. Differ. *15*, 867-878.

Giannoni, E., Buricchi, F., Raugei, G., Ramponi, G., and Chiarugi, P. (2005). Intracellular reactive oxygen species activate Src tyrosine kinase during cell adhesion and anchorage-dependent cell growth. Mol. Cell Biol. *25*, 6391-6403.

Giannoni, E., Fiaschi, T., Ramponi, G., and Chiarugi, P. (2009). Redox regulation of anoikis resistance of metastatic prostate cancer cells: key role for Src and EGFR-mediated pro-survival signals. Oncogene *28*, 2074-2086.

Gillies, R.J., Raghunand, N., Karczmar, G.S., and Bhujwalla, Z.M. (2002). MRI of the tumor microenvironment. J. Magn Reson. Imaging *16*, 430-450.

Goh, Y.Y., Pal, M., Chong, H.C., Zhu, P., Tan, M.J., Punugu, L., Lam, C.R., Yau, Y.H., Tan, C.K., Huang, R.L., Tan, S.M., Tang, M.B., Ding, J.L., Kersten, S., and Tan, N.S. (2010a). Angiopoietin-Like 4 Interacts with Integrins {beta}1 and {beta}5 to Modulate Keratinocyte Migration. Am. J. Pathol.

Goh, Y.Y., Pal, M., Chong, H.C., Zhu, P., Tan, M.J., Punugu, L., Tan, C.K., Huang, R.L., Sze, S.K., Tang, M.B., Ding, J.L., Kersten, S., and Tan, N.S. (2010b).

Angiopoietin-like 4 interacts with matrix proteins to modulate wound healing. J. Biol. Chem. *285*, 32999-33009.

Gonda, T.A., Tu, S., and Wang, T.C. (2009). Chronic inflammation, the tumor microenvironment and carcinogenesis. Cell Cycle *8*, 2005-2013.

Gonzalez-Muniesa, P., Bing, C., and Trayhurn, P. (2010). Upregulation of the expression of inflammatory and angiogenic markers in human adipocytes by a synthetic cannabinoid, JTE-907. Horm. Metab Res. *42*, 710-717.

Guo, W. and Giancotti, F.G. (2004). Integrin signalling during tumour progression. Nat. Rev. Mol. Cell Biol. *5*, 816-826.

Gupta, G.P. and Massague, J. (2006). Cancer metastasis: building a framework. Cell *127*, 679-695.

Hagag, N., Lacal, J.C., Graber, M., Aaronson, S., and Viola, M.V. (1987). Microinjection of ras p21 induces a rapid rise in intracellular pH. Mol. Cell Biol. *7*, 1984-1988.

Hanahan, D. and Weinberg, R.A. (2000). The hallmarks of cancer. Cell *100*, 57-70.

Hanahan, D. and Weinberg, R.A. (2011). Hallmarks of cancer: the next generation. Cell *144*, 646-674.

Hecht, S.S. (2003). Tobacco carcinogens, their biomarkers and tobacco-induced cancer. Nat. Rev. Cancer *3*, 733-744.

Hermann, L.M., Pinkerton, M., Jennings, K., Yang, L., Grom, A., Sowders, D., Kersten, S., Witte, D.P., Hirsch, R., and Thornton, S. (2005). Angiopoietin-like-4 is a potential angiogenic mediator in arthritis. Clin. Immunol. *115*, 93-101.

Herbst, R.S., Heymach, J.V., and Lippman, S.M. (2008). Lung cancer. N. Engl. J. Med. *359*, 1367-1380.

Hirpara, J.L., Clement, M.V., and Pervaiz, S. (2001). Intracellular acidification triggered by mitochondrial-derived hydrogen peroxide is an effector mechanism for drug-induced apoptosis in tumor cells. J. Biol. Chem. *276*, 514-521.

Honore, S., Kovacic, H., Pichard, V., Briand, C., and Rognoni, J.B. (2003). Alpha2beta1-integrin signaling by itself controls G1/S transition in a human adenocarcinoma cell line (Caco-2): implication of NADPH oxidase-dependent production of ROS. Exp. Cell Res. *285*, 59-71.

Hsieh, L.L. and Huang, Y.C. (1995). Loss of heterozygosity of APC/MCC gene in differentiated and undifferentiated gastric carcinomas in Taiwan. Cancer Lett. *96*, 169-174.

Hu, Z., Fan, C., Livasy, C., He, X., Oh, D.S., Ewend, M.G., Carey, L.A., Subramanian, S., West, R., Ikpatt, F., Olopade, O.I., van de Rijn, M., and Perou, C.M. (2009). A compact VEGF signature associated with distant metastases and poor outcomes. BMC. Med. *7*, 9.

Huber, E., Vlasny, D., Jeckel, S., Stubenrauch, F., and Iftner, T. (2004). Gene profiling of cottontail rabbit papillomavirus-induced carcinomas identifies upregulated genes directly Involved in stroma invasion as shown by small interfering RNA-mediated gene silencing. J. Virol. *78*, 7478-7489.

Iliopoulos, O., Levy, A.P., Jiang, C., Kaelin, W.G., Jr., and Goldberg, M.A. (1996). Negative regulation of hypoxia-inducible genes by the von Hippel-Lindau protein. Proc. Natl. Acad. Sci. U. S. A *93*, 10595-10599.

Irani, K., Xia, Y., Zweier, J.L., Sollott, S.J., Der, C.J., Fearon, E.R., Sundaresan, M., Finkel,T., and Goldschmidt-Clermont, P.J. (1997). Mitogenic signaling mediated by oxidants in Ras-transformed fibroblasts. Science *275*, 1649-1652.

Ito, Y., Oike, Y., Yasunaga, K., Hamada, K., Miyata, K., Matsumoto, S., Sugano, S., Tanihara, H., Masuho, Y., and Suda, T. (2003). Inhibition of angiogenesis and vascular leakiness by angiopoietin-related protein 4. Cancer Res. *63*, 6651-6657.

Itoh, M., Nagafuchi, A., Moroi, S., and Tsukita, S. (1997). Involvement of ZO-1 in cadherin-based cell adhesion through its direct binding to alpha catenin and actin filaments. J. Cell Biol. *138*, 181-192.

Jang, J.S., Cho, H.Y., Lee, Y.J., Ha, W.S., and Kim, H.W. (2004). The differential proteome profile of stomach cancer: identification of the biomarker candidates. Oncol. Res. *14*, 491-499.

Jenne, D.E., Reimann, H., Nezu, J., Friedel, W., Loff, S., Jeschke, R., Muller, O., Back, W., and Zimmer, M. (1998). Peutz-Jeghers syndrome is caused by mutations in a novel serine threonine kinase. Nat. Genet. *18*, 38-43.

Joneson, T. and Bar-Sagi, D. (1998). A Rac1 effector site controlling mitogenesis through superoxide production. J. Biol. Chem. *273*, 17991-17994.

Joyce, J.A. and Pollard, J.W. (2009). Microenvironmental regulation of metastasis. Nat. Rev. Cancer *9*, 239-252.

Kaddatz, K., Adhikary, T., Finkernagel, F., Meissner, W., Muller-Brusselbach, S., and Muller, R. (2010). Transcriptional profiling identifies functional interactions of TGF beta and PPAR beta/delta signaling: synergistic induction of ANGPTL4 transcription. J. Biol. Chem. *285*, 29469-29479.

Kalluri, R. (2009). EMT: when epithelial cells decide to become mesenchymal-like cells. J. Clin. Invest *119*, 1417-1419.

Kawamata, H., Tachibana, M., Fujimori, T., and Imai, Y. (2006). Differentiation-inducing therapy for solid tumors. Curr. Pharm. Des *12*, 379-385.

Kersten, S. (2005). Regulation of lipid metabolism via angiopoietin-like proteins. Biochem. Soc. Trans. *33*, 1059-1062.

Kersten, S., Mandard, S., Tan, N.S., Escher, P., Metzger, D., Chambon, P., Gonzalez, F.J., Desvergne, B., and Wahli, W. (2000). Characterization of the fasting-induced

adipose factor FIAF, a novel peroxisome proliferator-activated receptor target gene. J. Biol. Chem. *275*, 28488-28493.

Kersten, S., Seydoux, J., Peters, J.M., Gonzalez, F.J., Desvergne, B., and Wahli, W. (1999). Peroxisome proliferator-activated receptor alpha mediates the adaptive response to fasting. J. Clin. Invest *103*, 1489-1498.

Khwaja, A., Rodriguez-Viciana, P., Wennstrom, S., Warne, P.H., and Downward, J. (1997). Matrix adhesion and Ras transformation both activate a phosphoinositide 3-OH kinase and protein kinase B/Akt cellular survival pathway. EMBO J. *16*, 2783-2793.

Kim, H.K., Youn, B.S., Shin, M.S., Namkoong, C., Park, K.H., Baik, J.H., Kim, J.B., Park, J.Y., Lee, K.U., Kim, Y.B., and Kim, M.S. (2010). Hypothalamic Angptl4/Fiaf is a novel regulator of food intake and body weight. Diabetes *59*, 2772-2780.

Kim, I., Kim, H.G., Kim, H., Kim, H.H., Park, S.K., Uhm, C.S., Lee, Z.H., and Koh, G.Y. (2000). Hepatic expression, synthesis and secretion of a novel fibrinogen/angiopoietin-related protein that prevents endothelial-cell apoptosis. Biochem. J. *346 Pt 3*, 603-610.

Kliewer, S.A., Forman, B.M., Blumberg, B., Ong, E.S., Borgmeyer, U., Mangelsdorf, D.J., Umesono, K., and Evans, R.M. (1994). Differential expression and activation of a family of murine peroxisome proliferator-activated receptors. Proc. Natl. Acad. Sci. U. S. A *91*, 7355- Reference List

Klopper, J.P., Berenz, A., Hays, W.R., Sharma, V., Pugazhenthi, U., Janssen, J., Singh, M., Bissonnette, R.P., and Haugen, B.R. (2008). In vivo and microarray analysis of rexinoid-responsive anaplastic thyroid carcinoma. Clin. Cancer Res. *14*, 589-596.

Koliwad, S.K., Kuo, T., Shipp, L.E., Gray, N.E., Backhed, F., So, A.Y., Farese, R.V., Jr., and Wang, J.C. (2009). Angiopoietin-like 4 (ANGPTL4, fasting-induced adipose factor) is a direct glucocorticoid receptor target and participates in glucocorticoid-regulated triglyceride metabolism. J. Biol. Chem. *284*, 25593-25601.

Komarova, Y. and Malik, A.B. (2010). Regulation of endothelial permeability via paracellular and transcellular transport pathways. Annu. Rev. Physiol *72*, 463-493.

Komatsu, D., Kato, M., Nakayama, J., Miyagawa, S., and Kamata, T. (2008). NADPH oxidase 1 plays a critical mediating role in oncogenic Ras-induced vascular endothelial growth factor expression. Oncogene *27*, 4724-4732.

Kopfstein, L. and Christofori, G. (2006). Metastasis: cell-autonomous mechanisms versus contributions by the tumor microenvironment. Cell Mol. Life Sci. *63*, 449-468.

Koster, A., Chao, Y.B., Mosior, M., Ford, A., Gonzalez-DeWhitt, P.A., Hale, J.E., Li, D., Qiu, Y., Fraser, C.C., Yang, D.D., Heuer, J.G., Jaskunas, S.R., and Eacho, P. (2005). Transgenic angiopoietin-like (angptl)4 overexpression and targeted disruption of angptl4 and angptl3: regulation of triglyceride metabolism. Endocrinology *146*, 4943-4950.

Krause, K.H. (2004). Tissue distribution and putative physiological function of NOX family NADPH oxidases. Jpn. J. Infect. Dis. *57*, S28-S29.

Labat-Robert, J. and Robert, L. (2007). The effect of cell-matrix interactions and aging on the malignant process. Adv. Cancer Res. *98*, 221-259.

Langley, R.R. and Fidler, I.J. (2007). Tumor cell-organ microenvironment interactions in the pathogenesis of cancer metastasis. Endocr. Rev. *28*, 297-321.

Lampugnani M.G., Resnati M., Dejana E., Marchisio PC. (1991). The role of integrins in the maintenance of endothelial monolayer integrity. J Cell Biol; 112(3):479-90.

Le, J.S., Amy, C., Cazes, A., Monnot, C., Lamande, N., Favier, J., Philippe, J., Sibony, M., Gasc, J.M., Corvol, P., and Germain, S. (2003). Angiopoietin-like 4 is a proangiogenic factor produced during ischemia and in conventional renal cell carcinoma. Am. J. Pathol. *162*, 1521-1528.

Legry, V., Bokor, S., Cottel, D., Beghin, L., Catasta, G., Nagy, E., Gonzalez-Gross, M., Spinneker, A., Stehle, P., Molnar, D., Moreno, L.A., Amouyel, P., Dallongeville,

J., and Meirhaeghe, A. (2009). Associations between common genetic polymorphisms in angiopoietin-like proteins 3 and 4 and lipid metabolism and adiposity in European adolescents and adults. J. Clin. Endocrinol. Metab *94*, 5070-5077.

Lemberger, T., Desvergne, B., and Wahli, W. (1996). Peroxisome proliferator-activated receptors: a nuclear receptor signaling pathway in lipid physiology. Annu. Rev. Cell Dev. Biol. *12*, 335-363.

Lewis, A.M., Varghese, S., Xu, H., and Alexander, H.R. (2006). Interleukin-1 and cancer progression: the emerging role of interleukin-1 receptor antagonist as a novel therapeutic agent in cancer treatment. J. Transl. Med. *4*, 48.

Li, C. (2006). Genetics and regulation of angiopoietin-like proteins 3 and 4. Curr. Opin. Lipidol. *17*, 152-156.

Li, K.Q., Li, W.L., Peng, S.Y., Shi, X.Y., Tang, H.L., and Liu, Y.B. (2004). Anti-tumor effect of recombinant retroviral vector-mediated human ANGPTL4 gene transfection. Chin Med. J. (Engl.) *117*, 1364-1369.

Lichtenstein, L., Berbee, J.F., van Dijk, S.J., van Dijk, K.W., Bensadoun, A., Kema, I.P., Voshol, P.J., Muller, M., Rensen, P.C., and Kersten, S. (2007). Angptl4 upregulates cholesterol synthesis in liver via inhibition of LPL- and HL-dependent hepatic cholesterol uptake. Arterioscler. Thromb. Vasc. Biol. *27*, 2420-2427.

Lichtenstein, L., Mattijssen, F., de Wit, N.J., Georgiadi, A., Hooiveld, G.J., van der Meer, R., He, Y., Qi, L., Koster, A., Tamsma, J.T., Tan, N.S., Muller, M., and Kersten, S. (2010). Angptl4 Protects against Severe Proinflammatory Effects of Saturated Fat by Inhibiting Fatty Acid Uptake into Mesenteric Lymph Node Macrophages. Cell Metab *12*, 580-592.

Liou, G.Y. and Storz, P. (2010). Reactive oxygen species in cancer. Free Radic. Res. *44*, 479-496.

Lotem, J. and Sachs, L. (1996). Control of apoptosis in hematopoiesis and leukemia by cytokines, tumor suppressor and oncogenes. Leukemia *10*, 925-931.

Lu, B., Xu, F.Y., Taylor, W.A., Feingold, K.R., and Hatch, G.M. (2010). Cardiolipin Synthase-1 mRNA Expression Does Not Correlate with Endogenous Cardiolipin Synthase Enzyme Activity In Vitro and In Vivo in Mammalian Lipopolysaccharide Models of Inflammation. Inflammation.

MacFarlane, P.M., Satriotomo, I., Windelborn, J.A., and Mitchell, G.S. (2009). NADPH oxidase activity is necessary for acute intermittent hypoxia-induced phrenic long-term facilitation. J. Physiol *587*, 1931-1942.

Mandard, S., Zandbergen, F., Tan, N.S., Escher, P., Patsouris, D., Koenig, W., Kleemann, R., Bakker, A., Veenman, F., Wahli, W., Muller, M., and Kersten, S. (2004). The direct peroxisome proliferator-activated receptor target fasting-induced adipose factor (FIAF/PGAR/ANGPTL4) is present in blood plasma as a truncated protein that is increased by fenofibrate treatment. J. Biol. Chem. *279*, 34411-34420.

Mandard, S., Zandbergen, F., van, S.E., Wahli, W., Kuipers, F., Muller, M., and Kersten, S. (2006). The fasting-induced adipose factor/angiopoietin-like protein 4 is physically associated with lipoproteins and governs plasma lipid levels and adiposity. J. Biol. Chem. *281*, 934-944.

Mansure, J.J., Nassim, R., and Kassouf, W. (2009). Peroxisome proliferator-activated receptor gamma in bladder cancer: a promising therapeutic target
M2009. Cancer Biol. Ther. *8*, 6-15.

Markowitz, S.D. and Bertagnolli, M.M. (2009). Molecular origins of cancer: Molecular basis of colorectal cancer. N. Engl. J. Med. *361*, 2449-2460.

Marme, D. (2001). Tumor angiogenesis: new approaches to cancer therapy. Onkologie. *24 Suppl 1*, 1-5.

Martin, S.L. (1995). Characterization of a LINE-1 cDNA that originated from RNA present in ribonucleoprotein particles: implications for the structure of an active mouse LINE-1. Gene *153*, 261-266.

Maxwell, P.H., Wiesener, M.S., Chang, G.W., Clifford, S.C., Vaux, E.C., Cockman, M.E., Wykoff, C.C., Pugh, C.W., Maher, E.R., and Ratcliffe, P.J. (1999). The tumour suppressor protein VHL targets hypoxia-inducible factors for oxygen-dependent proteolysis. Nature *399*, 271-275.

Minn, A.J., Gupta, G.P., Padua, D., Bos, P., Nguyen, D.X., Nuyten, D., Kreike, B., Zhang, Y., Wang, Y., Ishwaran, H., Foekens, J.A., van, d., V, and Massague, J. (2007). Lung metastasis genes couple breast tumor size and metastatic spread. Proc. Natl. Acad. Sci. U. S. A *104*, 6740-6745.

Minn, A.J., Gupta, G.P., Siegel, P.M., Bos, P.D., Shu, W., Giri, D.D., Viale, A., Olshen, A.B., Gerald, W.L., and Massague, J. (2005). Genes that mediate breast cancer metastasis to lung. Nature *436*, 518-524.

Moll, U.M. and Schramm, L.M. (1998). p53--an acrobat in tumorigenesis. Crit Rev. Oral Biol. Med. *9*, 23-37.

Montgomery, A.M., Reisfeld, R.A., and Cheresh, D.A. (1994). Integrin alpha v beta 3 rescues melanoma cells from apoptosis in three-dimensional dermal collagen. Proc. Natl. Acad. Sci. U. S. A *91*, 8856-8860.

Morrison, D.K. (2009). The 14-3-3 proteins: integrators of diverse signaling cues that impact cell fate and cancer development. Trends Cell Biol. *19*, 16-23.

Mueller, M.M. and Fusenig, N.E. (2004). Friends or foes - bipolar effects of the tumour stroma in cancer. Nat. Rev. Cancer *4*, 839-849.

Mueller, M.M., Peter, W., Mappes, M., Huelsen, A., Steinbauer, H., Boukamp, P., Vaccariello, M., Garlick, J., and Fusenig, N.E. (2001). Tumor progression of skin carcinoma cells in vivo promoted by clonal selection, mutagenesis, and autocrine growth regulation by granulocyte colony-stimulating factor and granulocyte-macrophage colony-stimulating factor. Am. J. Pathol. *159*, 1567-1579.

Munzel, T., Afanas'ev, I.B., Kleschyov, A.L., and Harrison, D.G. (2002). Detection of superoxide in vascular tissue. Arterioscler. Thromb. Vasc. Biol. *22*, 1761-1768.

Murata, M., Yudo, K., Nakamura, H., Chiba, J., Okamoto, K., Suematsu, N., Nishioka, K., Beppu, M., Inoue, K., Kato, T., and Masuko, K. (2009). Hypoxia upregulates the expression of angiopoietin-like-4 in human articular chondrocytes: role of angiopoietin-like-4 in the expression of matrix metalloproteinases and cartilage degradation. J. Orthop. Res. *27*, 50-57.

Murphy, G.J. and Holder, J.C. (2000). PPAR-gamma agonists: therapeutic role in diabetes, inflammation and cancer. Trends Pharmacol. Sci. *21*, 469-474.

Nakagama, H. (2010). [PPARgamma and cancer]. Nippon Rinsho *68*, 323-329.

Nelen, M.R., van Staveren, W.C., Peeters, E.A., Hassel, M.B., Gorlin, R.J., Hamm, H., Lindboe, C.F., Fryns, J.P., Sijmons, R.H., Woods, D.G., Mariman, E.C., Padberg, G.W., and Kremer, H. (1997). Germline mutations in the PTEN/MMAC1 gene in patients with Cowden disease. Hum. Mol. Genet. *6*, 1383-1387.

Nesbit, M., Nesbit, H.K., Bennett, J., Andl, T., Hsu, M.Y., Dejesus, E., McBrian, M., Gupta, A.R., Eck, S.L., and Herlyn, M. (1999). Basic fibroblast growth factor induces a transformed phenotype in normal human melanocytes. Oncogene *18*, 6469-6476.

Oberley, L.W. (2001). Anticancer therapy by overexpression of superoxide dismutase. Antioxid. Redox. Signal. *3*, 461-472.

Oberley, T.D., Zhong, W., Szweda, L.I., and Oberley, L.W. (2000). Localization of antioxidant enzymes and oxidative damage products in normal and malignant prostate epithelium. Prostate *44*, 144-155.

Oike, Y., Akao, M., Kubota, Y., and Suda, T. (2005). Angiopoietin-like proteins: potential new targets for metabolic syndrome therapy. Trends Mol. Med. *11*, 473-479.

Padua, D., Zhang, X.H., Wang, Q., Nadal, C., Gerald, W.L., Gomis, R.R., and Massague, J. (2008). TGFbeta primes breast tumors for lung metastasis seeding through angiopoietin-like 4. Cell *133*, 66-77.

Paffenholz, R., Bergstrom, R.A., Pasutto, F., Wabnitz, P., Munroe, R.J., Jagla, W., Heinzmann, U., Marquardt, A., Bareiss, A., Laufs, J., Russ, A., Stumm, G., Schimenti, J.C., and Bergstrom, D.E. (2004). Vestibular defects in head-tilt mice result from mutations in Nox3, encoding an NADPH oxidase. Genes Dev. *18*, 486-491.

Pani, G., Galeotti, T., and Chiarugi, P. (2010). Metastasis: cancer cell's escape from oxidative stress. Cancer Metastasis Rev. *29*, 351-378.

Pani, G., Giannoni, E., Galeotti, T., and Chiarugi, P. (2009). Redox-based escape mechanism from death: the cancer lesson. Antioxid. Redox. Signal. *11*, 2791-2806.

Panigrahy, D., Huang, S., Kieran, M.W., and Kaipainen, A. (2005). PPARgamma as a therapeutic target for tumor angiogenesis and metastasis. Cancer Biol. Ther. *4*, 687-693.

Pervaiz, S. and Clement, M.V. (2002). A permissive apoptotic environment: function of a decrease in intracellular superoxide anion and cytosolic acidification. Biochem. Biophys. Res. Commun. *290*, 1145-1150.

Pervaiz, S. and Clement, M.V. (2007). Superoxide anion: oncogenic reactive oxygen species? Int. J. Biochem. Cell Biol. *39*, 1297-1304.

Pervaiz, S., Ramalingam, J.K., Hirpara,J.L., and Clement,M.V. (1999). Superoxide anion inhibits drug-induced tumor cell death. FEBS Lett. *459*, 343-348.

Pervaiz, S., Taneja, R., and Ghaffari, S. (2009). Oxidative stress regulation of stem and progenitor cells. Antioxid. Redox. Signal. *11*, 2777-2789.

Peters, J.M. and Gonzalez, F.J. (2009). Sorting out the functional role(s) of peroxisome proliferator-activated receptor-beta/delta (PPARbeta/delta) in cell proliferation and cancer. Biochim. Biophys. Acta *1796*, 230-241.

Petitclerc, E., Stromblad, S., von Schalscha, T.L., Mitjans, F., Piulats, J., Montgomery, A.M., Cheresh, D.A., and Brooks, P.C. (1999). Integrin alpha(v)beta3

promotes M21 melanoma growth in human skin by regulating tumor cell survival. Cancer Res. *59*, 2724-2730.

Porter, G.W., Khuri, F.R., and Fu, H. (2006). Dynamic 14-3-3/client protein interactions integrate survival and apoptotic pathways. Semin. Cancer Biol. *16*, 193-202.

Pyper, S.R., Viswakarma, N., Yu, S., and Reddy, J.K. (2010). PPARalpha: energy combustion, hypolipidemia, inflammation and cancer. Nucl. Recept. Signal. *8*, e002.

Qi, W., Liu, X., Qiao, D., and Martinez, J.D. (2005). Isoform-specific expression of 14-3-3 proteins in human lung cancer tissues. Int. J. Cancer *113*, 359-363.

Radisky, D.C., Levy, D.D., Littlepage, L.E., Liu, H., Nelson, C.M., Fata, J.E., Leake, D., Godden, E.L., Albertson, D.G., Nieto, M.A., Werb, Z., and Bissell, M.J. (2005). Rac1b and reactive oxygen species mediate MMP-3-induced EMT and genomic instability. Nature *436*, 123-127.

Rankin, E.B. and Giaccia, A.J. (2008). The role of hypoxia-inducible factors in tumorigenesis. Cell Death. Differ. *15*, 678-685.

Reginato, M.J., Mills, K.R., Paulus, J.K., Lynch, D.K., Sgroi, D.C., Debnath, J., Muthuswamy, S.K., and Brugge, J.S. (2003). Integrins and EGFR coordinately regulate the pro-apoptotic protein Bim to prevent anoikis. Nat. Cell Biol. *5*, 733-740.

Reuter, S., Gupta, S.C., Chaturvedi, M.M., and Aggarwal, B.B. (2010). Oxidative stress, inflammation, and cancer: how are they linked? Free Radic. Biol. Med. *49*, 1603-1616.

Rhee, S.G. (2006). Cell signaling. H2O2, a necessary evil for cell signaling. Science *312*, 1882-1883.

Sakaguchi, T., Suzuki, S., Higashi, H., Inaba, K., Nakamura, S., Baba, S., Kato, T., and Konno, H. (2008). Expression of tight junction protein claudin-5 in tumor vessels and sinusoidal endothelium in patients with hepatocellular carcinoma. J. Surg. Res. *147*, 123-131.

Salmon, S.E. (1984). Human tumor colony assay and chemosensitivity testing. Cancer Treat. Rep. *68*, 117-125.

Sangrar, W., Gao, Y., Scott, M., Truesdell, P., and Greer, P.A. (2007). Fer-mediated cortactin phosphorylation is associated with efficient fibroblast migration and is dependent on reactive oxygen species generation during integrin-mediated cell adhesion. Mol. Cell Biol. *27*, 6140-6152.

Sarsour, E.H., Kumar, M.G., Chaudhuri, L., Kalen, A.L., and Goswami, P.C. (2009). Redox control of the cell cycle in health and disease. Antioxid. Redox. Signal. *11*, 2985-3011.

Savagner, P. (2001). Leaving the neighborhood: molecular mechanisms involved during epithelial-mesenchymal transition. Bioessays *23*, 912-923.

Segal, M.S. and Beem, E. (2001). Effect of pH, ionic charge, and osmolality on cytochrome c-mediated caspase-3 activity. Am. J. Physiol Cell Physiol *281*, C1196-C1204.

Semenza, G.L. (2001). HIF-1 and mechanisms of hypoxia sensing. Curr. Opin. Cell Biol. *13*, 167-171.

She, Q.B., Solit, D.B., Ye, Q., O'Reilly, K.E., Lobo, J., and Rosen, N. (2005). The BAD protein integrates survival signaling by EGFR/MAPK and PI3K/Akt kinase pathways in PTEN-deficient tumor cells. Cancer Cell *8*, 287-297.

Shibanuma, M., Kuroki, T., and Nose, K. (1988). Superoxide as a signal for increase in intracellular pH. J. Cell Physiol *136*, 379-383.

Shibata, K., Nakayama, T., Hirakawa, H., Hidaka, S., and Nagayasu, T. (2010). Clinicopathological significance of angiopoietin-like protein 4 expression in oesophageal squamous cell carcinoma. J. Clin. Pathol. *63*, 1054-1058.

Shoji, M., Kawamoto, S., Setoguchi, Y., Mochizuki, K., Honjoh, T., Kato, M., Hashizume, S., Hanagiri, T., Yoshimatsu, T., and Nakanishi, K. (1994). The 14-3-3 protein as the antigen for lung cancer-associated human monoclonal antibody AE6F4. Hum. Antibodies Hybridomas *5*, 123-130.

Simone, N.L., Bonner, R.F., Gillespie, J.W., Emmert-Buck, M.R., and Liotta, L.A. (1998). Laser-capture microdissection: opening the microscopic frontier to molecular analysis. Trends Genet. *14*, 272-276.

Simpson, C.D., Anyiwe, K., and Schimmer, A.D. (2008). Anoikis resistance and tumor metastasis. Cancer Lett. *272*, 177-185.

Singh, S., Sadanandam, A., and Singh, R.K. (2007). Chemokines in tumor angiogenesis and metastasis. Cancer Metastasis Rev. *26*, 453-467.

Sinha, P., Kohl, S., Fischer, J., Hutter, G., Kern, M., Kottgen, E., Dietel, M., Lage, H., Schnolzer, M., and Schadendorf, D. (2000). Identification of novel proteins associated with the development of chemoresistance in malignant melanoma using two-dimensional electrophoresis. Electrophoresis *21*, 3048-3057.

Son, J.W., Kang, H.K., Chae, M.H., Choi, J.E., Park, J.M., Lee, W.K., Kim, C.H., Kim, D.S., Kam, S., Kang, Y.M., and Park, J.Y. (2006). Polymorphisms in the caspase-8 gene and the risk of lung cancer. Cancer Genet. Cytogenet. *169*, 121-127.

Sopori, M. (2002). Effects of cigarette smoke on the immune system. Nat. Rev. Immunol. *2*, 372-377.

Stam, J.C., Sander, E.E., Michiels, F., van Leeuwen, F.N., Kain, H.E., van der Kammen, R.A., and Collard, J.G. (1997). Targeting of Tiam1 to the plasma membrane requires the cooperative function of the N-terminal pleckstrin homology domain and an adjacent protein interaction domain. J. Biol. Chem. *272*, 28447-28454.

Steeg, P.S. (2006). Tumor metastasis: mechanistic insights and clinical challenges. Nat. Med. *12*, 895-904.

Stockton, R.A., Schaefer, E., and Schwartz, M.A. (2004). p21-activated kinase regulates endothelial permeability through modulation of contractility. J. Biol. Chem. *279*, 46621-46630.

Storz, P. (2005). Reactive oxygen species in tumor progression. Front Biosci. *10*, 1881-1896.

Struewing, J.P., Hartge, P., Wacholder, S., Baker, S.M., Berlin, M., McAdams, M., Timmerman, M.M., Brody, L.C., and Tucker, M.A. (1997). The risk of cancer associated with specific mutations of BRCA1 and BRCA2 among Ashkenazi Jews. N. Engl. J. Med. *336*, 1401-1408.

Stupack, D.G., Puente, X.S., Boutsaboualoy, S., Storgard, C.M., and Cheresh, D.A. (2001). Apoptosis of adherent cells by recruitment of caspase-8 to unligated integrins. J. Cell Biol. *155*, 459-470.

Stupack, D.G., Teitz, T., Potter, M.D., Mikolon, D., Houghton, P.J., Kidd, V.J., Lahti, J.M., and Cheresh, D.A. (2006). Potentiation of neuroblastoma metastasis by loss of caspase-8. Nature *439*, 95-99.

Suh, Y.A., Arnold, R.S., Lassegue, B., Shi, J., Xu, X., Sorescu, D., Chung, A.B., Griendling, K.K., and Lambeth, J.D. (1999). Cell transformation by the superoxide-generating oxidase Mox1. Nature *401*, 79-82.

Sukonina, V., Lookene, A., Olivecrona, T., and Olivecrona, G. (2006). Angiopoietin-like protein 4 converts lipoprotein lipase to inactive monomers and modulates lipase activity in adipose tissue. Proc. Natl. Acad. Sci. U. S. A *103*, 17450-17455.

Sullivan, R. and Graham, C.H. (2007). Hypoxia-driven selection of the metastatic phenotype. Cancer Metastasis Rev. *26*, 319-331.

Sun, Y. and Lodish, H.F. (2010). Adiponectin deficiency promotes tumor growth in mice by reducing macrophage infiltration. PLoS. One. *5*, e11987.

Suresh, S. (2007). Biomechanics and biophysics of cancer cells. Acta Biomater. *3*, 413-438.

Svineng, G., Ravuri, C., Rikardsen, O., Huseby, N.E., and Winberg, J.O. (2008). The role of reactive oxygen species in integrin and matrix metalloproteinase expression and function. Connect. Tissue Res. *49*, 197-202.

Taddei, M.L., Parri, M., Mello, T., Catalano, A., Levine, A.D., Raugei, G., Ramponi, G., and Chiarugi, P. (2007). Integrin-mediated cell adhesion and spreading engage different sources of reactive oxygen species. Antioxid. Redox. Signal. *9*, 469-481.

Talks, K.L., Turley, H., Gatter, K.C., Maxwell, P.H., Pugh, C.W., Ratcliffe, P.J., and Harris, A.L. (2000). The expression and distribution of the hypoxia-inducible factors HIF-1alpha and HIF-2alpha in normal human tissues, cancers, and tumor-associated macrophages. Am. J. Pathol. *157*, 411-421.

Talmadge, J.E. and Fidler, I.J. (2010). AACR centennial series: the biology of cancer metastasis: historical perspective. Cancer Res. *70*, 5649-5669.

Tamura, G., Sakata, K., Nishizuka, S., Maesawa, C., Suzuki, Y., Iwaya, T., Terashima, M., Saito, K., and Satodate, R. (1996). Inactivation of the E-cadherin gene in primary gastric carcinomas and gastric carcinoma cell lines. Jpn. J. Cancer Res. *87*, 1153-1159.

Tamura, M., Gu, J., Danen, E.H., Takino, T., Miyamoto, S., and Yamada, K.M. (1999). PTEN interactions with focal adhesion kinase and suppression of the extracellular matrix-dependent phosphatidylinositol 3-kinase/Akt cell survival pathway. J. Biol. Chem. *274*, 20693-20703.

Tan, N.S., Michalik, L., Desvergne, B., and Wahli, W. (2003). Peroxisome proliferator-activated receptor (PPAR)-beta as a target for wound healing drugs: what is possible? Am. J. Clin. Dermatol. *4*, 523-530.

Tan, S.H., Pal, M., Tan, M.J., Wong, M.H., Tam, F.U., Teo, J.W., Chong, H.C., Tan, C.K., Goh, Y.Y., Tang, M.B., Cheung, P.C., and Tan, N.S. (2009). Regulation of cell

proliferation and migration by TAK1 via transcriptional control of von Hippel-Lindau tumor suppressor. J. Biol. Chem. *284*, 18047-18058.

Tang, H.L., Le, A.H., and Lung, H.L. (2006). The increase in mitochondrial association with actin precedes Bax translocation in apoptosis. Biochem. J. *396*, 1-5.

Thangaraju, M., Sharma, K., Liu, D., Shen, S.H., and Srikant, C.B. (1999). Interdependent regulation of intracellular acidification and SHP-1 in apoptosis. Cancer Res. *59*, 1649-1654.

Thannickal, V.J. and Fanburg, B.L. (2000). Reactive oxygen species in cell signaling. Am. J. Physiol Lung Cell Mol. Physiol *279*, L1005-L1028.

Thiery, J.P. (2002). Epithelial-mesenchymal transitions in tumour progression. Nat. Rev. Cancer *2*, 442-454.

Tian, L., Zhou, J., Casimiro, M.C., Liang, B., Ojeifo, J.O., Wang, M., Hyslop, T., Wang, C., and Pestell, R.G. (2009). Activating peroxisome proliferator-activated receptor gamma mutant promotes tumor growth in vivo by enhancing angiogenesis. Cancer Res. *69*, 9236-9244.

Tsatsanis, C. and Spandidos, D.A. (2004). Oncogenic kinase signaling in human neoplasms. Ann. N. Y. Acad. Sci. *1028*, 168-175.

Tzivion, G., Gupta, V.S., Kaplun, L., and Balan, V. (2006). 14-3-3 proteins as potential oncogenes. Semin. Cancer Biol. *16*, 203-213.

Ushio-Fukai, M. and Nakamura, Y. (2008). Reactive oxygen species and angiogenesis: NADPH oxidase as target for cancer therapy. Cancer Lett. *266*, 37-52.

van Nieuw Amerongen, G.P. and van Hinsbergh, V.W. (2002). Targets for pharmacological intervention of endothelial hyperpermeability and barrier function. Vascul. Pharmacol. *39*, 257-272.

Varner, J.A., Emerson, D.A., and Juliano, R.L. (1995). Integrin alpha 5 beta 1 expression negatively regulates cell growth: reversal by attachment to fibronectin. Mol. Biol. Cell *6*, 725-740.

Verine, J., Lehmann-Che, J., Soliman, H., Feugeas, J.P., Vidal, J.S., Mongiat-Artus, P., Belhadj, S., Philippe, J., Lesage, M., Wittmer, E., Chanel, S., Couvelard, A., Ferlicot, S., Rioux-Leclercq, N., Vignaud, J.M., Janin, A., and Germain, S. (2010). Determination of angptl4 mRNA as a diagnostic marker of primary and metastatic clear cell renal-cell carcinoma. PLoS. One. *5*, e10421.

Vogelstein, B. and Kinzler, K.W. (2004). Cancer genes and the pathways they control. Nat. Med. *10*, 789-799.

Wagner, B.A., Evig, C.B., Reszka, K.J., Buettner, G.R., and Burns, C.P. (2005). Doxorubicin increases intracellular hydrogen peroxide in PC3 prostate cancer cells. Arch. Biochem. Biophys. *440*, 181-190.

Wagner, K.D. and Wagner, N. (2010). Peroxisome proliferator-activated receptor beta/delta (PPARbeta/delta) acts as regulator of metabolism linked to multiple cellular functions. Pharmacol. Ther. *125*, 423-435.

Wang, Y., Lam, K.S., Lam, J.B., Lam, M.C., Leung, P.T., Zhou, M., and Xu, A. (2007). Overexpression of angiopoietin-like protein 4 alters mitochondria activities and modulates methionine metabolic cycle in the liver tissues of db/db diabetic mice. Mol. Endocrinol. *21*, 972-986.

Wang, Z., Han, B., Zhang, Z., Pan, J., and Xia, H. (2010). Expression of angiopoietin-like 4 and tenascin C but not cathepsin C mRNA predicts prognosis of oral tongue squamous cell carcinoma. Biomarkers *15*, 39-46.

Ward, P.A., Adams, J., Faustman, J., Gebhart, G.F., Geistfeld, J.G., Imbaratto, J.W., Peterson, N.C., Quimby, F., Marshak-Rothstein, A., Rowan, A.N. (1999) Monoclona antibody production-a report of the committee on methods of producing monoclonal antibodies. National Academy Press, Washington, DC 1999.

Wei, L., Yang, Y., Zhang, X., and Yu, Q. (2004). Altered regulation of Src upon cell detachment protects human lung adenocarcinoma cells from anoikis. Oncogene *23*, 9052-9061.

Wenzlaff, A.S., Cote, M. L., Bock, C.H., Land, S.J., Santer, S.K., Schwartz, D.R., and Schwartz, A.G. (2005). CYP1A1 and CYP1B1 polymorphisms and risk of lung cancer among never smokers: a population-based study. Carcinogenesis *26*, 2207-2212.

Werner, E. and Werb, Z. (2002). Integrins engage mitochondrial function for signal transduction by a mechanism dependent on Rho GTPases. J. Cell Biol. *158*, 357-368.

Westhoff, M.A. and Fulda, S. (2009). Adhesion-mediated apoptosis resistance in cancer. Drug Resist. Updat. *12*, 127-136.

Woo, C.H., Eom, Y.W., Yoo, M.H., You, H.J., Han, H.J., Song, W.K., Yoo, Y.J., Chun, J.S., and Kim, J.H. (2000). Tumor necrosis factor-alpha generates reactive oxygen species via a cytosolic phospholipase A2-linked cascade. J. Biol. Chem. *275*, 32357-32362.

Wu, W.S. (2006). The signaling mechanism of ROS in tumor progression. Cancer Metastasis Rev. *25*, 695-705.

Wurtele, M., Jelich-Ottmann, C., Wittinghofer, A., and Oecking, C. (2003). Structural view of a fungal toxin acting on a 14-3-3 regulatory complex. EMBO J. *22*, 987-994.

Xu, A., Lam, M.C., Chan, K.W., Wang, Y., Zhang, J., Hoo, R.L., Xu, J.Y., Chen, B., Chow, W.S., Tso, A.W., and Lam, K.S. (2005). Angiopoietin-like protein 4 decreases blood glucose and improves glucose tolerance but induces hyperlipidemia and hepatic steatosis in mice. Proc. Natl. Acad. Sci. U. S. A *102*, 6086-6091.

Yang, Y.H., Wang, Y., Lam, K.S., Yau, M.H., Cheng, K.K., Zhang, J., Zhu, W., Wu, D., and Xu, A. (2008). Suppression of the Raf/MEK/ERK signaling cascade and inhibition of angiogenesis by the carboxyl terminus of angiopoietin-like protein 4. Arterioscler. Thromb. Vasc. Biol. *28*, 835-840.

Yin, J., Vogel, U., Ma, Y., Qi, R., Sun, Z., and Wang, H. (2007). The DNA repair gene XRCC1 and genetic susceptibility of lung cancer in a northeastern Chinese population. Lung Cancer *56*, 153-160.

Yoon, J.C., Chickering, T.W., Rosen, E.D., Dussault, B., Qin, Y., Soukas, A., Friedman, J.M., Holmes, W.E., and Spiegelman, B.M. (2000). Peroxisome proliferator-activated receptor gamma target gene encoding a novel angiopoietin-related protein associated with adipose differentiation. Mol. Cell Biol. *20*, 5343-5349.

Zang, L., Palmer, T.D., Hancock, W.S., Sgroi, D.C., and Karger, B.L. (2004). Proteomic analysis of ductal carcinoma of the breast using laser capture microdissection, LC-MS, and 16O/18O isotopic labeling. J. Proteome. Res. *3*, 604-612.

Zhan, M., Zhao, H., and Han, Z.C. (2004). Signalling mechanisms of anoikis. Histol. Histopathol. *19*, 973-983.

Zhang, Z., Vuori, K., Reed, J.C., and Ruoslahti, E. (1995). The alpha 5 beta 1 integrin supports survival of cells on fibronectin and up-regulates Bcl-2 expression. Proc. Natl. Acad. Sci. U. S. A *92*, 6161-6165.

Zhu, H., Li, J., Qin, W., Yang, Y., He, X., Wan, D., and Gu, J. (2002). Cloning of a novel gene, ANGPTL4 and the functional study in angiogenesis. Zhonghua Yi. Xue. Za Zhi. *82*, 94-99.

Zhu,P., Tan,M.J., Huang,R.L., Tan,C.K., Chong,H.C., Pal,M., Lam,C.R., Boukamp,P., Pan,J.Y., Tan,S.H., Kersten,S., Li,H.Y., Ding,J.L., and Tan,N.S. (2011). Angiopoietin-like 4 Protein Elevates the Prosurvival Intracellular O(2)(-):H(2)O(2) Ratio and Confers Anoikis Resistance to Tumors. Cancer Cell *19*, 401-415.

7. ATTACHED PUBLICATIONS

1) Zhu P, Tan MJ, Roystan H, Tan CK, Chong HC, Pal M, Lam CRI, Boukamp P, Pan JY, Tan SH, Kersten S, Li HY, Ding JL, Tan NS. The angiopoietin-like 4 sustains an elevated pro-survival intracellular O_2^-:H_2O_2 ratio and confers anoikis resistance to tumor. (*Cancer Cell 19, 401-4*).

Cancer Cell
Article

Angiopoietin-like 4 Protein Elevates the Prosurvival Intracellular O_2^-:H_2O_2 Ratio and Confers Anoikis Resistance to Tumors

Pengcheng Zhu,[1] Ming Jie Tan,[1] Royston-Luke Huang,[1] Chek Kun Tan,[1] Han Chung Chong,[1] Mintu Pal,[1] Chee Ren Ivan Lam,[1] Petra Boukamp,[2] Jiun Yit Pan,[3] Suat Hoon Tan,[3] Sander Kersten,[4] Hoi Yeung Li,[1] Jeak Ling Ding,[5] and Nguan Soon Tan[1,*]

[1]School of Biological Sciences, Nanyang Technological University, 60 Nanyang Drive, Singapore 637551, Singapore
[2]Division of Genetics of Skin Carcinogenesis, German Cancer Research Center (DKFZ), Im Neuenheimer Feld 280, D-69120 Heidelberg, Germany
[3]National Skin Centre, 1 Mandalay Road, Singapore 308205, Singapore
[4]Nutrition, Metabolism and Genomics Group, Wageningen University, 6700 EV Wageningen, The Netherlands
[5]Department of Biological Sciences, National University of Singapore, 14 Science Drive, Singapore 117543, Singapore
*Correspondence: nstan@ntu.edu.sg
DOI 10.1016/j.ccr.2011.01.018

SUMMARY

Cancer is a leading cause of death worldwide. Tumor cells exploit various signaling pathways to promote their growth and metastasis. To our knowledge, the role of angiopoietin-like 4 protein (ANGPTL4) in cancer remains undefined. Here, we found that elevated ANGPTL4 expression is widespread in tumors, and its suppression impairs tumor growth associated with enhanced apoptosis. Tumor-derived ANGPTL4 interacts with integrins to stimulate NADPH oxidase-dependent production of O_2^-. A high ratio of O_2^-:H_2O_2 oxidizes/activates Src, triggering the PI3K/PKBα and ERK prosurvival pathways to confer anoikis resistance, thus promoting tumor growth. ANGPTL4 deficiency results in diminished O_2^- production and a reduced O_2^-:H_2O_2 ratio, creating a cellular environment conducive to apoptosis. ANGPTL4 is an important redox player in cancer and a potential therapeutic target.

INTRODUCTION

In response to stresses such as hypoxia and inflammation in the tumor microenvironment, tumor cells exploit various signaling molecules to sustain and promote their growth, invasiveness, and metastasis (Singh et al., 2007). Aggressive tumor metastasis and invasiveness are the main cause of mortality in patients with cancer (Fidler, 1999). The constitutive activation of intracellular signaling by these molecules in tumor cells leads to cellular changes, including increased proliferation and the ability for cells to grow beyond their original confined milieu, leading to metastasis (Pani et al., 2009; Westhoff and Fulda, 2009). Among these changes, the loss of dependence on integrin-mediated extracellular matrix contact for growth (i.e., anoikis resistance) is an essential feature of tumor cells. However, the mechanism by which anoikis resistance is acquired remains an unsolved problem in cancer biology.

Although low levels of reactive oxygen species (ROS) regulate cellular signaling and play an important role in normal cell proliferation, recent studies show that tumors exhibit an excessive amount or persistent elevation of ROS (specifically the superoxide anion O_2^-) and utilize a redox-based mechanism to evade death by anoikis (Chiarugi, 2008; Giannoni et al., 2008; Pervaiz and Clément, 2007). Previous studies have indicated that ROS are involved in tumor initiation, progression, and maintenance. Furthermore, deregulated ROS production is also associated

Significance

We show here that elevated expression of ANGPTL4 is widespread in tumors, and tumor-derived ANGPTL4 confers anoikis resistance to tumors via autocrine adhesion mimicry. Our findings that ANGPTL4 hijacks integrin-mediated signaling to maintain an elevated, oncogenic O_2^-:H_2O_2 ratio and, therefore, confers anoikis resistance to tumor cells suggest ANGPTL4 as an important player in redox-mediated cancer progression. Treating cancer cells with ANGPTL4-targeted RNAi or monoclonal antibodies imparts a significant decrease in in vivo tumor growth and induces apoptosis in cancer cell lines upon anoikis challenge. Our findings suggest that anticancer strategies focusing on redox-based apoptosis induction in tumors are viable.

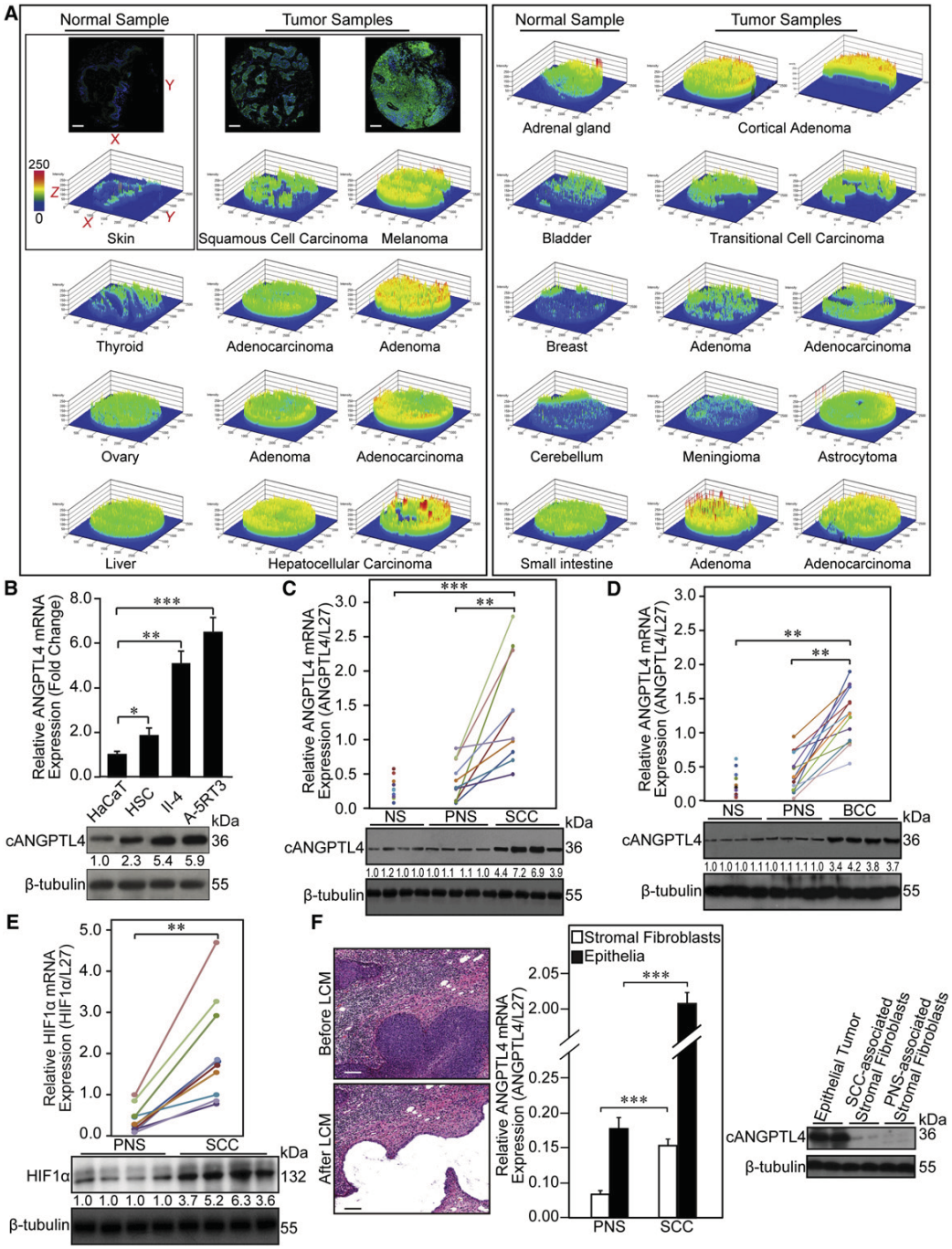

Figure 1. Elevated Expression of ANGPTL4 in Various Tumor Types

(A) ANGPTL4 expression varied among tumors procured from different anatomic sites. Heat map profiles generated from IF images. X, Y, and Z axes represent the length, width, and IF intensity, respectively. Representative images of normal skin and tumor samples with their corresponding heat maps are shown. Heat maps from same anatomic sites are grouped horizontally. Results are representative of two independent experiments performed in duplicate. Scale bars represent 200 μm.

(B) Relative ANGPTL4 mRNA and protein levels in nontumorigenic skin cell HaCaT and tumorigenic lines HSC, II-4, and A-5RT3.

(C and D) Relative ANGPTL4 mRNA and protein levels in paired human SCCs (C) or BCCs (D) and cognate PNSs. Normal human skin (NS) biopsies serve as additional controls. Three SSCs with the highest mRNA ANGPTL4 levels corresponded to an invasive prognosis.

with an invasive tumor phenotype. Oncogenic and mitogenic Ras activity is superoxide dependent, and a sustained increase in ROS following the overexpression of Nox1 (the catalytic subunit of NADPH oxidase) leads to cell transformation and aggressive tumor metastasis (Komatsu et al., 2008; Suh et al., 1999). Elevated production of ROS following activation of the c-Met proto-oncogene leads to cell transformation and malignant growth (Ferraro et al., 2006), and Rac-dependent redox signals increase the secretion of metalloproteinases and induce epithelial-mesenchymal transition (Wu, 2006), two key features of invasive cancers. Thus, a clear understanding of the underlying redox-based anoikis escape mechanism and its connection to malignancy will provide insight into therapeutic interventions.

The secreted protein angiopoietin-like 4 (ANGPTL4) was recently linked to tumor progression. ANGPTL4 was previously identified as a paracrine and, possibly, endocrine regulator of lipid metabolism (Oike et al., 2005) and a target of peroxisome proliferators-activated receptors (PPARs) (Kersten et al., 2000). ANGPTL4 is expressed in numerous cell types, such as adipocytes and hepatocytes, and is upregulated after fasting and hypoxia (Belanger et al., 2002; Kersten et al., 2000). Importantly, ANGPTL4 undergoes proteolytic processing to release its C-terminal fibrinogen-like domain (cANGPTL4), which circulates as a monomer but whose function remains unclear. The N-terminal coiled-coil domain of ANGPTL4 (nANGPTL4) mediates ANGPTL4 oligomerization and binds to lipoprotein lipase to modulate lipoprotein metabolism (Ge et al., 2004). Emerging studies also implicate tumor-derived ANGPTL4 in cancer metastasis via its effect on endothelial integrity. However, whether ANGPTL4 promotes or inhibits vascular permeability and, thus, cancer metastasis remains controversial. Several previous studies suggest that ANGPTL4 can prevent metastasis by inhibiting vascular leakiness (Galaup et al., 2006; Ito et al., 2003). Conversely, ANGPTL4 is also implicated as a pro-angiogenic factor (Le Jan et al., 2003). Recent reports demonstrate that *ANGPTL4* is one of the most highly predictive genes associated with breast cancer metastasis to the lung (Minn et al., 2005; Padua et al., 2008). ANGPTL4 expression is upregulated in clear cell renal-cell carcinoma (Le Jan et al., 2003) and oral tongue squamous cell carcinoma (SCC) (Wang et al., 2010). In addition, tumor-derived ANGPTL4 has been shown to promote metastasis by disrupting vascular integrity (Padua et al., 2008). The reasons for these conflicting results and the underlying mechanism of ANGPTL4 activity in tumor cells have not been clarified, hampering our understanding of its precise role in cancer metastasis. More importantly, the global expression pattern of ANGPTL4 in different types of tumors, to our knowledge, has yet to be fully investigated, and the pathological relevance of ANGPTL4 in cancer biology remains largely undefined. Thus, we set up to study the role of ANGPTL4 in tumor growth and metastasis.

RESULTS

Elevated Expression of ANGPTL4 in Various Tumor Types

To examine the expression profile of ANGPTL4 in human tumors, we screened its expression pattern on two human tumor tissue arrays, which cover most of the common benign, malignant, and metastatic tumors originating from various anatomic sites. Using immunofluorescence (IF) with an anti-cANGPTL4 antibody, we observed widespread, elevated ANGPTL4 expression in all epithelial tumor samples when compared to the corresponding normal tissues, regardless of the anatomic sites of origin (Figure 1A; see Figures S1A and S1B available online). However, the IF signal level varied among different types of tumors. Notably, the expression of ANGPTL4 increased as tumors progressed from a benign state to an invasive/metastatic state (Figure S1C). Next, we determined ANGPTL4 expression on three human skin tumorigenic lines (HSC, II-4, and A-5RT3), ten human SCC, and 13 basal cell carcinoma (BCC) biopsies by quantitative real-time PCR (qPCR) and immunoblot analyses. Consistent with our prior results, we observed increased ANGPTL4 mRNA and protein levels in these epithelial tumor cells compared with the nontumorigenic human skin line HaCaT or cognate peri-tumor normal samples (PNSs), respectively (Figures 1B–1D). No difference was observed between normal skin biopsies (NSs) and PNSs (Figures 1C and 1D). Interestingly, the three SCCs expressing the highest mRNA level of ANGPTL4 corresponded to an invasive prognosis (Figure 1C), underscoring our finding from tumor tissue arrays. In addition, polyclonal antibodies against either the N or C terminus of ANGPTL4 detected only cANGPTL4 in these tumor lines and SSCs (Figures 1B–1D; Figure S1D and S1E). To understand the reason for the increased expression of ANGPTL4 in tumor cells, we examined the expression of hypoxia-inducible factor 1 α (HIF1α) and PPARs in the SCCs. We found a concomitant upregulation of HIF1α with ANGPTL4 in SSCs than in PNSs (correlation coefficient = 0.88) (Figure 1E; Figures S1F). No clear correlation was observed between the expression of ANGPTL4 and the three PPAR isotypes (Figures S1G–S1I). These results suggested that at least for SCCs, the elevated ANGPTL4 expression reflects the tumor's hypoxic microenvironment. As a protein that is secreted by tumor cells, ANGPTL4 may perform paracrine or autocrine function in tumors. Therefore, we sought to determine the source of ANGPTL4 in tumors. We isolated epithelial tumor and stromal tissues, the latter consisting mainly of fibroblasts, from SCCs and PNSs, using laser capture microdissection (LCM). qPCR and immunoblot analyses revealed that epithelial tumor cells, rather than tumor stroma, were the major contributor of ANGPTL4 in SCCs (Figure 1F). Furthermore, only a low, baseline level of ANGPTL4 expression was found in normal PNS stroma and epithelia, suggesting that ANGPTL4 may have an autocrine role in tumors.

(E) Relative HIF1α mRNA and protein levels in paired SCCs and PNSs. For qPCR results, data points from the same individual are linked by colored lines.
(F) Relative ANGPTL4 mRNA and protein levels in LCM epithelial cells and stromal fibroblasts from paired SCCs and PNSs. Hematoxylin and eosin images of an SCC section before and after LCM of epithelial tissue are shown in left panel. Scale bars represent100 μm. Microdissected tissues were processed for qPCR (middle panel) and immunoblotting (right panel).
(B–F) mRNA data (mean ± SD) are from two independent qPCR experiments performed in triplicate. Ribosomal protein L27 (L27) serves as a reference housekeeping gene. *$p < 0.05$; **$p < 0.01$; ***$p < 0.001$. Immunoblot data are from three independent experiments performed in duplicate. β-Tubulin serves as a loading and transfer control. See also Figure S1.

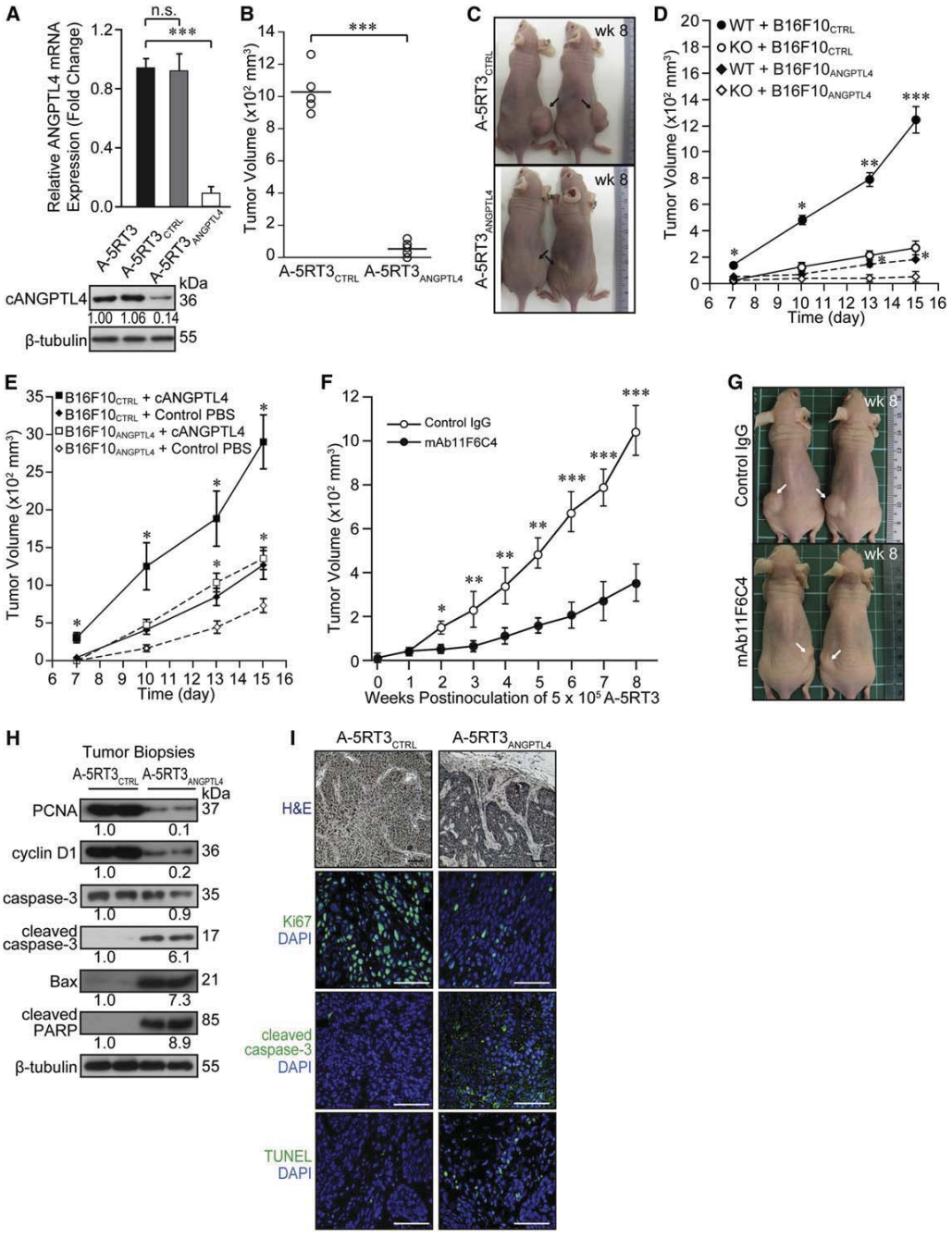

Figure 2. Suppression of ANGPTL4 Impairs Tumorigenicity

(A) Relative ANGPTL4 mRNA and protein levels in A-5RT3 (parental), A-5RT3$_{CTRL}$ (scrambled control), and A-5RT3$_{ANGPTL4}$ (knockdown) cells. Data (mean ± SD) are from three independent qPCR experiments performed in triplicate. Ribosomal protein L27 (L27) serves as a reference housekeeping gene. Immunoblot data are from three independent experiments performed in duplicate. β-Tubulin serves as a loading and transfer control.

(B) Size of xenograft tumors induced in nude mice by 5 × 10^5 of A-5RT3$_{ANGPTL4}$ or A-5RT3$_{CTRL}$ cells 8 weeks postinoculation (n = 5 per group). Each circle represents mean size from three measurements on each mouse at week 8 (wk 8).

(C) Representative pictures of A-5RT3$_{CTRL}$- and A-5RT3$_{ANGPTL4}$-induced tumors (wk 8) in (B). Black arrows indicate inoculation sites.

(D and E) Tumor volume induced in ANGPTL-KO and WT mice (D), and PBS- or recombinant cANGPTL4-treated C57BL/6J WT mice (E) by B16F10 melanoma (B16F10$_{CTRL}$, control) and ANGPTL4-knockdown (B16F10$_{ANGPTL4}$). Cells (1 × 10^6) were s.c. inoculated into each mouse (n = 6 per group). Mice (E) were treated i.v. with either 3 mg/kg of cANGPTL4 or vehicle PBS thrice a week. Values (mean ± SEM) are from three measurements of each mouse.

Suppression of ANGPTL4 Impairs Tumor Growth

Next, we investigated the biological relevance of elevated ANGPTL4 expression to tumor growth via RNAi. Four sets of siRNAs targeting different segments of the *ANGPTL4* sequence were stably introduced into the metastatic skin tumor line A-5RT3 (Mueller et al., 2001), and the subline with the highest knockdown efficiency (A-5RT3$_{ANGPTL4}$) was selected for subsequent studies. A nontargeting scrambled siRNA was also integrated into A-5RT3 (A-5RT3$_{CTRL}$) as a negative control. ANGPTL4 mRNA and protein levels were suppressed by >85% in A-5RT3$_{ANGPTL4}$ as compared with the parental A-5RT3 or A-5RT3$_{CTRL}$ (Figure 2A). The induction of interferon responses has been reported as a challenge to the specificity of some RNAi approaches (Bridge et al., 2003). To test whether the RNAi-mediated silencing of ANGPTL4 was associated with interferon responses, we measured the expression of several key interferon response genes by qPCR. No induction of *OAS1*, *OAS2*, *MX1*, or *ISGF3*γ was detected in A-5RT3$_{ANGPTL4}$ cells compared with either A-5RT3 or A-5RT3$_{CTRL}$ (Figure S2A).

As expected, the injection of A-5RT3$_{CTRL}$ cells into immunodeficient mice induced large primary tumors ($\sim$1000 mm^3) in all five mice at week 8, but A-5RT3$_{ANGPTL4}$-induced tumors displayed a 90% reduction in tumor growth (Figures 2B and 2C). A-5RT3$_{ANGPTL4}$-induced tumor growth was similarly reduced, albeit a 40% reduction, when mice were implanted with increasing number of tumor cells (Figure S2B). To strengthen the above observations, we subcutaneously (s.c.) implanted B16F10 cells into ANGPTL4-knockout (KO) and control (wild-type [WT]) mice. WT and KO mice were maintained in a C57BL/6J background, and the B16F10 melanoma was derived from the same background. Notably, B16F10 tumor cells implanted in KO mice grew slower than those implanted in WT mice; at day 15, the average tumor volume in KO mice was $\sim$6-fold less than in WT mice (Figure 2D). The injection of ANGPTL4-knockdown (B16F10$_{ANGPTL4}$) cells into KO mice induced little tumor growth and showed similar growth profile in WT mice compared to control B16F10 (B16F10$_{CTRL}$)-induced tumors in KO mice (Figure 2D). Conversely, WT mice implanted with B16F10$_{CTRL}$ cells and intravenously (i.v.) injected three times a week with recombinant N-terminal histidine-tagged cANGPTL4 showed greater tumor growth. The average tumor volume in cANGPTL4-treated mice was $\sim$3-fold larger than PBS-treated mice (Figure 2E; Figures S2C and S2D). B16F10$_{ANGPTL4}$-induced tumor growth was diminished in PBS-treated mice as compared to cANGPTL4-treated mice (Figure 2E). Next, we reasoned that treating mice injected with A-5RT3$_{CTRL}$ cells with an antibody that interferes with the action of ANGPTL4 would recapitulate the observation made with A-5RT3$_{ANGPTL4}$ cells. To this end the monoclonal human cANGPTL4-directed antibody mAb11F6C4 was identified and produced for our immunotherapy experiment based on its superior k_{on}, k_{off}, and K_D values, as determined by surface plasmon resonance (SPR) (Figure S2E and Supplemental Experimental Procedures). Notably, inhibition of ANGPTL4 with mAb11F6C4 attenuated tumor growth in immunodeficient mice, compared with control IgG-treated mice (Figures 2F and 2G). Immunoblot and IF analyses of A-5RT3$_{ANGPTL4}$-induced tumor biopsies indicated reduced cell proliferation and enhanced cell apoptosis than A-5RT3$_{CTRL}$-induced tumors (Figures 2H and 2I). A qPCR-focused array of A-5RT3$_{ANGPTL4}$-induced tumor biopsies further suggested increased expression of many pro-apoptotic genes, whereas expression of cell proliferation genes was diminished (Figure S2F and Table S1). Together, these observations clearly support a tumor-promoting role for cANGPTL4.

ANGPTL4-Deficient Tumor Cells Showed Increased Susceptibility to Anoikis

Anchorage-independent growth or anoikis resistance of tumor cells, a hallmark of tumor malignancy (Hanahan and Weinberg, 2000), was investigated by tumor colony formation in soft agar and anoikis assays (Salmon, 1984). Underscoring our in vivo findings, the colony-forming potential of A-5RT3$_{ANGPTL4}$ cells was undermined and formed fewer ($\sim$85%) tumor colonies on soft agar than A-5RT3$_{CTRL}$ (Figure 3A). Furthermore, A-5RT3$_{ANGPTL4}$ was more susceptible to anoikis, having 30% more apoptotic cells and enhanced caspase activities than A-5RT3$_{CTRL}$ cells after 2 hr of anoikis (Figures 3B and 3C). The addition of exogenous recombinant cANGPTL4 reduced the apoptotic index of A-5RT3$_{ANGPTL4}$ cells in a dose-dependent manner (Figure 3D). Similarly, ANGPTL4 deficiency in human keratinocytes rendered these cells $\sim$50% more susceptible to anoikis when compared to control keratinocytes, suggesting that a low amount of ANGPTL4 was also necessary to confer anoikis resistance in normal epithelial cells (Figure S3A). No difference in the apoptotic index was observed due to the deficiency of ANGPTL4 in adhered A-5RT3 cells or keratinocytes (Figures S3B and S3C).

ANGPTL4 Interacts with Integrins β1 and β5

The mechanism by which ANGPTL4 mediates anoikis resistance is an unanswered question. Previous studies have revealed that anoikis is an integrin-dependent process (Chiarugi, 2008; Zhan et al., 2004). Thus, we hypothesize that ANGPTL4 also exerts its role in tumor cells through integrins-mediated signaling. We examined if cANGPTL4 can interact with integrins. Indeed, SPR and ELISA results showed that ANGPTL4 specifically interacts with integrins β1 and β5, but not with β3 (Figures 3E and 3F), and these interactions were blocked by either mAb11F6C4 or

(F) Tumor volume in nude mice injected s.c. with 5 × 10^5 of A-5RT3 cells and treated i.v. with 30 mg/kg/week of either mAb11F6C4 or control IgG as a function of time (n = 6 per group). Each circle represents mean ± SEM from three measurements of each mouse.

(G) Representative pictures of control IgG- or mAb11F6C4-treated nude mice (wk 8) as described in (F). White arrows indicate inoculation sites.

(H) Immunoblot of proliferation (PCNA and cyclin D1), and apoptosis (cleaved caspase-3, Bax and cleaved PARP) markers in A-5RT3$_{ANGPTL4}$- and A-5RT3$_{CTRL}$-induced tumor biopsies. Immunoblot data are from three independent experiments performed in duplicate. β-Tubulin serves as a loading and transfer control.

(I) Hematoxylin and eosin (H&E) and IF staining of A-5RT3$_{CTRL}$- and A-5RT3$_{ANGPTL4}$-induced tumor sections. Proliferating (Ki67) and apoptotic (cleaved caspase-3 or TUNEL) cells were identified using the indicated antibodies or assay. Sections were counterstained with DAPI (blue). Scale bars represent 40 μm.

(H and I) All experiments were performed using tumor biopsies harvested from mice described in (B) and (C) at week 8 (wk 8). See also Figure S2 and Table S1.

*p < 0.05; **p < 0.01; ***p < 0.00; n.s., not significant.

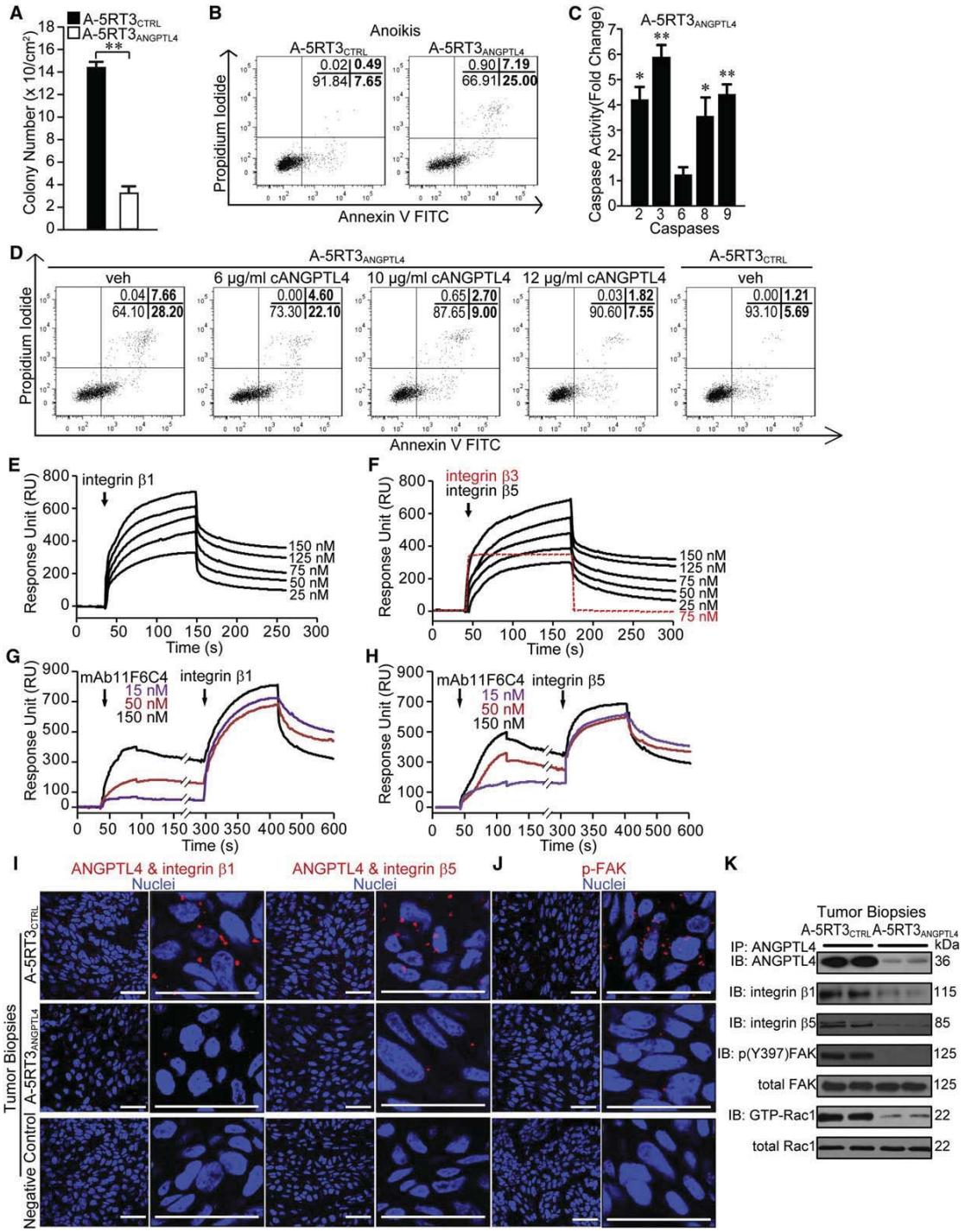

Figure 3. ANGPTL4 Interacts with Integrins β1 and β5 to Confer Tumor Cells Anoikis Resistance

(A) Quantification of A-5RT3$_{CTRL}$ and A-5RT3$_{ANGPTL4}$ tumor colonies on soft agar (left panel). Values (mean ± SD) are from four independent assays performed in triplicate. **$p < 0.01$.

(B) Percentage of apoptotic A-5RT3$_{CTRL}$ and A-5RT3$_{ANGPT4}$ cells after 2 hr of anoikis, as analyzed by FACS (5000 events). The sum of Annexin V^+/PI^- (early apoptosis) and Annexin V^+/PI^+ (late apoptosis) cells were considered apoptotic. Values (bold) denote apoptotic cells (%). Results are representative of three independent experiments.

integrin-specific antibodies (Figure 3G and 3H; Figures S3D–S3G). ANGPTL4 deficiency did not affect the expression of integrins β1, β3, and β5 (Figure S3H). An in situ proximity ligation assay (PLA) detected ANGPTL4-integrin complexes in both A-5RT3$_{CTRL}$ cells and tumors (Figure 3I; Figure S3I), confirming that this interaction also exists in vivo. Further investigation revealed that integrin activation by ANGPTL4 binding triggered focal adhesion kinase (FAK) in A-5RT3$_{CTRL}$ cells and tumors, which were reduced by >70% in A-5RT3$_{ANGPTL4}$ (Figure 3J; Figure S3J). All of these findings were corroborated by results from immunodetection of FAK on tumor biopsies (Figure 3K). Our findings suggest that ANGPTL4 secreted by epithelial tumor cells acts in an autocrine manner to hijack the integrin/FAK-regulated pathway, conferring anoikis resistance to tumors and, thus, sustaining tumor growth.

ANGPTL4 Elevates the O_2^- Level and Maintains a High O_2^-:H_2O_2 Ratio in Tumor Cells

ROS can be regulated through integrin engagement, and an elevated O_2^- level allows tumor cells to avoid anoikis (Pani et al., 2009; Pervaiz and Clément, 2007). In this regard we assessed whether ANGPTL4-integrin interaction regulates ROS production in tumor cells. Using electron paramagnetic resonance spectroscopy (EPR) in combination with 5-(diethoxyphosphoryl)-5-methyl-1-pyrroline-N-oxide (DEPMPO) spin trapping, we measured a decrease in the O_2^- level in A-5RT3$_{ANGPTL4}$ compared to A-5RT3$_{CTRL}$ cells (Figures 4A and 4B), suggesting that ANGPTL4 is vital in sustaining O_2^- production in tumor cells. To determine the source of O_2^-, similar experiments were performed using specific inhibitors that block the mitochondrial respiratory chain complex I and membrane-bound NADPH oxidase, which are two major producers of O_2^- in mammalian cells (Giannoni et al., 2008). Treatment of tumor cells with rotenone, a mitochondrial respiratory chain complex I inhibitor (Irani et al., 1997), did not alter cellular O_2^- level (Figures 4A and 4B), suggesting that this complex has little role in generating O_2^- in tumors. Further excluding mitochondria as the source of ANGPTL4-mediated O_2^- generation, qPCR analysis showed no change in the expression of selected genes in the methionine/homocysteine metabolic cycle (Figure S4A), as previously studied in diabetic rodent hepatocytes (Wang et al., 2007). In contrast the O_2^- level was abrogated by using two different NADPH oxidase inhibitors (Ushio-Fukai and Nakamura, 2008), diphenylene iodonium (DPI) and apocynin (Figures 4A and 4B). ROS generated through the involvement of the small GTPase Rac1 and NADPH oxidase upon integrin engagement exert a mandatory role in transmitting a prosurvival signal that ensures that tumor cells escape from anoikis (Giannoni et al., 2008; Jonesson and Bar-Sagi, 1998). Comparative immunoblot analyses of anti-cANGPTL4 immunoprecipitates from A-5RT3$_{CTRL}$- and A-5RT3$_{ANGPTL4}$-induced tumor lysates detected integrins β1 and β5, along with phosphorylated FAK and active GTP-bound Rac1, in A-5RT3$_{CTRL}$-induced tumors, all of which were reduced in A-5RT3$_{ANGPTL4}$-induced tumors (Figure 3K). To further validate the relevance of Rac1 in ANGPTL4-mediated O_2^- production, we transiently transfected A-5RT3$_{CTRL}$ and A-5RT3$_{ANGPTL4}$ cells with dominant-negative Rac1 (T17N) and constitutively active Rac1 (G12V), respectively. We measured a diminished O_2^- level in the former and, conversely, an obviously rescued O_2^- production in the latter. The percentage of inhibition and recovery was consistent with the ~65% transfection efficiencies, as estimated using a GFP-expressing vector. The requirement of Rac1 suggested a Rac1-engaged Nox (i.e., Nox1-3)-dependent mechanism for O_2^- production. Because Nox 3 is expressed predominantly in the inner ear (Paffenholz et al., 2004), we examined the expression of Nox1 and Nox2 in A-5RT3 (Figure S4B). Next, we performed Nox1 and Nox2 knockdown (Nox1 kd and Nox2 kd, respectively) in A-5RT3$_{CTRL}$ and A-5RT3$_{ANGPTL4}$ cells (Figure S4C), and measured the O_2^- level using EPR (Figures 4A and 4B). Results indicated that Nox1 NADPH oxidase is the predominant source of ANGPTL4-mediated O_2^- generation in tumor cells. The O_2^- level was completely abolished by superoxide scavenger Tiron, which serves as a negative control for superoxide measurements (Figures 4A and 4B). These data were reproduced by a chemiluminescence assay using 2-methyl-6-(4-methoxyphenyl)-3, 7-dihydroimidazo[1,2-a]pyrazin-3-one hydrochloride (MCLA) (Figure 4C) (Münzel et al., 2002). Next, we measured the level of H_2O_2 in tumor cells in the presence of a specific catalase inhibitor, 3-amino-l, 2, 4-triazole (Chance et al., 1979; Wagner et al., 2005). H_2O_2 levels were higher in A-5RT3$_{ANGPTL4}$ than A-5RT3$_{CTRL}$ cells (Figure 4D). Nox1 kd did not affect the H_2O_2 level, suggesting that ANGPTL4 modulated H_2O_2 production, linked to an unknown mechanism (Figure S4D). Notably, the lower O_2^- level and O_2^-:H_2O_2 ratio were concurrent with 3-fold more apoptosis and enhanced caspase activities within 2 hr of anoikis in A-5RT3$_{ANGPTL4}$ compared

(C) Relative activities of caspases 2, 3, 6, 8, 9 in A-5RT3$_{ANGPTL4}$ cells compared to A-5RT3$_{CTRL}$ cells (assigned value of one) after 2 hr of anoikis. Values (mean ± SD) are from three independent experiments performed in triplicate. *$p < 0.05$; **$p < 0.01$.

(D) Percentage of anoikis-induced apoptotic A-5RT3$_{ANGPT4}$ cells in the presence of increasing exogenous recombinant cANGPTL4, as analyzed by FACS (5000 events). Vehicle (PBS)-treated A-5RT3$_{CTRL}$ and A-5RT3$_{ANGPT4}$ cells served as controls for comparison. The apoptotic index is described in (B).

(E and F) Representative sensorgrams of three independent experiments showing binding profiles between immobilized-ANGPTL4 and integrin β1 (E) or integrin β5 (F). Integrin β3 (75 nM) did not show any detectable interaction (F, dotted red line). Sensorgrams were corrected against a reference flow cell with no immobilized protein. K_D ~10^{-7} M was determined after global fitting (Langmuir 1:1 model) using Scrubber2.

(G and H) Representative sensorgrams showing dose-dependent blocking of integrin β1 (G) and integrin β5 (H) to immobilized-ANGPTL4 by preinjection with the indicated concentrations of mAb11F6C4.

(I and J) In situ PLA detection of ANGPTL4:integrin β1 (I, left two panels), ANGPTL4:integrin β5 (I, right two panels), and phosphorylated FAK (J) in A-5RT3$_{ANGPTL4}$- and A-5RT3$_{CTRL}$-induced tumor biopsies. Higher magnification images are shown (I, second and fourth panels; J, right panel). PLA signals are shown in red, and nuclei are stained blue by Hoechst dye. Negative controls were performed with only anti-nANGPTL4 (I) or anti-FAK (J) antibodies. Scale bars represent 40 μm.

(K) Immunoprecipitation and immunodetection of ANGPTL4, integrin β1, integrin β5, total FAK, phosphorylated FAK (pY397FAK), total Rac1, and GTP-bound Rac1 (GTP-Rac1) from the indicated tumor sections. A configuration-specific monoclonal anti-Rac-GTP antibody was used for immunoprecipitation of GTP-Rac1. Total FAK serves as a loading and transfer control.

Experiments in (I)–(K) were performed using tumor biopsies described in Figures 2B and 2C. All experiments in (B)–(K) were repeated three times with consistent results. See also Figure S3.

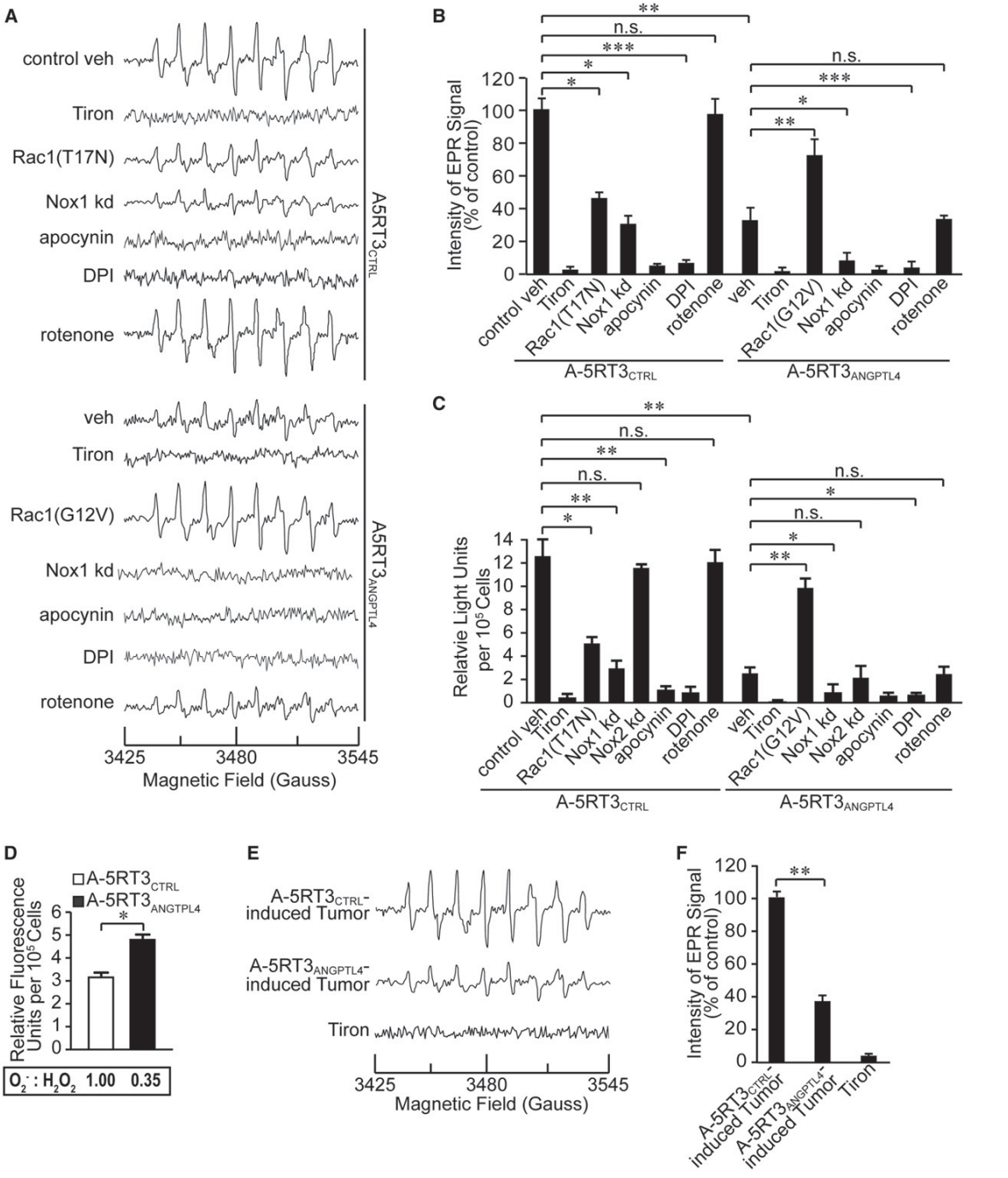

Figure 4. ANGPTL4 Elevates O_2^- Level and Maintains a Relatively High O_2^-:H_2O_2 Ratio in Tumor Cells

(A and E) Representative EPR spectra of DEPMPO-superoxide spin adduct from A-5RT3$_{CTRL}$ and A-5RT3$_{ANGPTL4}$ cells (A) or A-5RT3$_{CTRL}$- and A-5RT3$_{ANGPTL4}$-induced tumors (E) in the absence or presence of indicated chemicals or inhibitors. A-5RT3$_{CTRL}$ and A-5RT3$_{ANGPTL4}$ cells were transiently transfected either with vector expressing Rac1(T17N) or Rac1(G12V), or with ON-TARGETplus siRNA against either Nox1 (Nox1 kd) or Nox2 (Nox2 kd). The superoxide adduct of DEPMPO has hyperfine splitting constants of: a_N = 13.13 gauss; a_P = 55.61 gauss; a^{β}_H = 13.11 gauss; and a^{γ}_H = 0.71, 0.42, 0.7, 0.25, and 0.6 gauss.

(B and F) EPR signal intensity at 3480 gauss from A-5RT3$_{CTRL}$ and A-5RT3$_{ANGPTL4}$ cells in (A) or tumors in (E).Tiron-treated measurements serve as negative signal controls.

(C) Measurement of O_2^- levels using the MCLA assay in A-5RT3$_{CTRL}$ and A-5RT3$_{ANGPTL4}$ cells in the absence or presence of the indicated chemicals or inhibitors.

to A-5RT3$_{CTRL}$ cells (Figures 3B, 3C, and 4A–4D). Accordingly, we observed a reduced O_2^- level in A-5RT3$_{ANGPTL4}$-induced tumors compared to A-5RT3$_{CTRL}$-induced tumors (Figures 4E and 4F), which was associated with increased apoptosis (Figure 2H and 2I; Figure S2F).

To underscore the relevance of these findings to other cancers, similar experiments were performed using the breast cancer line MDA-MB-231, after using mAb11F6C4 to dose dependently neutralize endogenous cANGPTL4. We showed earlier that mAb11F6C4 was able to block cANGPTL4-integrin interaction (Figures 3G and 3H; Figures S3D–S3G). Consistent with the above results, the inhibition of cANGPTL4 in MDA-MB-231 reduced the O_2^- level (Figures S4E–S4G), lowered the O_2^-:H_2O_2 ratio (Figure S4H), and enhanced apoptosis and caspase activities (Figures S4I and S4J). Nox1 kd (Figure S4K) but not Nox2 kd reduced ANGPTL4-mediated O_2^- production (Figures S4E–S4G) with little effect on H_2O_2 production (Figure S4L). Together, these findings indicate that ANGPTL4 protects tumor cells from anoikis via an NADPH oxidase-dependent O_2^- generation mechanism.

ANGPTL4-Mediated O_2^- Activates the Src, PI3K/PKBα, and ERK Survival Pathways

Previous reports have shown that ROS produced via integrin engagement oxidizes and activates Src, which stimulates the ERK and PKBα prosurvival pathways (Giannoni et al., 2008, 2009; Pani et al., 2009). Both pathways regulate the subcellular localization or stability of BH3-only apoptotic proteins (e.g., Bad and Bim), which are essential for executing anoikis (Bouillet and Strasser, 2002). Thus, we asked whether ANGPTL4-integrin engaged O_2^- generation employs these downstream signaling pathways to modulate tumor cell behavior. Immunoblot analyses revealed diminished expression of oxidized/activated Src, phosphorylated PKBα, and ERK1 in A-5RT3$_{ANGPTL4}$-induced tumors and A-5RT3$_{ANGPTL4}$ cells (Figure 5A, and left panel of Figure 5B). Similar immunoblot analyses performed in the presence of DPI and with Nox1 kd cells revealed reduced Src, PKBα, and ERK1 activation, emphasizing the role of O_2^- in their activities (Figure 5B). The inhibition of PI3K by LY294002 and Wortmannin, a pivotal upstream mediator of PKBα, caused 4-fold more apoptosis of tumor cells upon anoikis challenge, reaching levels comparable to those of A-5RT3$_{ANGPTL4}$ cells (Figure 5C). In addition, inhibition of MEK1/2, the upstream signal of ERK1, by PD98059 also resulted in an enhancement of apoptotic cell numbers, albeit to a lesser extent (~50%) compared to PI3K inhibitors (Figure 5C). These results suggest that the PI3K/PKBα and ERK1/2 downstream survival pathways are modulated and exploited by ANGPTL4 engagement in tumor cells, the former being the predominant pathway.

The 14-3-3 adaptor protein is known to act downstream of the aforementioned survival pathways by sequestering pro-apoptotic Bad from the mitochondria to prevent apoptosis (She et al., 2005). In agreement with these previous findings, the number of 14-3-3/Bad complexes and 14-3-3β/σ proteins was reduced by ~70% in A-5RT3$_{ANGPTL4}$-induced tumors (Figures 5D–5F). The Na^+/H^+ exchanger 1 (NHE), which positively influences cell proliferation by maintaining an alkaline intracellular environment (Akram et al., 2006), was also diminished in A-5RT3$_{ANGPTL4}$-induced tumors (Figure 5D), indicating that NHE plays a subsidiary role in ANGPTL4-mediated tumor cell growth. Upon oxidant challenge in tumor cells, the induction of superoxide dismutase (SOD) expression is muted, allowing tumor cell proliferation (Oberley, 2001; Pervaiz and Clément, 2007). Indeed, we found that cytosolic Zn/CuSOD expression was enhanced in A-5RT3$_{ANGPTL4}$-induced tumors (Figure 5D), which contribute to a reduced O_2^-:H_2O_2 ratio via an indirect but linked mechanism (Figure 4D).

ANGPTL4 Deficiency Abrogates O_2^- Production and Sensitizes Cancer Cells to Anoikis

Our results revealed that the suppression of ANGPTL4, either by RNAi (Figures 4A–4C) or inhibition with mAb11F6C4 (Figures S4E–S4G), results in a dose-dependent reduction of O_2^- levels. To underscore the importance of ANGPTL4 in the regulation of O_2^- production, maintenance of a high O_2^-:H_2O_2 ratio, and, hence, tumor survival, we examined the impact of reduced ANGPTL4 on anoikis in nine different cancer cell lines, in addition to A-5RT3 and MDA-MB-231 cells. Treatment with mAb11F6C4 resulted in a dose-dependent reduction of O_2^- levels (40%–80% for 6 μg/ml mAb11F6C4) (Figure 6A; Figure S5A), a reduction in the O_2^-:H_2O_2 ratio (70%–90% for 6 μg/ml mAb11F6C4) (Figure 6B; Figure S5B), a 3- to 8-fold increase in the caspase activities (Figure 7A; Figure S6A), and 30%–60% more apoptotic tumor cells (Figure 7B; Figure S6B), all indicating weakened anoikis resistance. A higher percentage of apoptotic tumor cells was also observed using inducible RNAi against ANGPTL4 in the MDA-MB-231 line (Figure S6C). These findings indicate that ANGPTL4-mediated O_2^- production for anoikis resistance may be a common feature in tumor cells. Taken together, our study showed that tumor-secreted ANGPTL4 interacted with integrins in an autocrine fashion to stimulate NADPH oxidase-dependent generation of O_2^-, promoting a high O_2^-:H_2O_2 ratio, and consequently activating downstream PI3K/PKBα and ERK activities (Figure 8).

DISCUSSION

The loss of dependence on integrin-mediated ECM contact for growth (i.e., anoikis resistance) is an essential feature of tumor cells, but the mechanism by which anoikis resistance is acquired is a central problem in cancer biology. Our findings demonstrated that ANGPTL4-mediated integrin engagement activates ROS production, which leads to a prosurvival signal and sustained anchorage-related signals even in the absence of ECM and cell-cell contact. We showed that cANGPTL4 was detected and elevated in many human tumor cells and was predominantly secreted by proliferative tumor epithelial cells. cANGPTL4 specifically binds to integrins β1 and β5 on tumor cells and

(D) Measurement of H_2O_2 levels using the Amplex red assay in A-5RT3$_{CTRL}$ and A-5RT3$_{ANGPTL4}$ cells. Arbitrary relative O_2^-:H_2O_2 ratios are shown in boxes.
(B–D and F) Values were normalized to total proteins and presented as mean ± SEM. Data are from three independent experiments performed in triplicate. *$p < 0.05$; **$p < 0.01$; ***$p < 0.001$; n.s., not significant.
Vehicle-treated A-5RT3$_{CTRL}$ cells (B and C) and A-5RT3$_{CTRL}$-induced tumor (F) serve as cognate controls. See also Figure S4.

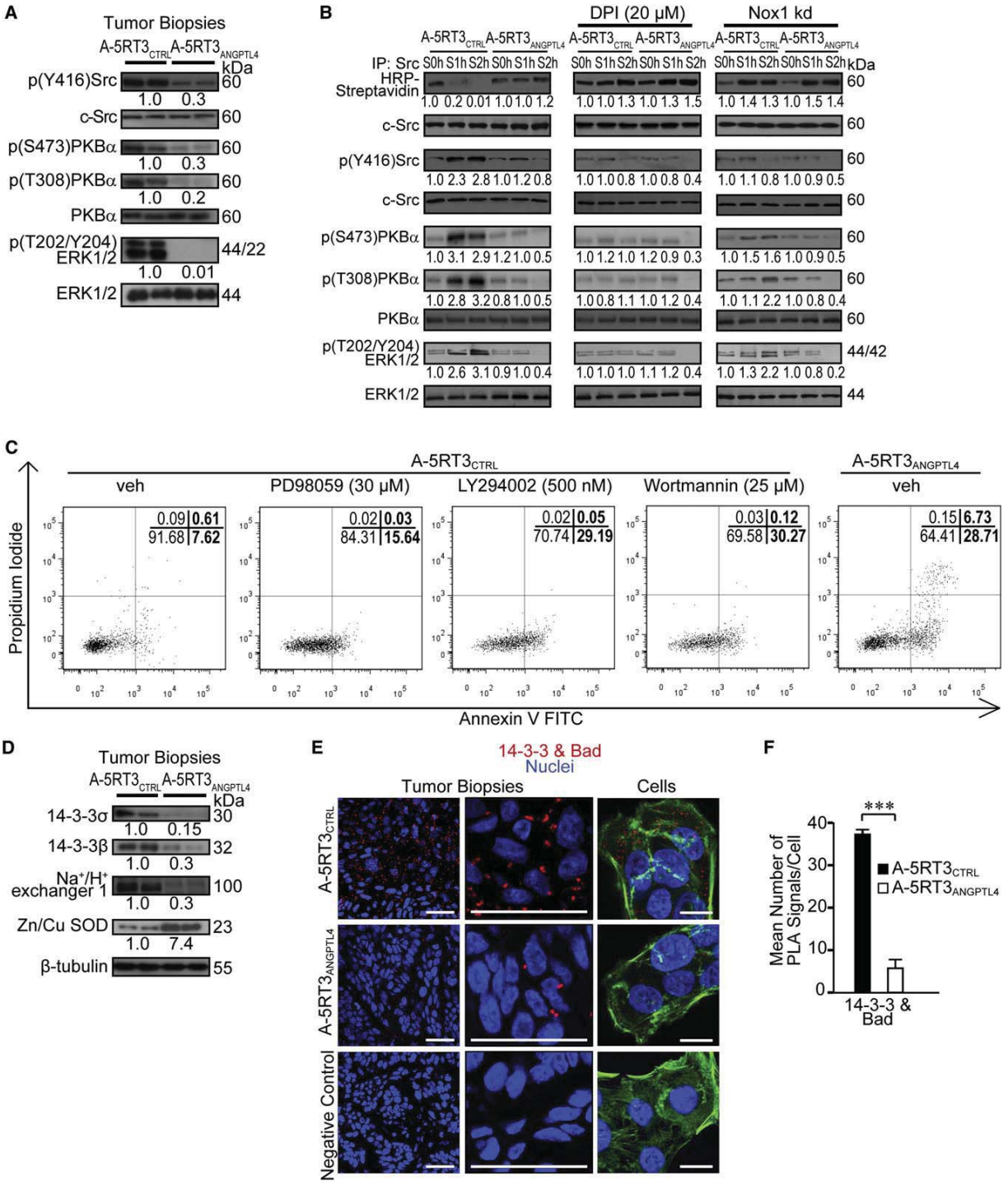

Figure 5. ANGPTL4-Mediated O_2^- Regulates Src and Promotes the PI3K/PKBα and ERK Survival Pathways

(A and D) Immunoblot of the indicated proteins in A-5RT3$_{ANGPTL4}$- and A-5RT3$_{CTRL}$-induced tumor biopsies. Values are mean from four independent experiments. c-Src (A) and β-tubulin (D) serve as loading and transfer controls, respectively.

(B) Immunoblot of the indicated proteins in A-5RT3$_{ANGPTL4}$ and A-5RT3$_{CTRL}$ cells in the absence or presence of 20 μM DPI, and in Nox1 kd A-5RT3$_{ANGPTL4}$ and A-5RT3$_{CTRL}$ cells. Cells were suspended for 0, 1, and 2 hr (S0h, S1h, and S2h, respectively). Cell lysates were labeled with 100 μM *N*-(biotinoyl)-*N*′-(iodoacetyl)

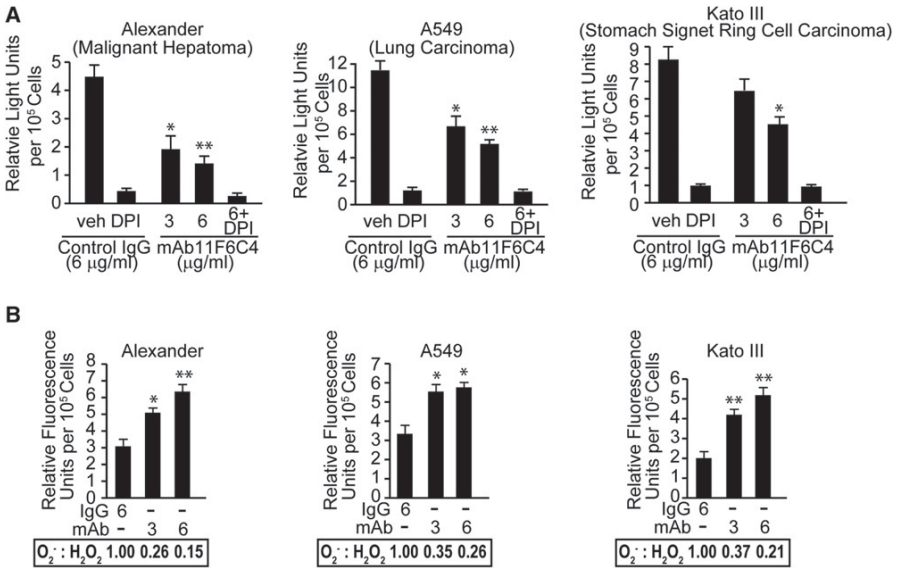

Figure 6. ANGPTL4 Maintains a Relatively High O_2^-:H_2O_2 Ratio in Tumor Cells

Measurement of O_2^- (A) and H_2O_2 (B) levels in three different tumor lines by MCLA assay and Amplex red assay, respectively. H_2O_2 was measured in the presence of the specific catalase inhibitor, 3-amino-l, 2, 4-triazole. Arbitrary relative O_2^-:H_2O_2 ratios (B) are shown in boxes. Values (mean ± SD) are normalized to the total protein content. Three independent experiments were performed with consistent results. *$p < 0.05$; **$p < 0.01$. See also Figure S5.

activates FAK and Rac1, which further stimulates NADPH oxidase-mediated O_2^- production via an autocrine pathway. However, it is conceivable that in tissues/organs, expressing high levels of cANGPTL4 in proximity to the tumor site may transmit a paracrine signal. Although integrins alone are not oncogenic, integrin-mediated signaling is often required to enable tumor survival and influence tumor growth (Desgrosellier and Cheresh, 2010). The pro-oxidant intracellular environment led to redox-mediated activation of the Src machinery and, therefore, stimulated downstream PI3K/PKBα and ERK prosurvival pathways. This further triggered the 14-3-3 adaptor protein to sequester the pro-apoptotic Bad protein from mitochondria, conferring resistance to anoikis and favoring tumor survival and growth.

The dysregulation of intracellular ROS levels, resulting in an excessive level or persistent elevation of ROS, has been linked to tumor growth, invasiveness, and metastasis. Indeed, elevated levels of ROS are detected in almost all cancers (Liou and Storz, 2010). An elevated O_2^- or O_2^-:H_2O_2 ratio is particularly important for cancer cells to sustain their tumorigenicity and metastatic potential (Clément and Pervaiz, 2001; Pervaiz and Clément, 2007). We found that the disruption of ANGPTL4-mediated redox signaling via genetic and antibody-mediated suppression of ANGPTL4 essentially reduced the activities of FAK, Rac1, and O_2^- production. These changes resulted in an increase in tumor cells' sensitivity to anoikis and impaired tumorigenesis. ANGPTL4-stimulated NADPH oxidase activity, leading to O_2^- production, can be inhibited NADPH oxidase inhibitors, but not by the mitochondrial complex I inhibitor rotenone. This suggests that O_2^- was "purposely" and enzymatically produced by NADPH oxidase, rather than as a by-product of mitochondrial activity. Two survival pathways, the PKBα and ERK, which have been shown to exert anoikis-suppressing effects (Westhoff and Fulda, 2009; Zhan et al., 2004), were complementarily employed by ANGPTL4 to confer resistance to anoikis in tumor cells.

The tumor-promoting role of inflammation in the tumor microenvironment is well recognized (Aggarwal and Gehlot, 2009). PPARγ and δ/β play major roles in the regulation of inflammation and are implicated in tumorigenesis (Peters and Gonzalez, 2009; Murphy and Holder, 2000). Although no correlation between the expression of either PPARγ or δ/β, and their target gene ANGPTL4, was observed in our analysis of PNSs and SCCs,

ethylenediamine to evaluate the Src redox state. An HRP-Streptavidin immunoblot performed on the anti-Src immunoprecipitate showing reduced Src. The immunoprecipitate was probed with anti-c-Src for normalization. Values (mean ± SD) represent the mean fold change against the value at S0h. Data shown are representatives of three independent experiments.

(C) Percentage of apoptotic A-5RT3$_{ANGPTL4}$ and A-5RT3$_{CTRL}$ cells, treated with either MEK inhibitor PD98059 or PI3K inhibitors LY294002 and Wortmannin, after 2 hr of anoikis challenge and analyzed by FACS (5000 events). Apoptotic index as described in Figure 3B. Sum of Annexin V^+/PI^- and Annexin V^+/PI^+ cells were considered apoptotic. Values are mean from three independent experiments.

(E) In situ PLA detection of 14-3-3:Bad complexes in indicated tumor sections and cells. PLA signals are red dots, and Hoechst-stained nuclei are in blue. Cells were counterstained with Alexa 488-phalloidin for actin stress fibers (green). Negative controls were performed with only anti-14-3-3 antibodies. Data shown are representative of three independent experiments. Scale bars represent 40 μm.

(F) Number (mean ± SD) of 14-3-3:Bad complexes (E, right panel) was calculated from 200 cells (n = 3; 600 cells total) using BlobFinder software. ***$p < 0.001$.

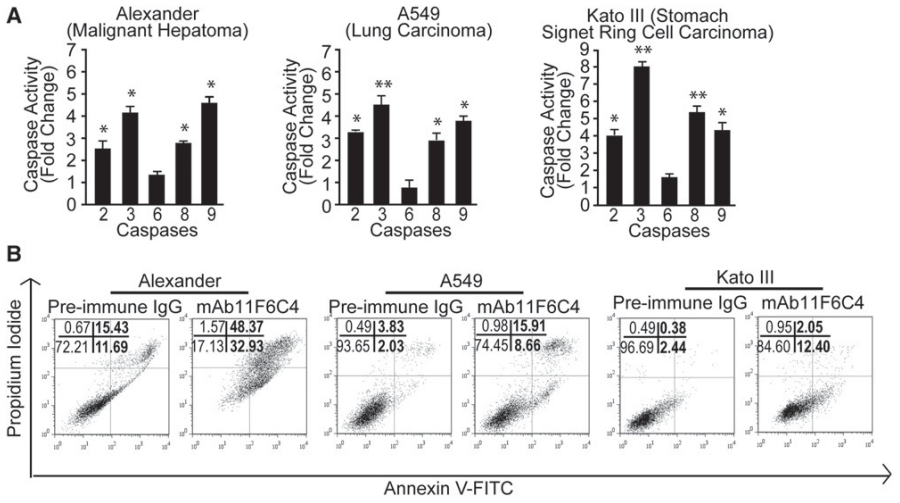

Figure 7. Deficiency of ANGPTL4 Activates Caspase Activities and Induces Apoptosis upon Anoikis in Tumor Cells

(A) Relative activities of caspases 2, 3, 6, 8, and 9 were measured after 2 hr of anoikis. Fold increase of caspase activities in mAb11F6C4 (6 μg/ml)-treated cells was calculated by comparing with the caspase activities of cells treated with preimmune IgG (6 μg/ml). Values (mean ± SD) are from three independent experiments with consistent results.*$p < 0.05$; **$p < 0.01$.

(B) Percentage of apoptotic cells in three tumor lines after 2 hr of anoikis as analyzed by FACS (5000 events). Tumor cells were treated with 10 μg/ml of control IgG or mAb11F6C4. Apoptotic index is as described in Figure 3B. Results are mean from three independent experiments. $p < 0.05$. See also Figure S6.

we cannot exclude their involvement and/or other oncogenic pathways or cell types in the tumor microenvironment, which enhanced the expression of cANGPTL4 in tumors. It is also conceivable that PPARs in cancer-associated fibroblasts play a more dominant role in the regulation of epithelial tumor growth. Indeed, PPARβ/δ-deficient fibroblasts can increase the proliferation of normal epithelial cells and SCCs via regulation of the interleukin-1 signaling pathway (Chong et al., 2009). A dysregulated inflammatory response promotes tumorigenesis and malignancy by stimulating ROS production (Aggarwal and Gehlot, 2009). Although not examined in this study, we cannot rule out the possibility that other mechanisms to produce O_2^-, such as cytosolic 5-lipooxygenase, may act in conjunction with ANGPTL4-stimulated NADPH oxidase activity to maintain an elevated intracellular O_2^- level for tumor growth (Chiarugi and Fiaschi, 2007). Despite inconclusive findings from clinical trials on the effect of antioxidants on cancer (Blot et al., 1993; Omenn et al., 1994; Hennekens et al., 1996; Lee et al., 1999), our findings that the specific inhibition of ANGPTL4-mediated integrin signaling and intracellular O_2^- production induce tumor cell apoptosis suggest that anticancer therapeutics focusing on redox-based apoptosis induction remain an exciting and viable strategy.

EXPERIMENTAL PROCEDURES

Human Tumor Samples

Human BCC biopsies and SCC biopsies along with their paired PNSs were provided by J.Y.P., S.H.T., and purchased from USA Asterand, plc., Detroit, MI. BCC samples, SCC samples, and PNSs, inclusive of epithelia and stroma, were subjected to protein and RNA extraction for immunoblotting and qPCR analyses, respectively. The study was approved by National Healthcare Group Domain-Specific Review Boards (NHG-DSRB). All the tumor samples had been de-identified prior to the analyses.

Tumorigenicity Assay

BALB/c athymic nude female mice (20–22 g), aged 5–6 weeks, and WT C57BL/6J female mice (20–25 g), aged 6–8 weeks, were purchased from A*STAR Biological Resources Centre (Singapore). C57BL/6J female WT and ANGPTL4-KO mice were used (Koster et al., 2005). The animal studies were approved and carried out in compliance with the regulation from Institutional Animal Care and Use Committee (IACUC0092), NTU. For nude mice experiments, 5×10^5 cells (A-5RT3$_{CTRL}$ or A-5RT3$_{ANGPTL4}$) were injected s.c. into the interscapular region of each nude mouse (n = 5). The injection site was rotated to avoid site bias. The injected tumor cells were allowed to grow for 8 weeks. The xenograft tumors were externally measured with a Vernier caliper every other day, and tumor volume was estimated using the equation: $V = (L \times W^2)/2$, where L and W are the length of the major and minor axis of the tumor, respectively. To test the effect of the number of injected cells on tumorigenicity, nude mice were inoculated with 0.5 ×, 2 ×, and 8 × 10^6 A-5RT3$_{CTRL}$ or A-5RT3$_{ANGPTL4}$ cells as above. Experiments were terminated at week 4 according to IACUC protocol because tumor volume in the 8 × 10^6 inoculation group approached 3000 mm^3.

For the antibody treatment, nude mice (n = 6) were implanted with A-5RT3 as above. One week postimplantation, 30 mg/kg/week of either mAb11F6C4 or isotype control IgG was i.v. administered for 4 weeks. The dose of antibody and delivery mode were consistent with studies using mAb14D12, another anti-ANGPTL4 mAb27 (Desai et al., 2007). KO mice and cANGPTL-treated C57BL/6J mice studies were performed as previously described (Sun and Lodish, 2010). Briefly, 1 × 10^6 B16F10$_{CTRL}$ (scrambled control) or B16F10$_{ANGPTL4}$ (ANGPTL4 knockdown) cells were s.c. injected into the interscapular region of the indicated mice (n = 4–6). Mice were i.v. treated with either 3 mg/kg of cANGPTL4 or control PBS three times a week. Animals were monitored and tumor volumes measured as above. Mice were sacrificed at the end of the experiment, and tumors were harvested for further analyses.

In Situ PLA

Duolink in situ PLA (Olink Bioscience) was performed on tumor biopsies or cells as described (Tan et al., 2009). The paired-primary antibodies used in the present study were rabbit anti-p(Y397)FAK and mouse anti-FAK antibodies, rabbit anti-pan-14-3-3 and mouse anti-BAD antibodies, and mouse anti-cANGPTL4 with either rabbit anti-β1, β3, or β5 integrin antibodies. As a

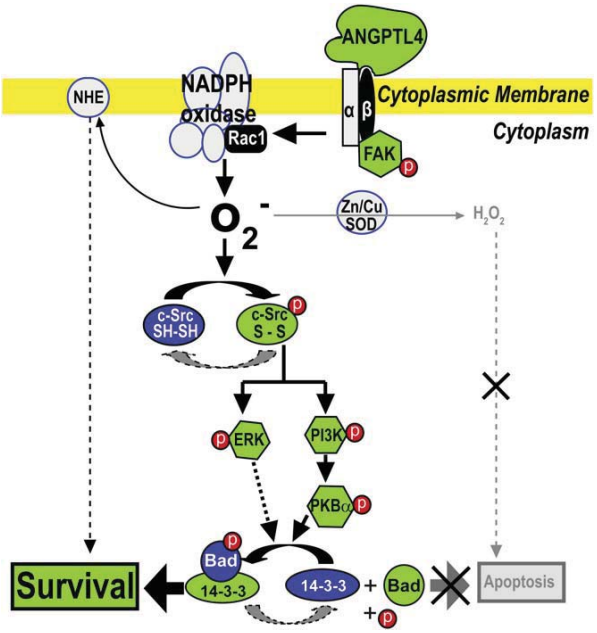

Figure 8. ANGPTL4-Mediated Regulation of O_2^- Production in Tumors

In an autocrine manner, tumor-derived ANGPTL4 specifically binds to integrins β1 or β5 and subsequently activates FAK and Rac1 activities, which further activates the NADPH oxidase-dependent generation of "*onco-ROS*" O_2^-, promoting a relatively high O_2^-:H_2O_2 ratio in tumor cells. This pro-oxidant intracellular milieu, which may subsidiarily be maintained through NHE, favors cell survival and proliferation by oxidizing/activating the Src machinery and, therefore, stimulates its downstream PI3K/PKBα- and ERK-mediated survival pathways. This further triggers the 14-3-3 adaptor protein to sequester pro-apoptotic Bad from mitochondria to prevent apoptosis and favor cell survival.

negative control, PLA was performed using only anti-FAK, anti-pan-14-3-3, or anti-nANGPTL4 antibodies, respectively. Briefly, sections/cells were fixed with 4% paraformaldehyde for 15 min. The slides were washed twice with PBS, blocked for 1 hr at room temperature with 2% BSA in PBS containing 0.1% Triton X-100, followed by incubation with the indicated antibody pairs overnight at 4°C. PLA was performed as recommended by the manufacturer. Images were taken using an LSM710 confocal laser scanning microscope with a Plan-Apochromat 63×/1.40 Oil objective and ZEN 2008 software (Carl Zeiss).

Measurement of O_2^- and H_2O_2

Production of O_2^- from tumor cells was measured using an O_2^--sensitive luciferin derivative, MCLA (Invitrogen). Cells (5×10^4) were trypsinized, washed, lysed in Krebs buffer, and treated either individually or combinatorially for 0.5 hr with the following chemicals: 10 mM Tiron, 20 μM diphenyleneiodonium chloride (DPI) or 500 μM apocynin, 50 μM rotenone, and 3 or 6 μg/ml monoclonal human anti-cANGPTL4 antibody mAb11F6C4. MCLA (2 μM) was added, and the luminescent signal was recorded immediately thereafter for 1 min with a GloMax 20/20 Luminometer (Promega). Intracellular H_2O_2 was measured as previously described (Wagner et al., 2005). We performed two control experiments to verify that we were measuring H_2O_2. The specificity of the assay for H_2O_2 was verified with catalase, and the degradation of H_2O_2 or inhibition of the assay system by the sample was analyzed by determining the recovery of exogenously added H_2O_2. The fold change in the O_2^-:H_2O_2 ratio of A-5RT3$_{ANGPTL4}$ and mAb11F6C4-treated tumor cells was determined by direct comparison with the value of either A-5RT3$_{CTRL}$ or control IgG-treated tumor cells, which were arbitrarily assigned the value of one.

Statistical Analyses

Statistical significance between two groups was analyzed using unpaired nonparametric test (Mann-Whitney test) or with a Student's t test (SPSS, Inc.). All statistical tests were two sided. A p value of ≤ 0.05 was considered significant.

SUPPLEMENTAL INFORMATION

Supplemental Information includes Supplemental Experimental Procedures, six figures, and one table and can be found with this article online at doi:10.1016/j.ccr.2011.01.018.

ACKNOWLEDGMENTS

This work was supported by grants from Ministry of Education, Singapore (ARC18/08), Nanyang Technological University (RG127/05, RG82/07), and Biomedical Research Council (10/1/22/19/644) to N.S.T.; a grant from the German Research Aid (Deutsche Krebshilfe: Tumorstammzellverbund) to P.B. We thank Dr. Samuel Ko and Anna Teo (Carl Zeiss, Singapore Pte Ltd.) for their expertise in laser capture microdissection with PALM Microbeam Axio Observer Z1 and image acquisition using LSM710 confocal microscope and MIRAX MIDI. The authors declare that they have no competing financial interests.

Received: July 5, 2010
Revised: November 11, 2010
Accepted: January 4, 2011
Published: March 14, 2011

REFERENCES

Aggarwal, B.B., and Gehlot, P. (2009). Inflammation and cancer: how friendly is the relationship for cancer patients? Curr. Opin. Pharmacol. *9*, 351–369.

Akram, S., Teong, H., Fliegel, L., Pervaiz, S., and Clément, M. (2006). Reactive oxygen species-mediated regulation of the Na^+-H^+ exchanger 1 gene expression connects intracellular redox status with cells' sensitivity to death triggers. Cell Death Differ. *13*, 628–641.

Belanger, A.J., Lu, H., Date, T., Liu, L.X., Vincent, K.A., Akita, G.Y., Cheng, S.H., Gregory, R.J., and Jiang, C. (2002). Hypoxia up-regulates expression of peroxisome proliferator-activated receptor γ angiopoietin-related gene (PGAR) in cardiomyocytes: role of hypoxia inducible factor 1α. J. Mol. Cell. Cardiol. *34*, 765–774.

Blot, W.J., Li, J.Y., Taylor, P.R., Guo, W., Dawsey, S., Wang, G.Q., Yang, C.S., Zheng, S.F., Gail, M., Li, G.Y., et al. (1993). Nutrition intervention trials in Linxian, China: supplementation with specific vitamin/mineral combinations, cancer incidence, and disease-specific mortality in the general population. J. Natl. Cancer Inst. *85*, 1483–1491.

Bouillet, P., and Strasser, A. (2002). BH3-only proteins- evolutionarily conserved proapoptotic Bcl-2 family members essential for initiating programmed cell death. J. Cell Sci. *115*, 1567–1574.

Bridge, A.J., Pebernard, S., Ducraux, A., Nicoulaz, A.L., and Iggo, R. (2003). Induction of an interferon response by RNAi vectors in mammalian cells. Nat. Genet. *34*, 263–264.

Chance, B., Sies, H., and Boveris, A. (1979). Hydroperoxide metabolism in mammalian organs. Physiol. Rev. *59*, 527–605.

Chiarugi, P. (2008). From anchorage dependent proliferation to survival: lessons from redox signalling. IUBMB Life *60*, 301–307.

Chiarugi, P., and Fiaschi, T. (2007). Redox signalling in anchorage-dependent cell growth. Cell. Signal. *19*, 672–682.

Chong, H.C., Tan, M.J., Philippe, V., Tan, S.H., Tan, C.K., Ku, C.W., Goh, Y.Y., Wahli, W., Michalik, L., and Tan, N.S. (2009). Regulation of epithelial-mesenchymal IL-1 signaling by PPARβ/δ is essential for skin homeostasis and wound healing. J. Cell Biol. *184*, 817–831.

Clément, M.V., and Pervaiz, S. (2001). Intracellular superoxide and hydrogen peroxide concentrations: a critical balance that determines survival or death. Redox Rep. *6*, 211–214.

Desai, U., Lee, E.C., Chung, K., Gao, C., Gay, J., Key, B., Hansen, G., Machajewski, D., Platt, K.A., Sands, A.T., et al. (2007). Lipid-lowering effects of anti-angiopoietin-like 4 antibody recapitulate the lipid phenotype found in angiopoietin-like 4 knockout mice. Proc. Natl. Acad. Sci. USA *104*, 11766–11771.

Desgrosellier, J.S., and Cheresh, D.A. (2010). Integrins in cancer: biological implications and therapeutic opportunities. Nat. Rev. Cancer *10*, 9–22.

Ferraro, D., Corso, S., Fasano, E., Panieri, E., Santangelo, R., Borrello, S., Giordano, S., Pani, G., and Galeotti, T. (2006). Pro-metastatic signaling by c-Met through RAC-1 and reactive oxygen species (ROS). Oncogene *25*, 3689–3698.

Fidler, I.J. (1999). Critical determinants of cancer metastasis: rationale for therapy. Cancer Chemother. Pharmacol. Suppl. *43*, S3–S10.

Galaup, A., Cazes, A., Le Jan, S., Philippe, J., Connault, E., Le Coz, E., Mekid, H., Mir, L.M., Opolon, P., Corvol, P., et al. (2006). Angiopoietin-like 4 prevents metastasis through inhibition of vascular permeability and tumor cell motility and invasiveness. Proc. Natl. Acad. Sci. USA *103*, 18721–18726.

Ge, H., Yang, G., Huang, L., Motola, D.L., Pourbahrami, T., and Li, C. (2004). Oligomerization and regulated proteolytic processing of angiopoietin-like 4. J. Biol. Chem. *279*, 2038–2045.

Giannoni, E., Buricchi, F., Grimaldi, G., Parri, M., Cialdai, F., Taddei, M.L., Raugei, G., Ramponi, G., and Chiarugi, P. (2008). Redox regulation of anoikis: reactive oxygen species as essential mediators of cell survival. Cell Death Differ. *15*, 867–878.

Giannoni, E., Fiaschi, T., Ramponi, G., and Chiarugi, P. (2009). Redox regulation of anoikis resistance of metastatic prostate cancer cells: key role for Src and EGFR-mediated pro-survival signals. Oncogene *28*, 2074–2086.

Hanahan, D., and Weinberg, R.A. (2000). The hallmarks of cancer. Cell *100*, 57–70.

Hennekens, C.H., Buring, J.E., Manson, J.E., Stampfer, M., Rosner, B., Cook, N.R., Belanger, C., LaMotte, F., Gaziano, J.M., Ridker, P.M., et al. (1996). Lack of effect of long-term supplementation with beta carotene on the incidence of malignant neoplasms and cardiovascular disease. N. Engl. J. Med. *334*, 1145–1149.

Irani, K., Xia, Y., Zweier, J.L., Sollott, S.J., Der, C.J., Fearon, E.R., Sundaresan, M., Finkel, T., and Goldschmidt-Clermont, P.J. (1997). Mitogenic signaling mediated by oxidants in Ras-transformed fibroblasts. Science *275*, 1649–1652.

Ito, Y., Oike, Y., Yasunaga, K., Hamada, K., Miyata, K., Matsumoto, S.I., Sugano, S., Tanihara, H., Masuho, Y., and Suda, T. (2003). Inhibition of angiogenesis and vascular leakiness by angiopoietin-related protein 4. Cancer Res. *63*, 6651–6657.

Joneson, T., and Bar-Sagi, D. (1998). A Rac1 effector site controlling mitogenesis through superoxide production. J. Biol. Chem. *273*, 17991–17994.

Kersten, S., Mandard, S., Tan, N.S., Escher, P., Metzger, D., Chambon, P., Gonzalez, F.J., Desvergne, B., and Wahli, W. (2000). Characterization of the fasting-induced adipose factor FIAF, a novel peroxisome proliferator-activated receptor target gene. J. Biol. Chem. *275*, 28488–28493.

Komatsu, D., Kato, M., Nakayama, J., Miyagawa, S., and Kamata, T. (2008). NADPH oxidase 1 plays a critical mediating role in oncogenic Ras-induced vascular endothelial growth factor expression. Oncogene *27*, 4724–4732.

Koster, A., Chao, Y., Mosior, M., Ford, A., Gonzalez-DeWhitt, P., Hale, J., Li, D., Qiu, Y., Fraser, C., and Yang, D. (2005). Transgenic angiopoietin-like (angptl)4 overexpression and targeted disruption of angptl4 and angptl regulation of triglyceride metabolism. Endocrinology *146*, 4943–4950.

Le Jan, S., Amy, C., Cazes, A., Monnot, C., Lamandé, N., Favier, J., Philippe, J., Sibony, M., Gasc, J.M., Corvol, P., et al. (2003). Angiopoietin-like 4 is a proangiogenic factor produced during ischemia and in conventional renal cell carcinoma. Am. J. Pathol. *162*, 1521–1528.

Lee, I.M., Cook, N.R., and Manson, J.E. (1999). Beta-carotene supplementation and incidence of cancer and cardiovascular disease: Women's Health Study. J. Natl. Cancer Inst. *91*, 2102–2106.

Liou, G.Y., and Storz, P. (2010). Reactive oxygen species in cancer. Free Radic. Res. *44*, 479–496.

Minn, A.J., Gupta, G.P., Siegel, P.M., Bos, P.D., Shu, W., Giri, D.D., Viale, A., Olshen, A.B., Gerald, W.L., and Massagué, J. (2005). Genes that mediate breast cancer metastasis to lung. Nature *436*, 518–524.

Mueller, M.M., Peter, W., Mappes, M., Huelsen, A., Steinbauer, H., Boukamp, P., Vaccariello, M., Garlick, J., and Fusenig, N.E. (2001). Tumor progression of skin carcinoma cells in vivo promoted by clonal selection, mutagenesis, and autocrine growth regulation by granulocyte colony-stimulating factor and granulocyte-macrophage colony-stimulating factor. Am. J. Pathol. *159*, 1567–1579.

Murphy, G.J., and Holder, J.C. (2000). PPARγ agonists: therapeutic role in diabetes, inflammation and cancer. Trends Pharmacol. Sci. *21*, 469–474.

Münzel, T., Afanas'ev, I.B., Kleschyov, A.L., and Harrison, D.G. (2002). Detection of superoxide in vascular tissue. Arterioscler. Thromb. Vasc. Biol. *22*, 1761–1768.

Oberley, L.W. (2001). Anticancer therapy by overexpression of superoxide dismutase. Antioxid. Redox Signal. *3*, 461–472.

Oike, Y., Akao, M., Kubota, Y., and Suda, T. (2005). Angiopoietin-like proteins: potential new targets for metabolic syndrome therapy. Trends Mol. Med. *11*, 473–479.

Omenn, G.S., Goodman, G., Thomquist, M., Grizzle, J., Rosenstock, L., Barnhart, S., Balmes, J., Cherniack, M.G., Cullen, M.R., Glass, A., et al. (1994). The beta-carotene and retinol efficacy trial (CARET) for chemoprevention of lung cancer in high risk populations: smokers and asbestos-exposed workers. Cancer Res. *54*, 2038s–2043s.

Padua, D., Zhang, X.H.F., Wang, Q., Nadal, C., Gerald, W.L., Gomis, R.R., and Massagué, J. (2008). TGFβ primes breast tumors for lung metastasis seeding through angiopoietin-like 4. Cell *133*, 66–77.

Paffenholz, R., Bergstrom, R.A., Pasutto, F., Wabnitz, P., Munroe, R.J., Jagla, W., Heinzmann, U., Marquardt, A., Bareiss, A., Laufs, J., et al. (2004). Vestibular defects in head-tilt mice result from mutations in Nox3, encoding an NADPH oxidase. Genes Dev. *18*, 486–491.

Pani, G., Giannoni, E., Galeotti, T., and Chiarugi, P. (2009). Redox-based escape mechanism from death: the cancer lesson. Antioxid. Redox Signal. *11*, 2791–2806.

Pervaiz, S., and Clément, M.V. (2007). Superoxide anion: oncogenic reactive oxygen species? Int. J. Biochem. Cell Biol. *39*, 1297–1304.

Peters, J.M., and Gonzalez, F.J. (2009). Sorting out the functional role(s) of PPARβ/δ in cell proliferation and cancer. Biochim. Biophys. Acta *1796*, 230–241.

Salmon, S.E. (1984). Human tumor colony assay and chemosensitivity testing. Cancer Treat. Rep. *68*, 117–125.

She, Q.B., Solit, D.B., Ye, Q., O'Reilly, K.E., Lobo, J., and Rosen, N. (2005). The BAD protein integrates survival signaling by EGFR/MAPK and PI3K/Akt kinase pathways in PTEN-deficient tumor cells. Cancer Cell *8*, 287–297.

Singh, S., Sadanandam, A., and Singh, R.K. (2007). Chemokines in tumor angiogenesis and metastasis. Cancer Metastasis Rev. *26*, 453–467.

Suh, Y.A., Arnold, R.S., Lassegue, B., Shi, J., Xu, X., Sorescu, D., Chung, A.B., Griendling, K.K., and Lambeth, J.D. (1999). Cell transformation by the superoxide-generating oxidase Mox1. Nature *401*, 79–82.

Sun, Y., and Lodish, H.F. (2010). Adiponectin deficiency promotes tumor growth in mice by reducing macrophage infiltration. PLoS ONE *5*, e11987.

Tan, S.H., Pal, M., Tan, M.J., Wong, M.H.L., Tam, F.U., Teo, J.W.T., Chong, H.C., Tan, C.K., Goh, Y.Y., Tang, M.B.Y., et al. (2009). Regulation of cell proliferation and migration by TAK1 via transcriptional control of von Hippel-Lindau tumor suppressor. J. Biol. Chem. *284*, 18047–18058.

Ushio-Fukai, M., and Nakamura, Y. (2008). Reactive oxygen species and angiogenesis: NADPH oxidase as target for cancer therapy. Cancer Lett. *266*, 37–52.

Wagner, B.A., Evig, C.B., Reszka, K.J., Buettner, G.R., and Burns, C.P. (2005). Doxorubicin increases intracellular hydrogen peroxide in PC3 prostate cancer cells. Arch. Biochem. Biophys. *440*, 181–190.

Wang, Y., Lam, K.S.L., Lam, J.B.B., Lam, M.C., Leung, P.T.Y., Zhou, M., and Xu, A. (2007). Overexpression of angiopoietin-like 4 alters mitochondria

activities and modulates methionine metabolic cycle in the liver tissues of db/db diabetic mice. Mol. Endocrinol. *21*, 972–986.

Wang, Z., Han, B., Zhang, Z., Pan, J., and Xia, H. (2010). Expression of angiopoietin-like 4 and tenascin C but not cathepsin C mRNA predicts prognosis of oral tongue squamous cell carcinoma. Biomarkers *15*, 39–46.

Westhoff, M.A., and Fulda, S. (2009). Adhesion-mediated apoptosis resistance in cancer. Drug Resist. Updat. *12*, 127–136.

Wu, W.S. (2006). The signaling mechanism of ROS in tumor progression. Cancer Metastasis Rev. *25*, 695–705.

Zhan, M., Zhao, H., and Han, Z.C. (2004). Signalling mechanisms of anoikis. Histol. Histopathol. *19*, 973–983.

Cancer Cell *19*

Supplemental Information

Angiopoietin-like 4 Protein Elevates the Prosurvival Intracellular O_2^-:H_2O_2 Ratio and Confers Anoikis Resistance to Tumors

Pengcheng Zhu, Ming Jie Tan, Royston-Luke Huang, Chek Kun Tan, Han Chung Chong, Mintu Pal, Chee Ren Ivan Lam, Petra Boukamp, Jiun Yit Pan, Suat Hoon Tan, Sander Kersten, Hoi Yeung Li, Jeak Ling Ding, and Nguan Soon Tan

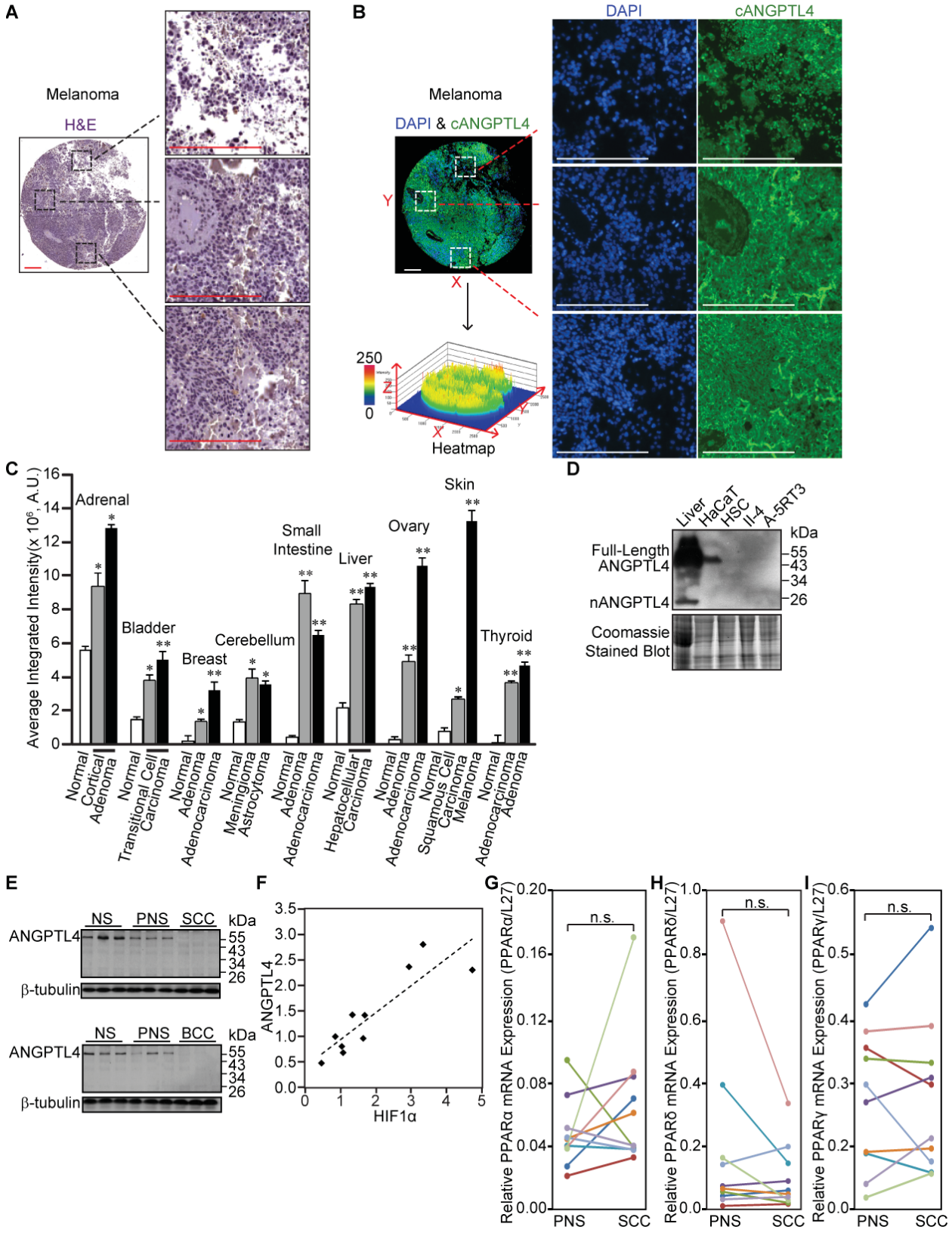

Figure S1, related to Figure 1. Elevated Expression of C-terminal ANGPTL4 (cANGPTL4) in Tumors

(A and B) Hematoxylin and eosin (H&E) image (A) and immunofluorescence image probed with an anti-cANGPTL4 antibody (B) on melanoma tumor tissue (representative of the tumor tissue array shown in Figure 1A). Higher magnification pictures on areas randomly selected from the melanoma tissue were shown on (A, right panel) and (B, DAPI on the middle and cANGPTL4 on the right panel), respectively. The heatmap (B, left bottom panel) was transformed from the immunofluorescence image (B, left upper panel) based on the gray scale value (immunofluorescence intensity) of cANGPTL4 as described in Figure 1A. Scale bars represent 200 μm.

(C) Average integrated gray scale value (immunofluorescence intensity) of cANGPTL4 from various normal and tumor tissues (also see Figure 1A). Tissues from same anatomic site were grouped and compared. A.U.: arbitrary unit. Values (mean ± SEM) were calculated from at least three biopsies and microscopic fields of each tissue. *$p < 0.05$; **$p < 0.01$.

(D-E) Immunoblot analysis using an anti-nANGPTL4 antibody of tumorigenic skin lines HSC, II-4, and A-5RT3 (D), and human skin squamous cell carcinomas (SCCs), basal cell carcinomas (BCCs) and cognate peri-tumor normal sample (PNS) (E). Liver, non-tumorigenic skin line HaCaT and normal skin biopsies (NS) served as cognate positive controls. Coomassie stained blot or β-tubulin served as a loading and transfer control. No full-length or nANGPTL4 was detected in indicated tumor cell line, BCCs or SCCs. Anti-nANGPTL4 antibody was previously described (Kersten et al., 2000).

(F) HIF1α with ANGPTL4 mRNA levels were concomitantly up-regulated in SSCs when compared with PNSs (correlation coefficient = 0.88).

(G-I) Relative mRNA expressions PPARα (G), PPARδ (H) and PPARγ (I) in paired human SCCs and PNSs as determined by qPCR. Data spots from same individual are linked by coloured lines. Data (means ± SD) are from two independent qPCR experiments performed in triplicate. Ribosomal protein L27 (L27) was used as a reference housekeeping gene. n.s. represents not significant in the comparison between paired SCCs and PNSs.

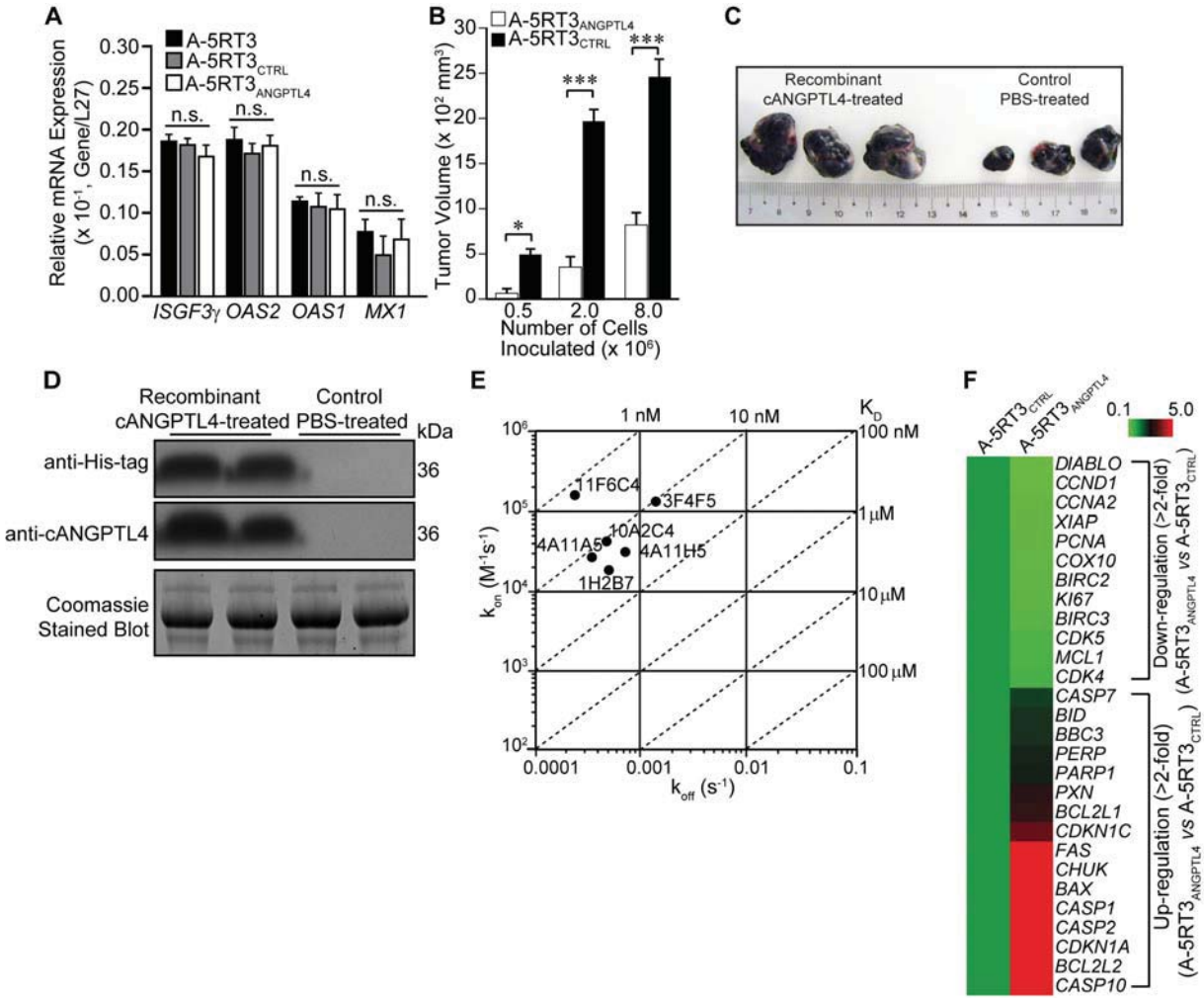

Figure S2, related to Figure 2. Suppression of ANGPTL4 Reduces Tumorigenicity and Exogenously Infused cANGPTL4 Accelerates Tumor Growth

(A) Relative mRNA levels of key interferon response genes: 2',5'-oligoadenylate synthetase isoforms 1 and 2 (*OAS1*, *OAS2*), interferon-induced myxovirus resistance 1 (*MX1*) and interferon-stimulated transcription factor 3γ (*ISGF3γ*) in A-5RT3 (parental cell), A-5RT3$_{CTRL}$ (scrambled control cell) and A-5RT3$_{ANGPTL4}$ (ANGPTL4 knockdown cell). Results (mean ± SD) are from three independent qPCR experiments performed in triplicate. Ribosomal protein L27 (L27) was used as a reference housekeeping gene. n.s. represents not significant in the comparisons between A-5RT3 and A-5RT3$_{ANGPTL4}$ cells or between A-5RT3$_{CTRL}$ and A-5RT3$_{ANGPTL4}$.

(B) Mean size of xenograft tumors induced in nude mice by 0.5×, 2× and 8×10^6 A-5RT3$_{ANGPTL4}$ or A-5RT3$_{CTRL}$ cells 4 weeks post-inoculation (per group). Values (mean ± SEM) are calculated from n = 5 (per group) mice. *p < 0.05; ***p<0.001

(C) Representative pictures of B16F10-induced tumors in C57BL/6J mice with *i.v.* treatments of either 3 mg/kg of cANGPTL4 or control PBS three times a week and dissected 15 days after injection (scale bar 10 mm).

(D) Immunoblot detection of recombinant cANGPTL4 using anti-His-tag and anti-cANGTPL4 antibodies. Plasma samples from C57BL/6J mice 1 day post-treatment with cANGPTL4 or control PBS (as described in Figure 2E) were used. Coomassie stained blot served as loading and transfer control. Experiments were repeated three times with consistent results.

(E) ANGPTL4 interaction kinetic maps for human mAbs, shown as association and dissociation rate constants (k_{on} and k_{off}), and a combination of k_{on} and k_{off} that results in the same affinity constant (K_D) values (diagonal lines) as determined by SPR. Labels in maps identify the six mAb clones. mAb11F6C4 was chosen for immunotherapy experiment based on its superior k_{on}, k_{off} and K_D values.

(F) Heatmap showing genes up- and down-regulated in A-5RT3$_{ANGPTL4}$-induced tumors relative to A-5RT3$_{CTRL}$-induced tumors as determined by qPCR. Results were generated from three pairs of indicated tumors. Experiments were performed using tumor biopsies harvested from mice described in Figures 2B-C at week 8.Three independent qPCR experiments performed in triplicate. Ribosomal protein L27 (L27) was used as a reference housekeeping gene. A detailed description of the genes and their expression is presented in Table S1.

Down-regulated (> 2-fold)		
Gene	**A-5RT3$_{CTRL}$**	**A-5RT3$_{ANGPTL4}$**
DIABLO	1.000	0.070
CCND1	1.000	0.102
CCNA2	1.000	0.119
XIAP	1.000	0.120
PCNA	1.000	0.177
COX10	1.000	0.223
BIRC2	1.000	0.247
KI67	1.000	0.269
BIRC3	1.000	0.345
CDK5	1.000	0.498
MCL1	1.000	0.500
CDK4	1.000	0.549

Up-regulated (> 2-fold)		
Gene	**A-5RT3$_{CTRL}$**	**A-5RT3$_{ANGPTL4}$**
CASP7	1.000	1.927
BID	1.000	2.051
BBC3	1.000	2.075
PERP	1.000	2.246
PARP1	1.000	2.308
PXN	1.000	2.947
BCL2L1	1.000	3.112
CDKN1C	1.000	3.609
FAS	1.000	6.171
CHUK	1.000	6.353
BAX	1.000	8.363
CASP1	1.000	10.499
CASP2	1.000	10.560
CDKN1A	1.000	13.037
BCL2L2	1.000	14.671
CASP10	1.000	24.740

Table S1, related to Figure 2. **Relative Fold Change of Gene Expressions in A-5RT3$_{ANGPTL4}$-induced Tumors as Compared with that of A-5RT3$_{CTRL}$-induced Tumors**
Note: The gene expression levels in A-5RT3$_{CTRL}$-induced tumors are assigned value one.

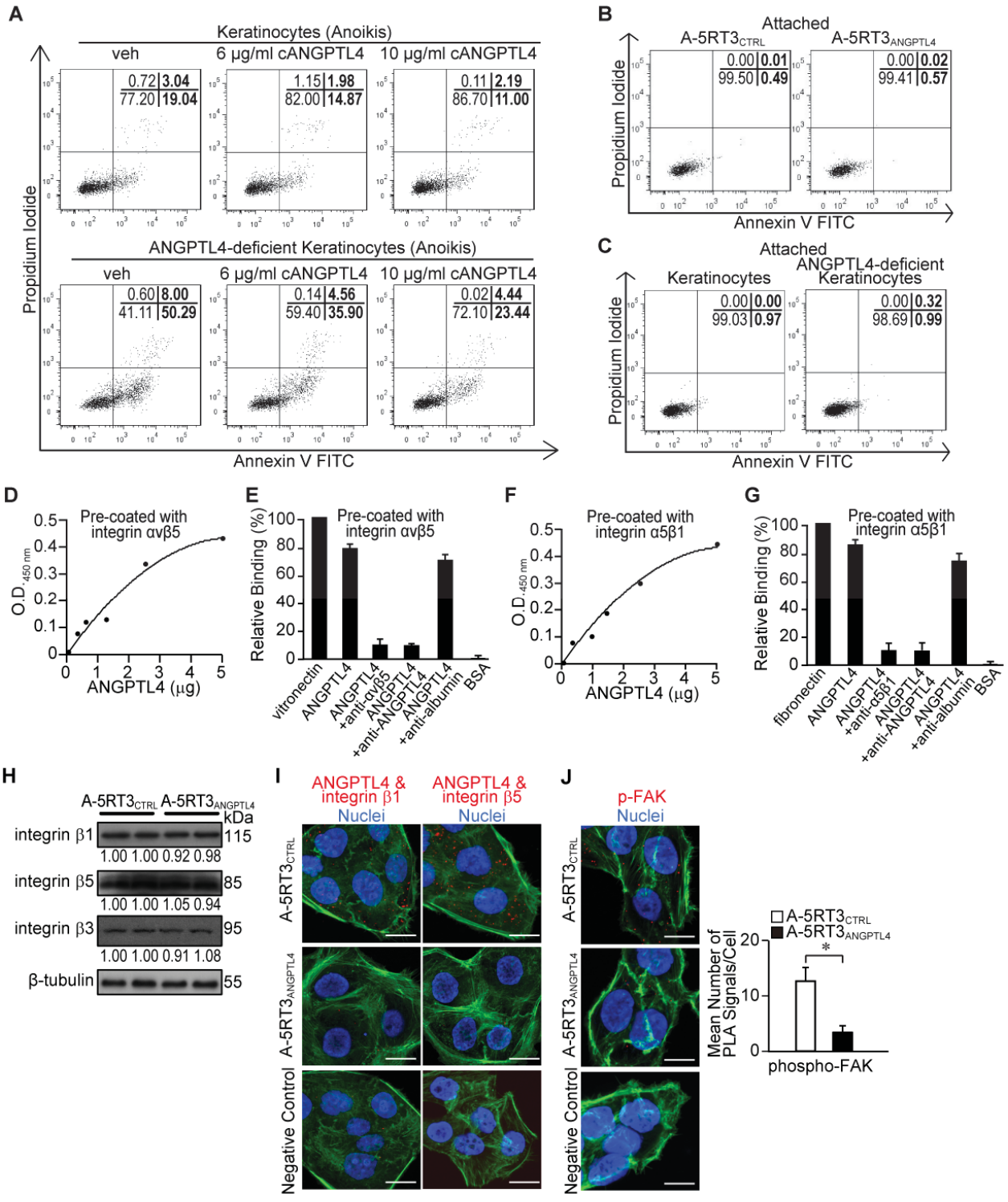

Figure S3, related to Figure 3. ANGPTL4 Effects on Keratinocytes and Its Interaction with Integrins to Activate FAK

(A) Percentage of anoikis-induced apoptotic skin keratinocytes and ANGPTL4-deficient keratinocytes in the presence of increasing exogenous recombinant cANGPTL4 as analysed by

FACS (5000 events). Vehicle (PBS)-treated keratinocytes and ANGPTL4-deficient keratinocytes served as cognate controls for comparison. Apoptotic index as described in Figure 3B.
(B-C) Apoptotic index of adhered epithelial cells. A-5RT3$_{CTRL}$ and A-5RT3$_{ANGPT4}$ cells (B), and normal skin keratinocytes and ANGPTL4-deficient keratinocytes (C) were detached by trypsin, subjected for Annexin V and PI staining, and immediately analysed by FACS (5000 events). The sum of Annexin V^+/PI^- (early apoptosis) and Annexin V^+/PI^+ (late apoptosis) cells were considered apoptotic. Values (bold) denote apoptotic cells (%). Results are representative of three independent experiments.
(D-G) Dose-dependent ANGPTL4 bindings to immobilized integrin αvβ5 (D and E) and integrin α5β1 (F and G), which were specifically blocked by anti-cANGPTL4 as determined by ELISA.
(H) Immunoblot detects no significant difference in the protein expressions of integrins β1, β5 and β3 between A-5RT3$_{CTRL}$ and A-5RT3$_{ANGPTL4}$ cells.
(I-J) *In situ* PLA detection of ANGPTL4:integrin β1 and ANGPTL4:integrin β5 complexes (I), and of phosphorylated FAK (J) in A-5RT3$_{CTRL}$ and A-5RT3$_{ANGPTL4}$ cells. PLA signals are shown in red and nuclei are stained blue by Hoechst dye. The cells were also counterstained with Alexa488-phalloidin for actin stress fibers (green). Negative controls were performed with only anti-nANGPTL4 (I) or anti-FAK (J) antibodies. Images were acquired in one z-plane using a Zeiss LSM710 confocal laser scanning microscope. Scale bars represent 40 μm. PLA images are representative of three independent experiments. Graph (J, right panel) showed mean number of phosphorylated FAK calculated from 200 A-5RT3$_{ANGPTL4}$ and A-5RT3$_{CTRL}$ cells (n = 3; total 600 cells) using BlobFinder software (Uppsula University). Error bars represent SD. *$p < 0.05$. All experiments were performed three or four times with consistent results.

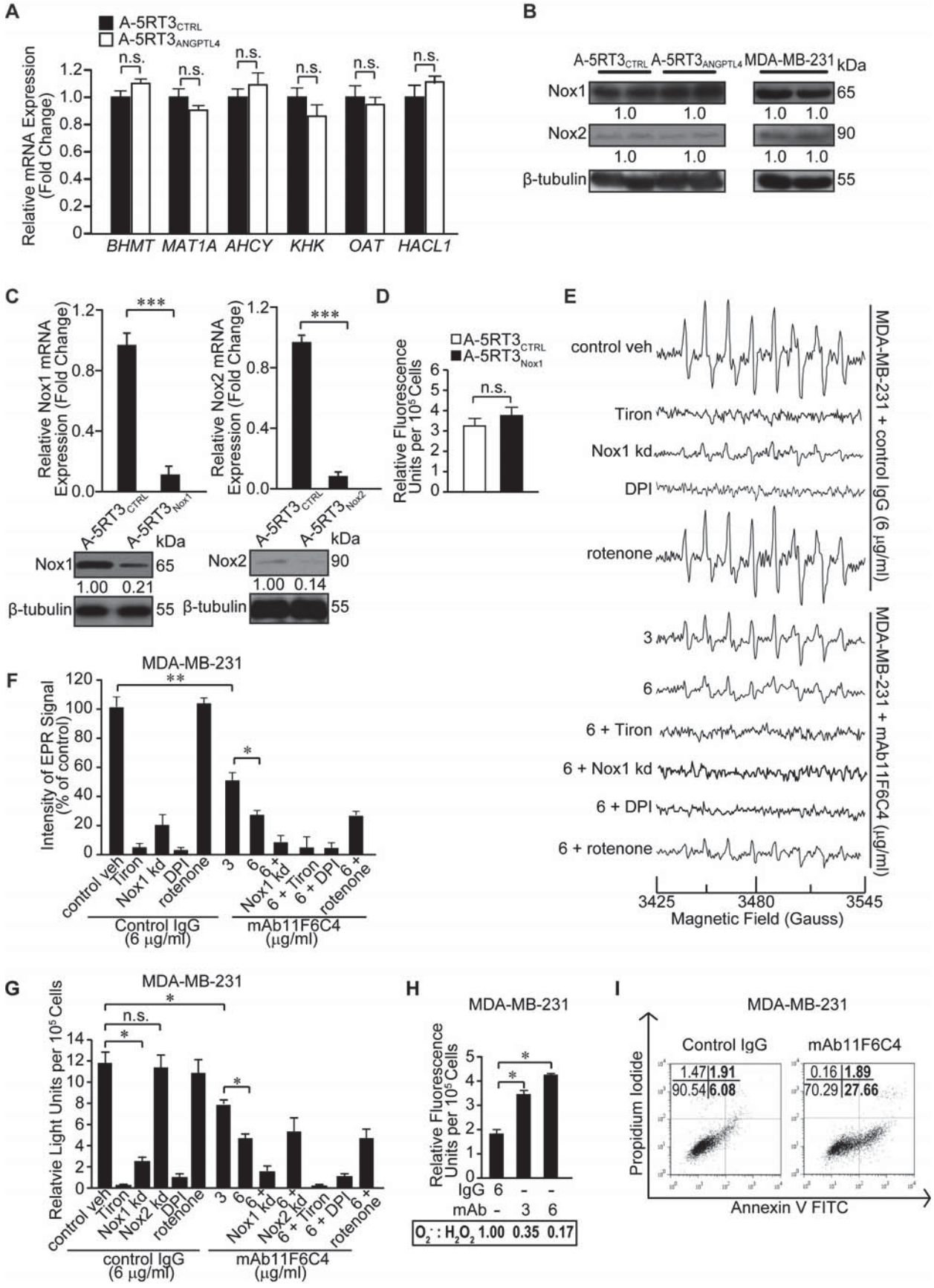

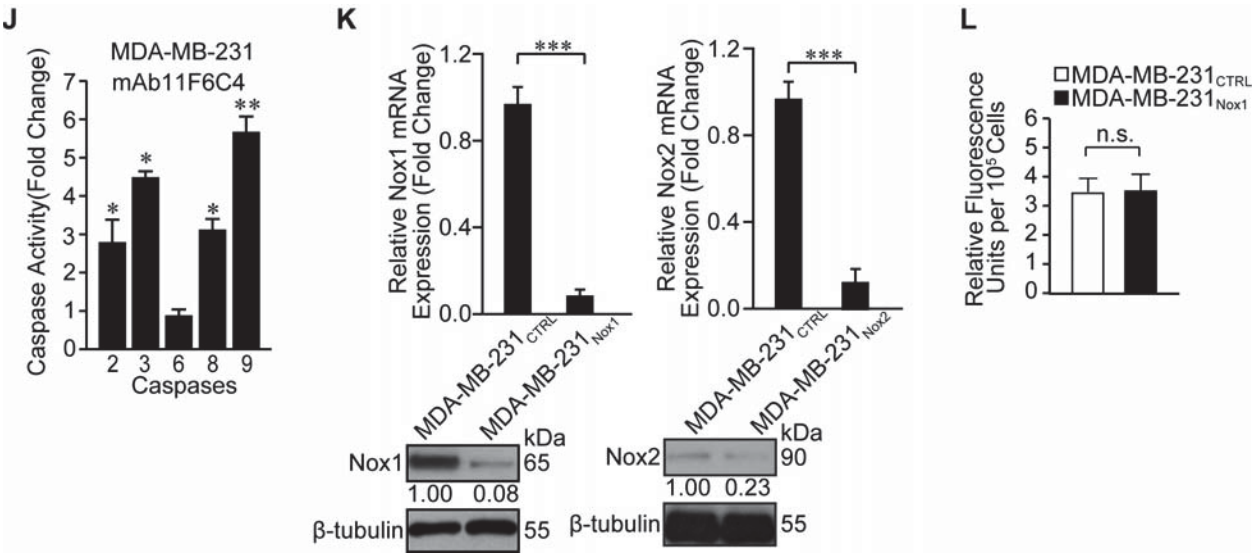

Figure S4, related to Figure 4. ANGPTL4 Elevates the O_2^- Level and Maintains a Relatively High O_2^-:H_2O_2 Ratio in Tumor Cells

(A) Suppression of ANGPTL4 has no effect in the methionine/homocysteine metabolic cycle of tumor cells. Relative mRNA level of *BHMT*, *MATLA*, *AHCY*, *KHK*, *OAT and HACL1* (representative genes in the methionine/homocysteine metabolic cycle) in A-5RT3$_{ANGPTL4}$ and A-5RT3$_{CTRL}$ cells as determined by qPCR.

(B) Immunoblot of Nox1 and Nox2 in A-5RT3$_{CTRL}$, A-5RT3$_{ANGPTL4}$ and MA-MB-231 cells. β-tubulin served as a loading and transfer control. Representative blots of three independent experiments are shown.

(C and K) Relative fold change in Nox1 and Nox2 mRNA and protein levels in A-5RT3$_{CTRL}$ (scrambled control), A-5RT3$_{Nox1}$ (Nox1 knockdown) and A-5RT3$_{Nox2}$ (Nox2 knockdown) cells (C), or in MDA-MB-231$_{CTRL}$ (scrambled control), MDA-MB-231$_{Nox1}$ (Nox1 knockdown) and MDA-MB-231$_{Nox2}$ (Nox2 knockdown) cells (K).

(D, H and L) Measurement of H_2O_2 levels using the Amplex red assay in A-5RT3$_{CTRL}$ and A-5RT3$_{Nox1}$ cells (D), in MDA-MB-231$_{CTRL}$ and MDA-MB-231$_{Nox1}$ cells (L); and in MDA-MB-231 cells treated with mAb11F6C4 (3 or 6 μg/ml) or control IgG (6 μg/ml) (H). Arbitrary relative O_2^-:H_2O_2 ratios are shown in boxes (J).

(E) Representative EPR spectra of DEPMPO-superoxide spin adduct from MDA-MB-231 cells in the absence or presence of indicated chemicals or inhibitors. MDA-MB-231 cells were treated with mAb11F6C4 (3 or 6 μg/ml) or control IgG (6 μg/ml). In indicated experiments, MDA-MB-231 cells were transiently transfected with ON-TARGETplus siRNA (Dharmacon) against either Nox1 (Nox1 kd) or Nox2 (Nox2 kd). The superoxide adduct of DEPMPO has hyperfine splitting constants of a_N=13.13 G; a_P=55.61 G; a^{β}_H=13.11 G; a^{γ}_H=0.71, 0.42, 0.7, 0.25, and 0.6 G.

(F) EPR signal intensity at 3480 G from MDA-MB-231 cells in (E). Tiron-treated measurement served as a negative signal control.

(G) Measurement of O_2^- levels using the MCLA assay in MDA-MB-231 cells treated with mAb11F6C4 (3 or 6 μg/ml) or control IgG (6 μg/ml) in the absence or presence of the indicated chemicals or inhibitors.

(I) Percentage of apoptotic MDA-MB-231 after 2 h of anoikis as analyzed by FACS (5000 events). Apoptotic index is described in Figure 3B. Values (bold) denote apoptotic cells (%) from three independent experiments.
(J) Relative activities of caspases 2, 3, 6, 8 and 9 in mAb11F6C4-treated MDA-MB-231 cells after 2 h of anoikis. Values (means ± SD) are from three independent experiments performed in triplicate. *$p < 0.05$; **$p < 0.01$. Fold-increase in caspase activity was calculated by comparison to pre-immune IgG-treated MDA-MB-231 cells.
(A, C and K) Error bars represent SD from three independent qPCR experiments performed in triplicate. Ribosomal protein L27 (L27) was used as a reference housekeeping gene. (D-H and L) Values were normalized to total proteins and presented as means ± SEM. Data were from three independent experiments performed in triplicate. *$p < 0.05$; **$p < 0.01$; ***$p < 0.001$; n.s. represents not significant. (E-G) Vehicle-treated MDA-MB-231 cells in the presence of control IgG (6 μg/ml) serve as cognate controls.

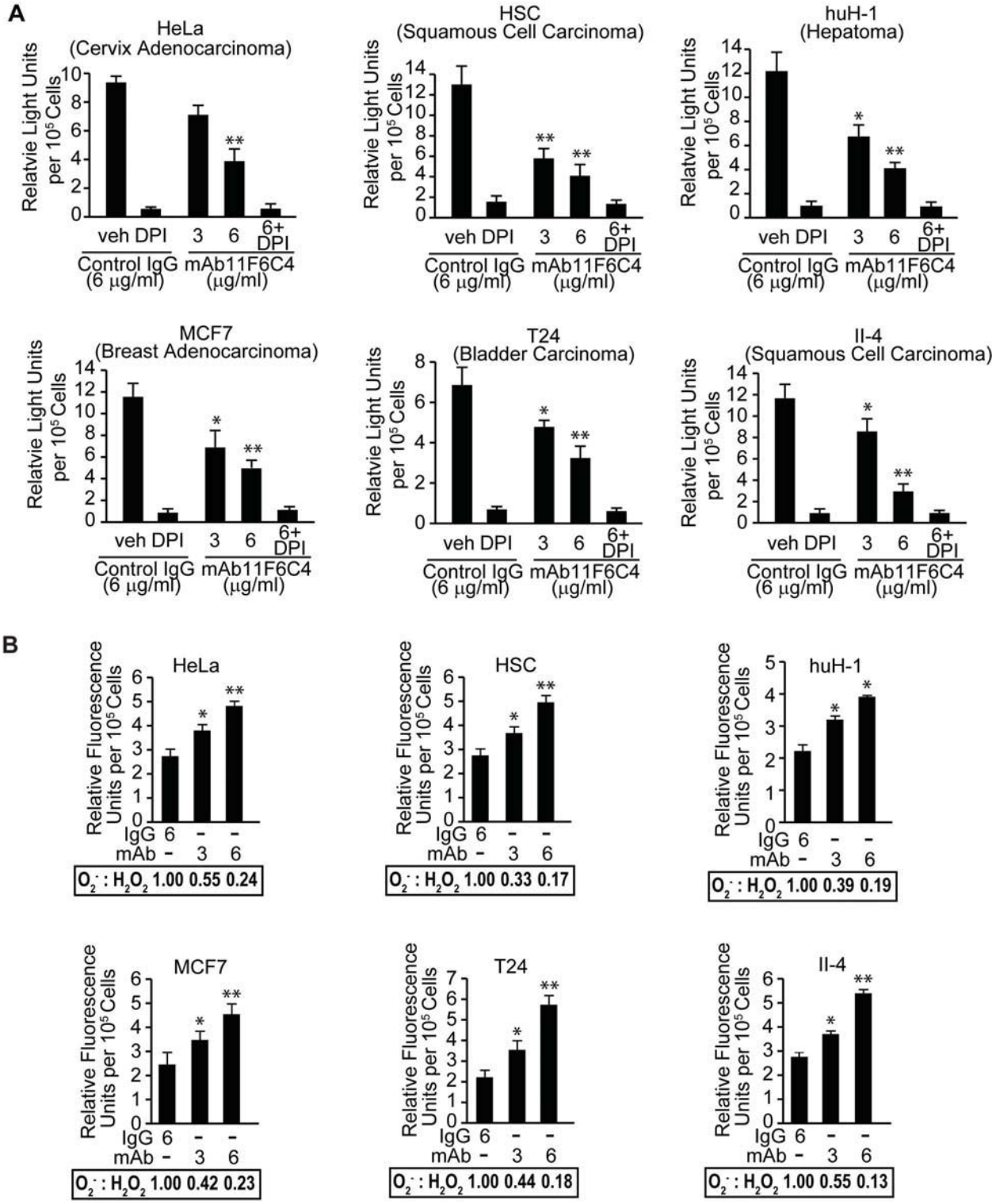

Figure S5, related to Figure 6. ANGPTL4 Maintains a Relatively High O_2^-:H_2O_2 Ratio In Tumor Cells

Measurement of O_2^- (A) and H_2O_2 (B) levels in six different tumor lines by MCLA assay and Amplex red assay, respectively. H_2O_2 was measured in the presence of the specific catalase inhibitor, 3-amino-l, 2, 4-triazole. Arbitrary relative O_2^-:H_2O_2 ratios (B) are shown in boxes.

Values (mean ± SD) are normalized to the total protein content. Three independent experiments were performed with consistent results. *p < 0.05; **p < 0.01.

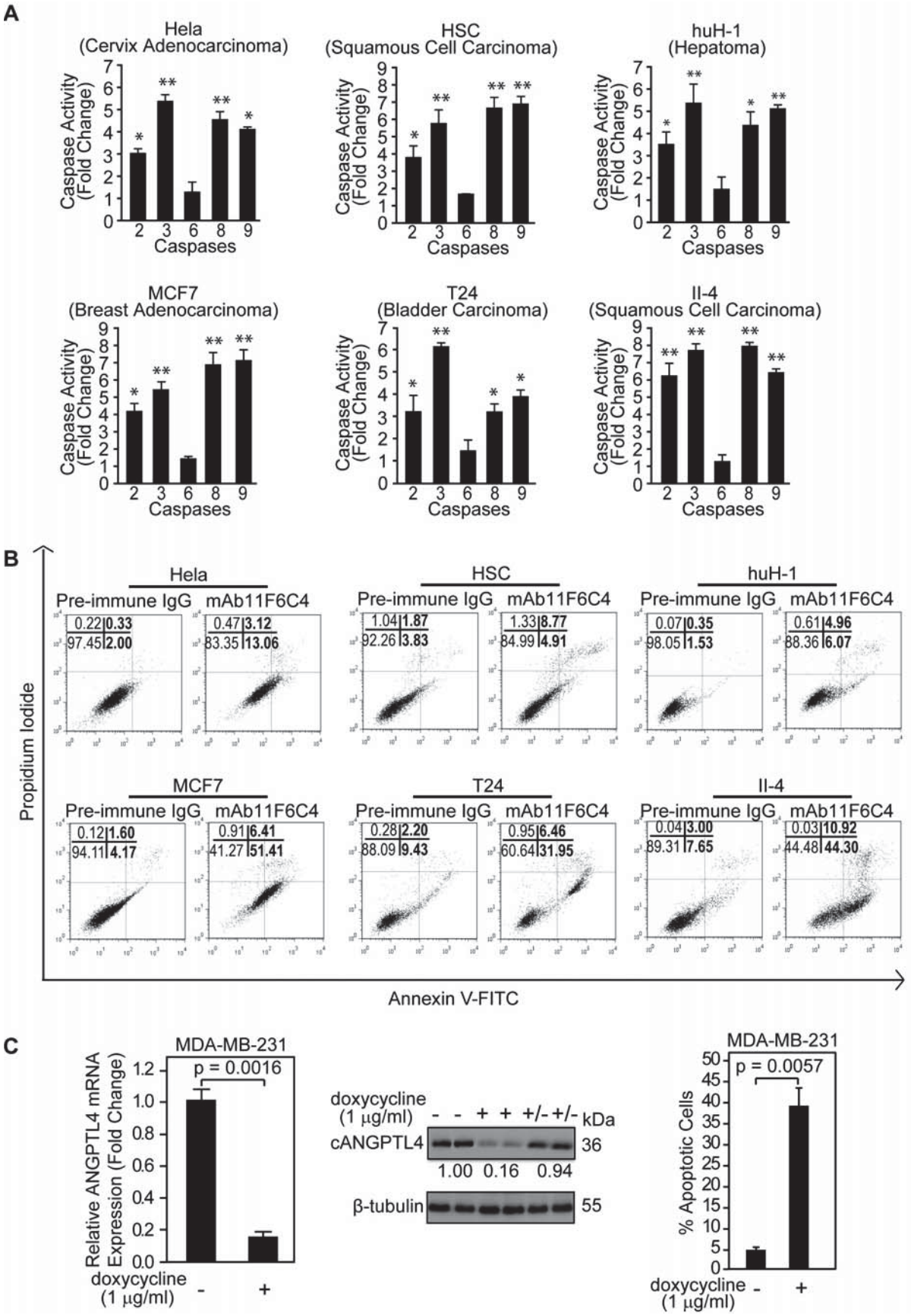

Figure S6, related to Figure 7. Deficiency in ANGPTL4 Activates Caspase Activities and Induces Apoptosis in Tumor Cells

(A) Relative activities of caspases 2, 3, 6, 8 and 9 were measured after 2 h of anoikis. Fold-increase of caspase activities in mAb11F6C4 (6 μg/ml)-treated cells was calculated by comparing with the caspase activities of cells treated with pre-immune IgG (6 μg/ml). Values (mean ± SD) are from three independent experiments with consistent results.*$p < 0.05$; **$p < 0.01$.

(B) Percentage of apoptotic cells in six tumor lines after 2 h of anoikis as analyzed by FACS (5000 events). Tumor cells were treated with 10 μg/ml of control IgG or mAb11F6C4. Apoptotic index is as described in Figure 3B. Results are mean from three independent experiments. $p < 0.05$. See also Figure S6.

(C) Relative ANGPTL4 mRNA (left panel) and protein (middle panel) levels in MDA-MB-231 cells, whose ANGPTL4 suppression was doxycycline-inducible. A stable MDA-MB-231 cell line that expresses an anti-ANGPTL4 shRNA (see supplemental experimental procedures) was produced using the Knockout Singe Vector System (Clontech). Cells were grown in the absence (-) or presence (+) of doxycycline (1 μg/ml) for 24 h. +/- denotes the removal of doxycycline after 24 h of treatment. The right panel shows the percentage of apoptotic MDA-MB-231 cells as evaluated by the anoikis assay. Values (mean ± SD) are from three independent experiments with consistent results.

Supplemental Experimental Procedures

Antibodies and Reagents

Antibodies and reagents used in this study: cyclinD1, integrins β1 and β5, (Chemicon); caspase-3, cleaved caspase-3 (R&D Systems); PCNA, β-tubulin, 14-3-3β, 14-3-3σ, Zn/Cu SOD, ERK1, p(T202/Y204)ERK1/2, Nox1, Nox2, secondary HRP-conjugated antibodies (Santa Cruz Biotechnology); c-Src, p(Y416)Src, FAK, p(Y397)FAK, PKBα, p(S473)PKBα, p(T308) PKBα (Cell Signaling Technology); pan-14-3-3 and BAD (Abcam); Na^+/H^+ exchanger 1 (NHE), Bax and cleaved PARP (Millipore); GTP-Rac1 and total Rac1 (Upstate Biotechnology); Ki67 (NovaCastra); secondary Alexa488-conjugated antibodies, 2-methyl-6-(4-methoxyphenyl)-3, 7-dihydroimidazo[1, 2-a]pyrazin-3-one, hydrochloride (MCLA) and Amplex® Red Hydrogen Peroxide/Peroxidase Assay Kit (Invitrogen). pFIV lentivirus-based siRNA vector and packaging kit were from System Biosciences. Acetyl ester was from Molecular Probes. Transfection reagent ExGen 500 and restriction enzymes were from Fermentas. Unless specified, all other reagents were obtained from Sigma.

Generation of cANGPTL4 and Antibodies

Recombinant ANGPTL4 proteins were purified from the conditioned medium of stable cANGPTL4-expressing S2 cells by preparative isoelectric membrane electrophoresis as previously described (Goh et al., 2010a, 2010b). Rabbit polyclonal antibodies against the C-terminal region and N-terminal region of human ANGPTL4 were produced in-house as previously described (Goh et al., 2010a, 2010b). Monoclonal antibodies (mAbs) against human cANGPTL4 (a.a. 186-406) were made according to standard protocols (Committee on Methods of Producing Monoclonal Antibodies et al., 1999). Briefly, mice were immunized with adjuvant conjugated-cAngptl4. The spleen of the mouse was then removed, and a single cell suspension was prepared. These cells were fused with myeloma cells and cultured in hybridoma selection medium (HAT; Gibco). The fused cells were cultured in microtiter plates with peritoneal macrophages for 48 h post-fusion ($2 - 4 \times 10^6$ cells/ml). The cultures were maintained in a 5% CO_2 humidified incubator for 7-21 days, and routinely fed with HAT medium. mAbs in medium were first screened using ELISA to identify positive clones. Positive clones were expanded and recloned by a limiting dilution technique to ensure monoclonality. Next, SPR was performed to determine the binding kinetics of mAbs. Global fitting of the data to a Langmuir 1:1 model was used to determine the association (k_{on}), dissociation (k_{off}) and affinity constant (K_D) using Scrubber2 (BioLogic Software Pte Ltd). mAb 11F6C4 was chosen for immunotherapy and other experiments based on its superior k_{on}, k_{off} and K_D values as well as its ability to block interaction between cANGPTL4 and integrins.

Human Tumor Array

Commercial tumor tissue arrays #MTU951 and #MET961 (Pantomics, Inc., USA) were utilized to study the expression profile of ANGPTL4 in a large human tumor set by immunofluorescence (IF) imaging. The #MTU951 human tumor tissue array contains 40 tumor types, covering most of the common benign, malignant and metastatic tumors originating from 27 anatomic sites, and the #MET961 human cancer metastasis tissue array consists of 48 cases of metastatic cancers from >8 anatomic sites. The two tissue arrays were probed with the anti-cANGPTL4 polyclonal antibody followed by Alexa488 goat-anti-rabbit IgG. Images were taken using MIRAX MIDI with Plan-Apochromatic 20x/0.8 objective (with equal exposure and gain), and each image was automatically stitched using MIRAX Scan software (Carl Zeiss). The 3D heatmaps were generated using IMARIS software (Bitplane Scientific Software). In the heatmaps, the X- and Y-axes represent the length and width, whereas the Z axis represents the IF intensity. The gray

value (IF intensity) was obtained from three biopsies using TissueQuest software (TissueGnostic GmbH).

Laser Capture Microdissection (LCM)

For LCM samples, epithelial and stromal fractions were microdissected from 8-μm-thick sectioned tissues using a PALM Microbeam Axio Observer Z1 (Carl Zeiss). LCM tissues were collected into microfuge tubes with opaque AdhesiveCaps (Carl Zeiss). RNA was extracted using Optimum™ FFPE RNA Isolation kit (Ambion) pooled from eight LCM tissues. Five ng of RNA was amplified using a Full Spectrum Complete Transcriptome RNA Amplification kit (System Biosciences) prior to qPCR as previously described (Chong et al., 2009; Goh et al., 2010a, 2010b).

Cell Culture

HaCaT is an immortalized but non-tumorigenic human keratinocyte line. II-4 and A-5RT3 are tumorigenic HaCaT derivatives kindly provided by the German Cancer Research Center (DKFZ, Germany). HSC is a human squamous cell carcinoma line provided by Prof. Aso (Yamagata University School of Medicine, Japan), and MDA-MB-231 (breast adenocarcinoma) by Dr. Lin (Nanyang Technological University). Other lines used were murine melanoma B16F10 and human tumor lines used were Alexander (malignant hepatoma), A549 (lung carcinoma), Hela (cervix adenocarcinoma), huH-1 (hepatoma), Kato III (stomach signet ring cell carcinoma), MCF7 (breast adenocarcinoma) and T24 (bladder carcinoma). All cells were maintained in Dulbecco's modified Eagle's medium (DMEM; Hyclone, USA) supplemented with 10% heat-inactivated fetal bovine serum (FBS, Hyclone), except for A549, huH-1, Kato III which were maintained in RPMI-1640 (Hyclone) with 10% FBS. Cells were cultured at 37 ºC, 5% CO_2 and 75% humidified incubator.

Suppression by RNA Interference (RNAi)

siRNAs against human ANGPTL4, mouse ANGPTL4, Nox1, Nox 2 and a scrambled sequence as control (control siRNA) were subcloned into the pFIV-H1/U6-puro pFIV/siRNA lentivirus system. The correct pFIV siRNA constructs were verified by sequencing using H1 primer. The sequences are shown in table below. Pseudovirus purification and transduction were performed (Chong et al., 2009). ANGPTL4-knockdown tumor cells were enriched by puromycin selection for 1 week. The A-5RT3 sub-cell line designated A-5RT3$_{ANGPTL4}$, with the highest knockdown efficiency was chosen in this study, and the non-targeted siRNA transduced line was denoted as A-5RT3$_{CTRL}$. The expression of endogenous ANGPTL4 in MDA-MB-231 cells was also suppressed using tetracycline-inducible pSingle-tTS-shRNA vector (Clontech). ANGPTL4 set 2 shRNA sequences were used (see table below). Knockdown efficiency of ANGPTL4 and relative expression level of indicated genes were determined by qPCR and immunoblot.

Table. Sequences of *ANGPTL4*, *Nox1*, *Nox2* and Control siRNAs.

siRNA	Sense Primer (5' → 3')	Antisense Primer (5' → 3')
ANGPTL4* set 1	AAAGCTGCAAGATGACCTCAGATGGAGGCTG	AAAACAGCCTCCATCTGAGGTCATCTTGCAG
***ANGPTL4* set 2#**	TCGAGGCAGCACCTGCGAATTCAGCATCTGCA TTCAAGAGATGCAGATGCTGAATTCGCAGGTG CTGCTTTTTTACGCGTA	AGCTTACGCGTAAAAAGCAGCACCTGCGAATT CAGCATCTGCATCTCTTGAATGCAGATGCTGA ATTCGCAGGTGCTGCC
***ANGPTL4* set 3**	AAAGCAGCAGGATCCAGCAACTCTTCCACAA	AAAATTGTGGAAGAGTTGCTGGATCCTGCTG
***ANGPTL4* set 4**	AAAGGCTTAAGAAGGGAATCTTCTGGAAGAC	AAAAGTCTTCCAGAAGATTCCCTTCTTAAGC
Nox1	AAAGGGCCACAGATGGCTCCCTTGCCTCCAT	AAAAATGGAGGCAAGGGAGCCATCTGTGGCC

Nox2	AAAGGGCCAGATGTTCTTTCTACAGAAGAAT	AAAAATTCTTCTGTAGAAAGAACATCTGGCC
Mouse *ANGPTL4*	AAAGCTGTGAGATGACTTCAGATGGAGGCTG	AAAACAGCCTCCATCTGAAGTCATCTCACAG
Control siRNA	AAAGCTGTCTTCAAGCTTGATATCGAAGACTA	AAAATAGTCTTCGATATCAAGCTTGAAGACAG

**ANGPTL4* Set 1 siRNA used for lentivirus-mediated RNA interference.

ANGPTL4 set 2 shRNA was cloned into pSingle-tTS-shRNA vector (Clontech) and used for doxycycline-inducible knockdown in MDA-MB-231 cells.

Rho GTPases Assay

Active GTP-bound Rac1 was quantified as previously described (Tan et al., 2009) with minor modifications. Briefly, 500 μg of the indicated tumor biopsies lysates were incubate with 2 μg of configuration-specific monoclonal anti-Rac1-GTP antibody (GTP-Rac1; NewEast Biosciences). GTP-Rac1-bounded antibodies were immunoprecipitated with Sepharose Protein G/A beads. Bound proteins were solubilised in Laemmli's buffer, resolved by SDS-PAGE, and immunoblotted using polyclonal antibody against Rac1. Total Rac1 was detected using total lysate. Anti-Rac1 antibodies for immunblot were from Cytoskeleton Inc.

Membrane Protein Extraction

HEK293T cells were transfected with either empty mammalian expression vector pEF1-mycA (Invitrogen) or vector carrying cDNAs encoding human integrins β1, β3 and β5 by means of ExGen 500. Forty-eight hours post-transfection, cell membranes were first isolated using ProteoExtractNative Protein Extraction Kit (Calbiochem) and subjected to enrichment by sucrose step gradient (Tang, 2006). The proteins were dialyzed against PBS prior to SPR analysis.

Immunoblot Analysis

Total protein was extracted from cells or tumor tissues/cells with ice-cold lysis buffer (20 mM $Na_2H_2PO_4$, 250 mM NaCl, 1% Triton-100, 0.1% SDS). Equal amount of protein extracts were resolved by SDS-PAGE and electrotransferred onto PVDF membranes. Membranes were processed according to standard procedure and proteins were detected by chemiluminesence (Millipore, USA). β-tubulin was used as loading and transfer control.

Detection of Src Oxidation by Carboxymethylation

The detection of reduced Src was performed as described (Giannoni et al., 2009) with minor modifications. Cells were subjected to anoikis as described above. At the indicated time, cells were then lysed with 500 μl lysis buffer (50 mM Tris-HCI, pH 7.5, 150 mM NaCl, 0.5% Triton X-100, 10 μg/ml aprotinin and 10 μg/ml leupeptin) containing 100 μM *N*-(biotinoyl)-*N*'-(iodoacetyl) ethylenediamine. Lysates were clarified by centrifugation and c-Src was immunoprecipitated using specific anti-c-Src antibodies. Immunocomplexes were resolved by SDS-PAGE and the biotinylated/reduced fraction of Src kinase was detected with horseradish peroxidase (HRP)-conjugated streptavidin and chemiluminesence.

Electron Paramagnetic Resonance (EPR) Measurement of O_2^-

Entire excised tumor biopsies were enzymatically dispersed into single cell suspensions. The tissue was minced and incubated in digestion buffer containing 1 mg/ml hyaluronidase, 1 mg/ml collagenase D and 100 unit/ml DNase (Sigma-Aldrich) in a 37°C shaking incubator for 2 h. The dispase and hyaluronidase digests were pooled and filtered through a 70 μm Nylon cell strainer. Cells were washed, pelleted and resuspended in PBS containing 3% FBS. Equal numbers of cells

were used for EPR measurement of O_2^-. Direct trapping of superoxide in aqueous media was performed using the spin trap DEPMPO, which forms a relatively stable superoxide adduct. EPR spectra were recorded at room temperature with a Bruker D-200 ER spectrometer, operating at X-band with a TM 110 cavity with a quartz flat cell. The EPR parameters were set at 100 KHz, X-band microwave frequency, 9.5 GHz; microwave power, 20 mW; modulation amplitude, 1 G; time constant, 160 s; scan time, 50 s; and receiver gain, 5 x 10^5. The EPR spectra represent the averaged signals of 10 scans. EPR signal amplitude at 3480 G represents the pure line corresponding only to the superoxide adduct. All experiments were performed in triplicates.

Total RNA Isolation and Quantitative Real-time PCR (qPCR)

Total RNA was extracted and qPCR was performed Expression was related to the housekeeping gene 60S ribosomal protein L27 (*L27*) which did not change under any of the experimental conditions studied. The sequence of primers is available in the table below. For focused mRNA array, genes whose expression was changed significantly (> 2-fold) were listed and heatmaps were generated using Orange Canvas 1.0 software.

Table. Sequences of qPCR Primers.

GenBank Accession	Official Symbol	Sense Primers (5' → 3')	Antisense Primers (5' → 3')
NM_004324	*BAX*	GGGTGGTTGGGTGAGACTC	AGACACGTAAGGAAAACGCATTA
NM_014417	*BBC3*	GACCTCAACGCACAGTACGAG	AGGAGTCCCATGATGAGATTGT
NM_138578	*BCL2L1*	TGCGTGGAAAGCGTAGACAAG	GCTGCTGCATTGTTCCCATA
NM_004050	*BCL2L2*	GCGGAGTTCACAGCTCTATAC	AAAAGGCCCCTACAGTTACCA
NM_001196	*BID*	GACAGCATGGACCGTAGCATC	AGGTGCGTAGGTTCTGGTTAATA
NM_001166	*BIRC2*	GTTTCAGGTCTGTCACTGGAAG	TGGCATACTACCAGATGACCA
NM_182962	*BIRC3*	TCCTGGATAGTCTACTAACTGCC	GCTTCTTGCAGAGAGTTTCTGAA
NM_033292	*CASP1*	TCCAATAATGGACAAGTCAAGCC	GCTGTACCCCAGATTTTGTAGCA
NM_001230	*CASP10*	ATTGGTCCCAAGACATGAAGAC	TGTTCCCTGTTTGTCCACTCT
NM_032982	*CASP2*	AAACGAGGTTCCTGGTACATCG	TCCTTGATAAGTGCGTTCACC
NM_033340	*CASP7*	AGTGACAGGTATGGGCGTTC	GAGGTTGCAGTCTTCCGAGAT
NM_001237	*CCNA2*	GATGGTAGTTTTGAGTCACCACA	CACGAGGATAGCTCTCATACTGT
NM_053056	*CCND1*	GCTGGAGCCCGTGAAAAAGA	CTCCGCCTCTGGCATTTTG
NM_000075	*CDK4*	CAGATGGCACTTACACCCGTG	GCAGCCCAATCAGGTCAAAGA
NM_004935	*CDK5*	GCCGCAATGTGCTACACAG	GAGTAACAGCGGACGGGAATC
NM_000389	*CDKN1A*	GTCACTGTCTTGTACCCTTGTG	CGGCGTTTGGAGTGGTAGAAA
NM_000076	*CDKN1C*	ACATCCACGATGGAGCGTC	GGAAGTCGTAATCCCAGCGG
NM_001278	*CHUK*	CAGCCATTTACCTGGCATGAG	GAGGGTCCCAATTCAACATCAA
NM_001303	*COX10*	CCAGCAAGTAAGACCCAAGCC	TCATCTCTTTCCACCGCTTTTC
NM_019887	*DIABLO*	GGTACAGACAGTGTTTGTGTGT	CTACTAAGGGAATGAGGCTCTGA
NM_000043	*FAS*	TATCACCACTATTGCTGGAGTCA	ACGAAGCAGTTGAACTTTCTGTT
NM_002417	*KI67*	TGTTCCCACTACACAATGTCTTG	ACTTACGCGAGACCAACAGTT
NM_021960	*MCL1*	GTGCCTTTGTGGCTAAACACT	AGTCCCGTTTTGTCCTTACGA
NM_001618	*PARP1*	GATGCCTATTACTGCACTGGG	CGGTCCTGCTTTTTAACCTTCAA
NM_022121	*PERP*	CAACCCTGCTGTCACTTACAT	AGGTCATCTTCGTAGTTGGGG
NM_182649	*PCNA*	ACACTAAGGGCCGAAGATAACG	CGGCATATACGTGCAAATTCAC
NM_002859	*PXN*	GCGGACTTGGAGTCTACCAC	TCCAGTTGGGTATGAGTAGGG
NM_001167	*XIA[*	GACAGGCCATCTGAGACACAT	GGGGTTAGGTGAGCATAGTCTG
NM_000687	*AHCY*	GCATCCGAGGCATCTCTGAG	GCCATAGAGGTTGTCAAACTTGC
NM_001713	*BHMT*	GACACCTTCATACCTTAGCTGC	ACAGGTTTACCGGATGCTATCAA
NM_012260	*HACL1*	CCTTCTTATCATCGGGAAAGGTG	CCCATAGGGGTGGGCAAAAAT
NM_000221	*KHK*	GCTATTCTGTGGACCTACGCT	AGTATAGGATGGTGCGGCTAC
NM_000429	*MATLA*	CATCAAGCACATCGGCTACGA	CCGAACATCAAACCCTGATCTC
NM_000274	*OAT*	TGCTGTCAACCAAGGGCATT	GCCTCCACTCCTGTATTCATAGG
NM_000988	*L27*	TGATGGCACCTCAGATCGC	AGAGTACCTTGTGGGCATTAGG

Note: Melt curve analysis was included to assure that only one PCR product was formed.

Surface Plasmon Resonance (SPR) Analysis

The purified fibrinogen-like fragment of ANGPTL4 (cANGPTL4) was immobilized onto ProteOn GLC chip by amine coupling, as recommended by the manufacturer (Bio-Rad). Different concentrations of integrins were introduced into the GLC chip at a flow rate of 25 µl/min for 5 min with running buffer (50 mM Tris, pH 8.0 and 100 mM NaCl). Polyclonal anti-cANGPTL4 antibodies against the immobilized cANGPTL4 determined the R_{max} value to be 423.1 resonance unit (RU). Global fitting of the data to a Langmuir 1:1 model was used to determine the association (k_{on}), dissociation (k_{off}) and affinity constants (K_D) using Scrubber2 (BioLogic Software Pte Ltd). The experimental R_{max} values of integrins β1 and β5 for cANGPTL4 were determined to be 365.6 and 341.9 RU, respectively. The affinity constants of the 6 mAbs for ANGPTL4 were determined using the One-Shot Kinetics protocol as described by manufacturer (Bio-Rad).

Soft Agar and Anoikis Assay

A-5RT3$_{CTRL}$ and A-5RT3$_{ANGPTL4}$ cells were used in soft agar assay. 0.6% Noble agar (Sigma Aldrich) in DMEM with 10% FBS was allowed to solidify in 6-well plates, and 1×10^4 cells were plated in 0.3% Noble agar in DMEM with 10% FBS on top. Tumor-cell colonies were stained with 1 mg/ml thiazolyl blue tetrazolium in PBS after 4 weeks.

Cells were subjected to an anoikis assay. Briefly, anoikis was induced by forced suspension, wherein 5.0×10^5 cells were seeded onto 1.0% serum-free DMEM equilibrated agarose in the presence of either 10 µg/ml of pre-immune IgG or mAb11F6C4. For MBA-MD-231, the cells were exposed to 1 µg/ml doxycyline for 24 h to knockdown ANGPTL4 prior anoikis. For rescue experiments, cells were subjected to anoikis in the presence of either the indicated concentrations of exogenous recombinant cANGPTL4 or vehicle (PBS). Cells were harvested at the indicated time points, and analyzed for apoptosis by FACS analysis. The apoptotic indices of attached cells were determined immediately after harvesting with trypsin.

Caspase Activity Assay

Cells were subjected to anoikis as described above. The activities of caspases 2, 3, 6, 8 and 9 were measured with Apotarget caspase colorimetric protease assay kit (Biosource International, Camarillo,CA) according to the manufacturer's instructions. The O.D.$_{405nm}$ was measured, and the fold increase in caspase activity was determined by direct comparison with the level of the A-5RT3$_{CTRL}$ or cognate pre-immune IgG treated cells.

Supplemental References

Committee on Methods of Producing Monoclonal Antibodies, Institute for Laboratory Animal Research, and Council, N.R., ed. (1999). Monoclonal Antibody Production.

Goh, Y.Y., Pal, M., Chong, H.C., Zhu, P.C., Tan, M.J., Punugu, L., Lam, C.R.I., Yau, Y.H., Tan, C.K., Huang, R.L., Tan, S.M., Tang, M.B.Y., Ding, J.L., Kersten, S. and Tan, N.S. (2010a). Angiopoietin-like 4 interacts with integrins β1 and β5 to modulate keratinocyte migration. Am. J. Pathol. *177*, 2791-2803.

Goh, Y.Y., Pal, M., Chong, H.C., Zhu, P., Tan, M.J., Punugu, L., Tan, C.K., Huang, R.L., Sze, S.K., Tang, M.B.Y., et al. (2010b). Angiopoietin-like 4 interacts with matrix proteins to modulate wound healing. J Biol Chem *285*, 32999-33009.

Tang, V.W. (2006). Proteomic and bioinformatic analysis of epithelial tight junction reveals an unexpected cluster of synaptic molecules. Biology direct *1*, 37.

2) Goh YY*, Pal M*, Chong HC*, **Zhu P**, Tan MJ, Punugu L, Yau YH, Tan CK, Roystan H, Tan SM, Tang MBY, Ding JL, Kersten S, Tan NS. Angiopoietin-like 4 interacts with integrins β1 and β5 to modulate keratinocyte migration (*Am. J. Pathol. 177, 2791-280,* *Authors contributed equally).

Uncorrected Version. Published on October 15, 2010 as DOI:10.2353/ajpath.2010.100129

The American Journal of Pathology, Vol. 177, No. 6, December 2010

DOI: 10.2353/ajpath.2010.100129

Epithelial and Mesenchymal Cell Biology

Angiopoietin-Like 4 Interacts with Integrins β1 and β5 to Modulate Keratinocyte Migration

Yan Yih Goh,* Mintu Pal,* Han Chung Chong,* Pengcheng Zhu,* Ming Jie Tan,* Lakshmi Punugu,* Chee Ren Ivan Lam,* Yin Hoe Yau,* Chek Kun Tan,* Royston-Luke Huang,* Suet Mien Tan,* Mark Boon Yang Tang,† Jeak Ling Ding,‡ Sander Kersten,§ and Nguan Soon Tan*

From the School of Biological Sciences, Nanyang Technological University, the National Skin Centre,† and the Department of Biological Sciences, National University of Singapore,‡ Singapore; and Wageningen University,§ Wageningen, The Netherlands*

Adipose tissue secretes adipocytokines for energy homeostasis, but recent evidence indicates that some adipocytokines also have a profound local impact on wound healing. Upon skin injury, keratinocytes use various signaling molecules to promote reepithelialization for efficient wound closure. In this study, we identify a novel function of adipocytokine angiopoietin-like 4 (ANGPTL4) in keratinocytes during wound healing through the control of both integrin-mediated signaling and internalization. Using two different *in vivo* models based on topical immuno-neutralization of ANGPTL4 as well as ablation of the *ANGPTL4* gene, we show that ANGPTL4-deficient mice exhibit delayed wound reepithelialization with impaired keratinocyte migration. Human keratinocytes in which endogenous ANGPTL4 expression was suppressed by either siRNA or a neutralizing antibody show impaired migration associated with diminished integrin-mediated signaling. Importantly, we identify integrins β1 and β5, but not β3, as novel binding partners of ANGPTL4. ANGPTL4-bound integrin β1 activated the FAK-Src-PAK1 signaling pathway, which is important for cell migration. The findings presented herein reveal an unpredicted role of ANGPTL4 during wound healing and demonstrate how ANGPTL4 stimulates intracellular signaling mechanisms to coordinate cellular behavior. Our findings provide insight into a novel cell migration control mechanism and underscore the physiological importance of the modulation of integrin activity in cancer metastasis. *(Am J Pathol 2010, 177:000–000; DOI: 10.2353/ajpath.2010.100129)*

Wound healing consists of a finely tuned pattern of integrated biological events aimed at reestablishing a new epithelial barrier. This process includes inflammation, cell migration, proliferation, and extracellular matrix (ECM) remodeling. Integrins are crucial mediators of cell migration that are essential throughout the wound healing process.[1] The binding of integrins to their cognate matrix proteins induces a conformational change that is propagated to the cytoplasmic domain and activates both focal adhesion kinase (FAK)-dependent and *FAK-independent* signaling pathways.[2] FAK is a nonreceptor protein tyrosine kinase that is involved in signal transduction from integrin-enriched focal adhesion sites that mediate cell contact with the matrix proteins. The multiple protein–protein interaction sites allow FAK to associate with adaptor and structural proteins to modulate the activities of mitogen-activated protein kinases, stress-activated protein kinases, and small GTPases.[2] Integrins can also cooperate with specific growth factor receptors to activate non–FAK-dependent pathways such as the phosphatidylinositol 3-kinase, mitogen-activated protein kinase, 14-3-3, and protein kinase C (PKC)-mediated pathways.[3–7] Although the importance of the cell-matrix interactions in wound healing is well-recognized, the mechanism underlying these events needs further study.

During the wound repair process, changes in ECM composition have a direct effect on cell–matrix communication and, consequently, the behavior of the epithelial cells. The ECM is composed of matrix structural proteins and matricellular proteins, among others. Matricellular proteins, such as secreted protein acidic and rich in cysteine (SPARC), thrombospondin, tenascin, and osteopontin, belong to a group of extracellular factors that

Supported by A*STAR BMRC grant (05/1/22/19/377), Ministry of Education, Singapore (ARC 18/08), Nanyang Technological University, Singapore (RGD 127/05, 158/06). M.P., L.P. and P.C.Z. are recipients of the Nanyang Research Scholarship. C.K.T. is recipient of ARC18/08 grant Scholarship.

Y.Y.G., M.P., and H.C.C. contributed equally to this work.

Accepted for publication August 13, 2010.

Supplemental material for this article can be found on *http://ajp.amjpathol.org*.

Address reprint requests to Nguan Soon Tan, Ph.D., School of Biological Science, 60 Nanyang Drive, Singapore 637551. E-mail: nstan@ntu.edu.sg.

modulate cell–matrix communication but do not serve primary structural roles.[8] They are expressed when tissues undergo events that require tissue renewal, tissue remodeling, or embryonic development. Despite the importance of matricellular proteins during wound repair, how these extracellular factors modulate the integrin-mediated signaling pathway that culminates in the appropriate cellular responses remain less well understood.[9]

Integrins on the cell surface are well suited to function as biosensors to constantly interrogate the wound environment and modulate cell responses accordingly. The binding of an integrin to its cognate matrix proteins activates intracellular signaling pathways to modulate a broad range of cellular processes, including cell migration.[10] Ligand-activated integrins are continuously internalized from the plasma membrane into the endosomal compartments and recycled back to the cell surface.[11] It is well established that integrin recycling contributes to the motility of rapidly migrating cells, such as wound keratinocytes, and permits constant monitoring of the wound cellular environment. The recycling process is apparently selective, with certain integrin heterodimers being cycled rapidly while others remain at the plasma membrane. However, the extracellular factors and mechanisms that provide such selectivity remain unclear.

Adipose tissue produces and secretes a variety of bioactive molecules called adipocytokines that are involved in energy homeostasis. Emerging evidence shows that certain adipocytokines, including leptin and plasminogen activator inhibitor type-1, also have a profound local impact on wound healing.[12,13] The angiopoietin-like 4 (ANGPTL4) protein is an adipocytokine that plays important roles in lipid and glucose metabolism.[14] Its expression is up-regulated by the nuclear hormone receptor peroxisome proliferator-activated receptor[15] and by hypoxia.[16] Its plasma abundance is increased by fasting and decreased by chronic high-fat feeding. ANGPTL4 decreases blood glucose and improves glucose tolerance in mice.[17] ANGPTL4 is also implicated in breast cancer metastasis via the regulation of vascular integrity.[18,19] The native ANGPTL4 is proteolytically cleaved, giving rise to the N-terminal coiled-coil fragment (nANGPTL4) and the C-terminal fibrinogen-like domain (cANGPTL4). The former assembles into multimeric structures and inhibits the activity of lipoprotein lipase.[20] cANGPTL4 exists as a monomer, whose function is still relatively unclear, but it has been implicated in the maintenance of vascular endothelial integrity.[21] Despite its multiple functions, the significance of the different cleaved fragments of ANGPTL4 is only beginning to be understood. Importantly, how ANGPTL4 relays its action from the cell surface and initiates intracellular signaling cascade remain unknown, which limits our understanding of the mechanisms by which ANGPTL4 contributes to wound healing and cancer metastasis.

Here we show that ANGPTL4 interacts with wound integrins β1 and β5. This interaction activates integrin-mediated intracellular signaling and allows for selective integrin recycling enhancing cell migration. ANGPTL4-deficient cells showed impaired cell migration and diminished FAK-Src-PAK1 activation. This defect was observed *in vivo* as delayed reepithelialization in *ANGPTL4*-knockout mice. Our results reveal a novel role of ANGPTL4 in modulating integrin-mediated signaling during wound healing. Considering the importance of cell migration to numerous pathophysiological processes, our findings fill crucial gaps in the understanding of integrin-mediated cell migration.

Materials and Methods

Wounding Experiment

Wounding and treatment were performed as described.[22] Wounds were topically treated daily with 50 μg of either preimmune IgG, anti-cANGPTL4 antibodies, or 10 μg recombinant ANGPTL4. The wounds were kept moist using occlusive Tegaderm (3M, USA) dressing. Treatments were rotated to avoid site bias. At the indicated days postinjury, wounds were excised for analysis. Pure-bred *ANGPTL4*$^{+/+}$ and *ANGPTL4*$^{-/-}$ mice on a C57Bl/6 background were used.[23] Animal experiments were approved by the University Institutional Animal Care and Use Committee (ARF-SBS/NIE-A-0093, −0078, and −004). Hematoxylin and eosin (H&E) stained images and histomorphometric measurements were taken using a MIRAX MIDI with Plan-Apochromatic ×20/0.8 objective and MIRAX Scan software (Carl Zeiss). Polyclonal antibodies against human (amino acids 186-406) and mouse (190-410) cANGPTL4 were produced in-house.

Knockdown of ANGPTL4 and Real-Time PCR

siRNA against human ANGPTL4 and a scrambled sequence as control were subcloned into the pFIV-H1/U6-puro pFIV/siRNA lentivirus system. Pseudovirus purification and transduction were performed as described.[22] Endogenous *ANGPTL4* in human keratinocytes was transiently suppressed using either siGLO control or ON-TARGETplus SMARTpool *ANGPTL4* siRNA (Dharmacon; L-007807-00) by means of DharmaFECT1. The knockdown efficiency and relative expression level of indicated genes were determined by qPCR using the KAPA FAST qPCR kit (KAPA Biosystems). All oligonucleotides and TaqMan probe sequences are provided in Table 1. The Interferon Response Detection Kit was from System Biosciences.

Recombinant ANGPTL4 Expression and Purification

The cDNAs encoding various domains of human ANGPTL4 were isolated by PCR, subcloned into pET30a vector and transformed into *E. coli* Rosetta-gami bacteria (Novagen). Protein expression was induced by 0.5 mmol/L IPTG and purified either by affinity nickel-Sepharose, size-exclusion or anion-exchange chormatographies according to standard procedures (Supplemental Figure 1, A and B at *http://ajp.amjpathol.org*). *Drosophila* S2 cells stably expressing either human integrin β1, β5, or β3 were maintained as previously described.[24] S2 cells were routinely cultured in serum-free medium. Cell membranes were first isolated using the ProteoExtract

Table 1. Oligonucleotide Sequences of siRNA and Real-Time PCR Primers Used in this Work

siRNA	
ANGPTL4 siRNA	
Sense	5′-AAAGCTGCAAGATGACCTCAGATGGAGGCTG-3′
Anti-sense	5′-AAAAGGCTTAAGAAGGGAATCTTCTGGAAGAC-3′
Control siRNA	
sense	5′-AAAGCTGTCTTCAAGATTGATATCGAAGACTA-3′
Anti-sense	5′-AAAATAGTCTTCGATATCAAGCTTGAAGACA-3′
Real-time qPCR*	
Human ANGPTL4	
Forward	5′-CTCCCGTTAGCCCCTGAGAG-3′
reverse	5′-AGGTGCTGCTTCTCCAGGTG-3′
Taqman probe	5′-(6-FAM)ACCCTGAGGTCCTTCACAGCCTGC(TAMRA)-3′
Mouse ANGPTL4	
Forward	5′-GCTTTGCATCCTGGGACGAG-3′
Reverse	5′-CCCTGACAAGCGTTACCACAG-3′
Taqman probe	5′-(6-FAM)ACTTGCTGGCTCACGGGCTGCTAC(TAMRA)-3′
L27	
Forward	5′-CTGGTGGCTGGAATTGACCGCTA-3′
Reverse	5′-CAAGGGGATATCCACAGAGTACCTTG-3′
Taqman probe	5′-(HEX)CTGCCATGGGCAAGAAGAAGATCGCC(BHQ1)-3′

*Melting curve analysis was performed to assure that only one PCR product was formed. Primers were designed to generate a PCR amplification product of 100 to 250 bp. Only primer pairs yielding unique amplification products without primer dimer formation were subsequently used for real-time PCR assays.

Native Protein Extraction Kit (Calbiochem) and were enriched by step sucrose gradient ultracentrifugation.[25]

In Vitro *Scratch-Wound Assay*

Scratch-wound assays were performed as described.[26] Images were taken at 2-minute intervals over 6 hours using a temperature-controlled, 5% CO_2-chambered Axiovert 200M microscope (Carl Zeiss) with a Plan-Neofluar ×10/0.3 or ×20/0.5 objective, CoolSNAP HQ^2 camera (Photometrics), and MetaMorph software (Molecular Devices). Preimmune IgG or anti-cANGPTL4 antibodies were used at 2 μg/ml, recombinant ANGPTL4 at 6 μg/ml.

Surface Plasmon Resonance

Surface plasmon resonance was used to determine the dissociation constants of the interactions of integrins β1, β5 with ANGPTL4 immobilized onto CM5 chip. Anti-cANGPTL4 antibodies against the immobilized ANGPTL4 determined the Rmax value of 251.8 resonance units (RU). Six concentrations (0.16, 0.32, 0.63, 1.25, 2.50, and 5.0 μmol/L) of various matrix proteins or integrins were used. Global fitting of the data to a Langmuir 1:1 model was used to determine the dissociation constant (K_D) using kinetic analysis calculated with the BiaEvaluation software (BIAcore, version 3.1). The experimental Rmax values of integrins β1 and β5 for ANGPTL4 were 261.1 RU and 229.3 RU, respectively. Values are mean ± SD of five independent preparations of recombinant proteins. Various anti-integrin α5β1 and αvβ5 antibodies from R&D Systems and Abnova.

Affinity Coprecipitation Assay

In vivo coimmunoprecipitation was performed using indicated antibodies as previously described.[27] The samples were lysed and coimmunoprecipitation was performed using resin immobilized with either anti-cANGPTL4, anti-integrin β1, or preimmune IgG. Immunoprecipitates were released by Laemmli's buffer and probed with the indicated antibodies. For specificity of coimmunoprecipitation, immunodetection of cytoplasmic ERK, which does not interact directly with integrins β1 and β5, was performed.

Rho GTPase Assay

Active GTP-bound Rac1 was quantified as previously described.[26] Briefly, 500 μg of cell lysates were incubated for 1 hour at 4°C with GST-p21 binding domain of PAK coupled to glutathione Sepharose beads. Bound proteins were solubilized in Laemmli's buffer, resolved by SDS-PAGE, and immunoblotted using the corresponding antibodies against Rac1. Total Rac1was detected using total cell lysate. Anti-Rac1 antibodies were from Cytoskeleton, Inc.

In Situ *Proximity Ligation Assay (PLA)*

Wound biopsies were frozen in Tissue-Tek OCT compound medium (Sakura). Keratinocytes subcultured onto glass chamber slides (Lab-Tek), or wound sections were fixed with 4% paraformaldehyde for 15 minutes. The slides were washed twice with PBS, blocked for 1 hour at 25°C with 2% BSA in PBS containing 0.1% Triton-X, followed by incubation overnight at 4°C with indicated antibody pairs. The slides were washed as described above. DUOlink *in situ* PLA was performed as recommended by the manufacturer (OLink Biosciences). The negative control was performed without primary antibody. Images were taken using an LSM710 META confocal laser scanning microscope with a Plan-Apochromat ×63/1.40 Oil objective and ZEN 2008 software (Carl Zeiss).

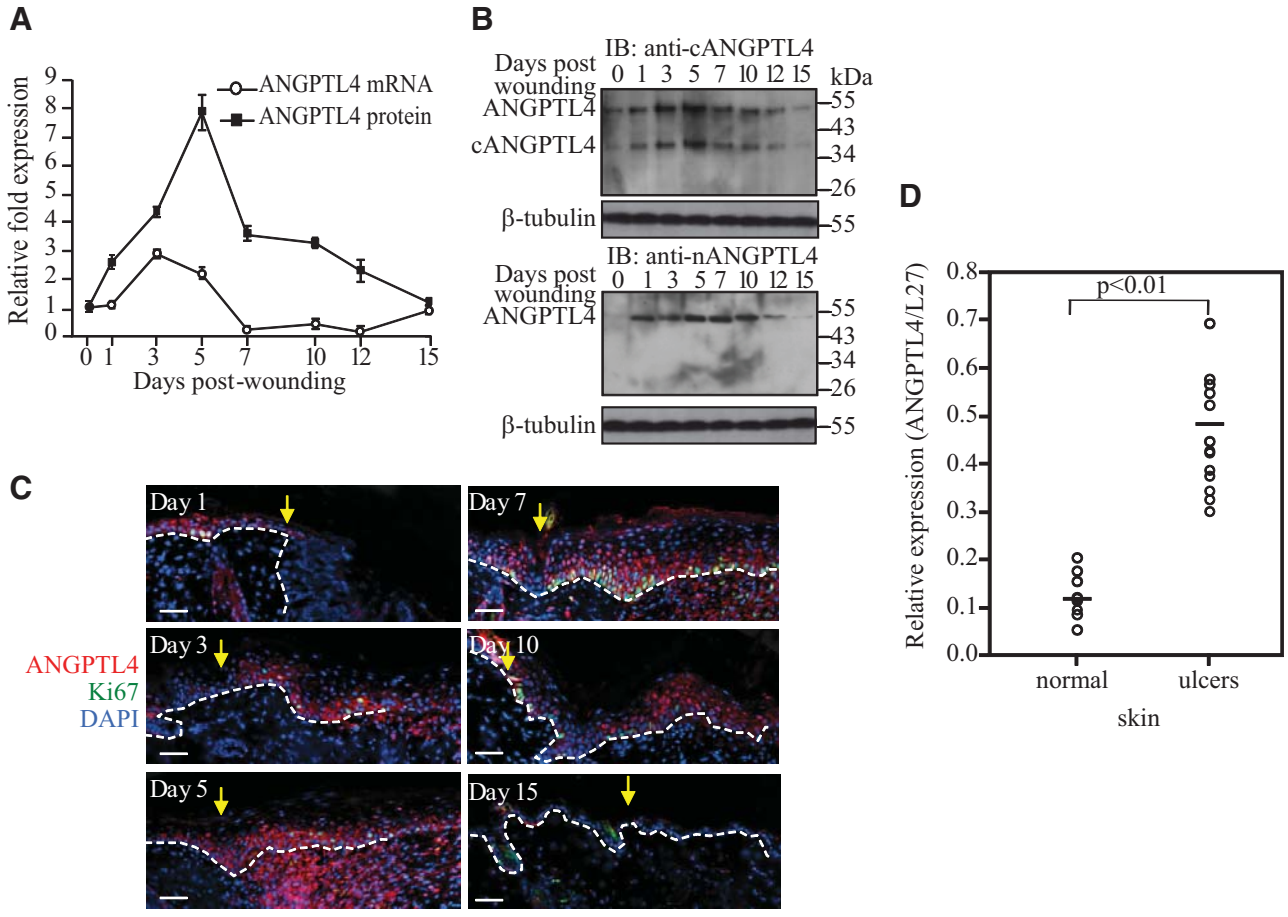

Figure 1. ANGPTL4 expression is elevated in wound biopsies. Expression profiles of ANGPTL4 (**A**) mRNA and (**B**) protein during wound healing determined by qPCR and immunoblotting, respectively. Ribosomal protein L27 was used as a normalizing reference gene. Polyclonal antibodies that recognized the N (anti-nANGPTL4) and C termini (anti-cANGPTL4) of ANGPTL4 were used. β-tubulin was used as loading and transfer control. Values at each time point are mean ± SEM of 15 mice. **C:** Immunofluorescence staining of ANGPTL4 in wound biopsies. Mouse skin wound biopsies at indicated days of postwounding were cryosectioned, stained for cANGPTL4 and Ki-67, and counterstained with DAPI. Representative pictures from the wound edge and adjacent wound bed are shown. **Arrow** denotes the wound edge at day 0. **Dotted white line** represents epidermal-dermal junction. Scale bar = 40 μm. **D:** Relative expression levels of *ANGPTL4* mRNA in normal human skin biopsies and ulcers determined by qPCR. Ribosomal protein L27 was used as a reference gene. Each circle shows the mean values of three different paraffin sections from an individual sample; horizontal bars show average values obtained from human skin biopsy or ulcers.

Integrin Internalization and FACS Analysis

Surface labeling of membrane receptors was performed on adherent cells as described,[28] with minor modifications. Surface proteins were directly labeled at 4°C with 0.2 mg/ml NHS-SS-biotin (Thermo) in PBS for 30 minutes. Labeled cells were washed twice with cold PBS and transferred to serum-free DMEM at 37°C to eliminate exogenous ANGPTL4 and to permit internalization. After removing biotin from all remaining surface proteins using 20 mmol/L MesNa for 15 minutes followed by 20 mmol/L IAA for 10 minutes, cells were lysed. Supernatants were corrected to equivalent protein concentrations, and biotinylated proteins were captured overnight by NeutrAvidin agarose resins (Thermo) at 4°C. Immobilized proteins were released using Laemmli's buffer and resolved by 10% SDS-PAGE, followed by immunoblot with the indicated antiintegrin antibodies. Cell surface expression of integrin at the indicated time was evaluated as previously described.[29]

Statistical Analysis

Statistical analysis was determined using the two-tailed Mann–Whitney test using SPSS software. $P < 0.05$ was considered statistically significant.

Results

Elevated ANGPTL4 Expression in Skin Wounds

We found that during the healing of a full-thickness excisional wound in mouse skin, *ANGPTL4* mRNA peaked at day 3–5 postwounding, as shown by quantitative PCR (qPCR) and immunodetection (Figure 1A). Using polyclonal antibodies that recognize either the N- or C-terminal region of ANGPTL4, only the native ANGPTL4 and cANGPTL4 were detected in wound biopsies (Figure 1B). Immunoblot showed the specificity of anti-cANGPTL4 (Supplemental Figure 1C at *http://ajp.amjpathol.org*). Dual

immunofluorescence staining revealed that the expression of ANGPTL4 increased progressively in both the wound epithelia and wound bed, coinciding with an increase in Ki-67–positive proliferating keratinocytes (Figure 1C). ANGPTL4 was detected only at basal levels in unwounded skin (Supplemental Figure 1D at *http://ajp.amjpathol.org*). A retrospective examination of human skin ulcers, which reflects a situation of impaired healing, also revealed higher ANGPTL4 expression in ulcers compared with normal skin (Figure 1D and Supplemental Figure 1E at *http://ajp.amjpathol.org*). Although ulcers are different from acute wounds, their examination can provide clues on ANGPTL4 expression in human wounds, as it was not possible for us to obtain equivalent biopsies from healthy volunteers. These observations suggest an important role of ANGPTL4 during wound healing.

ANGPTL4 *Deficiency Delays Wound Reepithelialization*

We examined the healing of full-thickness skin wound in wild type (*ANGPTL4*$^{+/+}$) and ANGPTL4-knockout (*ANGPTL4*$^{-/-}$) mice. Histomorphometric analysis of day 3–10 wound biopsies showed delayed reepithelialization of *ANGPTL4*$^{-/-}$ wounds when compared with *ANGPTL4*$^{+/+}$ wounds (Figure 2A). No difference in wound contraction was observed (Figure 2B). The length, thickness, and area of the epithelial tongue were reduced in *ANGPTL4*$^{-/-}$ wounds at days 3–5 postinjury (Figure 2, C–E). The *ANGPTL4*$^{+/+}$ wounds were completely reepithelialized by day 7, in contrast to *ANGPTL4*$^{-/-}$ wounds (Figure 2, A and F). The topical application of recombinant ANGPTL4 onto *ANGPTL4*$^{-/-}$ wounds resulted in complete reepithelialization at day 7 postapplication, in contrast to untreated *ANGPTL4*$^{-/-}$ wounds (Figure 2A). To eliminate a potential systemic effect of ANGPTL4 on wound closure, we examined the effect of topically applied anti-cANGPTL4 antibody on wound reepithelialization. We reasoned that the antibody might interfere with the action of ANGPTL4, and thus recapitulate *ANGPTL4*$^{-/-}$ wounds. Our analysis revealed impaired reepithelialization, reduced length and thickness of the epithelial tongue in wounds treated with anti-cANGPTL4 as compared to preimmune IgG-treated wounds (Supplemental Figure 2, A and B at *http://ajp.amjpathol.org*). No significant difference in wound contraction was observed (Supplemental Figure 2A at *http://ajp.amjpathol.org*). Images of serial sections encompassing complete wounds at days 3–10 postinjury showed that the impaired reepithelialization of the epidermis was not a local random alteration; rather it was distributed over the entire healing wound edge. Altogether, these results indicate ANGPTL4 is important for efficient wound healing.

ANGPTL4 *Deficiency Impairs Cell Adhesion and Migration*

To better understand the role of ANGPTL4, we examined the effect of ANGPTL4 on cell adhesion and migration using primary human keratinocytes. We suppressed endogenous *ANGPTL4* expression by RNA interference. Keratinocytes were either transduced with a lentivirus-mediated *ANGPTL4* siRNA (Figure 3A) or transiently transfected with ON-TARGETplus SMARTpool siRNAs (Supplemental Figure 2C at *http://ajp.amjpathol.org*). Lentivirus-mediated control scrambled siRNA and siGLO siRNA served as corresponding controls. The *ANGPTL4* expression level in *ANGPTL4*-knockdown keratinocytes ($K_{ANGPTL4}$) was reduced by 90% compared with control-siRNA keratinocytes (K_{CTRL}) (Figure 3A). The induction of interferon responses has been reported as a challenge to the specificity of some RNA interference approaches.[30] Therefore, we measured the expression of key interferon response genes by qPCR, which showed no induction in $K_{ANGPTL4}$ when compared with either wild-type nontransduced cells or K_{CTRL} (Figure 3B), suggesting no off-target effect. $K_{ANGPTL4}$ did not undergo spontaneous apoptosis in standard growth conditions, as determined by FACS analysis (Figure 3C). Next, we performed a cell adhesion assay on K_{CTRL} using serum-free medium. The results showed that cells attached more rapidly onto ANGPTL4-coated surfaces compared to control uncoated surfaces. The attachment rate was delayed in the presence of anti-cANGPTL4 antibody compared with preimmune IgG (Figure 3D), suggesting that ANGPTL4 facilitated cell attachment. *ANGPTL4*$^{-/-}$ mouse primary keratinocytes adhered poorly to the culture surface and underwent apoptosis, so we were unable to culture sufficient cells for experiments.

We examined the impact of ANGPTL4 on keratinocyte migration. In an *in vitro* scratch-wound assay, K_{CTRL} closed the wound by 6 hours, whereas $K_{ANGPTL4}$ took 18 hours, indicating impaired keratinocyte migration (K_{CTRL} vs. $K_{ANGPTL4}$:11.92 $\pm$ 0.31 vs. 6.66 $\pm$ 0.12 μm/h, $P < 0.05$) (Figure 4A). Similar observations were also made in transiently siRNA-transfected keratinocytes (5.87 $\pm$ 0.15 μm/h), indicating that the impaired migration was not due to an adaptation to the reduced ANGPTL4 level (Figure 4A). Similar experiments in the presence of mitomycin C showed that K_{CTRL} closed the wound by 8 hours, whereas $K_{ANGPLT4}$ and siRNA-transfected keratinocytes failed to close the wound even after 24 hours (Figure 4A). Importantly, the application of recombinant ANGPTL4 rescued the impaired migration of $K_{ANGPTL4}$ (12.03 $\pm$ 0.42 μm/h), regardless of mitomycin C treatment (9.24 $\pm$ 0.37 μm/h) (Figure 4A). Conversely, the presence of anti-cANGPTL4 antibody delayed K_{CTRL} migration (preimmune versus anti-cANGPTL4: 13.09 $\pm$ 0.23 vs. 6.80 $\pm$ 0.17 μm/h) (Supplemental Figure 2D at *http://ajp.amjpathol.org*). $K_{ANGPTL4}$ or anti-cANGPTL4-treated K_{CTRL} did not display pronounced lamellipodia at the leading edge of migrating cells (Figure 4B).

ANGPTL4 Interacts with Integrin β1 and β5

How ANGPTL4 mediates its action remains a central question in our understanding of ANGPTL4 in cell migration. Cell migration is an integrin-dependent process, and ANGPTL3, a close relative of ANGPTL4, binds to integrin $\alpha v\beta 3$.[31] This prompted us to inquire whether ANGPTL4

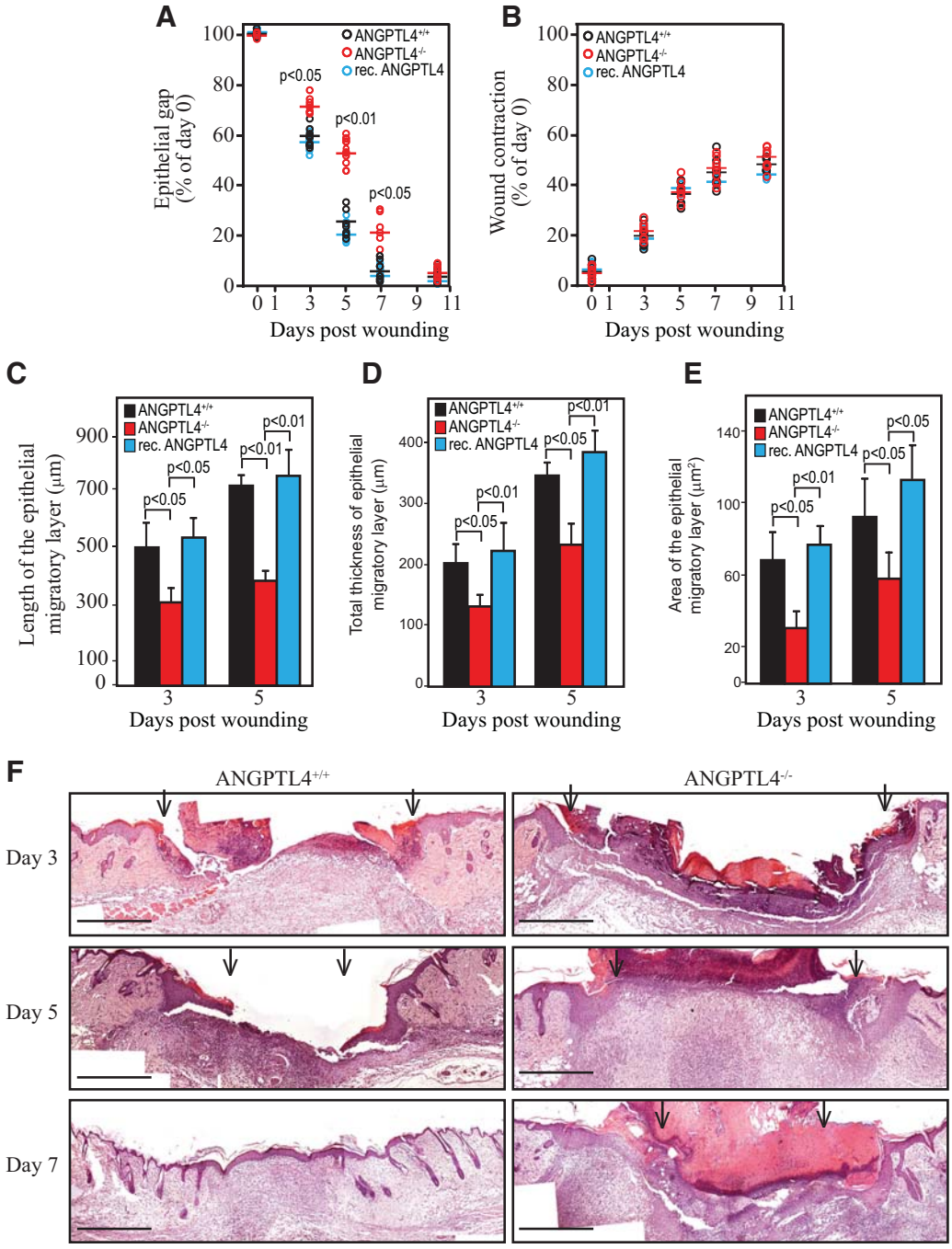

Figure 2. ANGPTL4 is important for efficient wound reepithelialization. Quantification of (**A**) epithelial gap, (**B**) wound contraction, (**C**) length, (**D**) thickness, and (**E**) area of wound epithelia in *ANGPTL4*$^{+/+}$, *ANGPTL4*$^{-/-}$, and recombinant ANGPTL4-treated *ANGPTL4*$^{-/-}$ wounds (rec. ANGPTL4). Each circle shows the mean values of 10 centrally dissected sections obtained from individual mouse; horizontal bars show average values obtained for each genotype or treatment. Values in **C** to **D** were mean of **left** and **right** wound epithelia measured using day-3 and day-5 wound biopsies from 10 mice. Epithelial gap and wound contraction are defined as the distance between the advancing edges of clear multiple layer neoepidermis and between the first hair follicle on both of the wound edge, respectively. The length of the wound epidermis measured from the first hair follicle to the tip of the wound epithelial tongue is used as an indicator of keratinocyte migration. **F:** Hematoxylin and eosin (H&E) pictures of postinjury wound edges from *ANGPTL4*$^{+/+}$ and *ANGPTL4*$^{-/-}$ mice. Scale bar = 500 μm. **Arrows** point to the epithelial wound edge. Representative pictures of centrally dissected wound sections are shown.

interacts with integrins, particularly integrins β1 and β5, which are essential for keratinocyte migration and whose expression is increased during wound healing.[32] We first bacterially expressed and purified the various domains of ANGPTL4 (Supplemental Figure 1B at *http://ajp.amjpathol.org*). Next, we ectopically expressed and purified human integrins β1, β3, and β5 in *Drosophila* S2 cells cultured in serum-free medium (Supplemental Figure 3A at *http://ajp.amjpathol.org*). Membrane extract enriched in either integrin β1, β3, or β5 was used for interaction studies with cANGPTL4 by surface plasmon resonance. Integrins β1 and β5, but not β3, interacted with cANG-

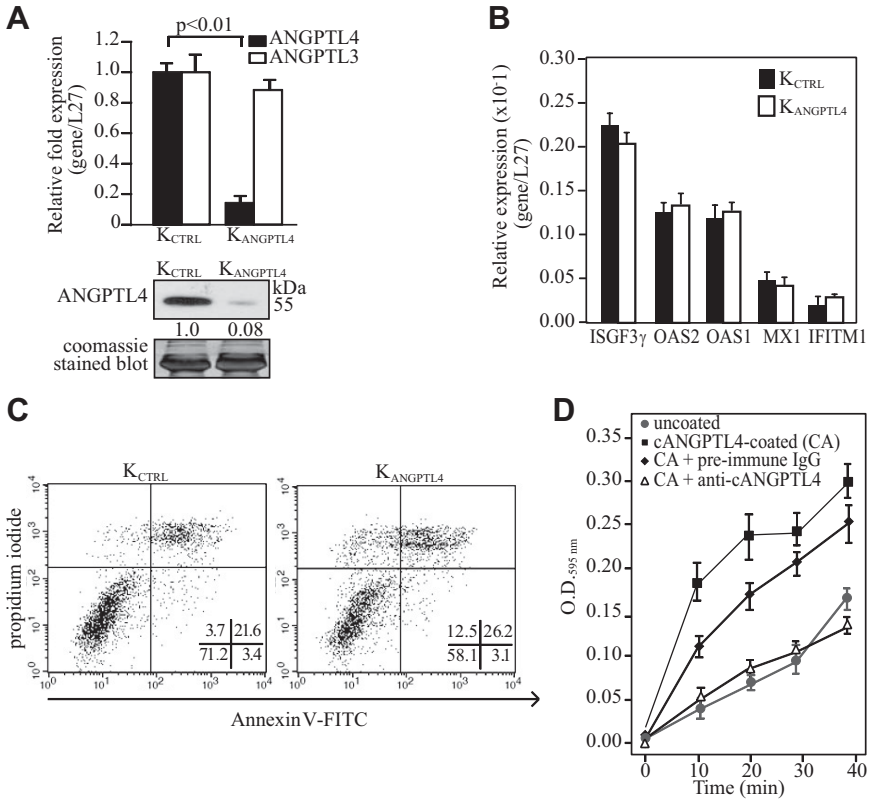

Figure 3. ANGPTL4 is important for cell adhesion. **A:** mRNA and/or protein levels of ANGPTL4 and ANGPTL3 in keratinocytes transduced with either control (K_{CTRL}) or *ANGPTL4* siRNA ($K_{ANGPTL4}$). Values below each band represent the mean fold differences in protein expression level compared with control from five independent experiments. Coomassie-stained blot showed equal loading. **B:** qPCR of interferon response genes in $K_{ANGPTL4}$ compared with K_{CTRL}. 2′,5′-oligoadenylate synthetase isoforms 1 and 2 (OAS1 and OAS2), interferon-induced myxovirus resistance 1 (MX1), interferon-inducible *trans*-membrane protein (IFITM), and interferon-stimulated transcription factor 3γ (ISGF3γ). Ribosomal protein L27 was used as a normalizing reference gene. **C:** FACS analysis of K_{CTRL} and $K_{ANGPTL4}$ stained with annexin V-FITC/PI. The percentage of apoptotic cells (**lower right** quadrant) is indicated in bold. **D:** Cell adhesion of K_{CTRL} onto cANGPTL4-coated surface in the presence of either preimmune IgG or anti-cANGPTL4.

PTL4 with K_D of $\sim 10^{-8}$ mol/L (Figure 5A). The interaction between ANGPTL4 and integrin β1 or β5 was specific, as it was reciprocally blocked with neutralizing antibodies raised against either integrins (α5β1 or αvβ5), or cANGTPL4 (Figure 5B-D). Thus, ANGPTL4 can directly interact with specific integrins, in the absence of cognate matrix proteins. We further confirmed this interaction by ELISA (Figure 5, E and F). *In situ* PLA performed using various antibody pairs on K_{CTRL} and day-5 wound sections confirmed that cANGPTL4 interacted with integrins β1 and β5 *in vivo* (Figure 5G). The PLA signal from each detected interacting protein pair is visualized as an individual red dot.[33] Double immunostaining performed using anti-vinculin and anti-cANGPTL4 on K_{CTRL} of an *"in vitro"* scratch wound revealed strong ANGPTL4 expression near focal contact regions, which was further confirmed using PLA (ANGPTL4 & integrin β1) and immunofluorescence (vinculin), underscoring the role of ANGPTL4 in keratinocyte migration (Supplemental Figure 3B at *http://ajp.amjpathol.org*). Immunoblot analysis of anti-cANGPTL4 and specific anti-integrin immunoprecipitates of *ANGPTL4*$^{+/+}$ and *ANGPTL4*$^{-/-}$ wound biopsy homogenates showed that the integrin β1 and β5 were present, as well as α3, α5, and αv subunits (Figure 5H, and Supplemental Figure 3C at *http://ajp.amjpathol.org*). Interaction of integrin β1 and β5 with ANGPTL4 did not compete with the binding of integrins to their natural cognate ligands, but rather they appeared to strengthen the integrin–matrix interactions. Consistent with the above findings, integrin β3 was not detected in anti-cANGPTL4 immunoprecipitates. Next, we performed cell adhesion assays and *in vitro* wound assays on fibronectin- and vitronectin-coated surfaces. The results showed that $K_{ANGPTL4}$ adhered more slowly to both coated surfaces than K_{CTRL} (Supplemental Figure 3, D and E at *http://ajp.amjpathol.org*). Cell migration assays were also performed on coated surfaces using K_{CTRL} and $K_{ANGPTL4}$ treated with mitomycin C, to exclude any effects of proliferation (Supplemental Figure 3F at *http://ajp.amjpathol.org*). The repopulation of the *in vitro* wound by K_{CTRL} and $K_{ANGPTL4}$ was faster on both matrix protein-coated surfaces compared with the cognate controls on uncoated surface (K_{CTRL} on coated versus uncoated: 6 hours vs. 8 hours; $K_{ANGPTL4}$ on coated versus uncoated: 19 hours vs. ≥24 hours). Notably, the application of recombinant ANGPTL4 accelerated the migration and closure of the *in vitro* wound by $K_{ANGPTL4}$ (compare Figure 4A and Supplemental Figure 3F at *http://ajp.amjpathol.org*). Taken together, these data indicate that integrins β1 and β5, but not β3, are novel interacting protein partners of ANGPTL4. This interaction aided cell migration.

ANGPTL4 Modulates Integrin-Mediated Signaling and Internalization

To gain insight into the intracellular signaling pathway, we performed *in vivo* coimmunoprecipitation using either anti-cANGPTL4 or anti-integrin β1 antibodies, followed by immunodetection of specific mediators of integrin-mediated signaling. ANGPTL4 bound to integrin β1 recruited more FAK-Src complex with more active Rac1-GTP and phosphorylated PAK1 in the membrane fraction of *ANGPTL4*$^{+/+}$ and ANGPTL4-treated *ANGPTL4*$^{-/-}$

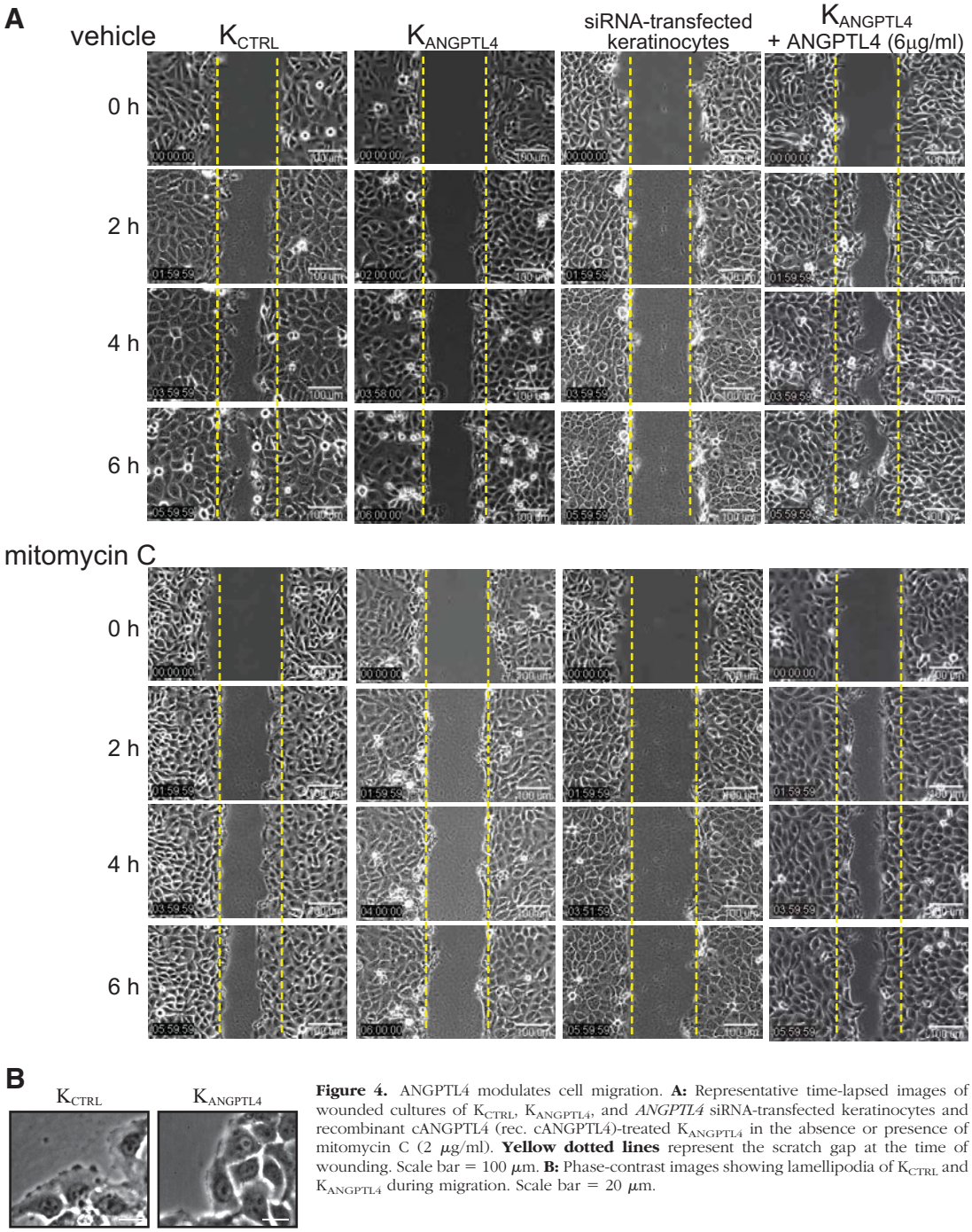

Figure 4. ANGPTL4 modulates cell migration. **A:** Representative time-lapsed images of wounded cultures of K_{CTRL}, $K_{ANGPTL4}$, and *ANGPTL4* siRNA-transfected keratinocytes and recombinant cANGPTL4 (rec. cANGPTL4)-treated $K_{ANGPTL4}$ in the absence or presence of mitomycin C (2 μg/ml). **Yellow dotted lines** represent the scratch gap at the time of wounding. Scale bar = 100 μm. **B:** Phase-contrast images showing lamellipodia of K_{CTRL} and $K_{ANGPTL4}$ during migration. Scale bar = 20 μm.

wounds than their cognate controls (Figure 6, A and B). We detected cytoplasmic ERK, which does not interact directly with integrin, only in the supernatant of the immunoprecipitates, indicating the specificity of the affinity coimmunoprecipitation (Figure 6, A and B). Neither integrin β1 nor ANGPTL4 was immunoprecipitated with preimmune IgG (Supplemental Figure 4A at *http://ajp.amjpathol.org*). Similar observations were also made in K_{CTRL} (Supplemental Figure 4, B and C at *http://ajp.amjpathol.org*), confirming that ANGPTL4 potentiates integrin-mediated signaling. Integrin recycling contributes to the motility of rapidly migrating cells and permits constant monitoring of the wound cellular environment.[34] We observed a selective internalization of cell-surface biotin-labeled integrins β1 and β5, but not integrin β3. Importantly, the rapid internalization of integrins β1 and β5 was reduced in ANGPTL4 deficiency (Figure 6C). The internalization of integrin β3 was similar under all examined conditions (Figure 6C). These observations were further corroborated by FACS analysis of the cell-surface expression of integrins (Figure 6D and Supplemental Figure 4D at *http://ajp.amjpathol.org*). Similar results were also observed in K_{CTRL} treated with anti-cANGPTL4 antibody (Supplemental Figure 4E at *http://ajp.amjpathol.org*).

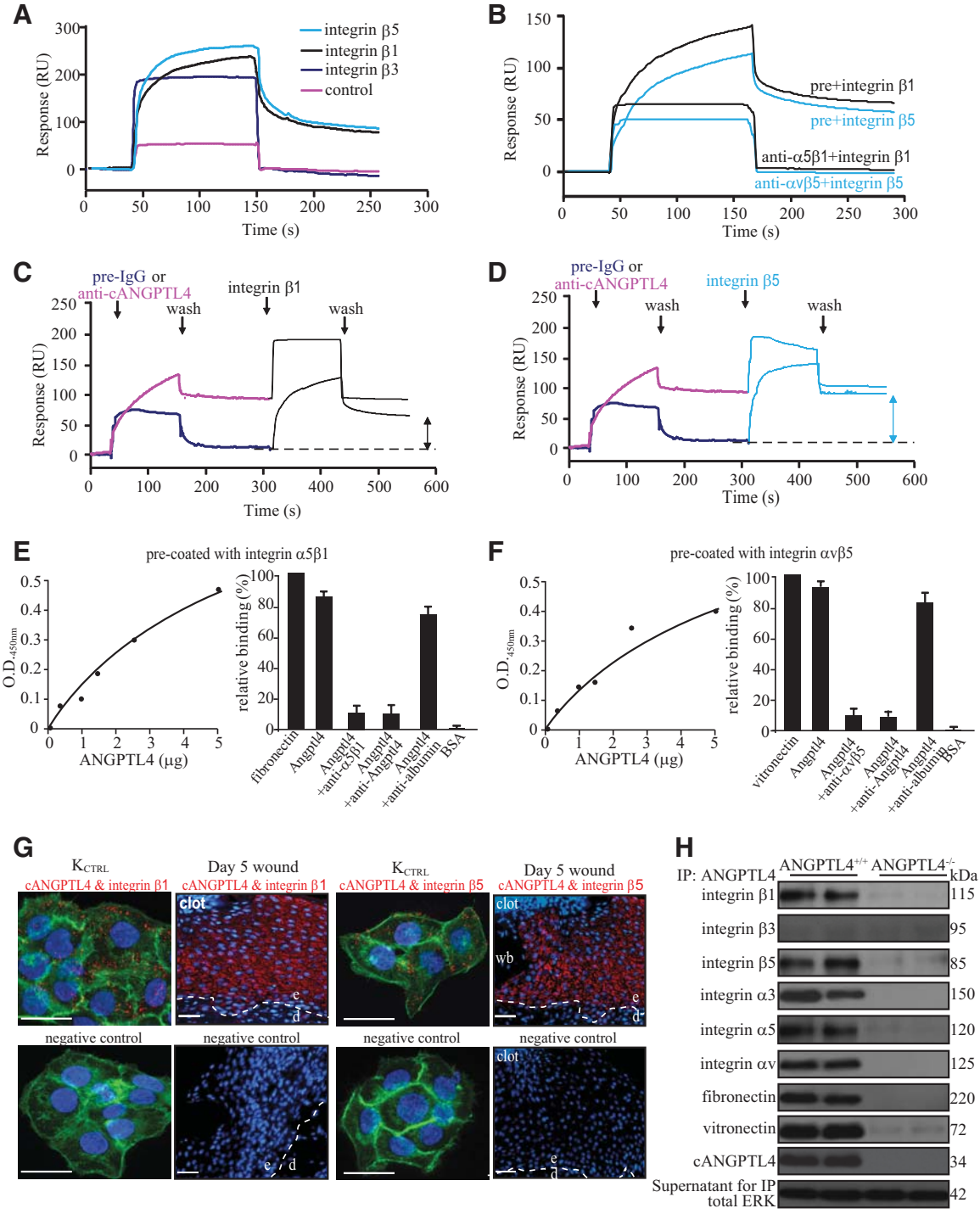

Figure 5. ANGPTL4 interacts with integrins $\beta 1$ and $\beta 5$. Representative sensorgrams showing binding profiles between immobilized cANGPTL4 and (**A**) S2-membrane extracts containing either control, integrin $\beta 1$, $\beta 3$, or $\beta 5$, or (**B**) integrin $\beta 1$ or $\beta 5$ preincubated with either preimmune IgG (pre) or cognate anti-integrin antibody. Integrin $\beta 1$ (**C**) or integrin $\beta 5$ (**D**) after preblocked with either preimmune IgG or anti-cANGPTL4 antibody. Each sensorgram was corrected by subtracting a sensorgram obtained from a reference flow cell with no immobilized protein. Anti-cANGPTL4 antibodies against the immobilized cANGPTL4 determined the Rmax value to be 138.2 resonance units (RU). Five independent experiments were performed. Dose-dependent ANGPTL4 binding to immobilized (**E**) integrin $\alpha 5\beta 1$ or (**F**) integrin $\alpha v\beta 5$, which was specifically blocked by anti-cANGPTL4, as determined by ELISA. Detection of (**G**) the ANGPTL4-integrin $\beta 1$ (**left panel**) and ANGPTL4-integrin $\beta 5$ (**right panel**) complexes in K_{CTRL} and in day-5 *ANGPTL4*$^{+/+}$ wound biopsies using DUOlink PLA. PLA signals (red) and Hoechst dye for nuclei (blue). For K_{CTRL}, the cells were counterstained with Alexa 488-phallodin for actin stress fibers. The nuclear image was acquired in one *z*-plane using a LSM510 META confocal laser-scanning microscope (Carl Zeiss). **Dotted white line** represents epidermal-dermal junction. Negative control was performed without primary antibodies. Representative pictures from wound sections with epidermis (e), dermis (d), wound bed (wb), and K_{CTRL} from six independent experiments or sections from three mice are shown. Scale bar = 40 μm. **H:** Immunodetection of indicated proteins from anti-cANGPTL4 immunoprecipitates of *ANGPTL4*$^{+/+}$ and *ANGPTL4*$^{-/-}$ wound biopsy homogenates. Total ERK from supernatant were used to verify equal loading.

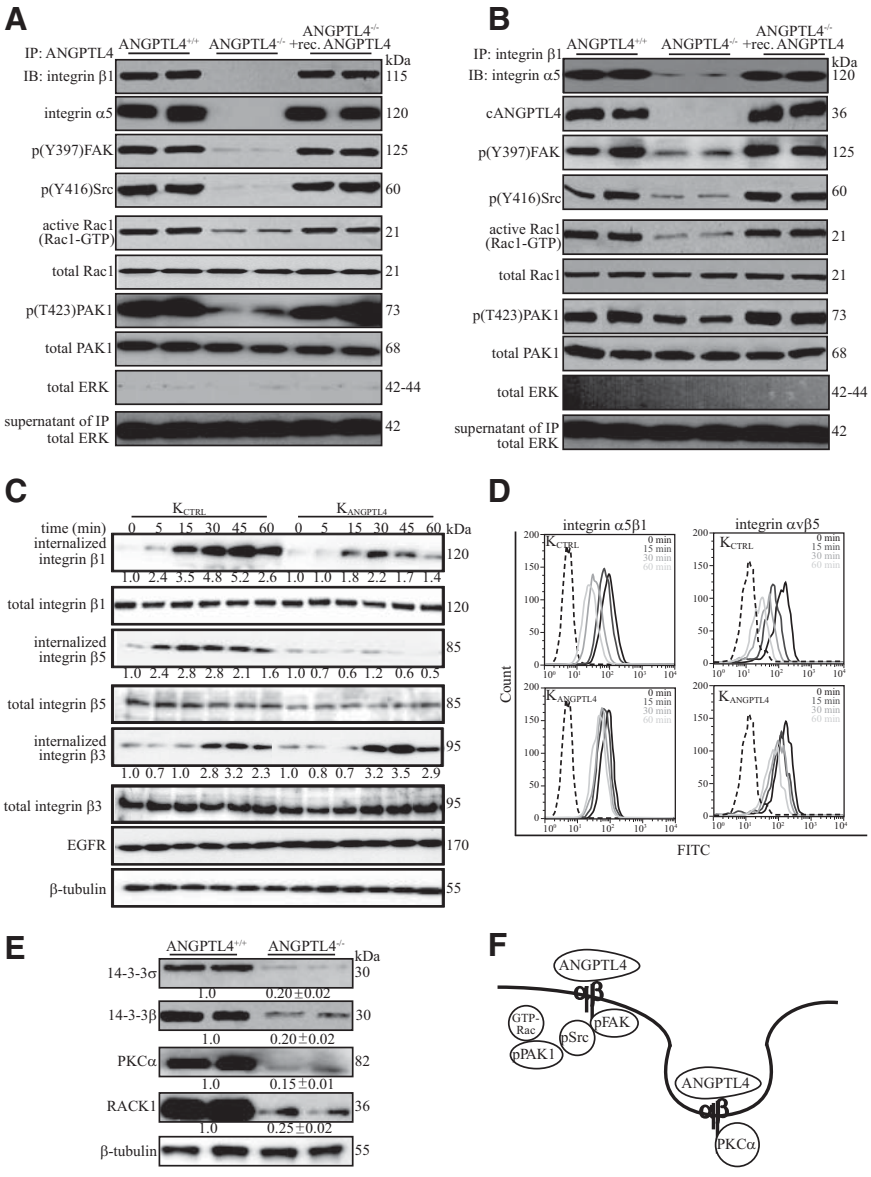

Figure 6. ANGPTL4 modulates integrin-mediated signaling and internalization. Immunodetection of indicated proteins in (**A**) anti-cANGPTL4 or (**B**) anti-integrin β1 immunoprecipitates (**top panel**); of Rac1-GTP and phosphorylated PAK1 (p(T423)PAK1) (**lower panels**) from membrane extract of indicated wound biopsies. Total PAK from total cell lysate were used to verify equal loading. Specificity of immunoprecipitation was verified by immunodetection of ERK in the immunoprecipitates and its supernatant. **C:** Kinetics of integrin internalization. Internalized biotinylated-integrins were detected using corresponding antibodies after immunoprecipitation with NeutrAvidin agarose resins. The level of total integrins β1, β3, and β5 were determined using total cell lysate before immunoprecipitation. EGFR and β-tubulin from total cell lysate were used to verify equal loading. Values denote mean fold change of three independent experiments compared to K_{CTRL} at time 0. **D:** Cell-surface expression of the integrins α5β1 and αvβ5 in K_{CTRL} and $K_{ANGPTL4}$ at the indicated time was determined by FACS. The negative control (only secondary antibody) is indicated by the dotted graph. **E:** Immunoblot analysis of membrane extracts from day-5 *ANGPTL4*$^{+/+}$ and *ANGPTL4*$^{-/-}$ wound biopsies for indicated proteins. Values below the band represent the mean fold differences in protein expression levels relative to *ANGPTL4*$^{+/+}$ from eight wound biopsies for each genotype. β-tubulin was used as loading and transfer control. **F:** Schematic illustration showing ANGPTL4 interacting with integrin, activating FAK-Src-PAK1 signaling and facilitating integrin internalization, which involves PKCα and 14-3-3σ/β, to aid cell migration.

Integrins β1 and β5 are internalized with the aid of adaptor protein 14-3-3σ and PKCα, which binds directly to integrin cytoplasmic tails.[35,36] Prompted by our above observations, we examined the membrane expression of these proteins in ANGPTL4-deficient keratinocytes and wound biopsies. Immunodetection showed that the expression of 14-3-3σ, β and PKCα was significantly reduced in *ANGPTL4*$^{-/-}$ wound biopsies when compared with their cognate controls (Figure 6E). Besides reduced expression of 14-3-3σ, β and PKCα, the *ANGPTL4*$^{-/-}$ wounds also exhibited decreased expression of RACK1,[37] indicating attenuated PKC-mediated signal transduction (Figure 6E). Similar findings were obtained in keratinocytes transiently transfected with *ANGPTL4*-siRNA, suggesting that the reduced levels of total signaling proteins observed is not an adaptation to the reduction in ANGPTL4 level (Supplemental Figure 4F at *http://ajp.amjpathol.org*). To examine whether ANGPTL4 has a direct effect on the expression of these signaling proteins, we examined their mRNA levels in $K_{ANGPTL4}$ treated with recombinant ANGPTL4 in the presence of either actinomycin D or cycloheximide. The increased mRNA levels of 14-3-3σ, β, and PKCα induced by ANGPTL4 was abolished in actinomycin D– but not cycloheximide-treated cells, suggesting a transcriptional regulatory mechanism (Supplemental Figure 4G at *http://ajp.amjpathol.org*). Thus, our results show that more activated FAK-Src complexes were formed when ANGPTL4 was bound to integrin β1, indicating that ANGPTL4 mediates its action at least partially via the FAK-Src-PAK1 axis. ANGPTL4 deficiency dysregulated 14-3-3σ and its effector PKCα expression, which would influence integrin internalization and thus keratinocyte migration. Altogether, our results reveal a novel function of ANGPTL4 in promoting keratinocyte migration during wound healing by activating integrin-mediated signaling and internalization.

Discussion

Wound healing is a complex process that involves a cascade of overlapping events, including inflammation, reepithelialization, and remodeling, all directed at the restoration of the epidermal barrier. Throughout the healing process, cellular interactions with ECM components coordinate the individual events, enabling temporal and spatial control. Reepithelialization is accomplished by increased keratinocyte proliferation and guided migration of the keratinocytes over the wound ECM. This process requires orderly changes in keratinocyte behavior and phenotype in which integrin-mediated signaling plays a crucial role. We reveal a newly discovered role of ANGPTL4 in cell migration via direct interaction with integrin β1 and β5 to modulate integrin-mediated FAK-Src-PAK1 signaling and internalization (Figure 6F).

Adipocytokines secreted by adipose tissue play important roles in energy homeostasis.[38] Emerging evidence points to additional nonmetabolic roles, such as wound healing, of some adipocytokines. We show that the expression of the adipocytokine ANGPTL4, while only weakly detectable in normal intact skin, was markedly elevated during the reepithelialization phase of wound healing. ANGPTL4 deficiency had a dramatic impact on cell migration *in vitro* and *in vivo*. Thus, in addition to its well-established role in energy homeostasis, we revealed an unsuspected role of ANGPTL4 as a matricellular protein in wound repair. Multiple functions of other matricellular proteins have been described, including SPARC, which is implicated in adipose tissue hyperplasia and adipogenesis.[39] ANGPTL4 undergoes proteolytic cleavage after secretion, to release the N-terminal coiled-coil domain (nANGPTL4) and a C-terminal fibrinogen-like domain (cANGPTL4). nANGPTL4 binds lipoprotein lipase and inhibits its activity,[20] but little is known about the role of cANGPTL4. Therefore, how ANGPTL4 triggers intracellular signaling to propagate its effect remains a central question in relation to its functions. Although ANGPTL4 is related to angiopoietins, it does not bind to the Tie receptors.[40] Using various methods, we identify integrin β1 and β5, but not β3, as novel interacting protein partners of ANGPTL4. We further show that the fibrinogen-like domain of ANGPTL4 associates with heterodimeric integrins, via the β1/β5 subunits and modulates integrin-mediated signaling, revealing crucial insight into its mechanism of action. This interaction modulates the FAK-Src-PAK1 signaling cascade, which is essential for keratinocyte migration.[2]

Integrins on cell surface are well suited to function as biosensors to constantly monitor changes in the wound microenvironment. They consist of α and β subunits that associate in various combinations to form at least 25 receptors. Each $\alpha\beta$ combination possesses specific binding and signaling properties. During wound healing, migrating keratinocytes enlarge their integrin repertoire concomitantly with changes in the extracellular matrix composition, suggesting a close interplay of these two groups of molecules during reepithelialization. ANGPTL4 interacts with the β subunits of $\alpha5\beta1$, $\alpha v\beta5$, and $\alpha3\beta1$ to enhance integrin-mediated signalings, integrin internalization, and keratinocyte migration. Consistent with the role of $\alpha5\beta1$and $\alpha v\beta5$ in facilitating cell migration and adhesion, their expression was increased in wound keratinocytes and their deficiencies have been associated with impaired cell migration, adhesion, or wound healing.[32,41,42] The role of integrin $\alpha3\beta1$ in cell migration is controversial,[43] depending on the complex of the various matrices present at the wound bed and, more importantly, on the context in which the intact matrix protein is presented to the cells. Small soluble matrix protein fragments generated by the action of proteases during reepithelialization can compete with substrate-anchored matrix proteins for integrin and impair cell migration.[44,45] We also showed that ANGPTL4 binding to specific integrins does not interfere with the association of integrins and their cognate matrix ligands. Although not studied herein, it is tempting to speculate that ANGPTL4 may also interact with specific matrix proteins and form a ternary complex with its cognate integrin receptor to further fine-tune cell-matrix communication which is crucial for cell migration.

During wound healing, migrating cells must display appropriate cellular behavior in response to the changing wound environment to enable effective wound closure. Interestingly, the deficiency in ANGPTL4 resulted in decreased expression of 14-3-3σ, β and PKCα, which also modulates cell migration via integrin internalization. The underlying mechanism by which ANGPTL4 regulates their expression remains to be determined. Thus, ANGPTL4 is a novel matricellular protein that modulates keratinocyte migration on at least two fronts. First, ANGPTL4 potentiates integrin-mediated signaling to facilitate cell migration. ANGPTL4 binding to specific integrins does not interfere with the association of integrins and their cognate matrix ligands. Second, ANGPTL4-bound integrins provide a novel means by which selective integrin signaling cascades can be activated, depending on the local context of the ECM. ANGPTL4 regulates 14-3-3σ and its effector PKCα expression, which would influence integrin internalization. This allows migrating wound keratinocytes to better scrutinize the changes in the wound ECM and fine-tune their cellular behavior.

Metastasis and wound repair share numerous characteristics during cell migration, so it is not surprising that ANGPTL4 has been implicated in cancer metastasis. Previous studies have reported that ANGPTL4 prevents metastasis by inhibiting vascular leakiness.[46,47] In contrast, recent work has revealed that one of the genes most highly associated with breast cancer metastasis to lung is *ANGPTL4*.[18] Tumor-derived ANGPTL4 was proposed to disrupt endothelial cell–cell contacts to aid the extravasation and metastasis of tumor cells.[48] Therefore, whether ANGPTL4 promotes or inhibits vascular leakiness and thus cancer metastasis remains controversial. Although this question is not directly addressed in this study, our data clearly showed that ANGPTL4 binds to integrin β1, and it has been shown that neutralizing antibody against integrin $\alpha5\beta1$ increases paracellular endothelial permeability.[49] Altogether, our finding that ANGPTL4 interacts with integrins β1 and β5 to modulate integrin-FAK-Src-PAK1 signaling and integrin internaliza-

tion provides valuable mechanistic insight into its roles in cancer metastasis.

Acknowledgments

We thank Dr. Samuel Ko and Anna Teo (Carl Zeiss, Singapore Pte Ltd.) for their expertise in image acquisition using LSM710 confocal microscope and MIRAX MIDI.

References

1. Hynes RO: Integrins: bidirectional, allosteric signaling machines. Cell 2002, 110:673–687
2. Schlaepfer DD, Mitra SK: Multiple connections link FAK to cell motility and invasion. Curr Opin Genet Dev 2004, 14:92–101
3. Mercurio AM, Rabinovitz I, Shaw LM: The alpha 6 beta 4 integrin and epithelial cell migration. Curr Opin Cell Biol 2001, 13:541–545
4. Dans M, Gagnoux-Palacios L, Blaikie P, Klein S, Mariotti A, Giancotti FG: Tyrosine phosphorylation of the beta 4 integrin cytoplasmic domain mediates Shc signaling to extracellular signal-regulated kinase and antagonizes formation of hemidesmosomes. J Biol Chem 2001, 276:1494–1502
5. Shaw LM, Rabinovitz I, Wang HH, Toker A, Mercurio AM: Activation of phosphoinositide 3-OH kinase by the alpha6beta4 integrin promotes carcinoma invasion. Cell 1997, 91:949–960
6. Fu H, Subramanian RR, Masters SC: 14-3-3 proteins: structure, function, and regulation. Annu Rev Pharmacol Toxicol 2000, 40:617–647
7. Dellambra E, Patrone M, Sparatore B, Negri A, Ceciliani F, Bondanza S, Molina F, Cancedda FD, De Luca M: Stratifin, a keratinocyte specific 14-3-3 protein, harbors a pleckstrin homology (PH) domain and enhances protein kinase C activity. J Cell Sci 1995, 108 (Pt 11):3569–3579
8. Bornstein P, Sage EH: Matricellular proteins: extracellular modulators of cell function. Curr Opin Cell Biol 2002, 14:608–616
9. Midwood KS, Williams LV, Schwarzbauer JE: Tissue repair and the dynamics of the extracellular matrix. Int J Biochem Cell Biol 2004, 36:1031–1037
10. Caswell PT, Norman JC: Integrin trafficking and the control of cell migration. Traffic 2006, 7:14–21
11. Caswell P, Norman J: Endocytic transport of integrins during cell migration and invasion. Trends Cell Biol 2008, 18:257–263
12. Frank S, Stallmeyer B, Kämpfer H, Kolb N, Pfeilschifter J: Leptin enhances wound re-epithelialization and constitutes a direct function of leptin in skin repair. J Clin Invest 2000, 106:501–509
13. Shimomura I, Funahashi T, Takahashi M, Maeda K, Kotani K, Nakamura T, Yamashita S, Miura M, Fukuda Y, Takemura K, Tokunaga K, Matsuzawa Y: Enhanced expression of PAI-1 in visceral fat: possible contributor to vascular disease in obesity. Nat Med 1996, 2:800–803
14. Oike Y, Akao M, Kubota Y, Suda T: Angiopoietin-like proteins: potential new targets for metabolic syndrome therapy. Trends Mol Med 2005, 11:473–479
15. Mandard S, Zandbergen F, Tan NS, Escher P, Patsouris D, Koenig W, Kleemann R, Bakker A, Veenman F, Wahli W, Müller M, Kersten S: The direct peroxisome proliferator-activated receptor target fasting-induced adipose factor (FIAF/PGAR/ANGPTL4) is present in blood plasma as a truncated protein that is increased by fenofibrate treatment. J Biol Chem 2004, 279:34411–34420
16. Belanger AJ, Lu H, Date T, Liu LX, Vincent KA, Akita GY, Cheng SH, Gregory RJ, Jiang C: Hypoxia up-regulates expression of peroxisome proliferator-activated receptor gamma angiopoietin-related gene (PGAR) in cardiomyocytes: role of hypoxia inducible factor 1alpha. J Mol Cell Cardiol 2002, 34:765–774
17. Xu A, Lam MC, Chan KW, Wang Y, Zhang J, Hoo RLC, Xu JY, Chen B, Chow WS, Tso AWK, Lam KSL: Angiopoietin-like protein 4 decreases blood glucose and improves glucose tolerance but induces hyperlipidemia and hepatic steatosis in mice. Proc Natl Acad Sci USA 2005, 102:6086–6091
18. Minn AJ, Gupta GP, Siegel PM, Bos PD, Shu W, Giri DD, Viale A, Olshen AB, Gerald WL, Massagué J: Genes that mediate breast cancer metastasis to lung. Nature 2005, 436:518–524
19. Bäckhed F, Crawford PA, O'Donnell D, Gordon JI: Postnatal lymphatic partitioning from the blood vasculature in the small intestine requires fasting-induced adipose factor. Proc Natl Acad Sci USA 2007, 104:606–611
20. Sukonina V, Lookene A, Olivecrona T, Olivecrona G: Angiopoietin-like protein 4 converts lipoprotein lipase to inactive monomers and modulates lipase activity in adipose tissue. Proc Natl Acad Sci USA 2006, 103:17450–17455
21. Yang YH, Wang Y, Lam KSL, Yau MH, Cheng KKY, Zhang J, Zhu W, Wu D, Xu A: Suppression of the Raf/MEK/ERK signaling cascade and inhibition of angiogenesis by the carboxyl terminus of angiopoietin-like protein 4. Arterioscler Thromb Vasc Biol 2008, 28:835–840
22. Chong HC, Tan MJ, Philippe V, Tan SH, Tan CK, Ku CW, Goh YY, Wahli W, Michalik L, Tan NS: Regulation of epithelial-mesenchymal IL-1 signaling by PPARbeta/delta is essential for skin homeostasis and wound healing. J Cell Biol 2009, 184:817–831
23. Köster A, Chao YB, Mosior M, Ford A, Gonzalez-DeWhitt PA, Hale JE, Li D, Qiu Y, Fraser CC, Yang DD, Heuer JG, Jaskunas SR, Eacho P: Transgenic angiopoietin-like (angptl)4 overexpression and targeted disruption of angptl4 and angptl3: regulation of triglyceride metabolism. Endocrinology 2005, 146:4943–4950
24. Tan NS, Ho B, Ding JL: High-affinity LPS binding domain(s) in recombinant factor C of a horseshoe crab neutralizes LPS-induced lethality. FASEB J 2000, 14:859–870
25. Tang VW: Proteomic and bioinformatic analysis of epithelial tight junction reveals an unexpected cluster of synaptic molecules. Biol Direct 2006, 1:37
26. Tan SH, Pal M, Tan MJ, Wong MHL, Tam FU, Teo JWT, Chong HC, Tan CK, Goh YY, Tang MBY, Cheung PCF, Tan NS: Regulation of Cell Proliferation and Migration by TAK1 via Transcriptional Control of von Hippel-Lindau Tumor Suppressor. J Biol Chem 2009, 284:18047–18058
27. IJpenberg A, Tan NS, Gelman L, Kersten S, Seydoux J, Xu J, Metzger D, Canaple L, Chambon P, Wahli W, Desvergne B: In vivo activation of PPAR target genes by RXR homodimers. EMBO J 2004, 23:2083–2091
28. Roberts M, Barry S, Woods A, van der Sluijs P, Norman J: PDGF-regulated rab4-dependent recycling of alphavbeta3 integrin from early endosomes is necessary for cell adhesion and spreading. Curr Biol 2001, 11:1392–1402
29. Sterk LM, Geuijen CA, Oomen LC, Calafat J, Janssen H, Sonnenberg A: The tetraspan molecule CD151, a novel constituent of hemidesmosomes, associates with the integrin alpha6beta4 and may regulate the spatial organization of hemidesmosomes. J Cell Biol 2000, 149:969–982
30. Bridge AJ, Pebernard S, Ducraux A, Nicoulaz AL, Iggo R: Induction of an interferon response by RNAi vectors in mammalian cells. Nat Genet 2003, 34:263–264
31. Camenisch G, Pisabarro MT, Sherman D, Kowalski J, Nagel M, Hass P, Xie MH, Gurney A, Bodary S, Liang XH, Clark K, Beresini M, Ferrara N, Gerber HP: ANGPTL3 stimulates endothelial cell adhesion and migration via integrin alpha vbeta 3 and induces blood vessel formation in vivo. J Biol Chem 2002, 277:17281–17290
32. Grose R, Hutter C, Bloch W, Thorey I, Watt FM, Fässler R, Brakebusch C, Werner S: A crucial role of beta 1 integrins for keratinocyte migration in vitro and during cutaneous wound repair. Development 2002, 129:2303–2315
33. Söderberg O, Leuchowius KJ, Gullberg M, Jarvius M, Weibrecht I, Larsson LG, Landegren U: Characterizing proteins and their interactions in cells and tissues using the in situ proximity ligation assay. Methods 2008, 45:227–232
34. Jones M, PT, JC: Endocytic recycling pathways: emerging regulators of cell migration. Curr Opin Cell Biol 2006, 18:549–557
35. Han DC, Rodriguez LG, Guan JL: Identification of a novel interaction between integrin beta1 and 14-3-3beta. Oncogene 2001, 20:346–357
36. Ng T, Shima D, Squire A, Bastiaens PI, Gschmeissner S, Humphries MJ, Parker PJ: PKCalpha regulates beta1 integrin-dependent cell motility through association and control of integrin traffic. EMBO J 1999, 18:3909–3923
37. Panetti TS, Wilcox SA, Horzempa C, McKeown-Longo PJ: Alpha v

beta 5 integrin receptor-mediated endocytosis of vitronectin is protein kinase C-dependent. J Biol Chem 1995, 270:18593–18597
38. Bulcão C, Ferreira SRG, Giuffrida FMA, Ribeiro-Filho FF: The new adipose tissue and adipocytokines. Curr Diabetes Rev 2006, 2:19–28
39. Bradshaw AD, Sage EH: SPARC, a matricellular protein that functions in cellular differentiation and tissue response to injury. J Clin Invest 2001, 107:1049–1054
40. Kim I, Kim HG, Kim H, Kim HH, Park SK, Uhm CS, Lee ZH, Koh GY: Hepatic expression, synthesis and secretion of a novel fibrinogen/angiopoietin-related protein that prevents endothelial-cell apoptosis. Biochem J 2000, 346 Pt 3:603–610
41. Bata-Csorgo Z, Cooper KD, Ting KM, Voorhees JJ, Hammerberg C: Fibronectin and alpha5 integrin regulate keratinocyte cell cycling. A mechanism for increased fibronectin potentiation of T cell lymphokine-driven keratinocyte hyperproliferation in psoriasis J Clin Invest 1998, 101:1509–1518
42. Huang X, Griffiths M, Wu J, Farese RV, Sheppard D: Normal development, wound healing, and adenovirus susceptibility in beta5-deficient mice. Mol Cell Biol 2000, 20:755–759
43. Wen T, Zhang Z, Yu Y, Qu H, Koch M, Aumailley M: Integrin alpha3 subunit regulates events linked to epithelial repair, including keratinocyte migration and protein expression. Wound Repair Regen 2010, 18:325–334
44. Giannone G, Sheetz MP: Substrate rigidity and force define form through tyrosine phosphatase and kinase pathways. Trends Cell Biol 2006, 16:213–223
45. Ginsberg MH, Partridge A, Shattil SJ: Integrin regulation. Curr Opin Cell Biol 2005, 17:509–516
46. Ito Y, Oike Y, Yasunaga K, Hamada K, Miyata K, Matsumoto SI, Sugano S, Tanihara H, Masuho Y, Suda T: Inhibition of angiogenesis and vascular leakiness by angiopoietin-related protein 4. Cancer Res 2003, 63:6651–6657
47. Galaup A, Cazes A, Le Jan S, Philippe J, Connault E, Le Coz E, Mekid H, Mir LM, Opolon P, Corvol P, Monnot C, Germain S: Angiopoietin-like 4 prevents metastasis through inhibition of vascular permeability and tumor cell motility and invasiveness. Proc Natl Acad Sci USA 2006, 103:18721–18726
48. Padua D, Zhang XHF, Wang Q, Nadal C, Gerald WL, Gomis RR, Massagué J: TGFbeta primes breast tumors for lung metastasis seeding through angiopoietin-like 4. Cell 2008, 133:66–77
49. Lampugnani MG, Resnati M, Dejana E, Marchisio PC: The role of integrins in the maintenance of endothelial monolayer integrity. J Cell Biol 1991, 112:479–490

3) Goh YY*, Pal M*, Chong HC, **Zhu P**, Tan MJ, Punugu L, Tan CK, Roystan H, Sze SK, Tang MBY, Ding JL, Kersten S, Tan NS. Angiopoietin-like 4 interacts with matrix proteins to modulate wound healing (*J.Biol.Chem. 285:32999-33009*, *Authors contributed equally).

Supplemental Material can be found at:
http://www.jbc.org/content/suppl/2010/09/07/M110.108175.DC1.html

THE JOURNAL OF BIOLOGICAL CHEMISTRY VOL. 285, NO. 43, pp. 32999–33009, October 22, 2010

Angiopoietin-like 4 Interacts with Matrix Proteins to Modulate Wound Healing*[S]

Received for publication, January 26, 2010, and in revised form, July 30, 2010 Published, JBC Papers in Press, August 21, 2010, DOI 10.1074/jbc.M110.108175

Yan Yih Goh[‡1], Mintu Pal[‡1], Han Chung Chong[‡], Pengcheng Zhu[‡], Ming Jie Tan[‡], Lakshmi Punugu[‡], Chek Kun Tan[‡], Royston-Luke Huang[‡], Siu Kwan Sze[‡], Mark Boon Yang Tang[§], Jeak Ling Ding[¶], Sander Kersten[‖], and Nguan Soon Tan[‡2]

From the [‡]School of Biological Sciences, Nanyang Technological University, 60 Nanyang Drive, Singapore 637551, the [§]National Skin Centre, 1 Mandalay Road, Singapore 308205, the [¶]Department of Biological Sciences, National University of Singapore, 14 Science Drive, Singapore 117543, and [‖]Wageningen University, 6700 EV Wageningen, The Netherlands

A dynamic cell-matrix interaction is crucial for a rapid cellular response to changes in the environment. Appropriate cell behavior in response to the changing wound environment is required for efficient wound closure. However, the way in which wound keratinocytes modify the wound environment to coordinate with such cellular responses remains less studied. We demonstrated that angiopoietin-like 4 (ANGPTL4) produced by wound keratinocytes coordinates cell-matrix communication. ANGPTL4 interacts with vitronectin and fibronectin in the wound bed, delaying their proteolytic degradation by metalloproteinases. This interaction does not interfere with integrin-matrix protein recognition and directly affects cell-matrix communication by altering the availability of intact matrix proteins. These interactions stimulate integrin- focal adhesion kinase, 14-3-3, and PKC-mediated signaling pathways essential for effective wound healing. The deficiency of ANGPTL4 in mice delays wound re-epithelialization. Further analysis revealed that cell migration was impaired in the ANGPTL4-deficient keratinocytes. Altogether, the findings provide molecular insight into a novel control of wound healing via ANGPTL4-dependent regulation of cell-matrix communication. Given the known role of ANGPTL4 in glucose and lipid homeostasis, it is a prime therapeutic candidate for the treatment of diabetic wounds. It also underscores the importance of cell-matrix communication during angiogenesis and cancer metastasis.

Skin repair after an injury proceeds via a finely tuned pattern of integrated biological events aimed at restoration of the epithelial barrier. The inflammatory stage of repair is followed by the proliferation and migration of keratinocytes, a process called re-epithelialization (1). These events are regulated spatiotemporally by several classical growth factors and cytokines, the effects of which have been well documented (2). Less studied are extracellular factors such as matricellular proteins and adipocytokines, both shown to have a profound local impact during wound repair (3, 4). Effective directed cell migration requires constant cellular interaction with the extracellular matrix (ECM)[3] in response to the changing wound environment. Although the importance of such cell-matrix communication in wound healing is well recognized, the mechanism that modifies the external wound microenvironment for coordinated keratinocyte behavior remains unclear.

Integrins on the cell surface often function as biosensors to constantly interrogate the wound environment and modulate cell responses accordingly. Binding of integrins to their cognate matrix proteins activates intracellular signaling pathways that modulate a broad range of cellular processes, including cell migration (5). Integrin-mediated signaling requires that integrins bind substrate-anchored matrix proteins. This interaction provides mechanical resistance that permits tensional forces to be generated via the actomyosin system (6). In contrast, small soluble matrix protein fragments generated by the action of proteases during re-epithelialization can compete with substrate-anchored matrix proteins for integrin binding and impair cell signaling (7). Thus, productive integrin signaling depends on the context in which the intact matrix protein is presented to cells. However, the way in which migrating wound keratinocytes coordinate the balance between substrate-anchored and small soluble matrix protein fragments by the specific induction of wound integrins requires further investigation.

Transcriptional regulation plays an important role in the control of keratinocyte behavior at the different phases of wound healing, but little is known about the mechanism that modifies the wound microenvironment to coordinate with changes in cellular behavior for cell-matrix communication. Effective cell-matrix communication is crucial for efficient wound healing. Several nuclear hormone receptors, one of the largest known classes of transcription factors, have been implicated wound repair (8, 9). Of interest, studies have shown that nuclear hormone receptor peroxisome proliferator-activated receptor β/δ

* This work was supported by A*STAR BMRC Grant 05/1/22/19/377, Ministry of Education Grant ARC 18/08, and Nanyang Technological University Grants RGD 127/05 and 158/06.

[S] The on-line version of this article (available at http://www.jbc.org) contains supplemental Figs. S1–S3 and Table S1.

[1] Both authors contributed equally to this work.

[2] To whom correspondence should be addressed. Tel.: 65-63162941; Fax: 65-67913856; E-mail: nstan@ntu.edu.sg.

[3] The abbreviations used are: ECM, extracellular matrix; ANGPTL4, angiopoietin-like 4; nANGPTL4, N-terminal coiled-coil fragment; $K_{ANGPTL4}$, human keratinocytes knockdown of ANGPTL4; cANGPTL4, C-terminal fibrinogen-like domain; K_{CTRL}, human keratinocytes with control scrambled siRNA; MMP, matrix metalloproteinase; PLA, proximity ligation assay; PPAR, peroxisome proliferator-activated receptor; SPR, surface plasmon resonance; WF, wound fluid/exudate; LCM, laser-capture microdissection; CM, conditioned medium; FACS, fluorescence-activated cell sorter.

(PPARβ/δ) is an early transcription factor that modulates keratinocyte response to inflammation during wound healing (10, 11). Most studies have focused on intracellular signaling or events mediated by PPARβ/δ that were important for keratinocyte survival and migration (10, 12, 13). However, the mechanism by which PPARβ/δ alters the wound microenvironment for effective cell-matrix communication remains unknown. Conceivably, as an intracellular transcription factor, PPARβ/δ is likely to exert such an effect via extracellular factors.

Angiopoietin-like 4 (ANGPTL4) belongs to a group of secreted factors that play important roles in lipid and glucose metabolism (14). Its expression is up-regulated by PPAR (15) and by hypoxia (16). ANGPTL4 is also implicated in breast cancer metastasis via the regulation of vascular integrity (17, 18). The native ANGPTL4 is proteolytically cleaved, giving rise to an N-terminal coiled-coil fragment (nANGPTL4) and a C-terminal fibrinogen-like domain (cANGPTL4). Despite multiple physiological and pathological functions, the significance of the different cleaved fragments of ANGPTL4 is only beginning to be understood. Importantly, the identity of the binding partners for ANGPTL4 and the mechanism by which ANGPTL4 modulates cell migration is unknown, hampering our understanding of its contribution to wound healing and cancer metastasis.

Here, we show that ANGPTL4 is a PPARβ/δ target gene in keratinocytes and that its expression is elevated after injury. We show that ANGPTL4 produced by wound keratinocytes coordinates cell-matrix communication. Specifically, ANGPTL4 interacts with vitronectin and fibronectin in the wound bed, delaying their proteolytic degradation by metalloproteinases and thereby regulating the availability of local extracellular matrix. This interaction does not interfere with the binding of matrix protein to its cognate integrin receptor or with integrin-mediated signaling. Our findings reveal a novel control of the wound environment by keratinocytes that coordinates the dynamic interactions between integrins and components of extracellular matrices.

EXPERIMENTAL PROCEDURES

Reagents—Sensor CM5 chips, amine coupling kits, and Immobiline pK buffers were from GE Healthcare. Purified vitronectin, fibronectin, and laminin were from Calbiochem. Transfection reagent ExGen 500 was from Fermentas. Real-time PCR KAPA SYBR Fast Master mix was from KAPABiosystem. DUOlink proximity ligation assay was from Olink Bioscience. *Drosophila* Schneider 2 (S2) expression vector harboring a proprietary secretory signal pSSAc5.1/V5-His A was as previously described (19). Double promoter pFIV-U1/H6-Puro lentivirus-based siRNA vector (catalog #SI110A-1) and pPACKF1 packaging plasmid kit were from System Biosciences. Purified matrix proteins were purchased from Sigma. All chemicals were from Sigma unless otherwise stated.

Antibodies—p21-activated kinase (PAK), LIMK1 (LIM kinase 2), PKBα, and their cognate phosphorylated forms were from Cell Signaling. Rac1 and cdc42 were from Cytoskeleton. β-Tubulin, His tag, laminin, fibronectin, matrix metalloproteinases (MMPs), and HRP-conjugated secondary antibodies were from Santa Cruz Biotechnology; vitronectin and integrin αvβ5 were from Chemicon; keratin 6 for wound keratinocytes and hair follicle, α-smooth muscle actin for myofibroblasts, F4/80 for macrophages, and CD31 for endothelial cells were from BioLegend. Anti-human PPARβ/δ monoclonal antibodies were from Perseus Proteomics Inc., Japan. Rabbit polyclonal antibodies against the C-terminal region of human (186–406 amino acid) and mouse (190–410 amino acids) ANGPTL4 were produced in-house. Briefly, female rabbits (New Zealand White, 2–2.5 kg) were injected intramuscularly with 300 μg of recombinant proteins homogenized with 500 μl of complete Freund's adjuvant solution. First and second booster immunization with the same immunization dose were performed 3 and 6 weeks after priming immunization using incomplete Freund's adjuvant, respectively. Final harvest was done by bleeding a whole blood volume, and the rabbits were then culled with injection of euthanasia into the marginal ear vein. The carcasses were disposed after confirming no heart beat and corneal reflex, pedal reflex reactions. Preimmune blood sampling was collected as the negative control. Antibodies were purified by Protein A affinity chromatography as recommended by manufacturer (GE Healthcare).

Keratinocyte Culture—Primary human keratinocytes (Cascade Biologics) were cultured in Quantum 153 medium supplemented with insulin, transferrin, EGF, cholera toxin, and 5% FBS (PAA Laboratories) in a 5% CO_2, 37 °C humidified incubator. This medium is a modification of the keratinocyte medium previously described (20, 21). Medium was changed every 3 days. Cells were subcultured upon reaching 70% confluence. Briefly, medium was removed, and the cells washed with PBS. Trypsin (0.25%), EDTA (1 mM) in PBS was added to the culture (0.08 ml/cm^2) and incubated at room temperature for 15 min. The flask was rapped gently to dislodge cells from the surface of the flask. PBS containing 1% dialyzed FBS was added, and the cells were collected by centrifugation. The cell pellet was resuspended with fresh medium and subcultured in new flask at 2.5×10^3 cells/cm^2.

Chromatin Immunoprecipitation (ChIP)—ChIP was performed according to the manufacturer's (Upstate Biotechnology) instructions with some modifications. Briefly, ChIP assay was performed using the monoclonal PPARβ/δ antibody. Cells were treated with 1% formaldehyde at 37 °C for 15 min. Cross-linked DNA was sonicated to form fragments ranging from 200 to 500 bp in length. DNA fragments were reverse cross-linked at 65 °C for 6 h. The DNA was subsequently purified using Qiaquick column (Qiagen). DNA was amplified by PCR for 20–23 cycles. The ChIP primers for the amplification of the PPAR-response element of the human ANGPTL4 gene were as previously described (22).

Skin Wounding Experiment—Wounding was performed as previously described (23, 24). Briefly, the hair follicle cycle of each mouse was synchronized by shaving the back of the animal 2 weeks before the start of the experiment. After anesthetizing, the mice were shaven. A full thickness mid-dorsal wound (0.5-cm^2, square-shaped) was created by excising the skin and the underlying panniculus carnosus. Wound closure was measured daily in a double-blinded fashion until it was complete. At indicated days post-wounding, the entire wound, including a 5-mm margin, was excised. Wounds were dissected

for immunohistochemistry, RNA, and protein analyses (23, 25). Six-week-old PPAR$\beta/\delta^{+/+}$ and $^{-/-}$ (24) and pure bred wild type (ANGPTL4$^{+/+}$) and ANGPTL4-knock-out (ANGPTL4$^{-/-}$) male mice were used (26). All mice used in this study had a C57BL/6 background and were individually caged, housed in a temperature-controlled room (23 °C) on a 10-h dark/14-h light cycle, and fed with the standard mouse chow diet. Animal experiments were approved by the University Institutional Animal Care and Use Committee (ARF-SBS/NIE-A-0093, ARF SBS/NIE-A-0078 and ARF SBS/NIE-A-004).

Western Blot and Immunofluorescence Assays—Cells or tissues were lysed in ice-cold lysis buffer (20 mM NaH_2PO_4, 250 mM NaCl, 1% Triton X-100, 0.1% SDS) supplemented with complete protease inhibitors (Roche Applied Science). Equal amounts of protein extracts were resolved by SDS-PAGE and electroblotted onto polyvinylidene difluoride membranes for Western analysis. Membranes were processed according to standard protocol and developed using chemiluminescence (Millipore). Equal loading/transfer was verified by Coomassie staining of gels or by immunodetection of β-tubulin. Wound biopsies were fixed with 4% paraformaldehyde in PBS for 2 h at 25 °C. The fixed tissues were centrally bisected, washed twice with PBS, and embedded in Tissue-Tek OCT compound medium (Sakura) overnight at 4 °C. The tissues were subsequently frozen at −70 °C for cryosectioning. Cryostat sections (8 μm) mounted on SuperFrost Plus slides were analyzed by immunofluorescence as previously described, except that anti-ANGPTL4 antibodies were used (23). The slides presenting the largest wound diameter was defined as the wound center. As a control for immunofluorescence staining, 10-fold more peptide antigen was preincubated with anti-ANGPTL4 at 4 °C for 1 h before use. Images were taken using a LSM710 confocal laser scanning microscope with a Plan-Apochromat 40×/1.40 oil objective and ZEN software (Carl Zeiss).

Flow Cytometry (FACS)—Wound tissues were subjected to FACS analysis as previously described (27). Entire excised skin wounds were dispersed enzymatically into single cell suspensions. The tissue was incubated with dispase I (1 mg/ml) overnight at 4 °C, minced, and incubated in digestion buffer containing hyaluronidase (1 mg/ml), collagenase D (1 mg/ml), and DNase (100 unit/ml) (Sigma) in a 37 °C shaking incubator for 2 h. The dispase and hyaluronidase digests were pooled and filtered through a 70-μm Nylon cell strainer. Cells were washed, pelleted, and resuspended in equal volume of PBS containing 3% FBS. For staining of surface marker, cells were first blocked with mouse BD Fc Block and then incubated with either phyoerythrin- or FITC-conjugated monoclonal antibodies specific for F4/80 (macrophages) and CD31 (endothelial cells) or control isotype IgG on ice for 30 min. After washing with PBS, the samples were subjected to flow cytometry on a FACSCalibur system (BD Biosciences). Data were analyzed using the CellQuest software (BD Biosciences). The analyzer threshold was adjusted on the flow cytometer channel to exclude most of the subcellular debris to reduce the background noise.

Laser-capture Microdissection (LCM)—Paraffin-embedded sections of PPAR$\beta/\delta^{+/+}$ and -$^{-/-}$ wounds (10 μm) were mounted onto MembraneSlides (Carl Zeiss). Hematoxylin- and eosin-stained sections were then subjected to LCM using PALM MicroBeam according to the manufacturer's instructions (Carl Zeiss). LCM tissues were collected into microcentrifuge tubes with opaque AdhesiveCaps (Carl Zeiss). RNA was extracted using Optimum^{TM} FFPE RNA Isolation kit (Ambion) pooled from eight LCM tissues. RNA was reverse-transcribed using random primers, and the resulting cDNA was used for real-time PCR.

Expression and Purification of Recombinant ANGPTL4 Proteins—The cDNA sequences encoding human full-length ANGPTL4, nANGPTL4, and cANGPTL4 were amplified by Pfu polymerase and subcloned into pSSAc5.1/V5-His-A (19). A histidine tag was introduced between the secretory signal and the ANGPTL4 cDNA. All ligated products were transformed into competent *Escherichia coli* Top 10 bacteria and selected on Luria broth agar plates containing 80 μg/ml ampicillin. Positive clones were confirmed by DNA sequencing. Positive constructs were co-transfected with hygromycin expression vector pCoHygro (Invitrogen) into S2 cells. Recombinant ANGPTL4 proteins were purified from the conditioned medium of stable ANGPTL4-expressing S2 cells by preparative isoelectric membrane electrophoresis as described (28).

Surface Plasmon Resonance (SPR) Coupled to Liquid Chromatography-Tandem Mass Spectrometry—Purified cANGPTL4 was immobilized onto a CM5-carboxylated dextran sensor chip by amine coupling using the Surface Prep Module of BIACORE 3000 as recommended by the manufacturer (BIAcore). Acute wound fluid/exudate (WF) was collected from two patients undergoing split-thickness skin grafting. The acute wound fluid was collected daily under sterile conditions from beneath a vapor-permeable membrane applied to the donor site and changed every 24 h for 3 days postoperatively. WF was centrifuged, aliquoted, and frozen at −70 °C. WF buffered with 50 mM Tris, pH 8.0, was introduced into the cANGPTL4-conjugated CM5 chip at a flow rate of 5 μl/min for 10 min with running buffer (50 mM Tris, pH 8.0, 100 mM NaCl). After incubation for 45 s, the chamber was washed with the same buffer, and the bound molecules were subsequently eluted using 10 mM glycine, pH 6.0, and collected in a recovery vial. The CM5 chip was reused to pool more samples after washing with running buffer for 10 min at 20 μl/min. The recovered cANGPTL4-binding proteins were digested with trypsin, reduced, alkylated, and then analyzed with a Finnigan Surveyor HPLC system coupled online to a LTQ-Orbitrap mass spectrometer (Thermo Electron) equipped with a nanospray source. Proteins were identified using a Mascot search. SPR was used to determine the dissociation constant of the interaction between fibronectin and vitronectin with recombinant cANGPTL4 immobilized onto a CM5 chip. Six concentrations (0.16, 0.32, 0.63, 1.25, 2.50, and 5.0 μM) of various matrix proteins were used. Each sensorgram was corrected by subtracting a sensorgram obtained from a reference flow cell with no immobilized protein. Anti-cANGPTL4 antibodies run against the immobilized cANGPTL4 determined the Rmax value to be 251.8 resonance units. Global fitting of the SPR data to a Langmuir 1:1 model was used to determine the dissociation constant (K_D) with Scrubber 2 software. Values are given as the

mean ± S.D. of five independent preparations of recombinant proteins.

Affinity Co-precipitation Assay—Purified recombinant His-tagged ANGPTL4, nANGPTL4, or cANGPTL4 was immobilized onto nickel-nitrilotriacetic acid resin (GE Healthcare). The resin was washed with wash buffer (50 mM Tris, pH 7.5, 150 mM NaCl, 0.1% Triton X-100) to remove excess ANGPTL4. An equal amount of ANGPTL4-bound resin was dispensed and incubated with 500 ng of purified matrix protein in PBS at 25 °C for 30 min. The resin was then thoroughly washed with wash buffer. The unbound fractions were pooled, and the bound fractions were released by SDS-PAGE loading dye. Both fractions were analyzed by immunoblotting with their indicated antibodies. Resin treated with Tris-buffered saline was used as a control. *In vivo* co-immunoprecipitation was performed using corresponding antibodies as previously described (29).

Sucrose Gradient Sedimentation Assay—Proteins (1 μg) were allowed to interact at 4 °C for 2 h in 150 μl of 50 mM Tris, pH 8.0, and 100 mM NaCl. The protein mixture was size-fractionated by ultracentrifugation for 16 h at 132,000 × *g* at 18 °C through a 5-ml sucrose density gradient (25–40%). Fractions of 300 μl were collected, chloroform/ethanol-precipitated, and analyzed by Western blot using their respective antibodies.

In Situ Proximity Ligation Assay (PLA)—Keratinocytes subcultured overnight on glass chamber slides (Lab-Tek) or cryosections of wound biopsies were fixed with 4% paraformaldehyde for 15 min. The slides were washed twice with PBS and blocked for 1 h at room temperature with 2% BSA in PBS containing 0.1% Triton X-100 followed by incubation with the indicated antibody pairs overnight at 4 °C. The slides were washed as described above. DUOlink™ *in situ* PLA was performed as recommended by the manufacturer (OLink Biosciences) using a slide incubated without primary antibody as a negative control. Triple PLA was performed as previously described with minor modifications (30). Rabbit anti-cANGPTL4 (in-house), mouse anti-integrin αvβ5, and goat anti-vitronectin antibodies (Chemicon) were used as proximity probes. DNA was ligated at 37 °C for 1 h. All probe sequences were as previously described (30) and were synthesized by Proligo (Sigma). As a negative control, rabbit anti-cANGPTL4 and mouse anti-integrin β5 proximity probes were omitted. Images were taken using a LSM710 confocal laser scanning microscope with a Plan-Apochromat 63×/1.40 oil objective and ZEN software (Carl Zeiss).

Knockdown of ANGPTL4 and Real-time PCR—siRNA against human ANGPTL4 and a scrambled sequence control were subcloned into the pFIV-H1/U6-puro siRNA lentivirus system (System Biosciences). An equimolar ratio of sense and antisense oligonucleotide mixture was heated to 95 °C for 5 min and allowed to anneal in 20 mM Tris, pH 7.8, 100 mM NaCl, and 0.2 mM EDTA by slow cooling to room temperature. The annealed oligonucleotide was phosphorylated using polynucleotide kinase before ligation with BbsI-linearized pFIV-H1/U6-puro siRNA vector. Ligated products were transformed into competent *E. coli* Top 10 bacteria and selected on Luria broth agar plates containing 80 μg/ml ampicillin. Positive clones were confirmed by DNA sequencing. Positive constructs were co-transfected with pPACK packing plasmids into 293TN cells using ExGen 500. Supernatant was collected 48 h post-transfection, and pseudovirus-containing precipitate was obtained by centrifugation at 50,000 × *g* for 90 min at 4 °C. Cells were transduced using Polybrene according to the manufacturer's recommendation. Transduced cells were enriched by 350 μg/ml puromycin selection for 2 weeks. Knockdown efficiency of ANGPTL4 and relative expression level of indicated genes were determined by quantitative PCR. All oligonucleotides and Taqman probes sequences were provided in supplemental Table S1. Control and ANGPTL4-knockdown keratinocytes were denoted as K_{CTRL} and $K_{ANGPTL4}$, respectively. The interferon response detection kit was from System Biosciences.

Matrix Protein Degradation Assay—Purified ECM proteins (200 ng) were first allowed to interact with various recombinant ANGPTL4 proteins (200 ng) before incubation at 37 °C with either WF or serum-free $K_{ANGPTL4}$-conditioned medium (CM). At the indicated times, aliquots of the reaction were stopped by the addition of SDS-PAGE loading dye. CM was prepared as follows; 3×10^6 $K_{ANGPTL4}$ cells were subcultured in a 10-cm dish the day before treatment. The next day cells were treated with 50 μg/ml TNF-α in 3 ml of serum-free basal Quantum 153 medium for 12 h. CM was collected, sterile-filtered, and stored at −80 °C for use in assays. Three independent experiments from two WF samples were performed. Protease inhibition assays were performed using the protease inhibitors pepstatin A (8 μM), EDTA (8 mM), and PMSF (1 mM) either alone or in indicated combinations in the CM. The matrix proteins were analyzed by Western blot using the corresponding antibodies.

Statistical Analysis—Data were analyzed statistically by two-tailed Mann-Whitney tests using SPSS software. Values were expressed as the mean ± S.E., and $p < 0.05$ was considered statistically significant.

RESULTS

ANGPTL4 Expression Is Regulated by PPARβ/δ in Keratinocytes—ANGPTL4 is a direct target gene of PPARβ/δ in HaCaT cells, a non-tumorigenic human keratinocyte cell line (22). However, the role, expression, and regulation of ANGPTL4 in skin wound healing is unclear. To this end, we first examined the expression level of ANGPTL4 in human keratinocytes after ligand activation of specific PPAR isotypes. Quantitative PCR revealed that ANGPTL4 mRNA was up-regulated by all three PPAR isotypes (Fig. 1*A*), with an ~8.5-fold induction with the specific PPARβ/δ ligand, GW501516. We found that serum, which contains undefined and complex mixture of lipid metabolites that can act as ligands for PPARs, also increased ANGPTL4 expression by ~5-fold (Fig. 1*A*). Next, the PPAR response element of the ANGPTL4 (22) from human keratinocytes was analyzed by ChIP using monoclonal anti-PPARβ/δ. Results showed that PPARβ/δ was bound to this site of the ANGPTL4 promoter region (Fig. 1*B*), indicating that ANGPTL4 is a direct target of PPARβ/δ in keratinocytes. Immunoblot analysis of day 3 wound biopsies using different polyclonal anti-ANGPTL4 antibodies detected the native ANGPTL4 and cANGPTL4 in the PPARβ/$\delta^{+/+}$ mice, whereas the expression of ANGPTL4 was reduced in PPARβ/$\delta^{-/-}$ littermates (Fig. 1*C*). The specificity of anti-cANGTPL4 is shown in supplemental Fig. S1*A* and specificity of anti-nANGPTL4 was as previously reported (15). Day 3 wound biopsies were

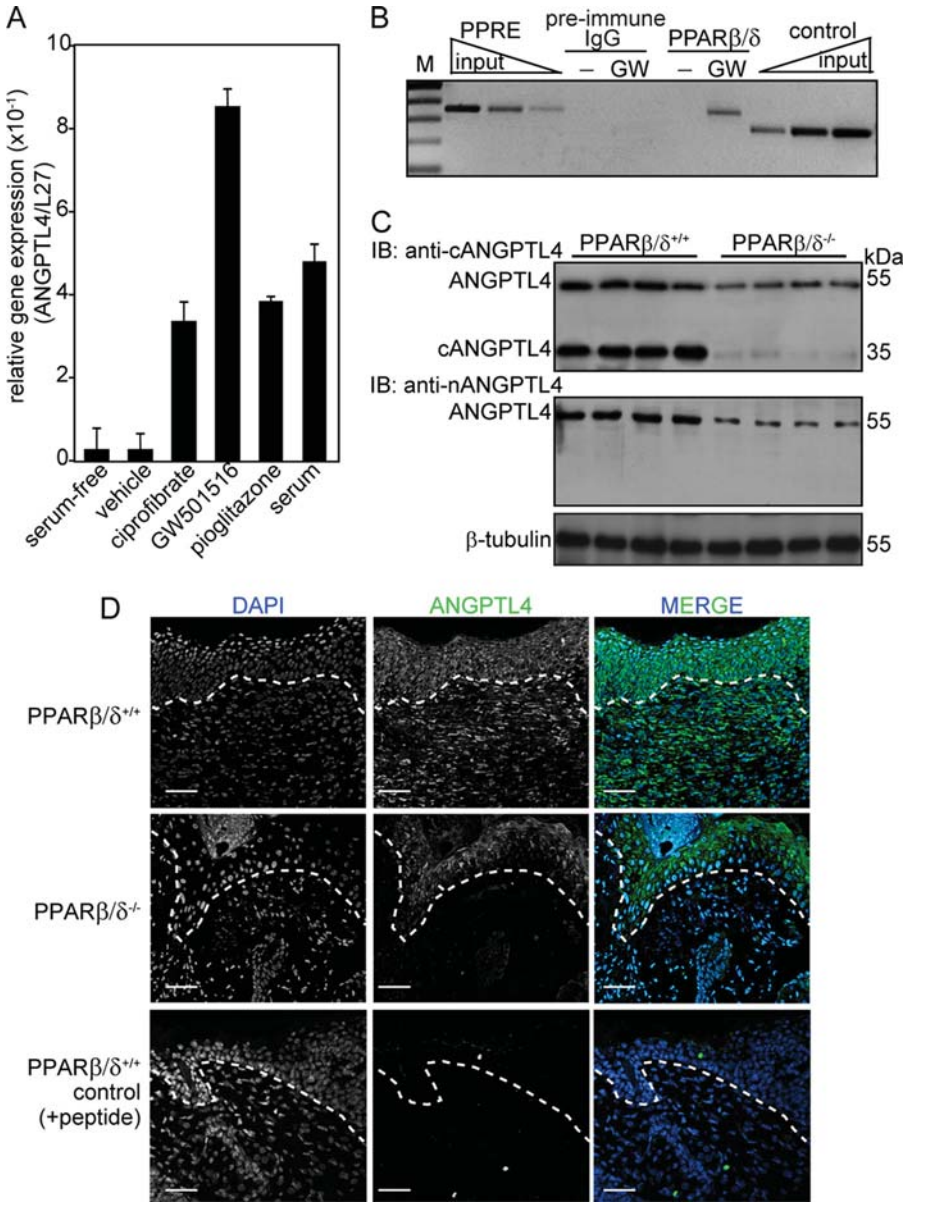

FIGURE 1. **Reduced expression of ANGPLT4 in PPAR$\beta/\delta^{-/-}$ mice wounds.** *A*, relative mRNA levels of ANGPTL4 in human keratinocytes treated with different agonists selective for each PPAR isotype, ciprofibrate (30 μM, PPARα), GW501516 (2 nM, GW, PPARβ/δ), and pioglitazone (500 nM, PPARγ) are shown. Values are mean ± S.E. of four independent studies. Ribosomal protein L27 used as a normalizing housekeeping gene. *B*, ChIP was done in keratinocytes using pre-immune IgG or monoclonal anti-PPARβ/δ. Regulatory region with the PPAR response element was immunoprecipitated with anti-PPARβ/δ and specifically amplified. No amplified signal was obtained with preimmune IgG. A control region upstream of PPAR response element served as the negative control. Aliquots of chromatin were analyzed before immunoprecipitation (*input*). *M*, 100-bp DNA marker. *C*, expression is shown of ANGPTL4 protein in day 3 post-wounding mice skin biopsies. Polyclonal antibodies that recognized the N-terminal (*anti-nANGPTL4*) and C-terminal (*anti-cANGPTL4*) of ANGPTL4 were used. β-Tubulin served as loading and transfer control. $n = 5$. *IB*, immunoblot. *D*, shown is immunofluorescence staining of ANGPTL4 in PPAR$\beta/\delta^{+/+}$ and PPAR$\beta/\delta^{-/-}$ day 3 wound biopsies using anti-cANGPTL4. Sections were counterstained with DAPI. Negative control is performed with anti-cANGPTL4 preincubated with antigen peptide. Representative images from wound epithelia and wound beds were shown ($n = 5$). The *dotted white line* denotes epidermal-dermal junction. *Scale bar*, 40 μm.

used because PPARβ/δ expression peaked at day 3 post-wounding (31). Immunofluorescence staining further confirmed that ANGPTL4 was highly expressed in both the wound epithelia and the wound bed in PPAR$\beta/\delta^{+/+}$ mice, whereas reduced expression was detected in their PPAR$\beta/\delta^{+/+}$ littermates (Fig. 1*D*). Quantitative PCR analysis of the LCM wound epithelium, dermis, and wound bed of day 3 wound biopsies from PPAR$\beta/\delta^{+/+}$ and PPAR$\beta/\delta^{+/+}$ mice showed that the wound epithelium was the major producer of ANGPTL4 (supplemental Fig. S1*B*). These results suggested that ANGPTL4 secreted by wound keratinocytes may play an important role during wound healing.

cANGPTL4 Interacts with Specific Matrix Proteins—To begin to understand the role of ANGPTL4 during wound healing, we sought to identify ANGPTL4-binding proteins using SPR-MS. Prompted by our initial observation (Fig. 1*D*), we hypothesized that WF may harbor ANGPTL4-interacting proteins. Using recombinant cANGPTL4 and WF as the bait and lysate, respectively, we identified the ECM proteins, vitronectin and fibronectin, as ANGPTL4 binding partners (supplemental Fig. S1*C*). Recombinant cANGPTL4 was expressed and purified from *Drosophila* S2 culture medium (supplemental Fig. S1*D*). Further analyses using SPR with purified vitronectin and fibronectin and ANGPTL4 revealed binding constants (K_D) of $\sim 10^{-7}$ M (ANGPTL4 with fibronectin and vitronectin, $3.80 \pm 1.74 \times 10^{-7}$ and $3.04 \pm 1.33 \times 10^{-7}$ M, respectively; cANGPTL4 with fibronectin and vitronectin, $3.52 \pm 1.41 \times 10^{-7}$ and 5.94 ± 1.79 M, respectively. Fig. 2, *A* and *B*). Specific anti-cANGPTL4 antibodies against immobilized cANGPTL4 determined the theoretical Rmax value to be 251.8 resonance units. The experimental Rmax values of fibronectin and vitronectin for cANGPTL4 were 238.6 and 218.5 resonance units, respectively, suggesting a 1:1 stoichiometry of binding. This interaction was specific, as the binding of anti-cANGTPL4 antibody, but not pre-immune IgG, to immobilized-ANGPTL4 blocked its interaction with vitronectin and fibronectin (Fig. 2, *C* and *D*). Specific interactions between cANGPTL4 with vitronectin and fibronectin were confirmed by *in vitro* affinity co-immunoprecipitation (Fig. 2*E*). In addition, we also examined the formation of the cANGPTL4-matrix protein complex by sedimentation using sucrose gradient ultracentrifugation, which separates proteins and protein complexes according to their native molecular weight, with larger proteins/

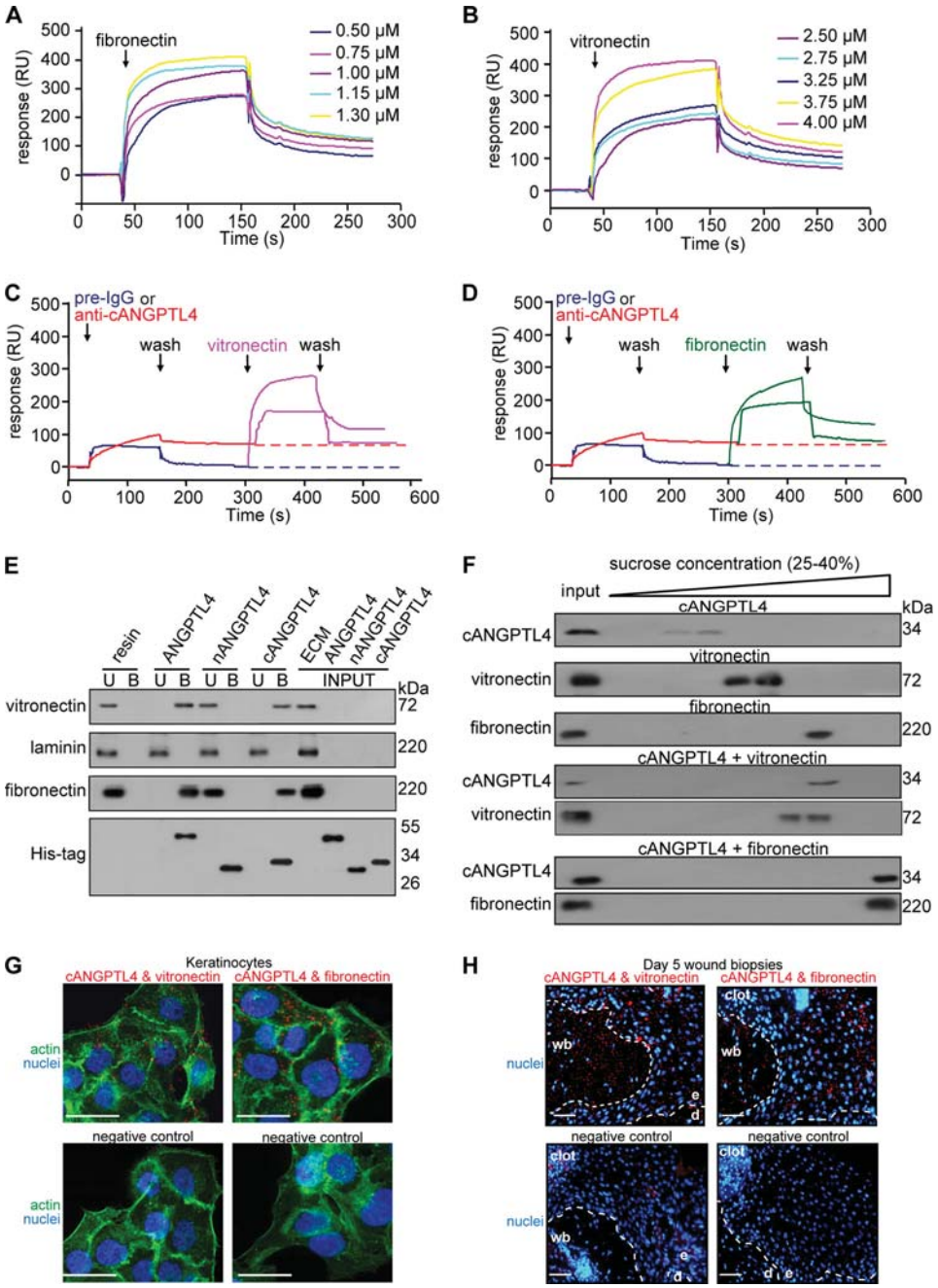

FIGURE 2. **cANGPTL4 interacts with vitronectin and fibronectin.** Sensograms show binding profiles between immobilized-cANGPTL4 and the indicated concentrations of either fibronectin (*A*) or vitronectin (*B*). A representative sensorgram ($n = 5$) shows binding profiles of vitronectin (*C*, *pink*) and fibronectin (*D*, *green*) with immobilized-cANGPTL4 CM5 chip after preblocking with either pre-immune IgG (*blue*) or anti-cANGPTL4 (*red*). *E*, co-immunoprecipitation assays ($n = 5$) were carried out by using different forms of His-tagged ANGPTL4 proteins immobilized on nickel-Sepharose and incubated with the indicated purified matrix molecules. Matrix proteins and ANGPTL4 were detected by immunodetected using corresponding antibodies and revealed by chemiluminescence. *U* and *B* denote the unbound/washed and bound fractions from the resin, respectively. *RU*, resonance units. *F*, shown is immunodetection of the indicated proteins from sucrose density gradient fractions. The proteins were allowed to interact in the indicated combinations before separation by sucrose gradient ultracentrifugation. Blots showed increasing sucrose density from *left* to *right*. An aliquot of the indicated protein, prior incubation, and centrifugation was also loaded (*input*) ($n = 5$). Detection of various complexes between ANGPTL4 and the indicated binding partners in K_{CTRL} (*G*) and in Day-5 (*H*) wound biopsies using PLA is shown. PLA signals (*red*), nuclei stained with Hoechst dye (*blue*), and actin stress fiber (*green*) by Alexa488-phalloidin is shown. The nuclei-image has been acquired in one z-plane using LSM710 confocal microscope. The *dotted white line* represents epidermal-dermal junction. Negative control is performed without primary antibodies. Representative pictures from wound section with epidermis (*e*), dermis (*d*), the adjacent wound bed (*wb*), and K_{CTRL} from six independent experiments or sections from three mice are shown. *Scale bar*, 40 μm.

complexes sedimenting at a higher sucrose density. Consistent with our previous results, immunodetection after sucrose gradient ultracentrifugation showed that cANGPTL4 associated with either vitronectin or fibronectin, which were detected in higher density fractions than the individual protein (Fig. 2*F*). No interaction between nANGPTL4 with identified matrix proteins was observed by either SPR analysis or co-immunoprecipitation (Fig. 2*E*).

In situ PLAs using indicated antibody pairs on primary human keratinocytes and day 5 wound sections were subsequently used to examine whether these interactions occur *in vivo*. These experimental PLA signals, visualized as individual *red dots*, were observed in the wound bed as well as in the wound epithelium (Fig. 2, *G* and *H*), confirming that cANGPTL4 interacts with vitronectin and fibronectin *in vivo*. As a positive control, vitronectin was shown to interact with integrin β5 (supplemental Fig. S2*A*), whereas the negative control recommended by the manufacturer revealed negligible nonspecific binding of PLA probes (Fig. 2, *G* and *H*, and supplemental Fig. S2*A*). Taken together, these data indicate that ANGPTL4 directly interacts with specific matrix proteins in the wound bed during wound healing.

ANGPTL4-bound Matrix Protein Can Interact with Integrins—Having shown that ANGPTL4 interacts with vitronectin and fibronectin, it was necessary to determine whether this interaction would interfere with integrin recognition of the matrix protein. To this end, we examined the ability of ANGPTL4-bound vitronectin to interact with the extracellular domain PSI-ILD of integrin β5. Purified recombinant cANGPTL4 with no histidine tag, histidine-tagged integrin β5 PSI-ILD, and vitronectin were allowed to interact in solution and then sedimented using sucrose gradient ultracentrifugation. When the three proteins were present together, all three proteins were detected at a higher sucrose density, suggest-

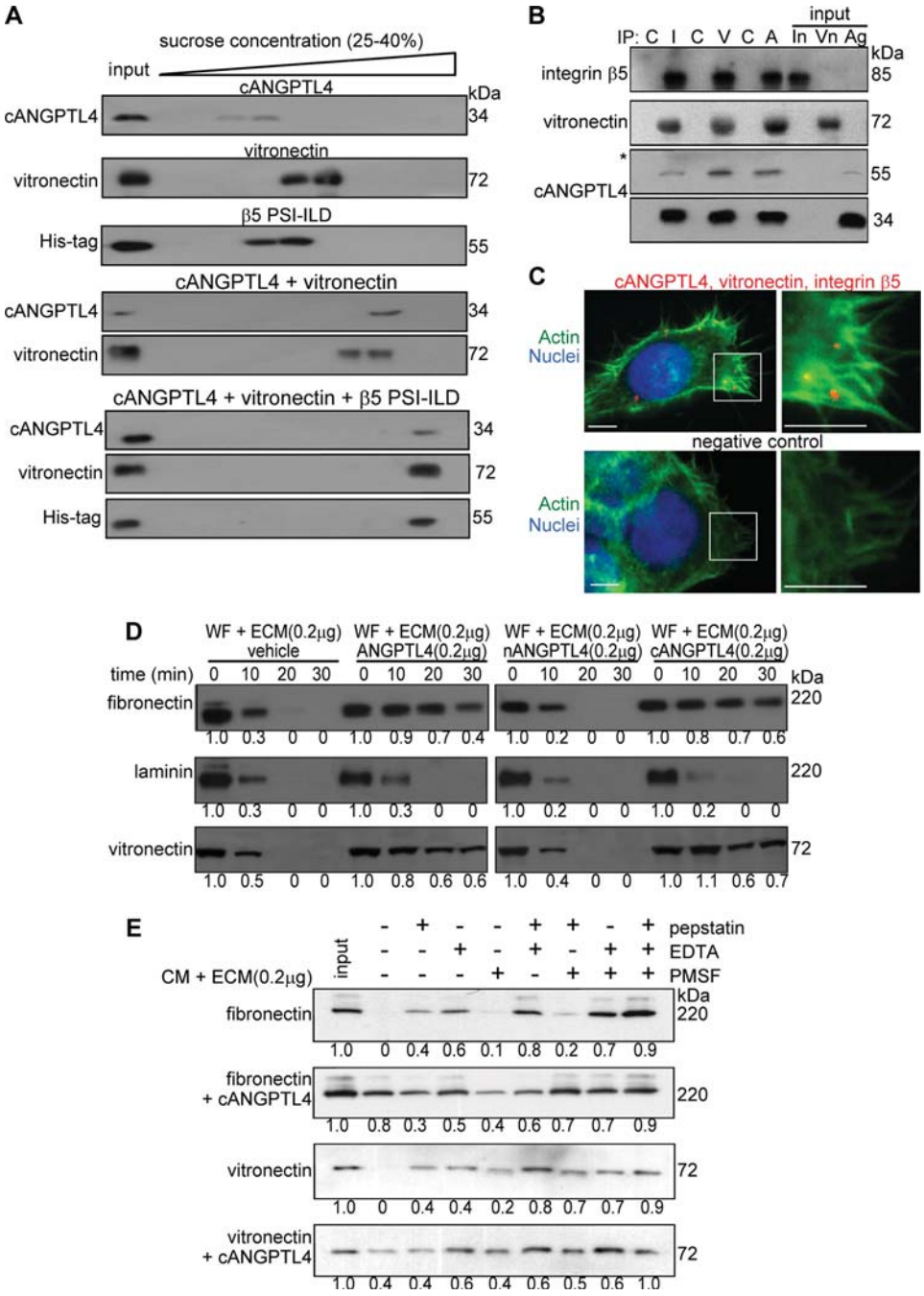

FIGURE 3. **ANGPTL4 modulates matrix protein degradation.** *A*, shown are immunoblots of cANGPTL4, His-tagged integrin β5 PSI-ILD, and vitronectin of sucrose density gradient fractions. The proteins were allowed to interact in the indicated combinations before separation by sucrose density gradient ultracentrifugation. Blots showed increasing sucrose density from *left* to *right*. *B*, *in vivo* co-immunoprecipitation (*IP*; $n = 3$) was performed by using antibodies against integrin β5 (*I*), vitronectin (*V*), and cANGPTL4 (*A*). As control, pre-immune IgG (*C*) was used. Antibodies were covalently cross-linked to Protein G on agarose beads were incubated with total keratinocyte cell lysate. Immunoprecipitates were detected by immunoblot using corresponding antibodies and revealed by chemiluminescence. Native ANGPTL4 of ~55 kDa was after longer exposure time as denoted by *asterisk*. Total cell lysate served as the input. (*In*, integrin β5; *Vn*, vitronectin; *Ag*, ANGPTL4). *C*, a triple PLA showed the ternary complex in keratinocytes. Triple PLA signals (*red*) nuclei were stained with Hoechst dye (*blue*) and Alexa488-phallodin for actin fiber (*green*). Representative PLA images from three independent experiments are shown. Negative control is without anti-cANGPLT4 and anti-integrin proximity probes. *Scale bar*, 40 μm. Immunodetection of the matrix proteins, vitronectin, and fibronectin after incubation for indicated time with WF (*D*) or TNF-α-treated $K_{ANGPTL4}$ (*E*) CM in the presence of indicated protease inhibitors is shown. Laminin, which does not interact with cANGPTL4, serves as control. Three independent experiments from two wound fluids were performed. Values below denote change in mean -fold expression compared with input.

ing that ANGPTL4-bound matrix protein could still interact with PSI-ILD of integrin β5 (Fig. 3*A*). *In vivo* co-immunoprecipitation and triple PLA were used to further confirm this observation. Co-immunoprecipitation from human keratinocyte lysate using antibodies against integrin αvβ5, vitronectin, or cANGPTL4 followed by immunodetection showed that the corresponding two proteins were also found in the immunoprecipitates (Fig. 3*B*). Finally, triple PLA further revealed the close proximity of ANGPTL4, integrin β5, and vitronectin at focal adhesions (Fig. 3*C*). In retrospect, the PLA signals from ANGPTL4 and matrix proteins detected in wound epithelium (Fig. 2*H*) represented ANGPTL4-bound matrix proteins that had interacted with their cognate integrins in keratinocytes. Taken together, our results suggest that the binding of ANGPTL4 to matrix proteins, such as vitronectin, does not prevent the matrix protein from associating with its cognate integrin.

ANGPTL4 Interacts with Matrix Proteins and Delays Their Degradation—Directed migration of wound keratinocytes over the provisional wound bed requires the controlled turnover of matrix proteins by proteases (32). We next examined the effect of the interaction between ANGPTL4 and matrix proteins on the turnover rate of matrix proteins. We preincubated purified ECM proteins with various recombinant ANGPTL4 proteins and subjected the mixture to WF. Our results revealed that the degradation of vitronectin and fibronectin was slower in the presence of ANGPTL4 and cANGPTL4 compared with either the vehicle control or nANGPTL4 (Fig. 3*D*). As a control, laminin-5, which does not bind to cANGPTL4, was degraded at a similar rate regardless of the presence of ANGPTL4 (Fig. 3*D*).

To eliminate the possible contribution of endogenous ANGPTL4 from WF, we performed a similar matrix degradation experiment with serum-free CM. We initially sup-

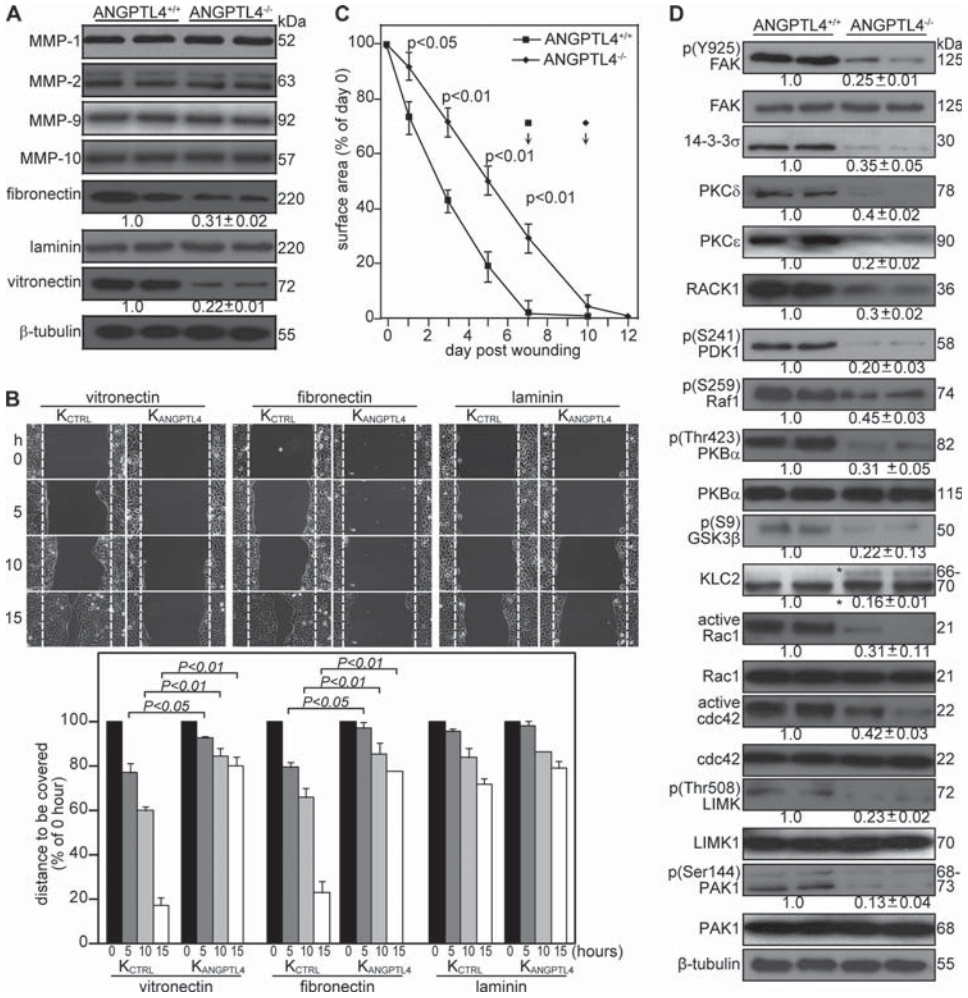

FIGURE 4. **ANGPTL4 knock-out mice displayed impaired wound re-epithelialization.** *A*, shown is an immunoblot analysis of MMP-1, -2, -9, -10, fibronectin, laminins, and vitronectin from day 5 wound biopsies of ANGPTL4$^{+/+}$ and ANGPTL4$^{-/-}$ mice. *Values below the band* represent the mean -fold differences in protein expression levels relative to ANGPTL4$^{+/+}$ from eight wound biopsies for each genotype. β-Tubulin served as loading and transfer controls. *B*, shown are wound closure kinetics of K_{CTRL} and $K_{ANGPTL4}$ treated with mitomycin C (2 μg/ml) on the indicated matrix protein-coated surfaces. Representative time-lapsed images of wounded cultures are shown. *Yellow dotted lines* represent the scratch gap at the time of wounding. The graph shows the distance to be covered by the migrating keratinocytes as the percentage of 0 h (=100%) *in vitro* wound gap distance (±S.E., $n = 5$, using the Mann-Whitney test). *C*, shown are the wound closure kinetics of ANGPTL4$^{+/+}$ and ANGPTL4$^{-/-}$ mice. Wound surface areas are plotted as percentage of day 0 (=100%) wound surface area (±S.E., $n = 10$, using the Mann-Whitney test). *Arrows* indicate the mean time for complete wound closure. *D*, shown are immunoblot analyses of the indicated proteins from ANGPTL4$^{+/+}$ and ANGPTL4$^{-/-}$ mice day 5 wound biopsies ($n = 5$). *Values below the bands* represent the mean -fold differences in protein expression levels when compared with ANGPTL4$^{+/+}$, which was assigned the value 1. *GSK-3*, glycogen synthase kinase-3; *KLC*, kinesin-light chain; *PAK*, p21-activated kinase; *PDK1*, 3-phosphoinositide-dependent kinase-1; *LIMK*, LIM kinase. β-Tubulin served as the loading and transfer control.

pressed endogenous ANGPTL4 expression by RNA interference in human keratinocytes. Keratinocytes were transduced with a lentivirus-mediated ANGPTL4 or control scrambled siRNA. The ANGPTL4 expression level in ANGPTL4-knockdown keratinocytes ($K_{ANGPTL4}$) was reduced by 90% compared with control siRNA keratinocytes (K_{CTRL}) (supplemental Fig. S2*B*). The expression of β-tubulin remained unchanged, as did the transfer and loading control. The expression of ANGPTL3, a closely related member of the family, remained unchanged, indicating the specificity of the knockdown. The induction of interferon responses has been reported as a challenge to the specificity of some RNAi approaches (33). Real-time PCR analysis of key interferon response genes OAS1, OAS2, MX1, and ISGF3γ revealed no significant difference between $K_{ANGPTL4}$ and either wild type non-transduced cells or K_{CTRL} (supplemental Fig. S2*C*). These data suggest that gene silencing is not associated with nonspecific interferon-response induction, namely, an off-target effect. Next, we stimulated the expression of proteases in $K_{ANGPTL4}$ by TNF-α treatment and used the resulting serum-free CM for a matrix protein degradation assay. Consistent with our previous results, the degradation of vitronectin and fibronectin was slower in the presence of ANGPTL4 and cANGPTL4 (supplemental Fig. S2*D*). Using different protease inhibitors, we further showed that ANGPTL4 mainly protected the degradation of vitronectin and fibronectin from MMPs (Fig. 3*E*). SPR analysis failed to detect any interaction between recombinant MMP2 or MMP9 and cANGPTL4, arguing against a direct role of ANGPTL4 in the inhibition of MMPs (supplemental Fig. S2*E*). Taken together, our results showed a physical interaction between ANGPTL4 with specific matrix proteins that resulted in the selective delay of the degradation of matrix proteins by MMPs during wound healing.

ANGPTL4 Deficiency Delays Wound Re-epithelialization—We showed that ANGPTL4 produced by keratinocytes interacts with vitronectin and fibronectin in the wound bed and delays their proteolytic degradation by MMPs. To underscore the *in vivo* relevance of ANGPTL4 in the degradation of specific matrix proteins by MMPs, we examined the expression of MMPs and matrix proteins in ANGPTL4$^{+/+}$ and ANGPTL4$^{-/-}$ wound biopsies. Keratinocytes synthesize and secrete mainly MMP-1, -2, -9 and -10, and their expression is required to regenerate the injured tissue (32). Immunoblot analysis of day 5 ANGPTL4$^{+/+}$ and ANGPTL4$^{-/-}$ wound biopsies showed that the protein levels of vitronectin and fibronectin, but not laminin, was reduced (Fig. 4*A*). Our analysis did not reveal significant differences in the protein level of major MMPs (Fig. 4*A*), indicating that the differential matrix protein level was a consequence of increased susceptibility of matrix proteins to proteolytic degradation.

We hypothesized that such actions would have a direct impact on wound healing. We first examined keratinocyte

migration using *in vitro* scratch wound assays on surfaces coated with matrix proteins using K_{CTRL} and $K_{ANGPTL4}$ treated with mitomycin C to exclude any effects of proliferation. Our results showed that $K_{ANGPTL4}$ re-populated the *in vitro* wound significantly more slowly on fibronectin- and vitronectin-coated surfaces compared with K_{CTRL} (Fig. 4*B*). No significant difference was observed on laminin-coated surfaces. Next, we examined the healing of full-thickness skin wounds in ANGPTL4$^{+/+}$ and ANGPTL4$^{-/-}$ mice. Our analysis of the day 3–10 wound biopsies showed a delayed re-epithelialization of ANGPTL4$^{-/-}$ wounds compared with ANGPTL4$^{+/+}$ (Fig. 4*C*). The length of the wound epidermis measured from the first hair follicle to the tip of the wound epithelial tongue is used as an indicator of keratinocyte migration, and this was also reduced in ANGPTL4$^{-/-}$ wounds (supplemental Fig. S3*A*). No difference in wound contraction, defined by the distance between the first hair follicle on either side of the wound edge, was observed. Immunohistochemical staining of wound biopsies for keratin 6 identifies the wound epithelia and hair follicles, whereas α-smooth muscle actin reveals the myofibroblasts (supplemental Fig. S3, *B* and *C*). We harvested the entire wound along with a 5-mm perimeter of the surrounding tissue. Cell counts indicated cell number per wound at day 3 (ANGPTL4$^{+/+}$ $3.20 \pm 0.39 \times 10^6$; ANGPTL4$^{-/-}$ $3.01 \pm 0.44 \times 10^6$, $n = 4$) and day 7 (ANGPTL4$^{+/+}$ $3.54 \pm 0.26 \times 10^6$; ANGPTL4$^{-/-}$ $3.33 \pm 0.54 \times 10^6$, $n = 4$). The cell suspension was analyzed on FACS after staining with antibodies against F4/80 for macrophages showed no significant difference between ANGPTL4$^{-/-}$ and ANGPTL4$^{+/+}$ biopsies (day 3, ANGPTL4$^{+/+}$ $15.1 \pm 1.2\%$; ANGPTL4$^{-/-}$ $14.1 \pm 2.1\%$; day 7, ANGPTL4$^{+/+}$ $18.3 \pm 2.6\%$; ANGPTL4$^{-/-}$ $18.7 \pm 3.8\%$ of cells in wound, $n = 3$) (supplemental Fig. S3*D*). We observed a consistently lower number of CD31$^+$ endothelial cells in ANGPTL4$^{-/-}$ compared with ANGPTL4$^{+/+}$ wounds (day 3, ANGPTL4$^{+/+}$ $15.7 \pm 2.4\%$; ANGPTL4$^{-/-}$ $10.1 \pm 1.8\%$; day 7, ANGPTL4$^{+/+}$ $19.7 \pm 3.6\%$; ANGPTL4$^{-/-}$ $14.7 \pm 2.8\%$ of cells in wound, $n = 3$) (supplemental Fig. S3*E*). Our results showed that ANGPTL4 deficiency delays wound re-epithelialization associated, at least in part, with an increase in matrix protein degradation.

ANGPTL4 Deficiency Affects Focal Adhesion Kinase- and 14-3-3σ-dependent Signaling Pathways—Given that integrins are receptors for matrix proteins and having shown that ANGPTL4 deficiency affects matrix protein integrity and wound healing, it is conceivable that the underlying mechanism involves integrin-mediated signaling. Indeed, the expression or phosphorylation of downstream effectors like focal adhesion kinase- and 14-3-3-dependent signaling cascades was reduced in ANGPTL4$^{-/-}$ compared with ANGPTL4$^{+/+}$ wounds (Fig. 4*D*). 14-3-3 associates with integrins to modulate cell migration via a focal adhesion kinase-independent mechanism involving protein kinase C (PKC) (34). ANGPTL4$^{-/-}$ wounds also showed decreased expression of RACK1, indicating an attenuated PKC-mediated signal transduction (Fig. 4*D*) (35). A reduced activation of focal adhesion kinase is also known to converge with a decreased activation of the Raf-MEK-ERK signaling pathway (36).

The downstream mediators of the PI3K cascade such as 3-phosphoinositide-dependent kinase-1 (PDK1), PKBα, and glycogen synthase kinase 3β (*GSK-3β*) were also altered (Fig. 4*D*). Glycogen synthase kinase 3β is a target of PKBα known to phosphorylate kinesin light chain and, thus, to negatively regulate kinesin-based motility and integrin recycling (37, 38). We observed hyperphosphorylated kinesin light chain 2 in ANGPTL4$^{-/-}$ wounds, which suggested that integrin recycling may be impaired in ANGPTL4-deficient keratinocytes (Fig. 4*D*). Small Rho GTPases are effectors of PI3K pathway. Among them, cdc42 and Rac1 are pivotal intracellular mediators for the formation of lamellipodia and cell migration. They activate downstream effectors such as p21-activated kinase, which in turn activate LIM kinases (39). ANGPTL4 deficiency led to a reduction in the phosphorylation of p21-activated kinase 1 (*PAK1*) and LIM kinase1 (*LIMK1*) (Fig. 4*D*). These would have a direct impact on lamellipodia formation and migration, consistent with our earlier observation that wound healing was delayed in $K_{ANGPTL4}$ (Fig. 4*B*). Taken together, our results show that ANGPTL4 deficiency impairs the activation of numerous integrin-initiated downstream signaling cascades, including focal adhesion kinase and 14-3-3, to mediate gene expression involved in cell migration.

DISCUSSION

Wound healing is a complex process that involves a cascade of overlapping events, including inflammation, re-epithelialization, and remodeling, all directed at the restoration of the epidermal barrier. Re-epithelialization is accomplished by increased keratinocyte proliferation and the guided migration of the keratinocytes over the wound. Cellular interactions with ECM proteins, *i.e.* cell-matrix communication, among others, coordinates the individual events, enabling temporal and spatial control as well as ordered changes in keratinocyte behavior and phenotype. We revealed a newly discovered cell-matrix communication role for ANGPTL4 in influencing wound re-epithelialization. ANGPTL4 binds and delays the degradation of specific matrix proteins; they are, thus, available as intact components of ECM to regulate cell-matrix communication.

During wound healing, migrating cells must display appropriate cellular behavior in response to the changing wound environment to enable effective wound closure. Integrins on the cell surface function as biosensors to constantly monitor changes in the microenvironment. Simultaneously, the context in which the cognate matrix protein is presented to the cells dictates productive integrin activation. At a low protein ratio of soluble to substrate-anchored matrix that is well below that required for blocking adhesion, one may observe an accelerated turnover of the integrin-matrix protein interaction (40). The deficiency in ANGPTL4 has a dramatic effect on wound closure. ANGPTL4 binds to specific matrix proteins via its C-terminal fibrinogen-like domain and delays their degradation by proteases. This association, however, does not interfere with integrin-matrix protein recognition. Instead, it directly affects integrin-mediated signaling by altering the balance between substrate-anchored matrix proteins and soluble matrix protein fragments, thereby modifying the availability of the local sub-

strate-anchored ECM and consequently modulating cellular behavior.

Numerous studies have shown that inflammation-induced PPARβ/δ is crucial for wound repair. PPARβ/δ confers anti-apoptotic properties to keratinocytes, in part via transcriptional control of the PKBα signaling pathway and by maintaining a sufficient number of viable wound keratinocytes at the wound edge (10, 12). Recently, PPARβ/δ was shown to potentiate cell polarization and directed migration during re-epithelialization (13). Most of these studies focused on intracellular signaling or events mediated by PPARβ/δ that were important for cell survival and migration. Clearly, cell-matrix communication is needed for effective directed cell migration during wound healing. However, the mechanism by which PPARβ/δ modifies the wound microenvironment to coordinate cell-matrix communication remains unknown. Conceivably, as an intracellular transcription factor, PPARβ/δ is likely to exert such an effect via an extracellular factor. The expression of ANGPTL4, only weakly detectable in normal intact skin, was markedly elevated during the re-epithelialization phase of wound healing, as was similarly observed in PPARβ/δ-knock-out mice (31). We provide evidence that PPARβ/δ stimulates the expression of the adipocytokine, ANGPTL4, in keratinocytes, which allows the migrating keratinocytes to modulate the wound microenvironment and to coordinate with cellular responses. Similar to its effect on integrin-matrix interactions, integrin-focal adhesion kinase-mediated signaling and key intracellular signaling cascades involved in actin polymerization and for the establishment of a leading lamellipodium in migrating cells are dependent on ANGPTL4. Besides regulating cell proliferation, PI3K/PKBα, PDK1, and glycogen synthase kinase-3β are involved in the coordinated assembly and disassembly of actin filaments and integrin recycling and contribute to the motility of rapidly migrating cells, such as wound keratinocytes (42). The ANGPTL4-knock-out mice did not have any obvious skin abnormalities but displayed altered epidermal differentiation (data not shown). This suggests that a low level of ANGPTL4 may be required for normal skin homeostasis and may play an important role during wound repair. The role of PPARβ/δ in epidermal differentiation and maintenance of a lipid barrier is well recognized, although the underlying mechanism remains unclear (43). Although not the focus of this study, we observed that the expression of 14-3-3, as assessed by immunoblot, was diminished in ANGPTL4$^{-/-}$ compared with ANGPTL4$^{+/+}$ mice, and this reduction may play a role in regulating epidermal differentiation. Studies have shown that 14-3-3 associates with PKC, which has a well established role in epidermal differentiation (44).

Emerging works have shown adipocytokines such as leptin, to have a profound local impact on wound healing (45). However, the mechanism for the observed beneficial effect on wound repair is unclear, and research efforts are currently directed toward understanding the molecular regulation. We identified ANGPTL4, an adipocytokine, as having a beneficial effect on wound healing in part due to its effect on the integrity of matrix proteins and cell-matrix communication. Given that ANGPTL4 is involved in lipid and glucose homeostasis and that ANGPTL4 decreases blood glucose and improves glucose tolerance in mice (41), it is a prime therapeutic candidate for diseases such as diabetes and for wound healing. A better understanding of its role in wound healing, especially in diabetic and chronic wounds, would provide better wound management. Altogether, ANGPTL4 modulates cell-matrix communications through its interactions with and effects on matrix proteins. Importantly, it provides a novel means by which migrating wound keratinocytes can scrutinize the changes in the wound ECM and modulate their cell behavior.

Acknowledgments—We thank Dr. Samuel Ko and Anna Teo (Carl Zeiss, Singapore Pte Ltd.) for expertise in image acquisition using the LSM710 confocal microscope, Mirax MIDI, and PALM Laser-capture microdissection.

REFERENCES

1. Hynes, R. O. (2002) *Cell* **110,** 673–687
2. Werner, S., and Grose, R. (2003) *Physiol. Rev.* **83,** 835–870
3. Bornstein, P., and Sage, E. H. (2002) *Curr. Opin Cell Biol.* **14,** 608–616
4. Bulcão, C., Ferreira, S. R., Giuffrida, F. M., and Ribeiro-Filho, F. F. (2006) *Curr. Diabetes Rev.* **2,** 19–28
5. Caswell, P. T., and Norman, J. C. (2006) *Traffic* **7,** 14–21
6. Ginsberg, M. H., Partridge, A., and Shattil, S. J. (2005) *Curr. Opin Cell Biol.* **17,** 509–516
7. Giannone, G., and Sheetz, M. P. (2006) *Trends Cell Biol.* **16,** 213–223
8. Tan, N. S., Michalik, L., Desvergne, B., and Wahli, W. (2003) *Am. J. Clin. Dermatol.* **4,** 523–530
9. Grose, R., Werner, S., Kessler, D., Tuckermann, J., Huggel, K., Durka, S., Reichardt, H. M., and Werner, S. (2002) *EMBO Rep.* **3,** 575–582
10. Tan, N. S., Michalik, L., Noy, N., Yasmin, R., Pacot, C., Heim, M., Flühmann, B., Desvergne, B., and Wahli, W. (2001) *Genes Dev.* **15,** 3263–3277
11. Tan, N. S., Michalik, L., Desvergne, B., and Wahli, W. (2004) *Expert Opin. Ther. Targets.* **8,** 39–48
12. Di-Poï, N., Tan, N. S., Michalik, L., Wahli, W., and Desvergne, B. (2002) *Mol. Cell* **10,** 721–733
13. Tan, N. S., Icre, G., Montagner, A., Bordier-ten-Heggeler, B., Wahli, W., and Michalik, L. (2007) *Mol. Cell. Biol.* **27,** 7161–7175
14. Oike, Y., Akao, M., Kubota, Y., and Suda, T. (2005) *Trends Mol. Med.* **11,** 473–479
15. Mandard, S., Zandbergen, F., Tan, N. S., Escher, P., Patsouris, D., Koenig, W., Kleemann, R., Bakker, A., Veenman, F., Wahli, W., Müller, M., and Kersten, S. (2004) *J. Biol. Chem.* **279,** 34411–34420
16. Belanger, A. J., Lu, H., Date, T., Liu, L. X., Vincent, K. A., Akita, G. Y., Cheng, S. H., Gregory, R. J., and Jiang, C. (2002) *J. Mol. Cell Cardiol.* **34,** 765–774
17. Minn, A. J., Gupta, G. P., Siegel, P. M., Bos, P. D., Shu, W., Giri, D. D., Viale, A., Olshen, A. B., Gerald, W. L., and Massagué, J. (2005) *Nature* **436,** 518–524
18. Padua, D., Zhang, X. H., Wang, Q., Nadal, C., Gerald, W. L., Gomis, R. R., and Massagué, J. (2008) *Cell* **133,** 66–77
19. Tan, N. S., Ho, B., and Ding, J. L. (2002) *Protein Eng.* **15,** 337–345
20. Rheinwald, J. G., and Green, H. (1977) *Nature* **265,** 421–424
21. Rheinwald, J. G., and Green, H. (1975) *Cell* **6,** 331–343
22. Schug, T. T., Berry, D. C., Shaw, N. S., Travis, S. N., and Noy, N. (2007) *Cell* **129,** 723–733
23. Chong, H. C., Tan, M. J., Philippe, V., Tan, S. H., Tan, C. K., Ku, C. W., Goh, Y. Y., Wahli, W., Michalik, L., and Tan, N. S. (2009) *J. Cell Biol.* **184,** 817–831
24. Tan, N. S., Michalik, L., Desvergne, B., and Wahli, W. (2005) *J. Biol. Chem.* **280,** 18163–18170
25. Tan, S. H., Pal, M., Tan, M. J., Wong, M. H., Tam, F. U., Teo, J. W., Chong, H. C., Tan, C. K., Goh, Y. Y., Tang, M. B., Cheung, P. C., and Tan, N. S. (2009) *J. Biol. Chem.* **284,** 18047–18058
26. Köster, A., Chao, Y. B., Mosior, M., Ford, A., Gonzalez-DeWhitt, P. A.,

Hale, J. E., Li, D., Qiu, Y., Fraser, C. C., Yang, D. D., Heuer, J. G., Jaskunas, S. R., and Eacho, P. (2005) *Endocrinology* **146,** 4943–4950
27. Chen, L., Tredget, E. E., Wu, P. Y., and Wu, Y. (2008) *PloS one* **3,** e1886
28. Tan, N. S., Ho, B., and Ding, J. L. (2000) *FASEB J.* **14,** 859–870
29. Tan, N. S., Michalik, L., Di-Poï, N., Ng, C. Y., Mermod, N., Roberts, A. B., Desvergne, B., and Wahli, W. (2004) *EMBO J.* **23,** 4211–4221
30. Söderberg, O., Gullberg, M., Jarvius, M., Ridderstråle, K., Leuchowius, K. J., Jarvius, J., Wester, K., Hydbring, P., Bahram, F., Larsson, L. G., and Landegren, U. (2006) *Nat. Methods* **3,** 995–1000
31. Michalik, L., Desvergne, B., Tan, N. S., Basu-Modak, S., Escher, P., Rieusset, J., Peters, J. M., Kaya, G., Gonzalez, F. J., Zakany, J., Metzger, D., Chambon, P., Duboule, D., and Wahli, W. (2001) *J. Cell Biol.* **154,** 799–814
32. Page-McCaw, A., Ewald, A. J., and Werb, Z. (2007) *Nat. Rev. Mol. Cell Biol.* **8,** 221–233
33. Bridge, A. J., Pebernard, S., Ducraux, A., Nicoulaz, A. L., and Iggo, R. (2003) *Nat. Genet.* **34,** 263–264
34. Dellambra, E., Patrone, M., Sparatore, B., Negri, A., Ceciliani, F., Bondanza, S., Molina, F., Cancedda, F. D., and De Luca, M. (1995) *J. Cell Sci.* **108,** 3569–3579
35. Schechtman, D., and Mochly-Rosen, D. (2001) *Oncogene* **20,** 6339–6347
36. Porter, G. W., Khuri, F. R., and Fu, H. (2006) *Semin Cancer Biol.* **16,** 193–202
37. Morfini, G., Szebenyi, G., Elluru, R., Ratner, N., and Brady, S. T. (2002) *EMBO J.* **21,** 281–293
38. Roberts, M. S., Woods, A. J., Dale, T. C., Van Der Sluijs, P., and Norman, J. C. (2004) *Mol. Cell. Biol.* **24,** 1505–1515
39. Knaus, U. G., and Bokoch, G. M. (1998) *Int. J. Biochem. Cell Biol.* **30,** 857–862
40. Legler, D. F., Wiedle, G., Ross, F. P., and Imhof, B. A. (2001) *J. Cell Sci.* **114,** 1545–1553
41. Xu, A., Lam, M. C., Chan, K. W., Wang, Y., Zhang, J., Hoo, R. L., Xu, J. Y., Chen, B., Chow, W. S., Tso, A. W., and Lam, K. S. (2005) *Proc. Natl. Acad. Sci. U.S.A.* **102,** 6086–6091
42. Enomoto, A., Murakami, H., Asai, N., Morone, N., Watanabe, T., Kawai, K., Murakumo, Y., Usukura, J., Kaibuchi, K., and Takahashi, M. (2005) *Dev. Cell* **9,** 389–402
43. Burdick, A. D., Kim, D. J., Peraza, M. A., Gonzalez, F. J., and Peters, J. M. (2006) *Cell. Signal.* **18,** 9–20
44. Denning, M. F. (2004) *Int. J. Biochem. Cell Biol.* **36,** 1141–1146
45. Frank, S., Stallmeyer, B., Kämpfer, H., Kolb, N., and Pfeilschifter, J. (2000) *J. Clin. Invest.* **106,** 501–509

4) Roystan H*, Teo Z*, Chong HC, **Zhu P**, Tan MJ, Tan CK, Lam CRI, SNG MK, David Leong, Tan SM, Ding JL, Li HY, Tan NS. Angiopoietin-like 4 disrupts endothelial integrity via integrin α5β1-mediated Rac/PAK signaling and declustering of VE-cadherin and claudin-5. (*Blood*, in press. *Authors contributed equally).

ANGPTL4 modulates vascular junction integrity by integrin signaling and disruption of intercellular VE-cadherin and claudin-5 clusters.

Royston-Luke HUANG[1,*], Ziqiang TEO[1,*], Han Chung CHONG[1], Pengcheng ZHU[1], Ming Jie TAN[1], Chek Kun TAN[1], Chee Ren Ivan LAM[1], Ming Keat SNG[1], David Tai Wei LEONG[2], Suet Mien TAN[1], Sander KERSTEN[3], Jeak Ling DING[4], Hoi Yeung LI[1], Nguan Soon TAN[1]

[1]School of Biological Sciences, Nanyang Technological University, 60 Nanyang Drive, Singapore 637551.

[2]Department of Chemical and Biomolecular Engineering, National University of Singapore, 4 Engineering Drive 4, Singapore 117576.

[3]Nutrition, Metabolism and Genomics group, Wageningen University, 6700 EV Wageningen, The Netherlands.

[4]Department of Biological Sciences, National University of Singapore, 14 Science Drive, Singapore 117543.

*R.L.H and Z.T. contributed equally to this work.

Abstract

Vascular disruption induced by interactions between tumor-secreted permeability factors and adhesive proteins on endothelial cells facilitates metastasis. The role of tumor-secreted angiopoietin-like 4 (cANGPTL4) in vascular leakiness and metastasis is controversial due to the lack of understanding of how cANGPTL4 modulates vascular integrity. Here, we show that cANGPTL4 instigated the disruption of endothelial continuity by directly interacting with three novel binding partners, integrin α5β1, VE-cadherin and claudin-5, in a temporally sequential manner, thus facilitating metastasis. We showed that cANGPTL4 binds and activates integrin α5β1–mediated Rac1/PAK signaling to weaken cell–cell contacts. cANGPTL4 subsequently associated with and declustered VE-cadherin and claudin-5, leading to endothelial disruption. Interfering with the formation of these cANGPTL4 complexes delayed vascular disruption. *In vivo* vascular permeability and metastatic assays performed using *ANGPTL4*-knockout and wild-type mice injected with either control or ANGPTL4-knockdown tumors confirmed that cANGPTL4 induced vascular leakiness and facilitated lung metastasis in mice. Thus, our findings elucidate how cANGPTL4 induces endothelial disruption. Our findings have direct implications for targeting cANGPTL4 to treat cancer and other vascular pathologies.

Introduction

Tumor metastasis is the main cause of mortality in cancer patients.[1] It is determined largely by vasculature leakiness and the critical steps of intravasation and extravasation, which involve the directional migration of tumor cells across the disrupted endothelium. The endothelium provides a semi-permeable boundary between the bloodstream and tumor. The paracellular permeability of the endothelium is mediated primarily by transmembrane endothelial adherens junction (AJ) and tight junction (TJ) proteins that are linked to the actin cytoskeleton[2], and connect adjacent endothelial cells (ECs).[3] Thus, the disruption of major components of AJs and TJs, such as the intercellular VE-cadherin and claudin-5 clusters leads to changes in the actin cytoskeleton, cell shape and the activation of intracellular signaling pathways, which partly via β-catenin initiate gene transcription.[4] Apart from AJs and TJs, integrins also strengthen EC-EC contacts and provide a scaffold for cytoskeletal reorganization during cell organization, proliferation and migration.[5] Specifically, the expression of integrin α5β1 regulates endothelial monolayer integrity.[6] Inherently, metastasis requires communication between tumor cells and ECs that culminates in the disruption of EC-EC contacts and the degradation of the vascular basement membrane. However, the molecular mechanisms that facilitate such communication are poorly understood.

In the tumor microenvironment, interactions among tumor cells, their secreted factors and the endothelium induce vascular permeability to aid tumor metastasis.[5,7] These factors bind to cognate cellular receptors, setting off a cascade of downstream molecular signaling events that determine the outcome of malignancy.[8,9] In this respect, angiopoietin-like 4 (ANGPTL4) protein has been implicated in cancer metastasis;[10] however, its precise role in vascular and cancer biology remains debatable. Earlier studies suggested that ANGPTL4 could prevent metastasis by inhibiting vascular leakiness.[11,12]

However, ANGPTL4 was identified as one of the most highly expressed genes in distant metastases[13] and it is associated with breast cancer metastasis to the lungs.[14,15] Our recent work revealed that tumors produced high levels of the C-terminal fibrinogen-like domain of ANGPTL4 (henceforth referred to as cANGPTL4). We also showed that cANGPTL4 stimulates integrin-mediated signaling to maintain an elevated, oncogenic $O_2^{\cdot-}$:H_2O_2 ratio to confer anoikis resistance to tumor cells via autocrine adhesion mimicry.[16] Furthermore, we have demonstrated that through interaction with matrix proteins, integrin β1 and integrin β5, cANGPTL4 facilitates cell migration and wound healing, both of which are processes highly reminiscent of metastasis.[17,18] Despite the plethora of evidence implicating ANGPTL4 in cancer metastasis, the heterotypic role of ANGPTL4 in vascular integrity remains unclear.

Here, we show that tumor-derived cANGPTL4 instigated the disruption of endothelial continuity by directly interacting with integrin α5β1, VE-cadherin and claudin-5 in a temporally sequential manner. Tumor-derived cANGPLT4 and recombinant human cANGPTL4 (rh-cANGPTL4) increased vascular permeability *in vitro* and *in vivo*. Using *ANGPTL4*-knockout and wild-type mice injected with either control or ANGPTL4-knockdown tumors confirmed that cANGPTL4 induced vascular leakiness and facilitated lung metastasis in mice. cANGPTL4 binds to and activates integrin α5β1-mediated PAK/Rac signaling which weakened EC-EC contacts and increased vascular leakiness. cANGPTL4 associated with the adhesive domains of VE-cadherin and claudin-5, resulting in their declustering and internalization, translocation of β-catenin to the nucleus and a leaky endothelium. These results identify cANGPTL4 as a novel upstream mediator of endothelium permeability and a potential target in the treatment of cancer and other vascular-related pathologies.

Materials and methods

Antibodies. Antibodies for PAK1 and pPAK1 (Ser199/Ser204) (Cell Signaling, USA) , integrin β1 [JB1A],α5β1[JBS5], β3[2008] and c-Jun (Millipore, USA); CD29/activated integrin β1 [HUTS-21] (BD, USA); β-tubulin, β-catenin [12F7], EGFR[1005] (Santa Cruz Biotechnologies, USA); VE-Cadherin [BV9], Claudin-5 (Abcam, USA); CD31 (DAKO, Denmark); Occludin (Invitrogen, USA); ZO-1(Zymed Laboratories, USA); Tie 1, Tie 2, JAM-C, β-tubulin, horseradish peroxidase (HRP)-conjugated goat anti-mouse, HRP-conjugated goat anti-rabbit, HRP-conjugated donkey anti-goat (Santa Cruz Biotechnologies, USA); mouse monoclonal anti-human cANGPTL4 mAb4A11H5 and rabbit polyclonal anti-human cANGPTL4 were produced in-house[16]; Secondary antibodies Alexa Fluor 488-conjugated goat anti-rabbit IgG and Alexa Fluor 594-conjugated goat anti-mouse IgG were also used (Molecular Probes, USA).

Cell Cultures. Primary human microvascular endothelial cells (HMVECs; Lonza, Switzerland) were cultured in EndoGRO-MV-VEGF medium (Millipore, USA) in a humidified atmosphere of 5% CO_2 at 37 °C. The culture surface was precoated with 0.1% gelatin in PBS. All other cell lines were cultured in DMEM supplemented with 10% FBS. Conditioned medium (CM) was obtained from 1 x 10^5 tumor cells grown in 1 ml of serum-free medium for three days.

Transient transfections assay. Transfections of HMVECs were carried out as per manufacturer's protocol (Promega, USA) with either constitutive-active Rac1 G12V or dominant-negative Rac1 T17N.

Expression and purification of recombinant cANGPTL4 proteins. The expression and purification of full-length ANGPTL4 and recombinant cANGPTL4 were performed as previously described[17,18].

***In Vivo* Tumorigenicity and Miles Vascular Permeability Assay.** Six-week-old BALB/c athymic female nude mice (20-22 g) were injected either cANGPTL4 (6 µg/ml) or 0.9% saline buffer was injected intradermally at adjacent locations on the back. To determine vascular permeability, tumor-bearing mice received an intravenous injection of Evans blue dye. Twenty min later, the mice were sacrificed and Evans blue extracted from the tumor and normal muscle as described in Miles vascular permeability assay.[19] The extravasated dye was extracted using formamide and the amount was quantified by measuring absorbance at 610nm. To determine the tumor vascular volume, 2MDa FITC conjugated dextran (10 mg/kg) was also injected intravenously for 20 min. Fluorescence readings was obtained using Nanodrop 3300 Fluorospectrometer.

For another set of experiments, mice were injected subcutaneously at the interscapular region with either 2×10^6 or 8×10^6 cells (A-5RT3$_{CTRL}$ or A-5RT3$_{\Delta ANGPTL4}$). Same procedures were carried out in C57B/L6J wild-type and ANGPTL4-knockout mice using B16F10$_{CTRL}$ or B16F10 $_{\Delta ANGPTL4}$ cells. Injection sites were rotated to avoid site bias. The injected tumor cells were allowed to grow for eight weeks.

***In Vivo* Metastasis Assay.** Wild type and ANGPTL4-knockout C57BL/6J mice were injected intravenously with either 5×10^5 B16F10$_{CTRL}$ or B16F10$_{\Delta ANGPTL4}$. For cANGPTL4 treatment, wild type C57BL/6J mice i.v injected with either 2×10^6 B16F10$_{CTRL}$ or B16F10$_{\Delta ANGPTL4}$ cells were treated with PBS or cANGPTL4 (3 mg/kg)

thrice weekly. After 3 weeks, the mice were sacrificed and the lungs were harvested for further analyses. Total metastatic burden were quantified by RT-PCR of melanin A. Total mRNA were extracted from lungs and reverse-transcribed as described previously.[17,18]

Proximity Ligation Assay (PLA). PLA was carried out according to the manufacturer's protocol (Olink Bioscience, Sweden) using indicated pairs of antibodies. Images were taken using a Zeiss LSM 710 confocal microscope with a Plan-APOCHROMAT 63x/1.4 oil DIC objective and ZEN 2009 software. PLA signals were quantified using BlobFinder software.[20]

Transendothelial Electrical Resistance (TER) measurement. TER was measured using an electrical cell-substrate impedance sensing system (ECIS, Applied BioPhysics). HMVECs were seeded on sterile 8-well gold-plated electrode arrays precoated with fibronectin at 2 x 10^5 cells/well and allowed to adhere and spread for 4 h at 37 °C. Data from the electrical resistance experiments were obtained over the experimental time course at 5 min intervals. Confluent HMVEC monolayers that had stable TERs for 1 h preceding administration of indicated treatments were used. As cells adhered and spread over the microelectrode, TER increased, whereas cell retraction, rounding or loss of adhesion was reflected by a decrease in TER. Resistance values for each microelectrode were normalized as the ratio of measured resistance to baseline resistance and plotted as a function of time.

Internalization assay. Confluent HMVECs monolayers were treated with either PBS or cANGPTL4 (6 µg/ml) for 3 h. At indicated time point, internalization assay was carried out as previously described.[17]

Immunofluorescence staining. Disrupted tight junctions were visualized by immunofluorescence staining for zona occludens-1 (ZO-1). HMVECs were fixed with 4% paraformaldehyde for 15 min, permeablized with 0.2% Triton-X 100 for 15 min and blocked with 2% bovine serum albumin (BSA) containing 0.1% Triton-X 100 in a humid chamber for 1 h at room temperature. Cells were incubated overnight at 4 °C with anti-human-ZO-1 antibodies (1:100) in 0.2% BSA. Following two washes in PBS, cells were incubated for 1 h at room temperature with Alexa488-secondary antibodies (1:250). Cells were counterstained with Alexa594-phalloidin for F-actin and DAPI for nuclei. Immunostainings performed without primary antibodies served as negative controls. For β-catenin staining, cells were fixed with 4% paraformaldehyde containing 5% sucrose for 15 min, permeablized with 0.5% Triton-X 100 in PBS for 4 min and blocked in 5% normal goat serum (NGS) with 0.1% Triton-X 100. Cells were incubated overnight at 4 ^{o}C with anti-human β-catenin antibodies (1: 200) in 3% NGS, followed by Alexa594-secondary antibodies. Images were acquired using Zeiss LSM 710 confocal microscope with a 63x objective and ZEN 2009 software.

Surface Plasmon Resonance (SPR). SPR was carried out as previously described[17,18] using a BIAcore 2000 system (BIAcore, Uppsala, Sweden). Six concentrations (0.16, 0.32, 0.63, 1.25, 2.50 and 5.0 μM) of recombinant integrin β1, first extracellular domain of VE-cadherin (ECD1), extracellular repeat 1 domain of VE-cadherin (EC1), occludin or JAM-A were used. Integrin was expressed in Drosophila S2 cells[17] and various extracellular domains of VE-cadherin and claudin-5 purchased from Abnova. Global fitting of the SPR data was performed as previously described to determine the K_D. Pre-injection or preincubation with the indicated antibodies or preimmune IgG was

performed to determine specific interactions. Each sensorgram was corrected by subtracting a sensorgram obtained from a reference flow cell with no immobilized protein. The Rmax value was determined to be 283.1 resonance units using anti-cANGTL4 antibodies against the immobilized cANGPTL4. Values are mean±S.D. (n=3)

Statistical Analysis. Statistical analyses were performed using two-tailed Mann-Whitney tests with SPSS software. All statistical tests were two-sided. p value of ≤ 0.05 is considered significant.

Results

Elevated cANGPTL4 expression in human tumors. To examine the expression profile of cANGPTL4 in tumors, we performed immunofluorescence using anti-cANGPTL4 antibody on two human tumor tissue arrays that covered benign, malignant and metastatic tumors originating from various anatomic sites. cANGPTL4 was elevated in all epithelial tumor samples compared to the corresponding normal tissue samples (Figures. S1A-C). Although fluorescence signals varied among different tumor types, they clearly showed that elevated cANGPTL4 was a common feature of tumors. Consistent with the above-mentioned observations, cANGPTL4 protein level was elevated in all cancer cell lines when compared to non-tumorigenic lines (HaCaT and BJ) (Figure S1D). Interestingly, we observed relatively higher cANGPTL4 levels in metastatic than in non-metastatic cancer cell lines, suggesting a role of cANGPTl4 in tumor metastasis. To further corroborate the role of cANGPTL4 in metastasis clinically, we determined cANGPTL4 mRNA and protein levels in six human basal cell carcinoma (benign) and melanoma (metastatic) biopsies by quantitative real-time PCR (qPCR) and immunoblot analyses. We observed significant upregulation of cANGPTL4 mRNA and protein levels in these epithelial cancers when compared with their cognate peri-tumor normal samples (PNSs). Notably, the melanomas expressed higher levels of cANGPTL4 mRNA and protein when compared to benign basal cell carcinoma (Figure 1A, B). Similar trend was observed when comparing cANGPTL4 protein levels of fine-needle aspirates (FNA) from three breast cancer patients to four human metastatic tumor lines (A-5RT3, MDA-MB231, MCF-7 and HT29) and two non-tumorigenic lines (HaCaT and BJ). The mean cANGPTL4 protein concentrations were 12.4 μg/ml (FNA), 5.9 μg/ml (metastatic lines) and 0.8 μg/ml (non-tumorigenic lines) (Figure S1E). These data suggest that epithelial tumors secrete elevated levels of cANGPTL4, which is consistent with our recent report

showing that tumor tissue expressed high levels of cANGPTL4 compared to basal level expression in the surrounding stroma.[16] Altogether, our findings implicate a role for cANGPTL4 in cancer metastasis.

cANGPTL4 increased vascular leakiness in *in vivo* tumors. We next explored the role of cANGPTL4 in tumorigenesis. Metastatic human squamous cell carcinoma cell line A-5RT3 and murine melanoma B16F10 were transduced with either scrambled (control) siRNA (A-5RT3$_{CTRL}$ or B16F10$_{CTRL}$) or siRNA against ANGPTL4 (A-5RT3$_{\Delta ANGPTL4}$ or B16F10$_{\Delta ANGPTL4}$) (Figure S2A) to suppress endogenous ANGPTL4, as previously described.[16,18] The injection of A-5RT3$_{CTRL}$ cells into immunodeficient mice induced large primary tumors at week 8, but A-5RT3$_{\Delta ANGPTL4}$–induced tumors displayed a 30% lower tumor volume (A-5RT3$_{CTRL}$ 1098±422 mm^3 v.s A-5RT3$_{\Delta ANGPTL4}$ 551±135mm^3, P<0.05, n=6) (Figure 1C). Miles assays revealed decreased vascular leakiness in A-5RT3$_{\Delta ANGPTL4}$-induced tumors (~5 fold lower), as evidenced by decreased extravasation of Evans blue dye (Figure 1D, Table 1). Differences in vascular volume among the tumor types were accounted for when determining tumor vascular permeability (Table 1). This differential vascular permeability was independent of the tumor volume, as observed in A-5RT3$_{CTRL}$- and A-5RT3$_{\Delta ANGPTL4}$-induced tumors (Figure 1D). Furthermore, none of the mice injected with A-5RT3$_{\Delta ANGPTL4}$ developed distant metastases to the lymph nodes, whereas 83% of mice injected with A-5RT3$_{CTRL}$ showed metastases (Figure S2B). Notably, rh-cANGPLT4 was sufficient to induce vascular leakiness when compared to the PBS control (rh-cANGPTL4 0.084±0.014 v.s PBS 0.04 ± 0.01, P<0.05, n=3) (Figures 1E, F). Consistent to the increased vascular volume in A-5RT3$_{CTRL}$- and B16F10$_{CTRL}$-induced tumors, the expression of EC marker CD31 was elevated when compared with their cognate ANGPTL4-deficient tumors (Figure 1G, H). Dual immunostaining for

CD31 and cANGPTL4 also confirmed that epithelial tumors were the major producer of cANGPTL4, consistent with earlier findings using laser-captured microdissected samples (Figures 1H).[16] Hence, these observations *in vivo* prompted us to investigate the molecular mechanism of cANGPTL4-induced endothelial permeability.

Confluent primary human microvascular ECs were cultured in 3-day-old CM from either A-5RT3$_{CTRL}$ or A-5RT3$_{\Delta ANGPTL4}$ cells. EC junction integrity was disrupted when the cells were cultured in A-5RT3$_{CTRL}$ CM, but not in A-5RT3$_{\Delta ANGPTL4}$ CM, as indicated by ZO-1 staining. Junction integrity was maintained in the presence of anti-cANGPTL4 monoclonal antibody, suggesting that tumor-secreted cANGPTL4 plays a major role in endothelial junction disruption (Figure 1I). We found that EC-EC junction integrity was disrupted when the cells were treated with only rh-cANGPTL4 (6 μg/ml) in the presence of either cycloheximide or actinomycin D, indicating that *de novo* protein synthesis and transcription were not required (Figure S2C). Treatment with cycloheximide, actinomycin D or vehicle alone did not induce any vascular lesions (Figure S2C). This disruption was mirrored by a decreased in the transendothelial electrical resistance (TER) of the monolayer, suggesting a rapid and dose-dependent increase in paracellular permeability (Figure 1J). No change in TER was observed in the PBS control (Figure 1J). This effect was not due to apoptosis, even after 6 h of rh-cANGPTL4 treatment (Figure S2D). Altogether, these results indicate that tumor-secreted cANGPTL4 disrupts endothelial integrity.

cANGPTL4 interacts with integrin α5β1, VE-cadherin and claudin-5. VE-cadherin and claudin-5 contribute to the control of paracellular permeability, while integrin α5β1, which is localized to EC-EC junctions, also mediates endothelial leakiness.[4,6] Hence, we hypothesized that tumor-derived cANGPTL4 induces vascular leakiness and ultimately

disrupts the endothelium barrier via direct interactions with specific junction proteins. Surface plasmon resonance (SPR) analysis revealed that cANGPTL4 interacted with VE-cadherin (K_D=1.12x10^{-7} M), claudin-5 (K_D=5.87x10^{-8} M) and integrin α5β1 (K_D= 1.26x10^{-8} M), but not with occludin or JAM-A (Figure 2A). More significantly, cANGPTL4 targeted the VE-cadherin EC1 domain and claudin-5 ECD1 domain, which are responsible for homophilic interactions between adjacent ECs, suggesting that the interactions of cANGPTL4 with VE-cadherin and claudin-5 could play an important role in regulating vascular permeability (Figure 2B).[21,22] No interactions were observed between cANGPTL4 and integrin β3[16,17] or other domains of VE-cadherin (EC3) and claudin-5 (ECD2), which also served as controls (Figure 2B). The observations of these interactions were corroborated by blocking with neutralizing antibodies against integrin α5β1 (Figure 2C), VE-cadherin (Figure 2D), claudin-5 (Figures 2E) and cANGPTL4 (Figures S3A-C). An *in situ* proximity ligation assay (PLA) detected complexes of integrin α5β1, claudin-5 or VE-cadherin with cANGPTL4 in both EC (integrin 22.50±5.01; VE-cadherin 16.43±2.46; claudin-5 12.35±3.44 PLA spots/cell calculated from 250 cells) and A-5RT3$_{CTRL}$-induced tumor biopsies (Figure 2F, S3D), confirming that these interactions also exists *in vivo*. No PLA signals, i.e. no interactions were observed between CD31 and cANGPTL4, claudin-5, VE-cadherin or integrin α5β1 (Figure S3E).

cANGPTL4 interacted directly with the EC1 and ECD1 adhesive domains of VE-cadherin and claudin-5, respectively, which may lead to disruption of intercellular VE-cadherin and claudin-5 cluster formation.[23] To examine this, membrane fractions of confluent ECs treated with cANGPTL4 were extracted, resolved under native conditions, and probed with either anti-VE-cadherin or anti-claudin-5. cANGPTL4 treatment resulted in smaller protein bands when compared with PBS (Figure 2G). Treatment with EDTA,

which disrupts intercellular adhesion, served as a positive control for declustered VE-cadherin and claudin-5. These findings confirm that cANGPTL4 interacts with integrin α5β1, VE-cadherin and claudin-5 to disrupt intercellular adhesion.

cANGPTL4 modulates endothelial integrity in a temporally sequential mechanism. Next, we sought a mechanistic explanation for the effect of cANGPTL4 on the endothelium. We monitored the temporal interactions of cANGPTL4 and its three binding partners through kinetic PLA. A bimodal interaction profile of the cANGPLT4:integrin α5β1 complex was detected within 30-60 min, followed by cANGPTL4:VE-cadherin and cANGPTL4:claudin-5 at 120 min post-cANGPTL4 treatment (Figure 3A). *In vitro* co-immunoprecipitation of cANGPTL4 and its various interacting partners validated our PLA and SPR results (Figure 3B). Except for integrin α5β1, which showed elevated expression only 2 h post-cANGPTL4 treatment, no change in protein level was observed for any other cANGPTL4-interacting partner, indicating that the bimodal cANGPTL4-protein interaction profiles did not result from increased protein expression (Figure S4A). We also showed that the initial cANGPTL4:integrin α5β1 interactions resulted in the complex being internalized into the cytoplasm at 40 min, followed by the internalization of the cANGPTL4:VE-cadherin and cANGPTL4:claudin-5 complexes between 120-150 min to result in the abrogation of the endothelial junctions (Figure 3C). This bimodal effect was not observed with the control treatment (Figure S4B). Notably, cANGPTL4:integrin α5β1 formation at 30-60 min coincided with a TER decrease, suggesting increased permeability (Figure 1K). Integrin β3, which does not interact with cANGPTL4, was internalized after 2 h in both vehicle and cANGPTL4-treated cells. Similar observations were also reported in wild-type and ANGPTL4-knockdown keratinocytes[17], suggesting that this may be inherent to either integrin β3 or

the experimental procedure. Thus, our results suggest that the initial interaction of cANGPTL4 with integrin α5β1 may be required to facilitate the subsequent interactions to mediate vascular disruption.

Inhibition of the cANGPTL4:integrin α5β1 complex delays cANGPTL4 interactions with VE-cadherin and claudin-5. Antibody to integrin α5β1 increased endothelial leakiness, but was insufficient to induce microscopic lesions at endothelial junctions.[6] Thus, we sought to understand the impact of the upstream cANGPTL4:integrin α5β1formation on the disruption of endothelial integrity. In the presence of monoclonal anti-integrin α5β1, cANGPTL4 required twice the length of time (6 h) to induce lesions along the EC-EC contact compared to the cANGPTL4 alone (Figure 4A). Anti-integrin α5β1 blocked the interaction with cANGPTL4 (Figure 2E). ECs treated with anti-integrin α5β1 alone did not induce any lesions, even after 6 h (Figure 4A). These results were corroborated by our TER data, which showed that the addition of anti-integrin α5β1 and cANGPTL4 (6 μg/ml) to ECs resulted in reduced endothelial permeability when compared with ECs treated only with 6 μg/ml cANGPTL4 (Figure 4B). Accordingly, anti-integrin α5β1 caused a concomitant delay of ~90 min in the interaction profile of cANGPTL4:VE-cadherin and cANGPTL4:claudin-5 when compared to control (compare Figures 4C and 3A). The mean fold change (0.4±0.12) in the interactions between cANGPTL4 and these 2 proteins remained similar, albeit with a non-significant decrease of ~10% for VE-cadherin, suggesting that interactions with these 2 proteins are required for endothelial disruption (Figure 4C). Thus, we treated HMVECs with cANGPTL4 for 90 min, which allowed for cANGPTL4:integrin α5β1 interactions and initiated endothelial leakiness, followed by its removal. Immunostaining for ZO-1 revealed that cANGPTL4:integrin α5β1 interactions alone is not sufficient to induce endothelial

disruption, and that the later interactions are necessary for the observed disruption. (Figure 4D). Interestingly, we observed from our TER data that the removal of rh-cANGPTL4 promoted a "reversal effect" on endothelial permeability, conceivably due to the "re-zipping" of the EC–EC contacts, thus reinforcing the important of cANGPTL4:integrin α5β1complex formation in the entire process of endothelial disruption (Figure 4E). Hence, our results suggest that although integrin α5β1 is an essential player, its interaction with cANGPTL4 alone is insufficient to induce an endothelial disruption/lesion. The data suggest that the binding of cANGPTL4 to integrin α5β1 triggers internalization of the complex and "un-zipping" of the endothelial junctions to first promote endothelial leakiness. This facilitates the subsequent cANGPTL4 interactions with the adhesive domains of VE-cadherin and claudin-5 that weaken their homophilic contacts, resulting in their declustering and internalization and finally culminating in the disruption of EC–EC contacts.

cANGPTL4-induced disruption of the endothelium involves integrin-mediated PAK/Rac signaling. The pivotal role of integrin α5β1 in the process of EC-EC contact disruption lead us to examine the detailed molecular events resulting from the cANGPTL4:intergrin α5β1 complex formation. *In vitro* co-immunoprecipitation of cANGPTL4 with activated integrin β1 (antibody clone Huts-21) indicated that integrin was activated upon association with cANGPTL4 (Figure 5A, B). No interactions were observed between cANGPTL4 and Tie1, Tie2, integrin β3 or the junction protein JAM-C (Figure 5B). Rac-GTP and PAK are downstream mediators of integrin signaling, whose roles in endothelial contractility and barrier function are well recognized.[24,25] Our co-immunoprecipitation results showed that ANGPTL4- activated integrin β1 also stimulates the activation of Rac1 and phosphorylation of PAK, when compared to PBS-treated ECs

(Figure 5C). The increased cANGPTL4:integrin α5β1 interaction and activation of PAK/Rac1 signaling coincided with endothelial leakiness (Figure 1J), possibly by modulating integrin-mediated intercellular adhesion and contractility.[24,26] To further underscore the role of Rac1, we transfected ECs with either constitutive active Rac1(G12V) or dominant-negative Rac1(T17N). Transfection of ECs with Rac1(G12V) accelerated the formation of cANGPTL4:VE-cadherin and cANGPTL4:claudin-5 complexes, while the expression of Rac1(T17N) delayed the complex delayed the complex formation (compare Figures 3A and 5D). This suggests that cANGPTL4 regulates endothelial integrity via the integrin α5β1-mediated Rac/PAK signaling axis, which functions via signaling cross-talk to facilitate cANGPTL4 interactions with VE-cadherin and claudin-5, ultimately leading to vascular disruption.

cANGPTL4 modulates the nuclear translocation of β-catenin. The perturbations and disassembly of VE-cadherin result in the translocation of membrane β-catenin to the nucleus.[27,28] Hence, we asked if cANGPTL4-induced declustering of VE-cadherin and claudin-5 resulted in nuclear translocation of β-catenin. In PBS-treated ECs, β-catenin formed a continuous lining along the cell margin as indicated by the immunofluorescence staining and intensity plot (Figure 6A and S5A), whereas treatment with either cANGPTL4 (6 μg/ml for 3 h) or 2.5 mM EDTA (positive control) resulted in the disappearance of the β-catenin margin and accumulation in the nuclei, indicating cell-cell junction disruption (Figure 6A and S5A). To better define the localization of β-catenin, we performed PLA that showed β-catenin in the nuclei at 180 min (β-catenin spots/nucleus increases from 1.2±0.81 at 0 min to 17.5±2.68 at 180 min, while those outside the nucleus decreases from 26.3±3.29 to 9.44±3.98); this timing coincided with the declustering of VE-cadherin and claudin-5 (Figure 6B). Immunoblot analysis

corroborated our PLA data (Figure 6C). Taken together, our data indicate that tumor-derived cANGPTL4 is a permeability-inducing factor capable of triggering endothelial disruption via sequential interactions with integrin α5β1, VE-cadherin and claudin-5, resulting in the accumulation of nuclear β-catenin (Figure 6D).

cANGPTL4 promotes metastasis to the lungs *in vivo*. To further investigate the role of cANGPTL4 in the metastatic process and to substantiate its biological relevance in cancer, we examined its effect on lung metastasis using two different mice models. Wild-type C57BL/6J mice (n=12 per group) were injected intravenously with either $B16F10_{CTRL}$ or $B16F10_{\Delta ANGPTL4}$ cells (2×10^6) and treated intravenously with either PBS or rh-cANGPTL4. Mice inoculated with $B16F10_{\Delta ANGPTL4}$ had significantly fewer lung metastases compared with $B16F10_{CTRL}$-injected mice. Intravenous administration of rh-cANGPTL4 enhanced lung metastases in both cases, as evidenced by real-time PCR analysis for melanin A, a marker of melanoma (Figure 7A, B). Cross-section staining of the lung tissues corroborated our *in vivo* data (Figure 7C and S5B), underscoring the biological metastatic potential of cANGPTL4 in tumor cells (Figure 7A, B). Additionally, we examined lung metastases using wild-type ($ANGPTL^{+/+}$) and *ANGPTL4*-knockout ($ANGPTL4^{-/-}$) mice injected with either 0.5×10^5 $B16F10_{CTRL}$ or $B16F10_{\Delta ANGPTL4}$. There was a significantly reduced number of tumor nodules in the lungs of $ANGPTL4^{-/-}$ when compared with $ANGPTL4^{+/+}$ mice, suggesting that metastasis of $B16F10_{CTRL}$ was impaired (Figure 7D, E). Altogether, our data indicate cANGPTL4 is a pro-metastatic tumor-derived factor and provide new insights into the mechanistic action of this protein in cancer.

Discussion

Metastasis requires dynamic tumor-endothelium communication through tumor-secreted vascular permeability factors to breach the endothelial barrier, thereby allowing the migration and invasiveness of the tumor cells across the endothelium. Hence, a better understanding of the mechanism by which such vascular permeability factors disrupt endothelial integrity could offer new therapeutic strategies. Recent studies have implicated a role for ANGPTL4 in metastasis,[10] yet the mechanism by which ANGPTL4 modulates endothelial junction integrity remains unknown. Here, we provide insight into the heterotypic role of cANGPTL4 in vascular integrity. We show that cANGPTL4 disrupts intercellular adhesion via a novel integrin α5β1-mediated Rac/PAK signaling pathway and the declustering and internalization of VE-cadherin and claudin-5, resulting in nuclear accumulation of β-catenin. Using two different mouse models, our *in vivo* vascular permeability and metastatic assays confirmed that cANGPTL4 acts as a vascular permeability factor by inducing vascular leakiness and disruption. Interestingly, ANGPTL4-deficient tumors also showed decreased vascularisation, suggesting that cANGPTL4 may facilitate metastasis through increased vascular permeability and volume.

EC-EC adhesion is mediated mainly by the α5β1 integrin and EC-specific adhesion complexes containing VE-cadherin and claudin-5. [6,29] Our work shows that cANGPTL4 interacts with these three adhesive complexes in a sequential manner to disrupt the endothelial junctions. A major route by which integrins regulate cell-cell contacts is the Rac/PAK pathway, leading to modulation of EC contractility.[24,30 31] We show that the initial interaction between cANGPTL4 and integrin α5β1 activates Rac and phosphorylate PAK, weakening cell–cell contacts and increasing endothelial leakiness. This facilitates cANGPTL4 access to the adhesive domains of VE-cadherin and claudin-5

to induce declustering of the adhesion molecules resulting in vascular disruption. We and others have shown that ANGPTL4 does not bind the angiopoietin receptor Tie1 or Tie2 to antagonize its action. Angiopoietin-1–mediated activation of Rac reduces vascular leak in the context of VEGF-induced vascular permeability. Thus, the role of Rac in vascular permeability is complex. The ligand and the cellular context that activate Rac will dictate its effect on vascular junction integrity.

The activation of Rac/PAK signaling trigger by cANGPTL4-bound integrin β1 is necessary to facilitate cANGPTL4 access to VE-cadherin and claudin-5 and to trigger vascular disruption. By preventing the association of cANGPTL4 with integrin β1 by anti-integrin β1, we observed delayed cANGPTL4:VE-cadherin and cANGPTL4:claudin-5 complexes formation and a concomitant decreased vascular permeability. Similar delay in cANGPTL4:VE-cadherin and cANGPTL4:claudin-5 complexes formation were also detected in ECs expressing dominant-negative Rac1, without affecting the cANGPTL4:integrin β1 formation. This indicates that the Rac/PAK signaling acts downstream of integrin and facilitates cANGPTL4 interactions with VE-cadherin and claudin-5. Interestingly, by preventing the subsequent cANGPTL4 interaction with VE-cadherin and claudin-5, the initial increased in vascular permeability due to the activation of integrin-mediated Rac/PAK signaling did not propagated to observable vascular lesions. This confirms that Rac/PAK signaling is necessary to potentiate the vascular disruptive effect of cANGPTL4.

The interactions of cANGPTL4 with the VE-cadherin ED1 and claudin-5 EDC1 domains disrupt VE-cadherin and claudin-5 clustering. The EC intercellular clustering of VE-cadherin and claudin-5, mediated by their extracellular domains, is important for the maintenance of a semi-permeable boundary between the bloodstream and the tumor.[21,22,32] Our results also reveal a time-dependent cellular trafficking of β-catenin

from the membrane to the nucleus in cANGPTL4-treated ECs, coinciding with endothelial disruption. The interactions between the cytoplasmic tail of VE-cadherin and the catenins are essential for the proper functioning of stable AJs.[28] The nuclear accumulation of β-catenin in leaky endothelium and release of β-catenin from AJ junctions into the nucleus is consistent with the declustering of AJs.[27,28,33] Moreover, the membrane-liberated β-catenin induces gene transcription that contributes to angiogenic responses of ECs following episodes of vascular leakage that promotes tumor metastasis.[34-36]

The role of ANGPTL4 in vascular leakiness, and thus metastasis, is controversial[10,12,37], and efforts to confirm it have been further hampered by the lack of understanding of the mechanistic action of ANGPTL4. We show that cANGPTL4 behaves as a vascular permeability factor and disrupts endothelial integrity via integrin α5β1-mediated Rac/PAK signaling and the declustering and internalization of VE-cadherin and claudin-5. The reason for the apparent discrepancy is unclear, but it may be due to the position of fusion tags in recombinant ANGPTL4. Studies that suggest an inhibitory role of ANGPTL4 in vascular leakiness have used a C-terminal fusion ANGPTL4, while our work and that of others who have presented evidence that ANGPTL4 is a pro-metastatic agent that induces endothelial permeability has utilize either an N-terminal fusion ANGPTL4 or un-tagged ANGPTL4. A dysfunctional endothelium usually presents as a leaky or disrupted vasculature and is characteristic of many pathological conditions, including inflammatory edema, diabetes, atherosclerosis, and cancer metastasis.[33,38] The disruption of EC-EC contacts is a major route exploited by primary tumors to promote metastasis. Our findings suggest that targeting cANGPTL4 to treat metastasis and vascular-related diseases could be a viable option.

Acknowledgements

This work was supported by grants from Ministry of Education, Singapore (ARC18/08), Nanyang Technological University, Singapore (RG127/05, RG82/07) and Biomedical Research Council (10/1/22/19/644).

Contribution: R.L.H and Z.T. performed experiments, analyzed the results and wrote the article; H.C.C., P.Z., M.J.T. C.K.T., C.R.I.L. and M.K.S. performed experiments; D.T.W.L. and S.M.T. performed experiments, contributed to discussion; S.K., J.L.D. and H.Y.L. analyzed the results, contributed to discussion, edited the article; N.S.T. analyzed the results, contributed to discussion, reviewed and edited the article.

Conflict-of-interest disclosure: The authors declare no competing financial interests.

Correspondence: Nguan Soon TAN, School of Biological Sciences, Nanyang Technological University, 60 Nanyang Drive, Singapore 637551; email: nstan@ntu.edu.sg; Tel: +65-6316-2941; Fax: +65-67913856

References

1. Yilmaz M, Christofori G, Lehembre F. Distinct mechanisms of tumor invasion and metastasis. *Trends Mol Med* 2007;13(12):535-541.

2. Dejana E. Endothelial cell-cell junctions: happy together. *Nat Rev Mol Cell Biol* 2004;5(4):261-270.

3. Komarova Y, Malik AB. Regulation of endothelial permeability via paracellular and transcellular transport pathways. *Annu Rev Physiol* 2010;72:463-493.

4. Bazzoni G, Dejana E. Endothelial cell-to-cell junctions: molecular organization and role in vascular homeostasis. *Physiol Rev* 2004;84(3):869-901.

5. Desgrosellier JS, Cheresh DA. Integrins in cancer: biological implications and therapeutic opportunities. *Nat Rev Cancer* 2010;10(1):9-22.

6. Lampugnani MG, Resnati M, Dejana E, Marchisio PC. The role of integrins in the maintenance of endothelial monolayer integrity. *J Cell Biol* 1991;112(3):479-490.

7. Joyce JA, Pollard JW. Microenvironmental regulation of metastasis. *Nat Rev Cancer* 2009;9(4):239-252.

8. Guo W, Giancotti FG. Integrin signalling during tumour progression. *Nat Rev Mol Cell Biol* 2004;5(10):816-826.

9. Thijssen VL, Barkan B, Shoji H et al. Tumor cells secrete galectin-1 to enhance endothelial cell activity. *Cancer Res* 2010;70(15):6216-6224.

10. Padua D, Zhang XHF, Wang Q et al. TGFbeta primes breast tumors for lung metastasis seeding through angiopoietin-like 4. *Cell* 2008;133(1):66-77.

11. Galaup A, Cazes A, Le JS et al. Angiopoietin-like 4 prevents metastasis through inhibition of vascular permeability and tumor cell motility and invasiveness. *Proc.Natl.Acad.Sci.U.S.A* 2006;103(49):18721-18726.

12. Ito Y, Oike Y, Yasunaga K et al. Inhibition of angiogenesis and vascular leakiness by angiopoietin-related protein 4. *Cancer Res.* 2003;63(20):6651-6657.

13. Hu Z, Fan C, Livasy C et al. A compact VEGF signature associated with distant metastases and poor outcomes. *BMC Med* 2009;7:9.

14. Minn AJ, Gupta GP, Siegel PM et al. Genes that mediate breast cancer metastasis to lung. *Nature* 2005;436(7050):518-524.

15. Minn AJ, Gupta GP, Padua D et al. Lung metastasis genes couple breast tumor size and metastatic spread. *Proc Natl Acad Sci U S A* 2007;104(16):6740-6745.

16. Zhu P, Tan MJ, Huang RL et al. Angiopoietin-like 4 protein elevates the prosurvival intracellular O2(-):H2O2 ratio and confers anoikis resistance to tumors. *Cancer Cell*

2011;19(3):401-415.

17. Goh YY, Pal M, Chong HC et al. Angiopoietin-Like 4 Interacts with Integrins {beta}1 and {beta}5 to Modulate Keratinocyte Migration. *Am J Pathol* 2010;177(6):2791-2803.

18. Goh YY, Pal M, Chong HC et al. Angiopoietin-like 4 interacts with matrix proteins to modulate wound healing. *J Biol Chem* 2010;285(43):32999-33009.

19. Ito Y, Oike Y, Yasunaga K et al. Inhibition of angiogenesis and vascular leakiness by angiopoietin-related protein 4. *Cancer Res.* 2003;63(20):6651-6657.

20. Allalou A, Wählby C. BlobFinder, a tool for fluorescence microscopy image cytometry. *Comput Methods Programs Biomed* 2009;94(1):58-65.

21. Wen H, Watry DD, Marcondes MCG, Fox HS. Selective decrease in paracellular conductance of tight junctions: role of the first extracellular domain of claudin-5. *Mol Cell Biol* 2004;24(19):8408-8417.

22. Taveau JC, Dubois M, Le Bihan O et al. Structure of artificial and natural VE-cadherin-based adherens junctions. *Biochem Soc Trans* 2008;36(Pt 2):189-193.

23. Taddei A, Giampietro C, Conti A et al. Endothelial adherens junctions control tight junctions by VE-cadherin-mediated upregulation of claudin-5. *Nat Cell Biol* 2008;10(8):923-934.

24. Stockton RA, Schaefer E, Schwartz MA. p21-activated kinase regulates endothelial permeability through modulation of contractility. *J Biol Chem* 2004;279(45):46621-46630.

25. Galan Moya EM, Le Guelte A, Gavard J. PAKing up to the endothelium. *Cell Signal* 2009;21(12):1727-1737.

26. Gimond C, van Der Flier A, van Delft S et al. Induction of cell scattering by expression of beta1 integrins in beta1-deficient epithelial cells requires activation of members of the rho family of GTPases and downregulation of cadherin and catenin function. *J Cell Biol* 1999;147(6):1325-1340.

27. Beckers CML, García-Vallejo JJ, van Hinsbergh VWM, van Nieuw Amerongen GP. Nuclear targeting of beta-catenin and p120ctn during thrombin-induced endothelial barrier dysfunction. *Cardiovasc Res* 2008;79(4):679-688.

28. Conacci-Sorrell M, Zhurinsky J, Ben-Ze'ev A. The cadherin-catenin adhesion system in signaling and cancer. *J Clin Invest* 2002;109(8):987-991.

29. Hanahan D, Weinberg RA. The hallmarks of cancer. *Cell* 2000;100(1):57-70.

30. Miyamoto Y, Reddig P, Juliano RL. Regulation of signal transduction by integrins. *Handb Exp Pharmacol* 2004;(165):197-216.

31. Hoang MV, Nagy JA, Senger DR. Active Rac1 improves pathologic VEGF neovessel architecture and reduces vascular leak: mechanistic similarities with angiopoietin-1. *Blood* 2011;117(5):1751-1760.

32. Sumpio BE, Riley JT, Dardik A. Cells in focus: endothelial cell. *Int J Biochem Cell Biol* 2002;34(12):1508-1512.

33. Harris ES, Nelson WJ. VE-cadherin: at the front, center, and sides of endothelial cell organization and function. *Curr Opin Cell Biol* 2010;22(5):651-658.

34. Skurk C, Maatz H, Rocnik E, Bialik A, Force T, Walsh K. Glycogen-Synthase Kinase3beta/beta-catenin axis promotes angiogenesis through activation of vascular endothelial growth factor signaling in endothelial cells. *Circ Res* 2005;96(3):308-318.

35. Conacci-Sorrell M, Zhurinsky J, Ben-Ze'ev A. The cadherin-catenin adhesion system in signaling and cancer. *J Clin Invest* 2002;109(8):987-991.

36. Beckers CML, García-Vallejo JJ, van Hinsbergh VWM, van Nieuw Amerongen GP. Nuclear targeting of beta-catenin and p120ctn during thrombin-induced endothelial barrier dysfunction. *Cardiovasc Res* 2008;79(4):679-688.

37. Le Jan S, Amy C, Cazes A et al. Angiopoietin-like 4 is a proangiogenic factor produced during ischemia and in conventional renal cell carcinoma. *Am J Pathol* 2003;162(5):1521-1528.

38. Fukumura D, Duda DG, Munn LL, Jain RK. Tumor microvasculature and microenvironment: novel insights through intravital imaging in pre-clinical models. *Microcirculation* 2010;17(3):206-225.

FIGURE LEGENDS

Figure 1: cANGPTL4 is elevated in metastatic tumors and disrupts endothelial junction integrity.

(A, B) Expression levels of cANGPTL4 mRNA (A) and protein (B) in basal cell carcinoma (BCCs) and metastatic melanoma paired with peri-tumor normal tissues as determined by qPCR and immunoblot, respectively (n=3). Data spots from same individual are linked by colored lines. Ribosomal protein L27 (L27) was used as a reference housekeeping gene. β-tubulin served as a loading and transfer control.

(C, D) Evan's blue dye extravasation induced by either A-5RT3$_{CTRL}$-, A-5RT3$_{\Delta ANGPTL4}$-induced tumors of different (C) or similar (D) tumor volume. (A-5RT3$_{CTRL}$ 1098±422 mm^3 v.s A-5RT3$_{\Delta ANGPTL4}$ 551±135mm^3, $P < 0.05$, n=6)

(E, F) Evan's blue dye extravasation induced by cANGPTL4 or PBS vehicle (G) and quantification (H) of extravasated Evan's blue dye by measurement of absorbance at 610nm. *, $P < 0.05$.

(G) Immunodetection of CD31 in A-5RT3$_{CTRL}$-, A-5RT3$_{\Delta ANGPTL4}$-induced tumors.

(H) Immunofluorescence staining for CD31 and cANGPTL4 in B16F10$_{CTRL}$- and B16F10$_{\Delta ANGPTL4}$-induced tumors. Scale bar: 100 μm.

(I) Immunofluorescence staining for ZO-1 in a confluent HMVEC monolayer. Cells were treated with either CM from A-5RT3$_{CTRL}$ in the presence or absence of anti-cANGPTL4, from A-5RT3$_{\Delta ANGPTL4}$ cells. HMVECs were counterstained with DAPI (blue) for nuclei and phalloidin (red) for actin stress fibers. Scale bar: 40 μm. White arrows indicate endothelial junction lesions.

(J) Transendothelial electrical resistance (TER) analysis of confluent monolayer HMVECs treated with the indicated amounts of cANGPTL4. PBS served as a vehicle control. Data (means±S.D.) from 3 independent experiments.

Figure 2: **cANGPTL4 interacts with integrin α5β1, VE-cadherin and claudin-5.**

(A-E) Representative sensorgrams showing binding profiles between immobilized-cANGPTL4 and integrin α5β1, VE-cadherin, claudin-5, occludin and junctional adhesion molecule A (JAM-A) (A); VE-cadherin extracellular repeat domain 1(EC1), claudin-5 first extracellular domain (ECD1), VE-cadherin EC3 and claudin-5 ECD2 (B); Integrin α5β1 (C),VE-cadherin (D) and claudin-5 (E) pre-blocked with either preimmune IgG or indicated cognate antibodies.

(F) *In situ* proximity ligation assay (PLA) of cANGPTL4 and indicated binding partners. PLA signals are in red (Integrin 22.50±5.01 v.s VE-cadherin 16.43±2.46 v.s claudin-5 12.35±3.44 PLA spots/cell for 250 cells, n=3). Cells were counterstained with Alexa488-phallodin for actin stress fibers (green) and Hoechst dye for nuclei (blue). Negative control was performed in the absence of anti-ANGPTL4. Scale bar: 40 μm.

(G) Immunodetection of VE-cadherin and claudin-5 from membrane extract of HMVECs treated with cANGPTL4 (3 or 6 μg/ml) for 3 h. Vehicle (v) is PBS, and E indicates treatment with 2.5 mM EDTA in PBS.

Figure 3: cANGPTL4 interacts with integrin α5β1, VE-cadherin and claudin-5 in a bimodal manner.

(A) *In situ* kinetic PLA detection of various complexes between cANGPTL4 and indicated binding partners in HMVECs treated with 6 μg/ml of cANGPTL4. Values (means±S.D.) represent mean fold change in the number of interactions compared to the zero time point, as determined from n=3 independent experiments (600 HMVECs) using BlobFinder. Experiments were terminated when microscopic lesions were observed at 180 min post-cANGPTL4 treatment.

(B) Immunodetection of integrin α5β1, VE-cadherin and claudin-5 in anti-cANGPTL4 immunoprecipitates from total protein lysates of HMVECs treated with 6 μg/ml rh-cANGPTL4.

(C) Immunodetection of integrins β1, integrin α5, integrin β3, VE-cadherin and claudin-5 from total protein lysate versus internalized fraction of HMVECs treated with cANGPTL4. Protein lysates were collected every 10 minutes (0-180 minutes). Values below each band represent the mean fold change in protein expression level compared with the cognate zero time point (n=3). *, $P < 0.05$; **, $P < 0.01$.

Figure 4: Inhibition of cANGPTL4:interacting partner complex formation delays endothelial disruption.

(A, B and D, E) Immunofluorescence staining for ZO-1 (A, D) and transendothelial electrical resistance (TER) measurement (B, E) in confluent HMVEC monolayer. Cells were treated with either 6 μg/ml of cANGPTL4 in the presence of increasing anti-integrin β1 concentrations (1:100, 1:50) (A, B) or 6 μg/ml of cANGPTL4 followed by removal of exogenous cANGPTL4 at 90 min (D, E). Treatments were for 3 or 6 h. HMVECs were counterstained with DAPI (blue) for nuclei and phalloidin (red) for actin stress fibers. Scale bar: 40 μm. White arrows indicate endothelial junction lesions. . Data (means±S.D.) from 3 independent experiments. *, $P < 0.05$; **, $P < 0.01$.

(C) *In situ* kinetic PLA detection of cANGPTL4: indicated binding partner complexes in cANGPTL4-treated HMVECs in the presence of anti-integrin β1. Values (means±S.D.) represent mean fold change in the number of interactions compared to the zero time point, as determined from n=3 independent experiments (~600 HMVECs) using BlobFinder. Experiments were terminated when microscopic lesions were observed (360 minutes post-cANGPTL4 treatment).

Figure 5: cANGPTL4-activated Integrin β1 mediates vascular permeability via activated Rac/PAK signaling axis.

(A, B) Immunodetection of indicated proteins in anti-Huts-21 (A) and anti-cANGPTL4 (B) immunoprecipitates from total protein lysates of rh-cANGPTL4-treated HMVECs (6 μg/ml). IgG immunoprecipitates serves as control.

(C) Immunodetection of indicated proteins from anti-Huts-21 immunoprecitates of HMVECs treated with either vehicle (PBS) or rh-cANGPTL4. Total integrin β1, Rac1 and PAK served as controls. Protein lysates were collected every 20 minutes (0-180 minutes). Values below each band represent the mean fold change in protein expression level from three independent experiments compared with the cognate zero time point. *, $P < 0.05$; **, $P < 0.01$.

(D) *In situ* kinetic PLA detection of cANGPTL4: indicated binding partner complexes in cANGPTL4-treated HMVECs transfected with either constitutive-active Rac1 G12V or dominant-negative Rac1 T17N. Values (means±S.D.) represent mean fold change in the number of interactions compared to the zero time point, as determined from n=3 independent experiments (~600 HMVECs) using BlobFinder. *, $P < 0.05$; **, $P < 0.01$.

Figure 6: cANGPTL4:interacting partner complex formation triggers the nuclear translocation of β-catenin.

(A) Immunofluorescence staining for β-catenin (green) in a HMVEC monolayer treated with either 6 μg/ml of cANGPTL4 or 2.5mM EDTA (as positive control) for 3 h. HMVECs were counterstained with DAPI (blue) for nuclei. Scale bar: 40 μm. White arrows indicate endothelial junction lesions associated with reduced β-catenin staining.

Representative fluorescence intensity plot of β-catenin and DAPI, indicated by the white dotted line across the nuclei, were quantified using Zen 2009 software (Carl Zeiss).

(B) *In situ* PLA assay for β-catenin and quantification of the number of PLA spots per nuclei of cANGPTL4-treated HMVECs at the indicated time points. (0 min, 1.2±0.81; 40 min, 3±1.23; 90 min, 7.9±1.93; 140 min, 13.3±2.44; 180 min, 17.5±2.68) PLA signals (red) revealed translocation of β-catenin into nuclei at 140 min after treatment (~250 HMVECs). Cells were counterstained with Hoechst dye for nuclei (blue). Scale bar: 40 μm. *, $P < 0.05$; **, $P < 0.01$.

(C) Immunodetection of β-catenin in membrane, cytosol and nuclei fractions of HMVECs treated with either vehicle (PBS) or cANGPTL4. Protein lysates were collected at the indicated times. Values (means±S.D.) below each band represent the mean fold change in protein expression level compared with the cognate zero time point (n=3). *, $P < 0.05$; **, $P < 0.01$.

(D) Schematic diagram of cANGPTL4-mediated disruption of endothelial junctions. (1) cANGPTL4:integrin α5β1 formation (30-50 min) coincides with (2) the activation of Rac-GTP and pPAK in ECs (40-60 min) and with vascular leakiness; (3) the interaction between cANGPTL4 with VE-cadherin and claudin-5 (120-140 min) disrupts intercellular contact formation, and stimulates (4) nuclear translocation of β-catenin (180 min).

Figure 7: cANGPTL4 facilitates metastasis

(A-C) Representative macroscopic images of lungs (A); relative expression of melanin A (B); representative eosin stained images of lung sections(C), from (3mg/kg, thrice weekly). Black nodules in (C) indicate intravasated melanoma (n=5). Scale bar: 100 μm

(D, E) Number of nodules (D) and weights of lungs (E) from wild type and ANGPTL4 knockout C57BL/6J mice intravenously injected with either 5 x 10^5 $B16F10_{CTRL}$ or $B16F10_{\Delta ANGPTL4}$ cells (n=12). **, $P < 0.01$; ***, $P < 0.001$.

Table 1. ANGPTL4 increases vascular permeability and vascular volume

Tumor (n=15)	**OD610 Evans blue/g**	**Fluorescent unit (FITC)/g**	**Ratio**	
	Vascular permeability	**Vascular volume**	**VP/VV**	**Fold change**
A-5RT3$_{CTRL}$	0.76 ± 0.09*	0.82 ± 0.17**	0.927	5.332
A-5RT3$_{\Delta ANGPTL4}$	0.073 ± 0.012	0.42 ± 0.09	0.174	1.000

Data represent the mean±SD of 15 animals. *, $P < 0.001$; **, $P < 0.01$

Huang et al. Figure 1

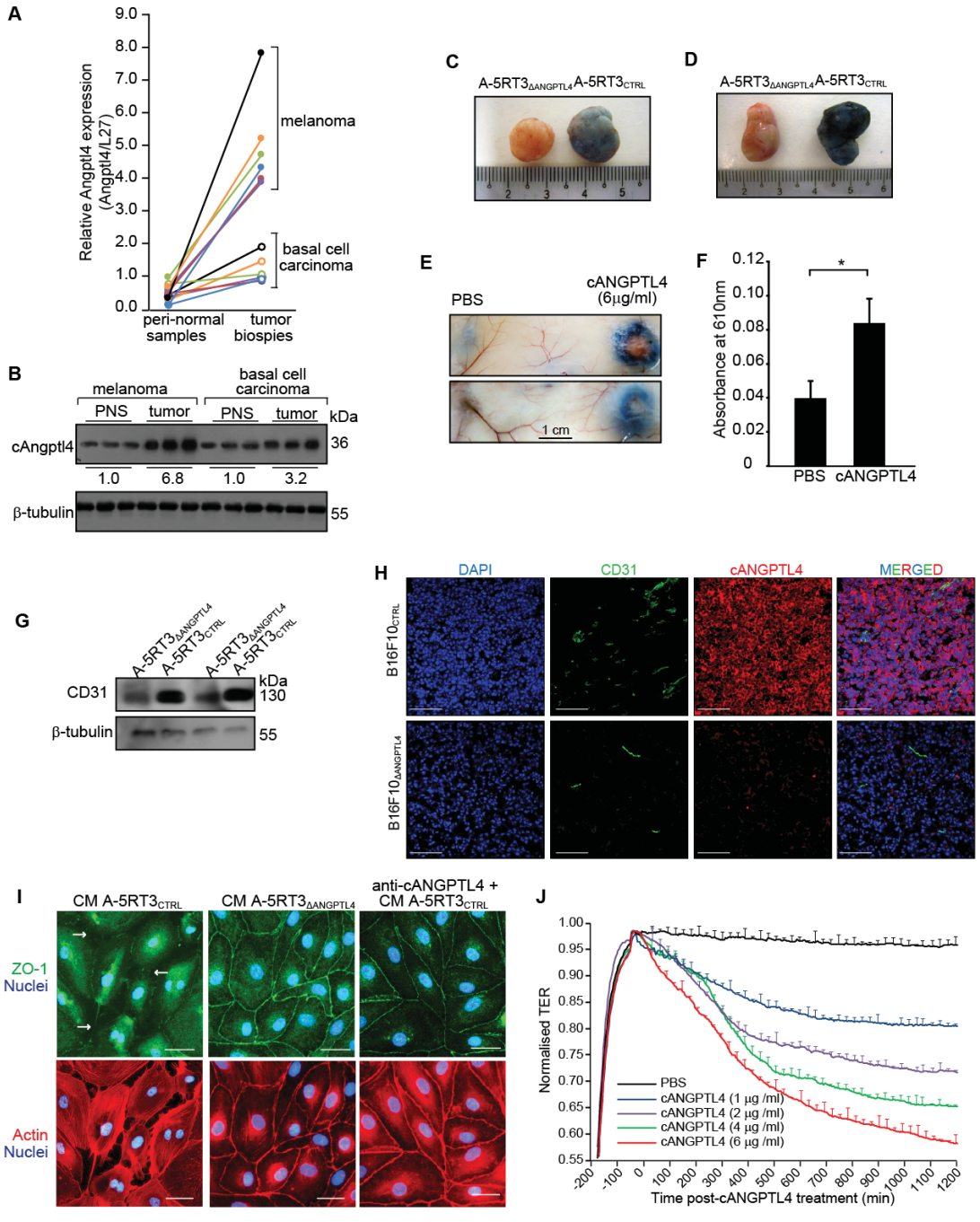

Huang et al, Figure 2

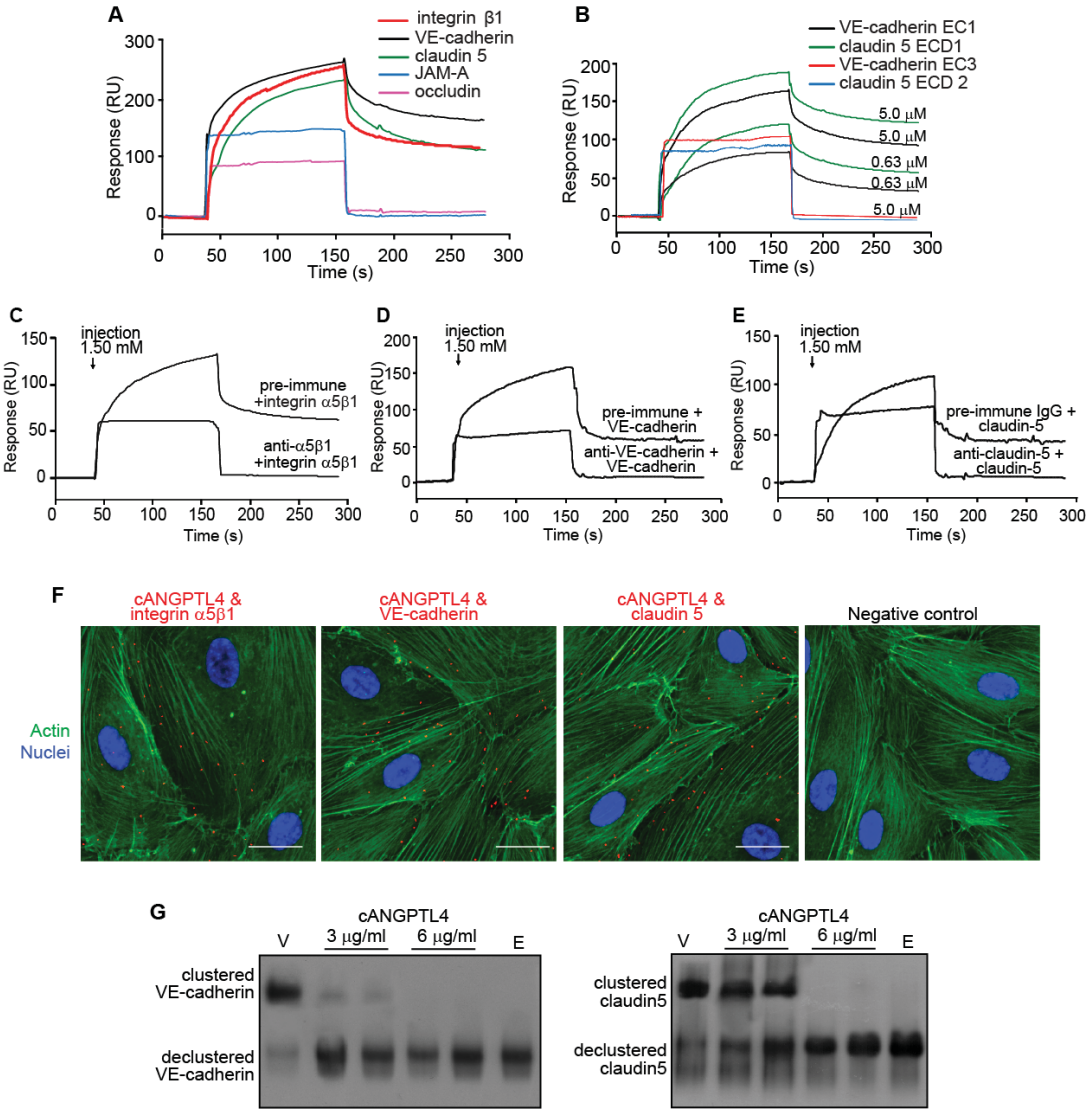

Huang et al, Figure 3

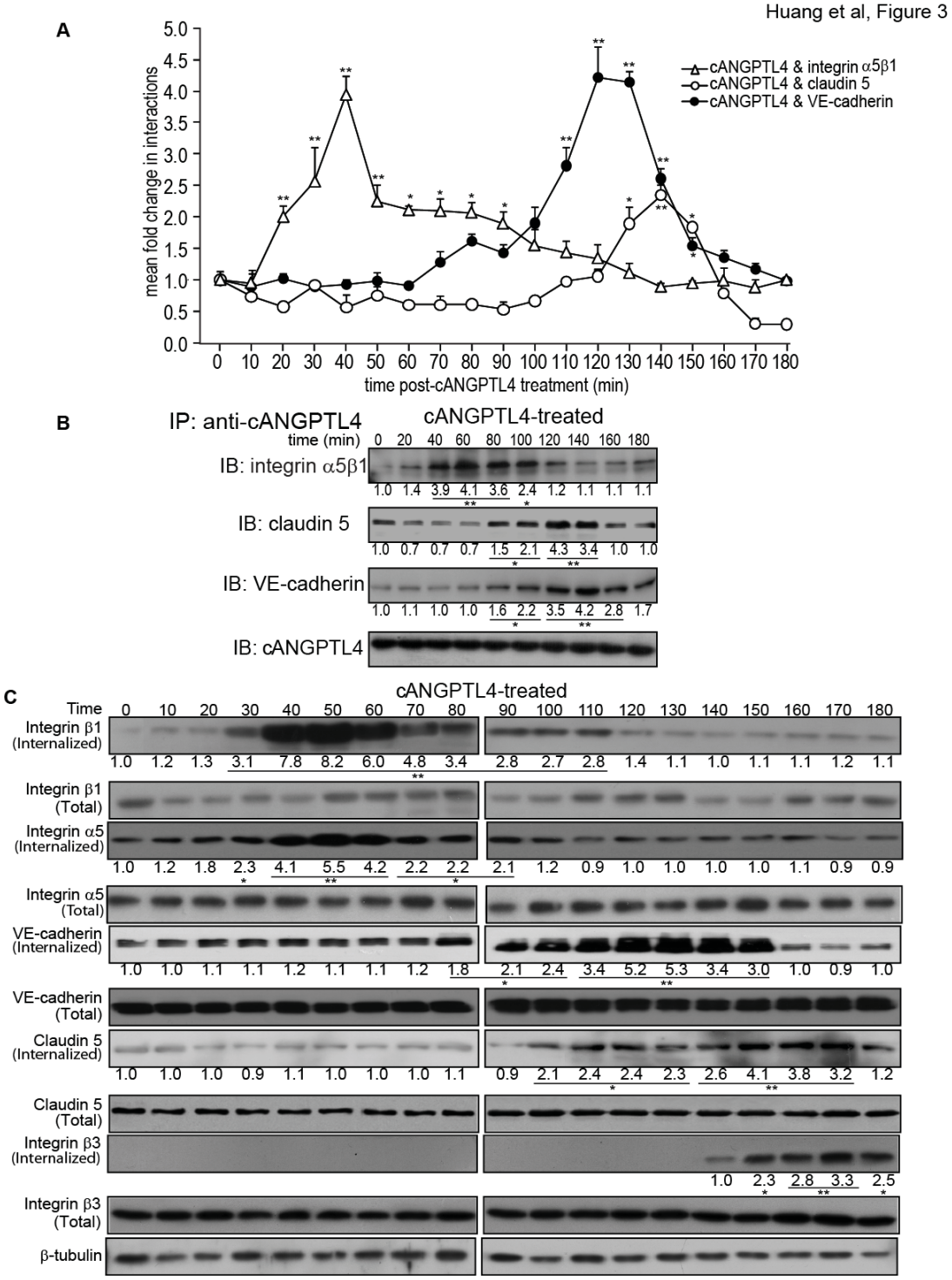

Huang et al, Figure 4

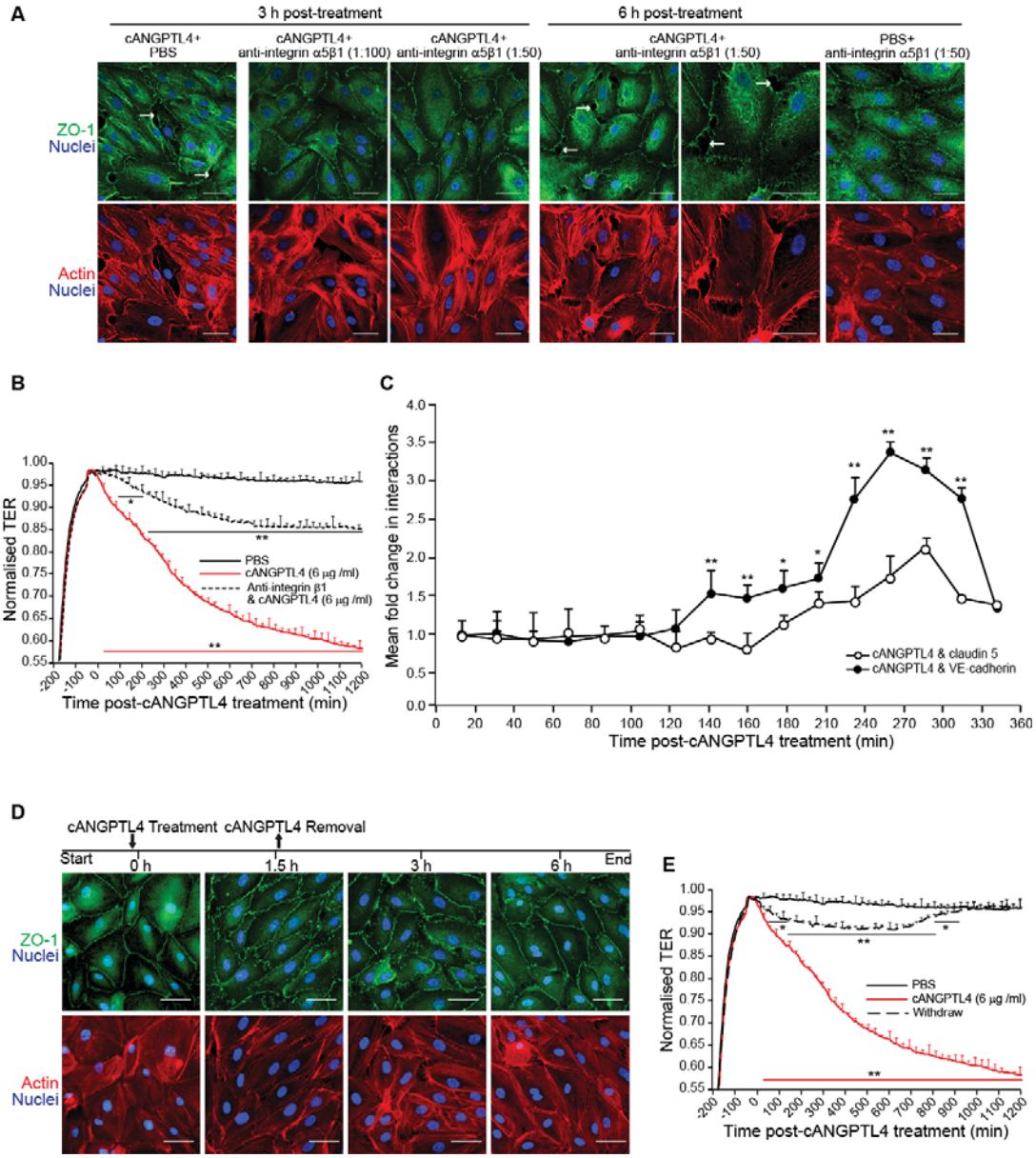

Huang et al, Figure 5

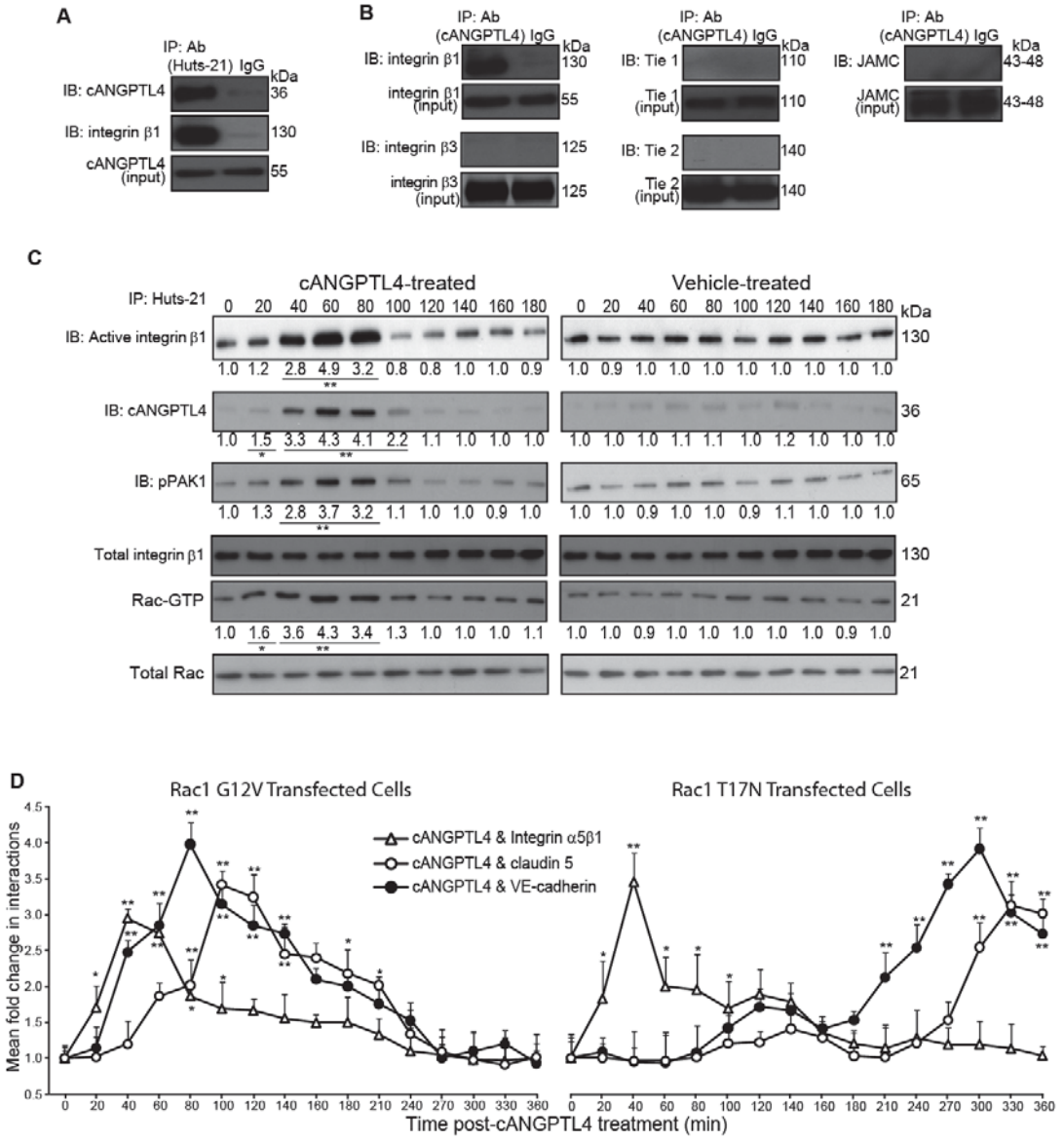

Huang et al, Figure 6

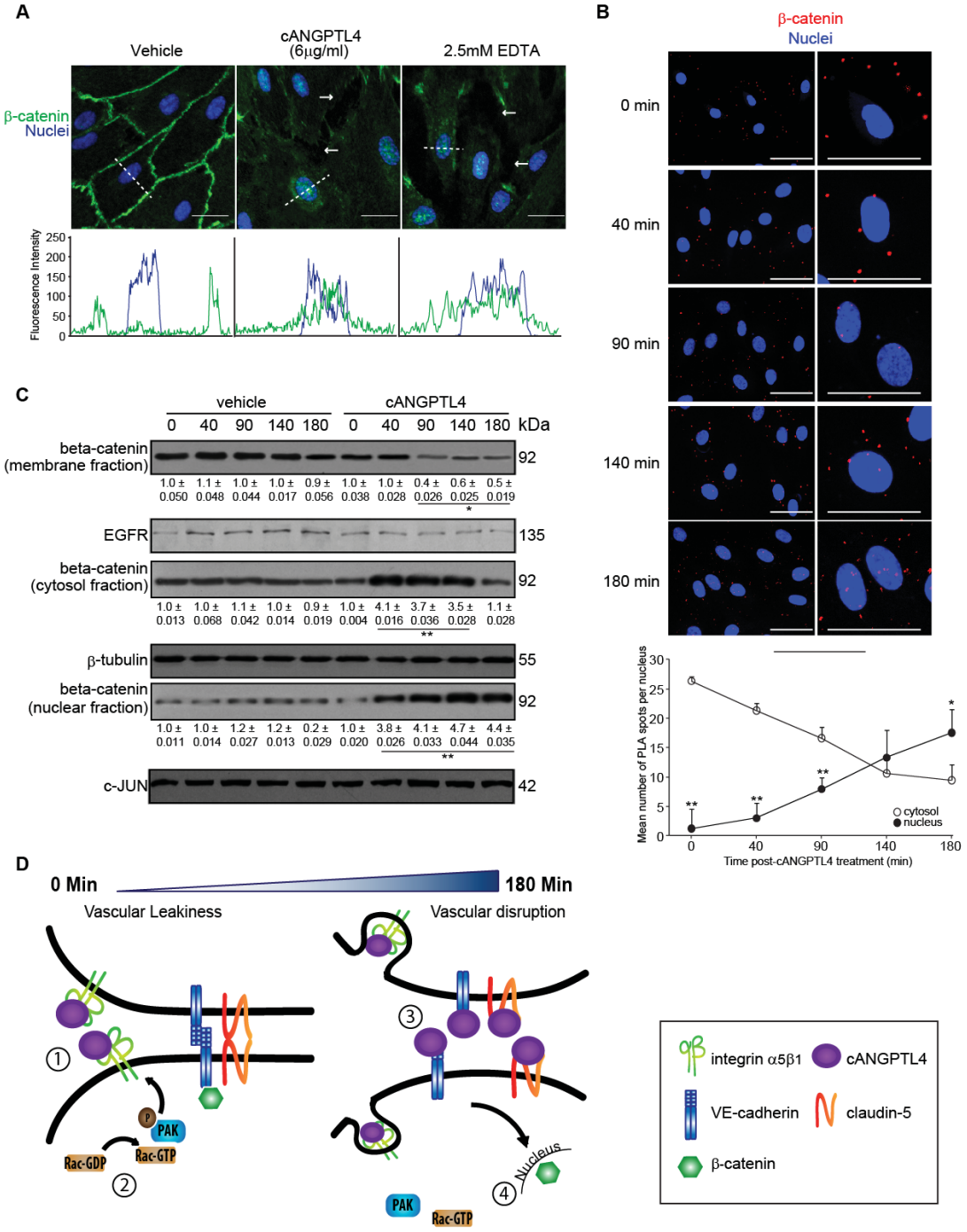

Huang et al, Figure 7

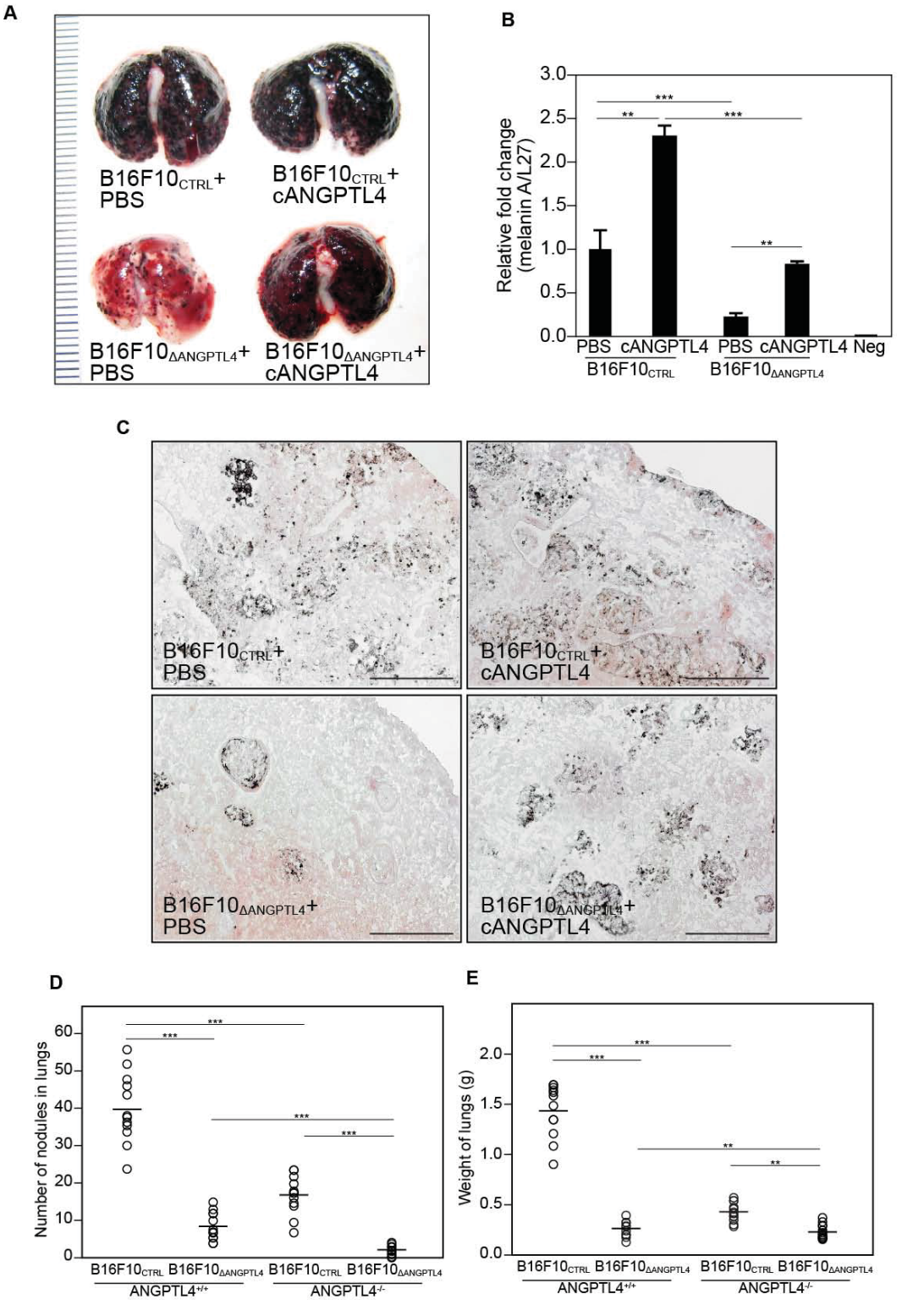

SUPPLEMENTARY INFORMATION

Supplemental Methods

Human Tumor Samples. Biopsies were subjected to protein and RNA extraction for immunoblotting and qPCR analyses, respectively. Commercial tumor tissue arrays #MTU951 and #MET961 (Pantomics, Inc., USA) were used to study the expression profile of cANGPTL4 in a large human tumor set by immunofluorescence (IF) imaging. The #MTU951 human tumor tissue array contains 40 tumor types, covering most of the common benign, malignant and metastatic tumors originating from 27 anatomic sites, and the #MET961 human cancer metastasis tissue array consists of 48 cases of metastatic cancers from >8 anatomic sites. The tissue arrays were probed with an anti-cANGPTL4 antibody and images acquired as previously described.[1] Gray scale values (i.e. immunofluorescence signals) were obtained using TissueQuest software (TissueGnostics GmbH).

Suppression of ANGPTL4 by RNA Interference (RNAi). An siRNA against human ANGPTL4 and a scrambled control siRNA were subcloned in the pFIV-H1/U6-puro pFIV/siRNA lentivirus system. The siRNA sequences were previously described.[2,3] The correct pFIV siRNA constructs were verified by sequencing using an H1 primer. Pseudovirus purification and transduction were performed.[1] ANGPTL4-knockdown tumor cells were enriched by puromycin selection for 1 week. The A-5RT3 sub-cell line designated A-5RT3$_{\Delta ANGPTL4}$, with the highest knockdown efficiency was chosen in this study, and the non-targeted siRNA transduced line was denoted A-5RT3$_{CTRL}$. Knockdown efficiency of ANGPTL4 and relative expression level of the indicated genes were determined by qPCR and immunoblot as previously described.[1,2]

Protein extraction, immunoprecipitation and immunoblot. Cell membrane fractions were obtained using ProteoJET^{TM} membrane protein extraction kit (Fermentas, USA) from 5 x 10^6 cells. For immunoprecipitation, HMVECs cells were treated with 6 µg/ml of rh-cANGPTL4 protein. At the indicated time, HMVECs cells were lysed. The lysate was then incubated with an anti-cANGPTL4 antibody overnight at 4 °C. Following that, the antibodies were pulled down using Sepharose protein A. Proteins were released by boiling for 10 min in Lamelli's buffer. Protein extracts were resolved using 10 % SDS-polyacrylamide gel electrophoresis (SDS-PAGE), and then electrotransferred (25 mM Tris, 192 mM glycine, 10% methanol, 0.05% SDS) onto a PVDF membrane for immunoblot analysis. Membranes were stripped and re-probed for other proteins as described.[4] Protein bands were detected using Immobilon^{TM} Western Chemiluminescent HRP substrate (Millipore, USA) and exposed onto X-ray film. For declustering experiments, confluent HMVECs cells were treated with rh-cANGPTL4 protein (3 and 6 µg/ml), 0.25 mM EDTA (as positive control) or control PBS. Membrane fractions were extracted as detailed above and resolved using 8 % native PAGE. Proteins were electrotransferred onto a PVDF membrane under reducing conditions (as above with 10 mM β-mercaptoethanol). Membranes were probed with antibodies against VE-cadherin or claudin-5.

FACS analysis. FACS analysis was carried out according to the manufacturer's protocol (BD Bioscience, USA). Briefly, cells were washed with cold PBS and then resuspended in 1X binding buffer. Next, 5 µl of FITC-Annexin V and 5 µl propidium iodide was added and the mixture was incubated for 15 min at 25°C in the dark. Four hundred microliters of 1X binding buffer was added before flow cytometry analysis using FACSCalibur and CellQuest software (BD Biosciences, USA).

Real-time PCR Primers

Gene	GenBank Accession	Forward primer	Reverse primer
Human Ribosomal protein L27	NM_011289	5'- CTG GTG GCT GGA ATT GAC CGC TA -3'	5'- CAA GGG GAT ATC CAC AGA GTA CCT TG -3'
Mouse Melanin A	XM_129166	5'- TGG ATA CAG AAC CTT GAT GAT GGA CA -3'	5' –GGG CTG ATG GGA TTT CTC TTG -3'
Human ANGPTL4	NM_139314	5' – ACC TCA ACG GCC AGT ACT TC -3'	5' – CCA TGG GCT GGA TCA ACA T -3'

References

1. Chong HC, Tan MJ, Philippe V, Tan SH, Tan CK, Ku CW, et al. Regulation of epithelial-mesenchymal IL-1 signaling by PPARbeta/delta is essential for skin homeostasis and wound healing. *J Cell Biol* 2009;184(6):817-831.

2. Goh YY, Pal M, Chong HC, Zhu P, Tan MJ, Punugu L, et al. Angiopoietin-Like 4 Interacts with Integrins {beta}1 and {beta}5 to Modulate Keratinocyte Migration. *Am J Pathol* 2010;177(6):2791-2803.

3. Goh YY, Pal M, Chong HC, Zhu P, Tan MJ, Punugu L, et al. Angiopoietin-like 4 interacts with matrix proteins to modulate wound healing. *J Biol Chem* 2010;285(43):32999-33009.

4. Yeung YG, Stanley ER. A solution for stripping antibodies from polyvinylidene fluoride immunoblots for multiple reprobing. *Anal Biochem* 2009;389(1):89-91.

Supplementary Figure Legends

Supplementary Figure 1: Elevated cANGPTL4 expression metastatic tumors.

(A, B) Representative H&E (A) and immunofluorescence (B) tumor tissue images probed with anti-cANGPTL4 antibody from colon adenocarcinoma tumor (representative of the tumor tissue array shown in S1C). Higher magnification pictures randomly selected from the adenocarcinoma tissue are shown (B, DAPI on the right panel and ANGPTL4 in the middle). Scale bars represent 200 μm.

(C) Average integrated gray value (immunofluorescence intensity) of cANGPTL4 level from the indicated normal and tumor tissues. Tissues from the same anatomic site were grouped. Values (mean±SEM) were calculated from at least three microscopic fields in each tissue. *P < 0.05; **$P < 0.01$.

(D) cANGPTL4 concentration in conditioned medium (CM) of the indicated tumorigenic and non-tumorigenic (as comparison controls) cell lines as determined by ELISA.

(E) Immunodetection of cANGPTL4 from fine-needle aspirates (FNA) of three breast cancer patients, CM of four tumorigenic (A-5RT3, MDA-MB231, MCF7-4.1 and HT29) and two non-tumorigenic lines (HaCaT and BJ). Known amounts of rh-cANGPTL4 (10-80 ng) corresponding to 1-8 μg/ml of cANGPTL4, served as calibration standards

Supplementary Figure 2: cANGPTL4-induced vascular disruption was not due to increased apoptosis.

(A) Relative expression of ANGPTL4 mRNA and protein in A-5RT3 tumor cells stably transfected with either the control scrambled siRNA (A-5RT3$_{CTRL}$) or the siRNA against ANGPTL4 (A-5RT3$_{\Delta ANGPTL4}$) as determined by qPCR and immunoblot, respectively.

(B) Histology of a representative metastasis to an axillary lymph node after injection of A-5RT3$_{CTRL}$ to the back of muscle fascia. The arrow marks foci of tumor cells invading

lymphatic tissue. Representative image of an enlarged axillary lymph node is seen in the insert next to a millimeter ruler.

(C) Immunofluorescence staining for ZO-1 in a confluent HMVEC monolayer. Cells were treated with 6 μg/ml of rh-cANGPTL4 in the presence or absence of cycloheximide and actinomycin for 3 h. HMVECs were counterstained with DAPI (blue) for nuclei and phalloidin (red) for actin stress fibers. Scale bar: 40 μm. White arrows indicate endothelial junction lesions.

(D) FACS analysis of vehicle (PBS)- or rh-cANGPTL4-treated HMVECs stained with annexin V-FITC/propidium iodide (PI). The percentage of apoptotic cells (upper- and lower-right quadrants) is indicated in bold. Data were obtained from three independent experiments.

Supplementary Figure 3: cANGTPL4 interacts with integrin α5β1, VE-cadherin and claudin-5

(A-C) Representative sensorgrams showing binding profiles between immobilized-cANGPTL4 with either integrin β1, VE-cadherin or claudin-5 pre-blocked with either preimmune IgG or an antibody to the C-terminus of ANGPTL4 (anti-ANGPTL4). Each sensorgram was corrected by subtracting a sensorgram obtained from a reference flow cell with no immobilized protein. The Rmax value was determined to be 283.1 resonance units (RU) using anti-cANGTL4 antibodies against the immobilized cANGPTL4.

(D) *In situ* proximity ligation assay (PLA) of cANGPTL4 and indicated binding partners in tumor biopsies. PLA signals are shown in red. Cells were counterstained DAPI for nuclei (blue). The negative control was performed only with anti-cANGPTL4. Scale bar: 40 μm.

(E) *In situ* proximity ligation assay (PLA) of CD31 and indicated proteins as negative control. Cells were counterstained with Alexa488-phallodin for actin stress fibers (green) and Hoechst dye for nuclei (blue).

Supplementary Figure 4: Expression level of integrin β1, β3, claudin-5, occludin and VE-cadherin in endothelial cells.

(A) Immunoblot of the indicated proteins from total protein lysate of HMVECs treated with rh-cANGPTL4 at the indicated time points. EGFR and β-tubulin were used as loading and transfer controls. Values below respective blots indicated fold-change in the band intensity compared to the time point at 0 h.

(B) Immunodetection of integrin β1, integrin α5, integrin β3, VE-cadherin and claudin-5 from total protein lysate versus internalized fraction of PBS treated HMVECs. Protein lysates were collected every 10 minutes (0-180 minutes). Values below each band represent the mean fold change in protein expression level compared with the cognate zero time point (n=3).

Supplementary Figure 5: cANGPTL4 stimulates nuclear translation of β-catenin in endothelial cells and potentiates lung metastasis.

(A) Immunofluorescence staining for β-catenin (green) in a HMVEC monolayer treated with either 6 μg/ml of cANGPTL4 or 2.5mM EDTA (as positive control) for 3 h. HMVECs were counterstained with DAPI (blue) for nuclei. Scale bar: 40 μm. White arrows indicate endothelial junction lesions associated with reduced β-catenin staining.

(B) Representative eosin stained images of normal lung section.